

**REPUBLIC OF TURKEY**  
**YILDIZ TECHNICAL UNIVERSITY**  
**GRADUATE SCHOOL OF NATURAL AND APPLIED SCIENCES**

**SYNTHESIS AND ANALYTICAL APPLICATIONS OF  
DENDRITIC LIGANDS**

**ALİ SEROL ERTÜRK**

**PhD. THESIS**  
**DEPARTMENT OF CHEMISTRY**  
**PROGRAM OF ANALYTICAL CHEMISTRY**

**ADVISER**  
**PROF. DR. ABDÜRREZZAK EMİN BOZDOĞAN**

**İSTANBUL, 2014**

**REPUBLIC OF TURKEY**  
**YILDIZ TECHNICAL UNIVERSITY**  
**GRADUATE SCHOOL OF NATURAL AND APPLIED SCIENCES**

**SYNTHESIS AND ANALYTICAL APPLICATIONS OF  
DENDRITIC LIGANDS**

A thesis submitted by Ali Serol Ertürk in partial fulfillment of the requirements for the degree of **PHILOSOPHY OF DOCTORATE** is approved by the committee on 0\*.0\*.2013 in Department of Chemistry, Analytical Chemistry Program.

**Thesis Adviser**

Prof. Dr. Abdürrezzak Emin BOZDOĞAN  
Yıldız Technical University

**Co- Adviser**

Assoc. Prof. Dr. Metin TÜLÜ  
Yıldız Technical University

**Approved By the Examining Committee**

Prof. Dr. Abdürrezzak Emin BOZDOĞAN  
Yıldız Technical University

\_\_\_\_\_

Prof. Dr. Filiz İMER, Member  
Yıldız Technical University

\_\_\_\_\_

Prof. Dr. Gönül KUNT  
Yıldız Technical University

\_\_\_\_\_

Assoc Prof. Dr. Mehmet ALTUN  
İstanbul University

\_\_\_\_\_

Assoc. Prof. Dr. Sezgin BAKIRDERE  
Yıldız Technical University

\_\_\_\_\_

Assoc. Dr. Amitav SANYAL

Boğaziçi University

---

This study was supported by Yıldız Technical University Scientific Research Projects Coordination Department (BAPK) Project No: 2012-01-02-DOP05.

## ACKNOWLEDGEMENTS

---

First of all, I would like to express my gratitude to my supervisor Prof. Dr. Abdürrezzak Emin BOZDOĞAN and second advisor Assoc. Prof. Dr. Metin TÜLÜ whose help, stimulating suggestions and encouragement helped me during the course of research and writing of this dissertation.

I would like also to thank Yıldız Technical University Scientific Research Project Coordination Department (BAPK) for funding my thesis with the Project No: 2012-01-02-DOP05.

I express my great thanks fully to my wife Müzeyyen ERTÜRK, my girl and family for their understanding, motivation and patience

Finally, I would like to thank Prof. Dr. Murat KOCA for his infinite support in every aspect of my academic research and life.

December, 2013

Ali Serol Ertürk

## TABLE OF CONTENTS

---

|   | Page |
|---|------|
| LIST OF SYMBOLS.....  | x    |
| LIST OF ABBREVIATIONS.....  | xi   |
| LIST OF FIGURES.....  | xiii |
| LIST OF TABLES .....  | xix  |
| ABSTRACT.....   | xxi  |
| ÖZET.....   | xxiv |
| CHAPTER 1   |      |
| INTRODUCTION.....   | 1    |
| 1.1 Literature Review.....  | 1    |
| 1.2 Objective of the Thesis.....  | 15   |
| 1.3 Hypothesis .....  | 15   |
| CHAPTER 2   |      |
| GENERAL INFORMATION.....  | 16   |
| 2.1 Introduction: Dendrimer Types and History .....   | 16   |
| 2.2 Chemical Synthesis of Dendrimers.....   | 19   |
| 2.2.1 Divergent Synthesis.....  | 19   |
| 2.2.2 Convergent Synthesis .....  | 19   |
| 2.3 Properties of Dendrimers.....   | 20   |
| 2.4 Applications of Dendrimers.....   | 22   |
| 2.4.1 Dendritic sensors .....   | 22   |
| 2.4.2 Dendrimers as Magnetic Resonance Imaging (MRI) Contrast in<br>Medical Applications..... | 24   |
| 2.4.3 Dendrimers-Encapsulated Metal Nanoparticles (DEMNs): Application<br>to Catalysis .....  | 25   |
| 2.4.3.1 Intradendrimer Complexes of PAMAMs with Cu <sup>2+</sup> .....                        | 25   |
| 2.4.3.2 Reduction of Dendrimer/Metal-Ion Composites.....                                      | 26   |
| 2.4.4 Dendrimers as Drug Delivery Devices .....   | 26   |
| 2.4.5 Dendrimers: Nanoarchitectures for Solubility Enhancement .....                          | 27   |

|                    |   |    |
|--------------------|---|----|
| 2.4.6              | Liquid Phase Polymer Retention (LPR): Dendrimer Enhanced Ultrafiltration (DEUF) .....           | 31 |
| 2.5                | Microwave Chemistry .....   | 33 |
| 2.5.1              | Microwave (MW) Theory .....   | 33 |
| 2.5.2              | Mechanism of Microwave (MW) Heating .....   | 33 |
| 2.5.3              | Solvent Selection in Microwave Chemistry .....  | 35 |
| 2.5.3.1            | Theory .....  | 35 |
| 2.5.3.2            | Choosing a Solvent .....  | 37 |
| 2.6                | Chemometrics .....  | 37 |
| 2.6.1              | PCA and Pattern Recognition .....   | 37 |
| 2.6.1.1            | PCA: Basic Concepts and Master Equations .....  | 38 |
| 2.6.1.2            | PCA NIPALS Algorithm .....  | 42 |
| 2.6.2              | EFA .....   | 43 |
| 2.6.2.1            | Abstract Factor Analysis .....  | 43 |
| 2.6.3              | MCR-Iterative Curve Resolution Methods .....  | 48 |
| 2.6.4              | MCR-ALS .....   | 49 |
| 2.6.5              | Classification: Cluster Analysis and Dendrograms .....  | 51 |
| 2.6.5.1            | Distance Measures in Cluster Analysis and Classification .....                                  | 51 |
| 2.6.5.2            | Cluster Analysis and Dendrograms .....  | 52 |
| 2.6.6              | Multivariate Regression .....   | 53 |
| 2.6.6.1            | Multivariate Calibration (MLR) .....  | 53 |
| 2.6.6.2            | Principal Component Regression (PCR) .....  | 54 |
| 2.6.6.3            | Partial Least Squares (PLS) .....   | 55 |
| 2.7                | Software Assisted Stability Constant Determination: Hyperquad & HypSpec .....                   | 57 |
| <br>CHAPTER 3      |   |    |
| EXPERIMENTAL ..... |   |    |
| 60                 |   |    |
| 3.1                | Materials .....   | 60 |
| 3.2                | Instrumentation & Software .....  | 60 |
| 3.3                | Characterization .....  | 61 |
| 3.4                | Microwave Assisted Synthesis of Amine Terminated PAMAMs .....                                   | 62 |
| 3.4.1              | General Procedure for the Synthesis of Half Generations (0.5-3.5) of PAMAMs .....               | 62 |
| 3.4.1.1            | Synthesis of EDA Cored Half Generations (E0.5-E3.5) .....                                       | 62 |
| 3.4.1.2            | Synthesis of DETA Cored Half Generations (D0.5-D3.5) .....                                      | 64 |
| 3.4.1.3            | Synthesis of Jeffamine <sup>®</sup> T-403 Cored Half Generations (P0.5-P3.5) .....              | 65 |
| 3.4.2              | General Procedure for the Synthesis of Full Generations (1-4.NH <sub>2</sub> ) .....            | 67 |
| 3.4.2.1            | Synthesis of EDA Cored Full Generations (E1-E4.NH <sub>2</sub> ) .....                          | 67 |
| 3.4.2.2            | Synthesis of DETA Cored Full Generations (D1-D4.NH <sub>2</sub> ) .....                         | 69 |
| 3.4.2.3            | Synthesis of Jeffamine <sup>®</sup> T-403 Cored Full Generations (P1-P4.NH <sub>2</sub> ) ..... | 71 |
| 3.4.2.4            | LPR Experiment .....  | 72 |
| 3.5                | Synthesis of Water Soluble PAMAM Derivatives .....  | 72 |
| 3.5.1              | General Procedure for the Synthesis of Carboxyl Terminated PAMAMs .....                         | 72 |
| 3.5.1.1            | Synthesis of E3.COOH .....  | 73 |
| 3.5.1.2            | Synthesis of E4.COOH .....  | 73 |

|          |  |    |
|----------|--|----|
| 3.5.1.3  | Synthesis of D3.COOH .....   | 73 |
| 3.5.1.4  | Synthesis of D4.COOH .....   | 74 |
| 3.5.1.5  | Synthesis of P3.COOH .....   | 74 |
| 3.5.1.6  | Synthesis of P4.COOH .....   | 74 |
| 3.5.2    | General Procedure for the Synthesis of Tris Terminated PAMAMs ..   | 75 |
| 3.5.2.1  | Synthesis of E3.TRIS .....   | 75 |
| 3.5.2.2  | Synthesis of E4.TRIS .....   | 76 |
| 3.5.2.3  | Synthesis of D3.TRIS .....   | 76 |
| 3.5.2.4  | Synthesis of D4.TRIS .....   | 76 |
| 3.5.2.5  | Synthesis of P3.TRIS.....  | 77 |
| 3.5.2.6  | Synthesis of P4.TRIS.....  | 77 |
| 3.6      | Determination of the Protonation Constants of PAMAMs by Hyperquad<br>Program .....   | 78 |
| 3.6.1    | Potentiometric Titrations and Measurements.....  | 78 |
| 3.7      | Spectroscopic Investigation of the Protonation Constants of PAMAMs by<br>Chemometric Approaches and HypSpec Program .....                | 79 |
| 3.7.1    | Spectroscopic Titrations and Measurements.....   | 79 |
| 3.7.2    | Protonation Constants .....  | 79 |
| 3.7.3    | Hierarchical Cluster Analysis (HCA).....   | 80 |
| 3.7.4    | Principal Component Analysis (PCA).....  | 80 |
| 3.7.5    | Data Treatment and Spectral Factor Analysis (SPFA) .....   | 80 |
| 3.8      | Analysis of Co(II)-PAMAM Dendrimer Complexes by UV-VIS<br>Spectroscopy.....  | 81 |
| 3.8.1    | Potentiometric Titrations and Measurements.....  | 81 |
| 3.8.2    | UV-VIS Measurements.....   | 82 |
| 3.9      | Removal of Metal Ions from Aqueous Solutions by Dendrimer Enhanced<br>Ultrafiltration (DEUF).....  | 82 |
| 3.9.1    | Analytical Methods.....  | 82 |
| 3.9.2    | Batch Complexation and Polymer Assisted Ultrafiltration (PAUF) ...   | 83 |
| 3.10     | Synthesis and Characterization of Cu-DENs.....   | 84 |
| 3.10.1   | Binding Studies .....  | 84 |
| 3.10.2   | Spectroscopic Titration of Dendrimers with Cu <sup>2+</sup> ions .....   | 84 |
| 3.11     | P4.NH <sub>2</sub> as Solubility Enhancer of Carvedilol .....  | 86 |
| 3.11.1   | Phase Solubility Studies.....  | 86 |
| 3.11.2   | Drug Binding Constants.....  | 87 |
| 3.12     | Determination of Different Generations from Binary Mixtures of<br>Jeffamine <sup>®</sup> T-403 Cored PAMAMs by UV-VIS Spectroscopy ..... | 87 |
| 3.12.1   | UV-VIS Spectroscopy Analysis .....   | 87 |
| 3.12.1.1 | Design and Analysis of Experiments.....  | 87 |
| 3.12.1.2 | Preparation of Dendrimer Solutions .....   | 88 |
| 3.12.2   | Data Set.....  | 88 |
| 3.12.3   | Variable Selection .....   | 89 |

## CHAPTER 4

|                              |  |    |
|------------------------------|--|----|
| RESULTS AND DISCUSSION ..... | 91   |    |
| 4.1                          | Microwave Assisted Synthesis of Amine Terminated PAMAMs .....                | 91 |
| 4.1.1                        | Synthesis of Generation 1-4 PAMAMs .....                                     | 91 |
| 4.1.2                        | Comparison of Microwave Assisted Amidation with Conventional<br>Methods..... | 97 |

|         |  |     |
|---------|--|-----|
| 4.1.3   | Gel Permeation Chromatography (GPC) Analysis of Jeffamine® T-403 Cored PAMAMs.....   | 99  |
| 4.2     | Synthesis of Water soluble PAMAM Derivatives .....   | 101 |
| 4.2.1   | Surface Modification of PAMAMs .....   | 101 |
| 4.3     | Determination of the Protonation Constants of PAMAMs by Hyperquad Program .....  | 106 |
| 4.3.1   | Potentiometric Titrations and Measurements.....  | 106 |
| 4.3.2   | Primary Amine Terminated PAMAMs.....   | 108 |
| 4.3.3   | Effect of Ionic Strength on Potentiometric Titration Curves of Amine Terminated PAMAMs .....   | 110 |
| 4.3.4   | Tris Terminated PAMAMs .....   | 112 |
| 4.3.5   | Determination of the Protonation Constants by Hyperquad .....  | 115 |
| 4.3.5.1 | Protonation Constants of PAMAM E3.NH <sub>2</sub> and E4.NH <sub>2</sub> .....   | 116 |
| 4.3.5.2 | Protonation Constants of PAMAM D3.NH <sub>2</sub> and D4.NH <sub>2</sub> .....   | 118 |
| 4.3.5.3 | Protonation Constants of P3.NH <sub>2</sub> and P4.NH <sub>2</sub> PAMAMs .....  | 120 |
| 4.4     | Spectroscopic Investigation of the Protonation Constants of PAMAMs by Chemometric Approaches and HypSpec Program .....                               | 122 |
| 4.4.1   | Determination of the number of UV-VIS Absorbing Species (Pure Components) by PCA and EFA .....   | 122 |
| 4.4.1.1 | Amine Terminated PAMAMs.....   | 124 |
| 4.4.1.2 | Tris Terminated PAMAMs .....   | 126 |
| 4.4.1.3 | Carboxyl Terminated PAMAMs .....   | 128 |
| 4.4.2   | Exploratory Data Analysis .....  | 130 |
| 4.4.2.1 | Hierarchical Cluster Analysis (HCA).....   | 130 |
| 4.4.2.2 | Pattern Recognition .....  | 135 |
| 4.4.3   | MCR-ALS .....  | 145 |
| 4.4.3.1 | Amine Terminated PAMAMs.....   | 146 |
| 4.4.3.2 | Tris Terminated PAMAMs .....   | 147 |
| 4.4.3.3 | Carboxyl Terminated PAMAMs .....   | 149 |
| 4.4.4   | Refinement of Protonation Constants by HypSpec Program.....  | 150 |
| 4.4.5   | Species Distribution Curves.....   | 155 |
| 4.4.5.1 | Amine Terminated PAMAMs.....   | 155 |
| 4.4.5.2 | TRIS Terminated PAMAMs.....  | 156 |
| 4.4.5.3 | Carboxyl Terminated PAMAMs .....   | 158 |
| 4.5     | Analysis of Co(II)-PAMAM Dendrimer Complexes by UV-VIS Spectroscopy.....   | 159 |
| 4.5.1   | Potentiometric Measurements .....  | 159 |
| 4.5.2   | UV-VIS Characterization of P4.NH <sub>2</sub> .....  | 161 |
| 4.5.3   | UV-VIS Characterization of Co (II)-P4.NH <sub>2</sub> Complex.....   | 162 |
| 4.6     | Removal of Metal Ions from Aqueous Solutions by Dendrimer Enhanced Ultrafiltration .....   | 163 |
| 4.6.1   | Generation Effect of P3.NH <sub>2</sub> and P4.NH <sub>2</sub> PAMAMs on the Simultaneous Retention of Cu (II), Co (II), Ni (II), Cd (II), Zn (II) . | 163 |
| 4.6.2   | Effect of EOP on Metal Binding Abilities of P3.NH <sub>2</sub> and P4.NH <sub>2</sub> ...  | 172 |
| 4.6.3   | Effect of Initial Free Metal Ion Concentration on Dendrimer Metal Complexation .....   | 175 |
| 4.7     | Synthesis and Characterization of Cu-Dendrimer Encapsulated Nanoparticles .....  | 176 |
| 4.7.1   | Spectroscopic Titrations of Tris and Carboxyl Terminated Dendrimers .....  | 176 |

|                  |  |     |
|------------------|--|-----|
| 4.7.2            | Synthesis and UV-VIS Characterization of Cu-DENs .....   | 185 |
| 4.8              | P4.NH <sub>2</sub> as Solubility Enhancer of Carvedilol .....  | 189 |
| 4.8.1            | Effect of PAMAM Concentration on Solubility of Carvedilol .....  | 189 |
| 4.8.2            | Drug Binding Constants and Encapsulation Efficiency of P4.NH <sub>2</sub> -<br>CAR Complexes .....                                       | 191 |
| 4.9              | Determination of Different Generations from Binary Mixtures of<br>Jeffamine <sup>®</sup> T-403 Cored PAMAMs by UV-VIS Spectroscopy ..... | 192 |
| 4.9.1            | UV-VIS Spectroscopy Analysis of PAMAMs .....   | 192 |
| 4.9.2            | Design of Experiments and Data Processing .....  | 193 |
| 4.9.3            | Determination of the Number of Variables .....   | 194 |
| 4.9.4            | Multivariate Models: MLR, PCR and PLS .....  | 195 |
| 4.9.4.1          | Comparison of Models .....   | 195 |
| 4.9.4.2          | Validation .....   | 196 |
| 4.10             | General Results and Summary .....  | 199 |
| REFERENCES       | .....  | 204 |
| APPENDIX-A       | .....  | 225 |
| CURRICULUM VITAE | .....  | 239 |

## LIST OF SYMBOLS

---

|                     |                                |
|---------------------|--------------------------------|
| $\mu\text{L}$       | Microliter                     |
| $\mu\text{m}$       | Micrometer                     |
| $^{\circ}\text{C}$  | Centigrade                     |
| $^{13}\text{C NMR}$ | Carbon NMR                     |
| $^1\text{H NMR}$    | Proton NMR                     |
| hr                  | Hour                           |
| L                   | Liter                          |
| M                   | Molar                          |
| mg                  | Milligram                      |
| min.                | Minute                         |
| mL                  | Milliliters                    |
| mM                  | Millimolar                     |
| nm                  | Nanometer                      |
| NMR                 | Nuclear magnetic resonance     |
| ppm                 | Parts per million              |
| R%                  | Percent retention              |
| $C_f$               | Concentration of feed solution |
| $C_p$               | Concentration of permeate flux |
| $\lambda$           | Wavelength                     |
| m $\Omega$          | Milliohm                       |

## LIST OF ABBREVIATIONS

---

|         |  |
|---------|--|
| AAS     | Atomic absorption spectroscopy                               |
| ALS     | Alternating least squares                                    |
| CAR     | Carvedilol   |
| CLS     | Classical least squares                                      |
| DAB     | Diamino butane   |
| DEMNs   | Dendrimer encapsulated metal nanoparticles                   |
| DENs    | Dendrimer encapsulated nanoparticles                         |
| DETA    | Diethylene triamine  |
| DEUF    | Dendrimer enhanced ultrafiltration                           |
| EDA     | Ethylene diamine   |
| EFA     | Evolving factor analysis                                     |
| EOB     | Extent of binding  |
| EOP     | Extent of protonation  |
| FA      | Factor analysis  |
| G       | Generation   |
| GPC     | Gel permeation chromatography                                |
| HCA     | Hierarchical cluster analysis                                |
| HPLCDAD | High performance liquid chromatography-diode array detection |
| IE      | Imbedded error   |
| ILS     | Inverse least squares  |
| ITTFA   | Iterative target transformation factor analysis              |
| LMCT    | Ligand to metal charge transfer                              |
| LPR     | Liquid phase retention                                       |
| LV      | Latent Variable  |
| MA      | Methyl acrylate  |
| MALS    | Multiangle light scattering                                  |
| MAS     | Microwave assisted synthesis                                 |
| MCR     | Multivariate curve resolution                                |
| MCR-ALS | Multivariate curve resolution-alternating least squares      |
| MLR     | Multivariate calibration                                     |
| Mn      | Nominal molecular weight                                     |
| MW      | Microwave  |
| Mw      | Molecular weight   |
| MWCO    | Molecular weight cut-off                                     |
| NIPALS  | Non-linear iterative partial least squares                   |
| PAMAM   | Poly(amido) amine  |

|        |  |
|--------|--|
| PAMAMs | Poly(amido) amine dendrimers               |
| PAUF   | Polymer assisted ultrafiltration           |
| PBS    | Phosphate buffered saline                  |
| PC     | Principal component                        |
| PCA    | Principle component analysis               |
| PCR    | Principle component regression             |
| PDI    | Poly dispersity index                      |
| PEUF   | Polyelectrolyte-enhanced ultrafiltration   |
| PF     | Polymer filtration                         |
| PLS    | Partial least squares                      |
| PPI    | Poly propylene imine                       |
| PPIs   | Poly propylene imine dendrimers            |
| PSU    | Polymer supported ultrafiltration          |
| RE     | Real error                                 |
| RFA    | Resolution factor analysis                 |
| RMSEC  | Root mean square error of calibration      |
| RMSECV | Root mean square error of cross validation |
| RMSEP  | Root mean square error of prediction       |
| SEC    | Size exclusion chromatography              |
| SMCR   | Self modelling curve resolution            |
| SPFA   | Spectra factor analysis                    |
| Tris   | Tris (hydroxymethyl) aminomethane          |
| UF     | Ultrafiltration                            |
| UV-VIS | Ultraviolet-visible                        |
| XE     | Extracted error                            |

## LIST OF FIGURES

|             |  | Page |
|-------------|--|------|
| Figure 2.1  | A comparison of complexity as a function of molecular architecture, strategy, quantized building blocks, and technological age .....   | 17   |
| Figure 2.2  | Common commercially available dendrimers. Top left: PPI (G5). Top right: PAMAM (G3). Bottom: PAMAM (G5). Each generation is marked with a circle .....   | 18   |
| Figure 2.3  | Schematically depicted dendrimer synthesis. Top: Divergent strategy. Bottom: Convergent strategy.....  | 20   |
| Figure 2.4  | The ‘dendritic box’ .....  | 22   |
| Figure 2.5  | PPI dendrimer, containing 32 units at the terminal: fluorescent sensor for the detection of $\text{Co}^{2+}$ ions .....  | 23   |
| Figure 2.6  | PAMAM-based dendritic sensor .....   | 24   |
| Figure 2.7  | Synthesis of DEMNs.....  | 25   |
| Figure 2.8  | UV-VIS monitoring of the synthesis of DEMNs. Dashed line (spectrum 1): G4-OH/ $\text{Cu}^{2+}$ solution; solid line (spectrum 2): reduction with 5-fold molar excess of $\text{NaBH}_4$ ; solid line (spectrum 3): same condition for G4- $\text{NH}_2$ instead G4-OH.....   | 26   |
| Figure 2.9  | Solubility profile of Indomethacin in the presence of differing concentrations of G4- $\text{NH}_2$ , G4-OH, and G-4.5 dendrimers at pH 7.0 .....  | 28   |
| Figure 2.10 | Possible mechanisms of dendrimer-mediated solubility enhancement .....   | 29   |
| Figure 2.11 | Top row: Three dimensional depiction of conformational change of an amino-terminated PAMAM dendrimer at increasing pH Middle row: Two-dimensional depiction of the conformational change of an amino-terminated PAMAM dendrimer upon increasing pH. Bottom row: Two-dimensional depiction of the conformational change of a carboxyl-terminated PPI dendrimer at increasing pH ..... | 30   |
| Figure 2.12 | Scheme of the process of metal-ion retention by an aqueous soluble polymer in a UF system .....  | 31   |
| Figure 2.13 | Liquid phase retention instrumental arrangement. UF cell with polymeric and / or metal ion solution; (2) membrane filtrate; (3) magnetic stirrer; (4) pressure trap; (5) selector; (6) reservoir with water.....   | 32   |
| Figure 2.14 | Water treatment by DEUF.....   | 32   |
| Figure 2.15 | Systematic representation of sample heating by conduction and microwaves.....  | 34   |
| Figure 2.16 | Data matrix $\mathbf{X}$ , consisting of $I$ rows, ‘objects’, each characterized by $K$ columns, ‘variables’ .....   | 38   |
| Figure 2.17 | PCA projects the columns of $\mathbf{X}$ onto a loading vector $\mathbf{p}_1\mathbf{T}$ and the rows of $\mathbf{X}$ into the complementary score vector $\mathbf{t}_1$ , constituting the ‘first principal component (PC)’ .....  | 39   |

|             |  |     |
|-------------|--|-----|
| Figure 2.18 | Matrix $\mathbf{X}$ decomposed into a set of rank 1 outer products ( $A$ terms, corresponding to the effective rank, $A$ ) and the residual matrix, $E$ .....  | 39  |
| Figure 2.19 | A sample Cross validation PRESS curve of P4.NH <sub>2</sub> . 5 PCs. ....  | 42  |
| Figure 2.20 | (A) Typical structure of data that are subjected to EFA, the rows of the matrix are formed by spectra measured as a function of an independent variable; (B) Hyperspectral data. Spectra are measured as a function of the two coordinates of an image.....    | 44  |
| Figure 2.21 | The dimensions of $\mathbf{U}$ , $\mathbf{S}$ , and $\mathbf{V}^T$ . Only the shaded parts are relevant .....  | 45  |
| Figure 2.22 | Submatrices analyzed by traditional EFA (A) forward EFA; (B) backward EFA .....  | 46  |
| Figure 2.23 | The combination of appearance and disappearance of significant singular values results in concentration windows. species distribution curve, forward EFA, backward EFA and species existence range as a function of pH from top the bottom, respectively ..... | 47  |
| Figure 2.24 | Example of linking in cluster analysis and resulting dendrograms .....   | 52  |
| Figure 3.1  | Systematic diagram of batch complexation and PAUF .....  | 83  |
| Figure 3.2  | Schematic representation of metal complexation of P4.NH <sub>2</sub> .....   | 84  |
| Figure 4.1  | ATR monitoring and time dependency from ester to amide ( <b>P0.5</b> to <b>P1.NH<sub>2</sub></b> ) PAMAMs.....   | 95  |
| Figure 4.2  | ATR spectra of pure, ester, and amine terminated dendrimers respectively.....  | 95  |
| Figure 4.3  | Synthesis and structure development of generation (1-4) PAMAMs, a) Alkylation step and b) Amidation step .....   | 96  |
| Figure 4.4  | ATR monitored conversion spectrum from <b>P0.5</b> to <b>P1.NH<sub>2</sub></b> .....   | 97  |
| Figure 4.5  | Conversion of P0.5 to P1.NH <sub>2</sub> .....   | 98  |
| Figure 4.6  | GPC of P4.NH <sub>2</sub> .....  | 100 |
| Figure 4.7  | Tris and carboxyl surface modification of esteric generations.....   | 102 |
| Figure 4.8  | <sup>1</sup> H NMR spectrum monitoring of the conversion of D3.5 (bottom) to D4.COOH (middle) and D4.TRIS (Top) .....  | 104 |
| Figure 4.9  | ATR monitoring and time dependency from ester to amide (D2.5 to D3.COOH) PAMAMs .....  | 105 |
| Figure 4.10 | ATR monitoring and time dependency from ester to amide (D2.5 to D3.TRIS) PAMAMs .....  | 105 |
| Figure 4.11 | Potentiometric pH titration curves for E4.NH <sub>2</sub> at ionic strength of 0, 10, 25, 50, and 100 mM respectively.....   | 111 |
| Figure 4.12 | Potentiometric pH titration curves for D4.NH <sub>2</sub> at ionic strength of 0, 10, 25, 50, and 100 mM respectively.....   | 111 |
| Figure 4.13 | Potentiometric pH titration curves for P4.NH <sub>2</sub> at ionic strength of 0, 10, 25, 50, and 100 mM respectively.....   | 112 |
| Figure 4.14 | Potentiometric pH titration curve for E4.TRIS at ionic strength 100 mM .....   | 113 |
| Figure 4.15 | Potentiometric pH titration curve for D4.TRIS at ionic strength 100 mM .....   | 114 |
| Figure 4.16 | Potentiometric pH titration curve for P4.TRIS at ionic strength 100 mM .....   | 114 |
| Figure 4.17 | Species distribution curves for the E3.NH <sub>2</sub> system vs. pH at 25 ± 0.1 °C, I=100 mM NaCl.....  | 117 |
| Figure 4.18 | Species distribution curves for the E4.NH <sub>2</sub> system vs. pH at 25 ± 0.1 °C, I=100 mM NaCl.....  | 117 |

|             |   |     |
|-------------|---|-----|
| Figure 4.19 | Species distribution curves for the D3.NH <sub>2</sub> system vs. pH at 25 ± 0.1 °C, I=100 mM NaCl.....   | 119 |
| Figure 4.20 | Species distribution curves for the D4.NH <sub>2</sub> system vs. pH at 25 ± 0.1 °C, I=100 mM NaCl.....   | 119 |
| Figure 4.21 | Species distribution curves for the P3.NH <sub>2</sub> system vs. pH at 25 ± 0.1 °C, I=100 mM NaCl.....   | 121 |
| Figure 4.22 | Species distribution curves for the P4.NH <sub>2</sub> system vs. pH at 25 ± 0.1 °C, I=100 mM NaCl.....   | 121 |
| Figure 4.23 | 3D plots of UV spectroscopic titration of (A) E4.NH <sub>2</sub> (1.08x 10 <sup>-3</sup> M) (B) D4.NH <sub>2</sub> (4.98 x 10 <sup>-4</sup> M) (C) P4.NH <sub>2</sub> (4.483 x 10 <sup>-4</sup> M) solution with 0.098 N HCl at 25 ± 01 °C, I=100 mM NaCl ..... | 124 |
| Figure 4.24 | Determination of the number of absorbing species (PCs-Factors) by cross validation (left side of (A), (B), (C)) and FA (right side of (A), (B), (C) ) for E4.NH <sub>2</sub> , D4.NH <sub>2</sub> and P4.NH <sub>2</sub> , respectively. ....                   | 125 |
| Figure 4.25 | 3D plots of UV spectroscopic titration of (A) E4.TRIS (7.08x 10 <sup>-4</sup> M) (B) D4.TRIS (3.70 x 10 <sup>-4</sup> M) (C) P4.TRIS (6.06 x 10 <sup>-4</sup> M) solution with 0.098 N HCl at 25 ± 01 °C, I=100 mM NaCl .....                                   | 126 |
| Figure 4.26 | Determination of the number of absorbing species (PCs-Factors) by cross validation (left side of (A), (B), (C)) and FA (right side of (A), (B), (C) ) for E4.TRIS, D4.TRIS and P4.TRIS, respectively. ....  | 127 |
| Figure 4.27 | 3D plots of UV spectroscopic titration of (A) E4.COOH (8.24 x 10 <sup>-4</sup> M) (B) D4.COOH (8.50 x 10 <sup>-4</sup> M) (C) P4.COOH (9.14 x 10 <sup>-4</sup> M) solution with 0.098 N HCl at 25 ± 01 °C, I=100 mM NaCl.....                                   | 128 |
| Figure 4.28 | Determination of the number of absorbing species (PCs-Factors) by cross validation (left side of (A), (B), (C)) and FA (right side of (A), (B), (C) ) for E4.COOH, D4.COOH and P4.COOH, respectively.....   | 129 |
| Figure 4.29 | Dendogram for HCA analysis of E4.NH <sub>2</sub> titration data.....  | 131 |
| Figure 4.30 | Dendogram for HCA analysis of D4.NH <sub>2</sub> titration data. ....   | 131 |
| Figure 4.31 | Dendogram for HCA analysis of P4.NH <sub>2</sub> titration data. ....   | 132 |
| Figure 4.32 | Dendogram for HCA analysis of E4.TRIS titration data .....  | 132 |
| Figure 4.33 | Dendogram for HCA analysis of D4.TRIS titration data.....   | 133 |
| Figure 4.34 | Dendogram for HCA analysis of P4.TRIS titration data.....   | 133 |
| Figure 4.35 | Dendogram for HCA analysis of E4.COOH titration data.....   | 134 |
| Figure 4.36 | Dendogram for HCA analysis of D4.COOH titration data .....  | 134 |
| Figure 4.37 | Dendogram for HCA analysis of P4.COOH titration data.....   | 135 |
| Figure 4.38 | Score plots of E4.NH <sub>2</sub> titration data for (A) PC 1 vs. PC3 (B) PC1 vs. PC3 and (C) pattern recognition results on maximum absorbance at 282 nm vs. pH graph for E4.NH <sub>2</sub> .....   | 136 |
| Figure 4.39 | Score plots of D4.NH <sub>2</sub> titration data for (A) PC 1 vs. PC2 (B) PC1 vs. PC3 and (C) pattern recognition results on maximum absorbance at 282 nm vs. pH graph for D4.NH <sub>2</sub> .....   | 137 |
| Figure 4.40 | Score plots of P4.NH <sub>2</sub> titration data for (A) PC 1 vs. PC2 (B) PC1 vs. PC3 and (C) pattern recognition results on maximum absorbance at 280 nm vs. pH graph for P4.NH <sub>2</sub> .....   | 138 |
| Figure 4.41 | Score plots of E4.TRIS titration data for (A) PC 1 vs. PC2 (B) PC1 vs. PC4 and (C) pattern recognition results on maximum absorbance at 284 nm vs. pH graph for E4.TRIS.....  | 139 |
| Figure 4.42 | Score plots of D4.TRIS titration data for (A) PC 1 vs. PC2 (B) PC1 vs. PC3 and (C) pattern recognition results on maximum absorbance at 286 nm vs. pH graph for D4.TRIS. ....   | 140 |

|             |  |     |
|-------------|--|-----|
| Figure 4.43 | Score plots of P4.TRIS titration data for (A) PC 1 vs. PC2 (B) PC1 vs. PC3 and (C) pattern recognition results on maximum absorbance at 284 nm vs. pH graph for P4.TRIS..... | 141 |
| Figure 4.44 | Score plots of E4.COOH titration data for (A) PC 1 vs. PC2 (B) PC1 vs. PC3 and (C) pattern recognition results on maximum absorbance at 286 nm vs. pH graph for E4.COOH..... | 142 |
| Figure 4.45 | Score plots of D4.COOH titration data for (A) PC 1 vs. PC2 (B) PC1 vs. PC3 and (C) pattern recognition results on maximum absorbance at 286 nm vs. pH graph for D4.COOH..... | 143 |
| Figure 4.46 | Score plots of P4.COOH titration data for (A) PC 1 vs. PC2 (B) PC1 vs. PC4 and (C) pattern recognition results on maximum absorbance at 286 nm vs. pH graph for D4.COOH..... | 144 |
| Figure 4.47 | Molar absorbance spectrum of E4.NH <sub>2</sub> .....  | 146 |
| Figure 4.48 | Molar absorbance spectrum of D4.NH <sub>2</sub> .....  | 146 |
| Figure 4.49 | Molar absorbance spectrum of P4.NH <sub>2</sub> .....  | 147 |
| Figure 4.50 | Molar absorbance spectrum of E4.TRIS.....  | 147 |
| Figure 4.51 | Molar absorbance spectrum of D4.TRIS .....   | 148 |
| Figure 4.52 | Molar absorbance spectrum of P4.TRIS .....   | 148 |
| Figure 4.53 | Molar absorbance spectrum of E4.COOH .....   | 149 |
| Figure 4.54 | Molar absorbance spectrum of D4.COOH.....  | 149 |
| Figure 4.55 | Molar absorbance spectrum of P4.COOH .....   | 150 |
| Figure 4.56 | Species distribution curve of E4.NH <sub>2</sub> in the pH range of 2-11. %<br>Concentrations of free E4.NH <sub>2</sub> .....   | 155 |
| Figure 4.57 | Species distribution curve of D4.NH <sub>2</sub> in the pH range 2-11. %<br>Concentrations of free D4.NH <sub>2</sub> : .....  | 155 |
| Figure 4.58 | Species distribution curve of P4.NH <sub>2</sub> in the pH range 2-11. %<br>Concentrations of free P4.NH <sub>2</sub> .....  | 156 |
| Figure 4.59 | Species distribution curve of E4.TRIS in the pH range of 2-11. %<br>Concentrations of free E4.TRIS .....   | 156 |
| Figure 4.60 | Species distribution curve of D4.TRIS in the pH range of 2-11. %<br>Concentrations of free D4.TRIS.....  | 157 |
| Figure 4.61 | Species distribution curve of P4.TRIS in the pH range of 2-11. %<br>Concentrations of free P4.TRIS.....  | 157 |
| Figure 4.62 | Species distribution curve of E4.COOH in the pH range of 2-11. %<br>Concentrations of free E4.COOH.....  | 158 |
| Figure 4.63 | Species distribution curve of D4.COOH in the pH range of 2-12. %<br>Concentrations of free D4.COOH .....   | 158 |
| Figure 4.64 | Species distribution curve of P4.COOH in the pH range of 2-12. %<br>Concentrations of free P4.COOH .....   | 159 |
| Figure 4.65 | A sample structure of Jeffamine <sup>®</sup> T-403 cored PAMAMs. Third generation P3.NH <sub>2</sub> structure .....   | 160 |
| Figure 4.66 | Illustration of forward and back potentiometric titration curves of P4.NH <sub>2</sub> with 2 <sup>nd</sup> derivative of back titration curve.....                          | 160 |
| Figure 4.67 | PAMAM dendrimer characteristic absorption band in between 280-285 nm.....  | 161 |
| Figure 4.68 | Representative absorption spectra of P4.NH <sub>2</sub> .....  | 162 |
| Figure 4.69 | Observation of Co(II)-P4.NH <sub>2</sub> complexation bands at 585-635 nm for the alternating concentrations of Co(II):P4.NH <sub>2</sub> ratios .....                       | 162 |
| Figure 4.70 | Illustration of the complex formation between Co(II) ions and P4.NH <sub>2</sub> .   | 163 |

|             |  |     |
|-------------|--|-----|
| Figure 4.71 | Cu (II) retention in aqueous solutions of (A) in P3.NH <sub>2</sub> and (B) in P4.NH <sub>2</sub> solutions as a function of solution pH.....                            | 165 |
| Figure 4.72 | Co (II) retention in aqueous solutions of (A) in P3.NH <sub>2</sub> and (B) in P4.NH <sub>2</sub> solutions as a function of solution pH.....                            | 166 |
| Figure 4.73 | Ni (II) retention in aqueous solutions of (A) in P3.NH <sub>2</sub> and (B) in P4.NH <sub>2</sub> solutions as a function of solution pH.....                            | 167 |
| Figure 4.74 | Cd (II) retention in aqueous solutions of (A) in P3.NH <sub>2</sub> and (B) in P4.NH <sub>2</sub> solutions as a function of solution pH.....                            | 168 |
| Figure 4.75 | Zn (II) retention in aqueous solutions of (A) in P3.NH <sub>2</sub> and (B) in P4.NH <sub>2</sub> solutions as a function of solution pH.....                            | 169 |
| Figure 4.76 | Cu (II), Co (II), Ni (II), Cd (II), Zn (II) retention profiles in aqueous solutions of (A) P3.NH <sub>2</sub> and (B) P4.NH <sub>2</sub> as a function of solution pH... | 171 |
| Figure 4.77 | Extend of Protonation ( $\alpha$ ) of primary and tertiary amine groups of (A) P3.NH <sub>2</sub> and (B) P4.NH <sub>2</sub> dendrimer .....                             | 172 |
| Figure 4.78 | % proton binding curve for (A) P3.NH <sub>2</sub> and (B) P4.NH <sub>2</sub> .....   | 174 |
| Figure 4.79 | Precipitation diagram of metal hydroxides at 25 °C.....  | 176 |
| Figure 4.80 | Absorption spectra of E4.TRIS dendrimer (0.228 mM) solution titrated with Cu <sup>2+</sup> (81.54 mM) at 680 nm .....  | 177 |
| Figure 4.81 | Absorption spectra of D4.TRIS dendrimer (0.202 mM) solution titrated with Cu <sup>2+</sup> (80.14 mM) at 680 nm .....  | 178 |
| Figure 4.82 | Absorption spectra of P4.TRIS dendrimer (0.148 mM) solution titrated with Cu <sup>2+</sup> (81.54 mM) at 680 nm .....  | 178 |
| Figure 4.83 | Absorption spectra of E4.COOH dendrimer (0.321 mM) solution titrated with Cu <sup>2+</sup> (80.14 mM) at 680 nm .....  | 179 |
| Figure 4.84 | Absorption spectra of D4.COOH dendrimer (0.268 mM) solution titrated with Cu <sup>2+</sup> (80.50 mM) at 680 nm .....  | 179 |
| Figure 4.85 | Absorption spectra of P4.COOH dendrimer (0.200 mM) solution titrated with Cu <sup>2+</sup> (79.86 mM) at 680 nm .....  | 180 |
| Figure 4.86 | Spectroscopic titration curve of the E3.TRIS dendrimer with Cu <sup>2+</sup> ions.....   | 181 |
| Figure 4.87 | Spectroscopic titration curve of the E4.TRIS dendrimer with Cu <sup>2+</sup> ions.....   | 181 |
| Figure 4.88 | Spectroscopic titration curve of the E3.COOH dendrimer with Cu <sup>2+</sup> ions.....   | 181 |
| Figure 4.89 | Spectroscopic titration curve of the E4.COOH dendrimer with Cu <sup>2+</sup> ions.....   | 182 |
| Figure 4.90 | Spectroscopic titration curve of the D3.TRIS dendrimer with Cu <sup>2+</sup> ions.....   | 182 |
| Figure 4.91 | Spectroscopic titration curve of the D4.TRIS dendrimer with Cu <sup>2+</sup> ions.....   | 182 |
| Figure 4.92 | Spectroscopic titration curve of the D3.COOH dendrimer with Cu <sup>2+</sup> ions.....   | 183 |
| Figure 4.93 | Spectroscopic titration curve of the D4.COOH dendrimer with Cu <sup>2+</sup> ions.....   | 183 |
| Figure 4.94 | Spectroscopic titration curve of the P3.TRIS dendrimer with Cu <sup>2+</sup> ions.....   | 183 |
| Figure 4.95 | Spectroscopic titration curve of the P4.TRIS dendrimer with Cu <sup>2+</sup> ions.....   | 184 |
| Figure 4.96 | Spectroscopic titration curve of the P3.COOH dendrimer with Cu <sup>2+</sup> ions.....   | 184 |

|   |     |
|---|-----|
| Figure 4.97 Spectroscopic titration curve of the P4.COOH dendrimer with Cu <sup>2+</sup> ions.....                                | 184 |
| Figure 4.98 Change in color during the synthesis of Cu-DENs.....  | 186 |
| Figure 4.99 UV-VIS absorption spectra of the formation of Cu-E4.TRIS.....   | 187 |
| Figure 4.100 UV-VIS absorption spectra of the formation of Cu-E4.COOH.....  | 187 |
| Figure 4.101 UV-VIS absorption spectra of the formation of Cu-D4.TRIS.....  | 187 |
| Figure 4.102 UV-VIS absorption spectra of the formation of Cu-D4.COOH.....  | 188 |
| Figure 4.103 UV-VIS absorption spectra of the formation of Cu-P4.TRIS.....  | 188 |
| Figure 4.104 UV-VIS absorption spectra of the formation of Cu-P4.COOH.....  | 188 |
| Figure 4.105 Representative illustration of the CAR-dendrimer inclusion complex....   | 189 |
| Figure 4.106 Phase solubility diagram of P4.NH <sub>2</sub> .....   | 190 |
| Figure 4.107 Increase in the absorbance of CAR by increasing P4.NH <sub>2</sub> concentration and hypsochromic shift.....         | 191 |
| Figure 4.108 UV-VIS spectra of different generation PAMAMs and their mixtures at $\lambda$ maximum.....                           | 193 |
| Figure 4.109 RMSECV levels of P2.NH <sub>2</sub> and P3.NH <sub>2</sub> for (a) PLS (b) PCR model.....                            | 195 |
| Figure 4.110 Y measured and Y predicted values of (a) MLR model (b) PCR model (c) PLS model for P2.NH <sub>2</sub> component..... | 198 |
| Figure 4.111 Y measured and predicted values of (a) MLR model (b) PCR model (c) PLS model for P3.NH <sub>2</sub> component.....   | 199 |

## LIST OF TABLES

|            |   | Page |
|------------|---|------|
| Table 2.1  | Dielectric constant ( $\epsilon'$ ), $\tan\delta$ , and dielectric loss ( $\epsilon''$ ) for 30 common solvents (measured at room temperature and 2450 MHz) .....   | 36   |
| Table 3.1  | Concentrations used to titrate aqueous solutions of tris and carboxyl terminated dendrimers with $\text{Cu}^{2+}$ ions .....  | 85   |
| Table 3.2  | Number of amine groups on tris terminated PAMAMs available for binding with $\text{Cu}^{2+}$ ions .....   | 86   |
| Table 3.3  | Number of amine groups on carboxyl terminated PAMAMs available for binding with $\text{Cu}^{2+}$ ions .....   | 86   |
| Table 3.4  | $3^2$ Full Factorial Design Layout.....   | 88   |
| Table 4.1  | Preparation of EDA cored ester terminated PAMAMs by conventional method.....  | 92   |
| Table 4.2  | Preparation of DETA cored ester terminated PAMAMs by conventional method.....   | 93   |
| Table 4.3  | Preparation of Jeffamine <sup>®</sup> T-403 cored ester terminated PAMAMs by conventional method.....   | 93   |
| Table 4.4  | Preparation of EDA cored amine terminated PAMAMs by MAS .....   | 93   |
| Table 4.5  | Preparation of DETA cored amine terminated PAMAMs by MAS .....  | 94   |
| Table 4.6  | Preparation of Jeffamine <sup>®</sup> T-403 cored amine terminated PAMAMs by MAS .....  | 94   |
| Table 4.7  | Optimization of reaction conditions for the synthesized dendrimers from P1.NH <sub>2</sub> to P4.NH <sub>2</sub> .....  | 99   |
| Table 4.8  | Molecular weight dependency of different generation of PAMAMs .....   | 100  |
| Table 4.9  | Preparation of Tris terminated PAMAMs .....   | 106  |
| Table 4.10 | Preparation of carboxyl terminated PAMAMs.....  | 106  |
| Table 4.11 | Experimental potentiometric titration conditions for different PAMAMs .....   | 107  |
| Table 4.12 | Physico-chemical Properties of different generation EX.NH <sub>2</sub> , DX.NH <sub>2</sub> , PX.NH <sub>2</sub> PAMAMs.....  | 108  |
| Table 4.13 | Corresponding amine numbers to 1 <sup>st</sup> and 2 <sup>nd</sup> end points of the potentiometric titration curves.....   | 110  |
| Table 4.14 | pKa values of the tris terminated PAMAMs at the corresponding inflection point.....   | 113  |
| Table 4.15 | Physico chemical properties of some Tris terminated PAMAMs .....  | 115  |
| Table 4.16 | Stability constants ( $\log\beta$ values, which refer to $\text{L}_q + \text{H}_r \rightleftharpoons \text{L}_q\text{H}_r$ ) of E3.NH <sub>2</sub> and E4.NH <sub>2</sub> PAMAMs at $25 \pm 0.1$ °C ( I = 100 mM NaCl)..... | 116  |
| Table 4.17 | Stability constants ( $\log\beta$ values, which refer to $\text{L}_q + \text{H}_r \rightleftharpoons \text{L}_q\text{H}_r$ ) of D3.NH <sub>2</sub> and D4.NH <sub>2</sub> PAMAMs at $25 \pm 0.1$ °C ( I = 100 mM NaCl)..... | 118  |

|            |   |     |
|------------|---|-----|
| Table 4.18 | Stability constants ( $\log\beta$ values, which refer to $L_q + H_r \rightleftharpoons L_qH_r$ ) of the proton and P3.NH <sub>2</sub> and P4.NH <sub>2</sub> PAMAMs at $25 \pm 0.1$ °C ( I = 100 mM NaCl) ..... | 120 |
| Table 4.19 | Stability constants of E3.NH <sub>2</sub> and E4.NH <sub>2</sub> .....  | 151 |
| Table 4.20 | Stability constants of D3.NH <sub>2</sub> and D4.NH <sub>2</sub> .....  | 152 |
| Table 4.21 | Stability constants of P3NH <sub>2</sub> and P4.NH <sub>2</sub> .....   | 152 |
| Table 4.22 | Stability constants E3.TRIS and E4.TRIS .....   | 153 |
| Table 4.23 | Stability constants of D3.TRIS and D4.TRIS .....  | 153 |
| Table 4.24 | Stability constants of P3.TRIS and P4.TRIS.....   | 153 |
| Table 4.25 | Stability constants of E3.COOH and E4.COOH .....  | 154 |
| Table 4.26 | Stability constants of D3.COOH and D4.COOH .....  | 154 |
| Table 4.27 | Stability constants of P3.COOH and P4.COOH .....  | 154 |
| Table 4.28 | Extent of protonation of (A) tertiary amines and (B) primary amines of evaluated P3.NH <sub>2</sub> and P4.NH <sub>2</sub> .....  | 173 |
| Table 4.29 | Selected properties of Jeffamine <sup>®</sup> T403 cored PAMAMs.....  | 175 |
| Table 4.30 | Solubility Products of metal hydroxides at 25 °C [274] .....  | 176 |
| Table 4.31 | Number of amine groups on TRIS terminated DENs available for binding with Cu <sup>2+</sup> ions .....   | 185 |
| Table 4.32 | Comparison of RMSEC, RMSECV and RMSEP on MLR, PCR and PLS models .....  | 196 |

## ABSTRACT

---

# SYNTHESIS AND ANALYTICAL APPLICATIONS OF DENDRITIC LIGANDS

Ali Serol ERTÜRK

Department of Chemistry

PhD. Thesis

Adviser: Prof. Dr. Abdürrezzak Emin Bozdoğan

Co-adviser: Assoc. Prof. Dr. Metin TÖLÜ

Dendrimers are highly branched, star shaped and three dimensional macromolecules with nanometer scale. Their structure composition and controlled synthesis allow them to be designed with different shapes and sizes with interior cores and attaching surface groups. Surface modification of dendrimers affects some physical or chemical properties; such as solubility, chelating ability, encapsulation efficiency, absorption capacity and many others. Depending on these attained features, dendrimers can be used for a wide range of applications including drug delivery, gene therapy, catalysis, antibacterial agents and many others.

Starting from ethylene diamine (EDA), diethylene triamine (DETA) and commercially available polymer Jeffamine<sup>®</sup>T-403 cores, amine terminated, and tris and carboxyl surface modified water soluble PAMAM derivatives up to fourth generation were synthesized. Synthesis of amine terminated and tris terminated PAMAMs were performed by new developed microwave assisted synthesis (MAS) methods. By this way, amidation step was shortened up to 30-80 min. from 5-8 days while tris surface modification up to 110-130 min. from two days. Amine terminated DETA and surface modified DETA and Jeffamine<sup>®</sup> T-403 cored PAMAMs are the novel molecules in literature synthesized in this thesis. Synthesized dendrimers were purified by Liquid phase polymer retention (LPR) technique and characterized by <sup>1</sup>HNMR, <sup>13</sup>CNMR, IR and UV-VIS spectroscopy. Results revealed that synthesized dendrimers are in high purity and good yields and larger scales in shorter times.

Protonation mechanism of synthesized dendrimers were investigated by potentiometric and spectroscopic titrations. Data driven from titrations were evaluated with recent computer programs Hyperquad and HypSpec for pKa calculations. Number of absorbing

species in aqueous solutions of dendrimers to establish equilibrium chemical models were determined with spectral factor analysis (SPFA) with the aid of evolving factor analysis (EFA), root mean square error cross validation (RMSECV). Thus, without using any law of mass action, number of species present in aqueous dendrimer solutions were determined and pKa calculations were performed. A positive correlation between number of protonated species and generation numbers of amine terminated dendrimers was observed. On the other hand, variety of surface functional group was determined as to be deterministic on the number of spectroscopically active species and so calculated pKa values.

By means of species distribution plots obtained from titration experiments, protonation behaviors of synthesized dendrimers were characterized. Properties of a model fourth generation Jeffamine<sup>®</sup> T-403 cored P4.NH<sub>2</sub> dendrimer on the Co(II) binding ability and a low bioavailable drug Carvedilol (CAR) were investigated. P4.NH<sub>2</sub>-Co(II) complex and P4.NH<sub>2</sub>-CAR inclusion complexes characterized by UV-VIS spectroscopy. Stable and miscible ion pairs of CAR with P4.NH<sub>2</sub>'s internal basic tertiary amines were observed by UV-VIS spectroscopy.

The ability of simultaneous metal complexation of P3.NH<sub>2</sub> and P4.NH<sub>2</sub> was investigated with the removal of uncomplexed Cu (II), Co (II), Ni (II), Cd (II), and Zn (II) from metal dendrimer mixture solution with LPR technique. Retentate metal concentrations were determined by atomic absorption spectroscopy (AAS). pH role and effect of Jeffamine<sup>®</sup> T-403 cored PAMAM dendrimer generation on the simultaneous removal of metal ions from aqueous solutions were also investigated. High affinity of both P3.NH<sub>2</sub> and P4.NH<sub>2</sub> towards metal ions were observed in the decreasing order Zn(II) > Co(II) > Ni(II) > Cu(II) > Cd(II) at pH 9. Only the Cu(II) retention increases with increasing generation and pH. Zn(II) and Co(II) are retained most over % 90 retention for both generations at pH 9. In this way, novel metal chelating abilities of polydentate ligands P3.NH<sub>2</sub> and P4.NH<sub>2</sub> were characterized by LPR technique and explained by extent of protonation EOP profiles in different pH values. Over neutral pH, P3.NH<sub>2</sub> and P4.NH<sub>2</sub> are stable enough to simultaneously bind Co (II), Ni (II), Cd (II), and Zn (II).

Synthesis of Cu-DENs nanoparticles were performed from EDA, DETA and Jeffamine<sup>®</sup> T-403 cored, tris and carboxyl terminated PAMAM derivatives. Maximum metal loading capacity of these derivatives were determined by using spectroscopic titrations. Cu-DENs were characterized by UV-VIS spectroscopy. Disappearance of d-d transition band and ligand to metal charge transfer (LMCT) peak and formation of monotonically increasing exponential band were used as the evidence of the successful synthesis of Cu-Dens in addition to color change of dendrimer metal mixture solutions from blue to golden brown.

Finally, full factorial three level experimental design was used to construct multivariate MLR, PCR, PLS calibration models for the simultaneous determination P2.NH<sub>2</sub> and P3.NH<sub>2</sub> from binary mixtures of Jeffamine<sup>®</sup> T403 PAMAMs by UV-VIS spectroscopy. Different binary mixture solutions of P2.NH<sub>2</sub>-P3.NH<sub>2</sub> were prepared and spectral data collected by UV-VIS spectroscopy between the wavelengths ranges of 250-350 nm. Constructed models were compared in terms of prediction powers from relative mean square error of prediction (RMSEP) values.

**Key words:** Dendrimer, microwave assisted synthesis (MAS), liquid phase retention (LPR), spectral factor analysis (SPFAC), removal of metals, multivariate calibration

---

**YILDIZ TECHNICAL UNIVERSITY**  
**GRADUATE SCHOOL OF NATURAL AND APPLIED SCIENCES**

---

## DENDRİTİK LİGANDLARIN SENTEZİ VE ANALİTİK UYGULAMALARI

Ali Serol ERTÜRK

Analitik Kimya Anabilim Dalı

Doktora Tezi

Tez Danışmanı: Prof. Dr. Abdürrezzak Emin BOZDOĞAN

Eş Danışman: Prof. Dr. Metin TÜLÜ

Dendrimerler nano boyutta, oldukça dallanmış, yıldız şeklinde üç boyutlu moleküllerdir. Yapısal oluşumları ve kontrol edilebilir bir şekilde sentezlenebilmeleri, dendrimerlerin farklı çekirdek ve yüzey gruplarına sahip olan farklı şekillerde ve boyutlarda sentezlenebilmelerini mümkün kılmaktadır. Dendrimerlerin yüzey modifikasyonu, çözünürlük, şelat yetenekleri, kapsülleme verimliliği, absorpsiyon kapasitesi gibi birçok fiziksel ve kimyasal özelliklerini etkilemektedir. Bu kazanılan özelliklere dayalı olarak, dendrimerler ilaç taşıma sistemleri, gen terapisi, katalizör, anti-bakteriyel ajan ve buna benzer birçok uygulamayı içeren geniş bir uygulama alanında kullanılabilirler.

Etilen diamin (EDA), dietilen diamin (DETA) ve ticari olarak elde edilebilir olan Jeffamine® T-403 çekirdeğinden yola çıkarak, amin sonlu ve yüzeyi tris ve karboksili fonksiyonel grupları ile değiştirilmiş suda çözünür dördüncü jenerasyona kadar PAMAM dendrimerler ve türevleri sentezlenmiştir. Amin sonlu ve tris sonlu dendrimerlerin sentezi yeni geliştirilmiş olan mikrodalga destekli sentez (MAS) metotları kullanılarak gerçekleştirilmiştir. Bu şekilde, amitleme aşaması 5-8 günden 30-80 dk. indirirlerken, tris yüzey değişimi iki günden 110-130 dk. gibi kısa bir süreye indirilmiştir. Bu çalışmada sentezlenen, amin sonlu DETA ve yüzeyi değiştirilmiş olan DETA ve Jeffamine® T-403 çekirdekli PAMAMlar daha önce literatürde karşılaşılmayan yeni dendrimerlerdir. Sentezlenen dendrimerler sıvı fazlı polimer destekli alıkonma (LPR) tekniği kullanılarak saflaştırıldı ve dendrimerler <sup>1</sup>HNMR, <sup>13</sup>CNMR, IR ve UV-VIS spektroskopisi kullanılarak karakterize edildi. Elde edilen sonuçlara göre, dendrimerler yüksek saflıkta, iyi verimlerde, kısa sürede ve büyük ölçeklerde sentezlenmişlerdir.

Sentezlenen dendrimerlerin protonlanma mekanizmaları potansiyometrik ve spektroskopik titrasyon çalışmaları ile incelenmiştir. Titrasyonlardan elde edilen veriler Hyperquad ve HypSpec bilgisayar programları kullanılarak pKa hesaplamalarında kullanılmıştır. Kimyasal denge modelleri kurabilmek amacıyla, dendrimerlerin sulu çözeltilerinde içerdikleri absorbans yapan tür sayıları spektral faktör analizi (SPFA) kullanılarak; faktör analizi (EFA) ve RMSECV yardımıyla belirlenmiştir. Bunun sonucunda, herhangi bir yük ve denkliği kullanılmaksızın, sulu dendrimer çözeltilerinde var olan tür sayıları belirlenmiş ve pKa hesaplamaları gerçekleştirilmiştir. Protonlanan türler ile jenerasyon sayıları arasında amin sonlu dendrimerler için pozitif bir uyuma rastlanırken, yüzey fonksiyonel grubu çeşitliliğinin, spektroskopik olarak aktif tür sayısının belirlenmesinde belirleyici ve buna bağlı olarak hesaplanan pKa değeri sayılarında da belirleyici olduğu gözlemlenmiştir.

Titrasyon çalışmalarından elde edilen tür dağılım eğrileri sayesinde, sentezlenen dendrimerlerin protonlanma davranışları karakterize edildi. Dördüncü nesil P4.NH<sub>2</sub> dendrimerin Co(II) ve biyolojik olarak elde edilebilirliği düşük olan carvedilol (CAR) bağlama yetenekleri araştırıldı. P4.NH<sub>2</sub> - Co(II) kompleksi ve P4.NH<sub>2</sub>-CAR içerik kompleksi UV-VIS spektroskopisi kullanılarak karakterize edildi. CAR'ın P4.NH<sub>2</sub>'nin iç tersiyer amin grupları ile kararlı ve karışabilen iyon çiftleri oluşturduğu gözlemlendi.

P3.NH<sub>2</sub> ve P4.NH<sub>2</sub> dendrimerlerin eş zamanlı olarak metal kompleksi oluşturma yetenekleri, sulu çözeltilerde kompleks yapmamış Cu (II), Co (II), Ni (II), Cd (II), ve Zn (II) iyonlarının ortamdan LPR tekniği kullanılarak uzaklaştırılması incelenerek araştırıldı. Alıkonan metal konsantrasyonları, atomik absorpsiyon spektroskopisi (AAS) kullanılarak tayin edildi. Jeffamine<sup>®</sup> T-403 çekirdekli PAMAM dendrimerlerin sulu çözeltilerden eş zamanlı olarak metal iyonlarının uzaklaştırılmasına pH'nın etkisi ayrıca araştırıldı. P3.NH<sub>2</sub> ve P4.NH<sub>2</sub> dendrimerlerin metal iyonlarına karşı pH 9'da ilgisinin Zn(II) > Co(II) > Ni(II) > Cu(II) > Cd(II) olmak üzere düşen oranda olduğu gözlemlendi. Sadece Cu(II) iyonlarının alıkonmasının, pH attıkça arttığı gözlemlendi. Zn (II) ve Co(II) iyonları, her iki jenerasyon için, nesil sayısı arttıkça % 90 üzerinde doğru orantılı olarak alıkonmuşlardır. Bu şekilde, Jeffamine<sup>®</sup> T-403 çekirdekli çok dişli P3.NH<sub>2</sub> ve P4.NH<sub>2</sub> ligantlarının yeni metal bağlama kabiliyetleri karakterize edildi ve farklı pH değerlerinin protonlanma süreleri ile açıklandı. Nötral pH'ın üzerinde, P3.NH<sub>2</sub> ve P4.NH<sub>2</sub> Co (II), Ni (II), Cd (II), and Zn (II) iyonlarını eş zamanlı olarak bağlayabilmek için yeteri kadar kararlı olduğu görüldü.

EDA, DETA ve Jeffamine<sup>®</sup> T-403 çekirdekli, tris ve karboksili son gruplu PAMAM türevlerinden, Cu-DENs nanopartiküller sentezlendi. Bu dendrimer türevlerinin, maksimum metal bağlama kapasiteleri, spektroskopik titrasyonlar kullanılarak belirlendi. Cu-DENs nanopartiküller UV-VIS spektroskopisi kullanılarak karakterize edildi. d-d kompleks oluşum bandının ve ligandan metale yük aktarımı (LMCT) bantlarının kaybolması ve yerini düşük dalga boylarına doğru azalan üstel bir banda bırakması; dendrimer metal karışımları renginin maviden altın sarısına dönmesine ek olarak kanıt olarak kullanılmıştır.

Son olarak, ful faktöriyel üç seviyeli deneysel tasarımı kullanılarak, MLR, PCR ve PLS modeller; P2.NH<sub>2</sub> ve P3.NH<sub>2</sub> moleküllerinin Jeffamine<sup>®</sup> T-403 çekirdekli ikili dendrimer karışımlarından eş zamanlı olarak tayininde kullanılmak üzere oluşturuldu. Farklı P2.NH<sub>2</sub>-P3.NH<sub>2</sub> çözelti karışımları hazırlandı ve 250-350 nm dalga boyları arasında UV-VIS spektroskopisi kullanılarak spektral veri toplandı. Oluşturulan modeller tahmin güçleri RMSEP değerleri kullanılarak kıyaslandı.

**Anahtar Kelimeler:** Dendrimer, mikrodalga destekli sentez (MAS), sıvı fazlı alıkonma (LPR), spektral faktör analizi (SPFA), metallerin uzaklaştırılması, çok deęişkenli kalibrasyon

### INTRODUCTION

#### 1.1 Literature Review

Dendrimers are three dimensional, highly branched, relatively monodisperse macromolecules. They have received much attention in recent years due to their unique structures, which make them important for a wide range of applications including drug delivery [1-3], gene therapy [4-6], catalysis [7-10], antibacterial agents [11-13] and many others [14]. Dendrimers are conventionally synthesized by divergent [15-22] and convergent [23-26] methods. In poly (amidoamine) PAMAM dendrimer synthesis, divergent synthesis method is used. This method involves the alkylation of a central core usually ethylene diamine (EDA) or ammonia with methyl acrylate (MA), and amidation of the resulting product with excess EDA. While alkylation steps produce ester terminated dendrimers called as half generations, second steps-amidations produce amine terminated full generations. By the successive repetition of the alkylation and amidation steps, higher generation PAMAMs can be obtained. However, the synthesis of higher generation PAMAMs requires quantitative consumptions of the reactants, long time preparations and tedious purification steps especially for the removal of excess EDA. Therefore, the synthesis of higher generation PAMAMs with high purity in a short time has significant limitations. These limitations are mostly depended on the amidation step. This step takes five to eight days [27, 28] for the higher generations. In order to overcome these limitations, it has been generated recent research interests on the fast, facile and precise approaches for PAMAM dendrimer synthesis [27, 28]. For example, in industrial applications, it is difficult to apply dendrimers in large scales because of their huge cost and preparations [29]. Massive production of higher generation PAMAMs are mostly

restricted by the amidation step [15, 27, 28, 30]. That's why there are many attempts to increase the amidation yield and to diminish the reaction time [31].

Microwave assisted chemistry (MAS) could be an alternative to many classical reactions with some advantages. These are short reaction times, better yields and fewer by-products [32-35]. These advantages of MAS could be attributed to microwave effect or thermal effects, which are the consequence of dielectric constant of used solvent. Selective heating of highly absorbing compounds in less polar reaction media and superheating of solvents under proper temperature and ambient pressure are the dominant factors for accelerating reaction proceedings [34]. Thus, once reactions could not be performed with conventional synthetic methods can be performed with microwave (MW) chemistry and can give the desired products with efficient rates and yields [36, 37]. However, MAS is not a complete alternative of conventional chemistry. There are many debates about the MW energy which cannot break the molecular bonds to undergo chemical reactions [33, 38]. These debates claim that endothermic reactions are best performed by providing necessary thermal energy. As long as this energy is supplied either by conventional heating or microwave system which initially contains some type of polar solvents conducting homogenous heat transfer, the reactions can proceed in a desired direction.

On the other hand, Hoz et al. [39] claim about the microwave effect proposing as "microwave irradiation in organic synthesis is a combination of thermal effects, arising from the heating rate, superheating or "hot spots" and the selective absorption of radiation by polar substances". Even, in both cases, temperature is an important parameter and its homogeneity can be maintained better in microwave conditions. Therefore, IR or preferably by fiber optic (FO) sensors should be used to control this parameter [40].

In the synthesis of dendrimers, purification is an important target as much as obtaining high yield and ideal growth. In the purification of higher generations, there are some advanced techniques; such as, liquid phase retention (LPR) [41], and membrane dialysis [42]. Structural heterogeneity of PAMAMs results from undesired side-reactions and trailing generation defects occurring during the synthesis. These structural defects have been described by several groups [43-46]. It was reported that commercially available dendrimers could have low monodispersity [47, 48] and membrane dialysis of PAMAMs improves the uniformity [42].

The choice of core, repeating branches, and terminal functional groups can play an important role on the characteristics of the overall physical and chemical properties of dendrimers [49]. While EDA is the most general core used in PAMAM dendrimer synthesis, there is a great interest seeking for the discovery of the chemical and physical properties of new type of dendrimers, which have new cores different than EDA. DETA is a structural analogue of diethylene glycol. Its chemical properties resemble those for EDA, and it has similar uses [50]. It is a weak base and its aqueous solution is alkaline. This property of DETA make it proper to be used as a core for higher generation PAMAM dendrimer synthesis. On the other hand, polymeric cored dendrimers have become a common field of interest because of their wide range of applications [51, 52]. Jeffamine<sup>®</sup> T-403 is a polymer, which has large and unsymmetrical chains having propylene oxide repeating units. These large repeating units can retard the steric hindrance, but, enhance the reactivity and water solubility. Conventional synthesis and characterization of Jeffamine<sup>®</sup> T-3000 cored water soluble dendritic macromolecules was reported and their antibacterial activity as a novel water soluble dendrimer was explored in a recent study [53]. In addition, as e new trend, it has been recently investigated the comprehensive cytotoxicity evaluation and *in vitro* characterization of Jeffamine<sup>®</sup>-cored PAMAMs on L929 cell lines for oral drug delivery purposes and showed that Jeffamine-cored carboxylic acid-terminated PAMAMs can be a promising option for oral drug delivery of poorly water-soluble drugs [54]. Although both monomeric and polymeric cored dendrimers can be synthesized by conventional divergent approach, there have been little attention paid to the MAS of PAMAMs. In order to increase the yield of amidation reaction and reduce the reaction times and the formation of by products, MAS method could be an alternative to the classical divergent method. This method has been applied to the synthesis of EDA cored first generation PAMAMs [55]. Unfortunately, in that study, the reaction times are long and small amount of dendrimers could have been synthesized. Besides, the amount of reactants and solvents are almost in the same amount with classical divergent method.

PAMAMs are highly branched polydentate chelating agents with their interior amide, tertiary amine and terminal amino groups [16], and possible various surface functional groups such as carboxyl, hydroxyl and so forth [56]. Metal binding properties of PAMAMs with controllable size and structure by modifying the core, repeating units and

surface functional groups make them affinitive for metal ions in aqueous solutions [57]. Proton binding sites of dendrimers which are tertiary and primary amines allow dendrimers to bind many metal simultaneously and show interesting characteristics. By means of these properties, PAMAMs are used as MRI contrasting agents in target drug delivery [58], cancer therapy [59], gene delivery [60] and tumor screening [61]. Given the fact that, not only physical properties of dendrimers like intrinsic viscosity, metal absorption affinity, molecular conformation but also many molecular properties of PAMAMs and surface functionalized derivatives are depend on the molecular charge and useful for many applications, it is important to develop necessary approach to accurately characterize protonation constant ( $pK_a$ ) values of the proton binding sites of both amine terminated and surface functionalized PAMAMs.

Charge of PAMAMs are pH dependent. Maiti et al. [62] reported that decreasing the pH of the solutions of EDA cored PAMAMs from high pH  $\sim 10$  to towards neutral pH  $\sim 7$  and low pH  $\sim 4$  leads successively to no protonation, only primary amine protonation, and tertiary amines protonation. In a recent study, Böhme et al. [63] also used PAMAMs as model system to investigate effective charge for spherical polyelectrolytes and observed from NMR study that all amino groups of generation (G) two PAMAM are unprotonated at pH  $\sim 10.5$ . At pH 7.7 all amino groups are protonated while the tertiary amine groups are unprotonated. This followed by the 55 % of the tertiary amine protonation at pH 5.5 and finally all amino groups are protonated at pH  $\sim 3$ . Likewise, the protonation behavior of polypropylene imine (PPI) dendrimers with amine terminal groups in aqueous solutions have also displayed the same manner [64].

The stability constants for the formation of a single isomer is called a micro-constant. Microscopic charging mechanism of PPIs and PAMAMs are not clear yet and there have been an improving interest and discussions in the literature [64-70]. The result of these studies is that PPIs protonate in two steps with an intermediate plateau at a degree of protonation of  $2/3$ . First protonation step, at around pH 10, involves the protonation of primary amine groups and the odd shells of tertiary amine groups. Second step is around pH 5, and involves the protonation of even shells consisting the tertiary amine groups. Others claim that primary and tertiary amine groups of PPIs protonates almost independently [67]. On the other hand, some others assert that protonation mechanism of the PPIs and PAMAMs should be similar [71]. Cakara et al. [65] have shown that the

protonation mechanism of PAMAMs is very different from the PPIs. This difference was explained by firstly with the distance between the amine groups which is smaller in PPI dendrimers and secondly the onion like protonation structure of PPI dendrimers. That is, in the first step of the protonation not only primary amines protonates but also tertiary amines residing in odd shells protonate. It has been also shown in the same study and supported recently by the study of Pande et. al. [72] by examining the microscopic protonation mechanism of PAMAMs that the primary amine groups at the periphery protonates at high pH, while the tertiary amine groups in the central core protonate only at lower  $\text{pH} < 2$ .

Polydentate chelating abilities of PAMAMs have been generated a common interest to evaluate their complexation abilities in aqueous solutions, especially with Cu (II) ions. The tertiary and primary amine groups of large PAMAMs are Lewis bases that they can bind many metal ions simultaneously. However, the amine groups do not always bind to metal ions because of the pH characteristic of the media. When the extend of protonation (EOP) of amine groups is out of the pH range of metal binding or all amine groups are protonated, they are not available for metal ion coordination [56]. LPR technique has been shown as efficient method [41, 73] for the determination of metal ion-polymer complexes with AAS.

Diallo et al. [74] have measured the extend of binding (EOB) of Cu (II) ions in aqueous solutions of G3-G8 PAMAMs by combining ultrafiltration (UF) technique with AAS. It has been shown clearly as a result of this study that dendrimers exhibit distinctive advantage over traditional chelating agents and macrocycles. This is accomplished by the increasing binding ability of nitrogen ligands on conformationally flexible PAMAM dendrons with covalent attachment. In this way, it was reported that PAMAMs can serve as high capacity nanoscale containers for toxic metal ions like Cu (II).

Uptake of metal ions by dendrimers like PAMAM has still needed to be well understood in terms of effect of dendrimer core chemistry, terminal group chemistry, metal ion binding capacity, selectivity and structure and structure with any metal ions complexes [56, 74]. This was tried to be accomplished by investigating the protonation mechanism of dendrimers in aqueous solutions [67, 68, 75].

Koper et al. [68] characterized the protonation of diamino butane (DAB) cored PPIs in aqueous solutions with potentiometric titrations and Ising-like site binding model of

protonation. They have proposed that when these dendrimers titrated with excess acid 2/3 of intermediate plateau of dendrimers protonates in two consecutive steps. In the first step, terminal amine groups and odd number of tertiary amine shells protonate together at pH 10 and this is followed by the even shells of tertiary amine shells at pH 5.

Kabanov et al. [64] conducted potentiometric titrations to estimate the protonation behavior of DAB cored PPIs with terminal amine groups in aqueous solutions by applying Henderson-Hasselbach equation. In this way, they estimated the pKa values of surface amine groups and tertiary amine groups as equal to 9.80 and 6.00, respectively.

Cakara et al. [65] investigated the protonation behavior of generation 0 to 6 PAMAMs by potentiometric (acid-base) titrations and analyzed the resulting titration curves with site binding model. They used the limited number of interaction parameters involving the nearest neighbor pair interaction to explain microscopic ionization constants. Regardless of higher generations, these parameters were calculated from lower generation 0 and 1 and generalized for the explanation of the degree of protonation of higher generation PAMAMs. Results of this study [65] revealed that the protonation of PAMAMs involves first the protonation of periphery amine groups at high pH, this is followed by the tertiary amine groups as the pH decreased while central tertiary amines could be protonated at low pH.

Niu et al. [76] used Frumkin adsorption isotherm and multishell structural model together to enlighten the protonation mechanism of four generation hydroxyl and amine terminated PAMAMs in aqueous solutions. During analysis, they used two binding parameters. These are intrinsic binding constant and a constant characterizing the strength of possible electrostatic interactions among proton binding sites. They could calculate overall intrinsic protonation constant value of pKa 6.30 and 9.23 for hydroxyl and amine terminated PAMAMs. On the other hand, Diallo et al [56] calculated primary amine pKa values as 9.90, while tertiary amine pKa values as 6.52, 6.85 and 7.16 for amine terminated G3, 4 and 5 PAMAMs, respectively. The method they used was the fitting each titration with sigmoid function by Mathematica software to find the inflection point of each titration curve. The primary amine pKa values found by Diallo et al. [56] shift 1-1.5 pKa units from Cakara et al. [65] and Niu et al. [76]. Diallo et al. [56] questioned about the significance of this difference by asserting that “Although these investigators have employed theoretically derived protonation models to analyze their titration data,

independent experimental measurements and/or atomistic simulations have not validated their models". Diallo et al. [56] calculated the extend of protonation of PAMAMs with different surface functionality by using the Henderson- Hasselbach equation which uses an effective  $p\tilde{K}_a^i$  that takes into electrostatic repusions between the protonated nearest neighbor sites  $i$  and  $j$  [65], [68], [75]. In the end of their acid base titrations, they observed that EOP values they found were in good agreement with those of Cakara et al. [65] and Niu et al. [76]. Finally, they indicated that tertiary and terminal groups of EDA cored PAMAMs protonate independently, surface functionality and dendrimer generation did not have a significant effect on EOP of tertiary amine groups of EDA cored PAMAMs.

Cakara and Barkovec [77] conducted comparative study on the protonation mechanism of PAMAM and PPI dendrimers. They defined EDA cored PAMAMs with a core with short core chain with two carbon atoms and long amido –amine arms. On the other hand, they defined PPI dendrimers with core chain with long four carbon atom and with shorter-arms. They also interpreted the potentiometric titration of PAMAMs and PPIs by site binding model which involves a limited number of parameters to get an insight into both macroscopic and microscopic protonation mechanisms. The result of their study revealed that PAMAMs and PPIs exhibit different protonation behaviors due to pH of the aqueous media. While PAMAMs show a protonation mechanism of core shell structure, PPI dendrimers show onion like structure.

Many physical properties like intrinsic viscosity, molecular confirmation, adsorption and absorption affinity and many others of dendrimer are dependent on the protonation state molecular charge. These properties are important as dendrimers used in a wide range of applications as above before mentioned. Protonation mechanism of dendrimers can show differences according to their structures (e.g: PAMAM or PPI). There have been some attempts to determine proton binding constants and explain protonation behavior of dendrimers by potentiometric titrations combined with some mathematical models [65, 69, 76, 78], nuclear magnetic resonance (NMR) [68]. However, a little attention has been paid to spectroscopic titration to explain protonation mechanism of dendrimers [79]. In comparison, even if NMR data give microscopic information on the protonation behavior, it requires costly experiments with limited accuracy when compared to potentiometric titrations [68], [77]. Furthermore, it was presented that microscopic titrations can be obtained from potentiometric titration data by using site binding model and this model

can be applied to dilute solutions on the contrary to NMR studies to get more accurate data [65]. On the other hand, spectroscopic titrations and measurements could be useful in equilibrium studies as they give access the regions of equilibrium not otherwise attainable [80], allow the investigation of polyfunctional acids while potentiometric methods without model application can only estimate macro-constants [81], help to understand complexation model, make possible to calculate spectra of the various absorbing species at the equilibrium and so make possible to get insight on the chemical behavior of the studied system [82].

Equilibrium of solutions have long been studied with spectrophotometric methods and great number of approaches were developed to obtain information about equilibria. These methods mostly were based on the single wavelength measurement or graphical or numerical methods for calculating the equilibrium constants [82]. Development of technology in recent decades had led to easy access to computer facilities. These facilities were maintained to manage rapid calculation and data acquisition. Thus, chemometric approaches or chemometric data handling have come to focal point to extract information from a large number of experimental data, especially for spectral data involving not only a single wavelength but also full range of required wavelength [82]. A large number of computer programs have been published in order to explain equilibrium of solutions, species distributions and equilibrium constants predominantly from potentiometric, spectroscopic and NMR data [83]. Some of them are BEST [84], HYPERQUAD [85], HYPERNMR [86], MINQUAD [87], SPECFIT [88], SUPERQUAD [89] and TITFIT [90] while the most recent ones are Reactlab EQUILIBRIA [91] (potentiometric and spectroscopic data), HYPERQUAD2008 [83] (potentiometric data), HypNMR (NMR data) [83], HypSPEC (Spectroscopic data) [83].

Tauler and Casassas [92] were applied principal component analysis (PCA) to determine rank of the data matrix-the number of absorbing complex species from spectral data. By means of this method, they determine the chemical model without using or concerning any assumption for law of mass action or mass balance restrictions, and using any stoichiometric coefficients or formation constant of formed species. Simultaneous determination of the number of species present in a solution could be determined with several methods. One of the first determined of these methods is matrix triangularization (Gauss elimination method) is based on the determination of the rank of Data matrix

D(NSOLN, N WAVE), which is built from the spectral data of number of solutions and waves where absorbance readings recorded [93, 94]. The main drawbacks of this method were indicated as accurate estimation of errors, uncertainties when its applied to low concentrations [92]. More robust method was applied by Malinowski [95, 96]. This method is based on the application of error analysis to PCA. The main aim of the method is to obtain significant number of actual factors. The distinction with the significant eigenvalues and experimental error was defined by the use of some functions which are standard deviation of residual error, real error (RE), extracted error (XE) and imbedded error (IE) and the indicator function (Ind). On the other hand, Cartwright [97] was applied factor analysis (FA-submatrix analysis) of titration data as a function of pH to the different protonation species of phosphate when the pH increased and plotted the logarithm of eigenvalues versus pH to observe the actual and error functions at each titration point. Alternatively, evolving factor analysis (EFA) was used to visualize important factors in the same direction with experiment and reverse direction. To do so, appearance and disappearance of absorbing species can be visualized on the pH domain [98]. Application of the both the submatrix analysis and EFA were proposed as soundness of the proposed chemical model (stability constants and set of species) [92].

PCA, FA and EFA were applied to investigation of the multi-equilibria systems to get information about the number of absorbing species in a solution simultaneously [92]. SPFA (spectra factor analysis) procedure [92, 99, 100] was applied to spectrophotometric titrations and has been broadened to study macromolecular ligands, which have a field of great interest because of their biological and environmental importance [101]. SPFA is a method that can be used without having an initial model assumption (model free-hypothesis free) or applying a law of mass action. In this way, spectroscopic titration can be used for the analysis of macromolecular species in aqueous solutions with chemometric methods and come to robust methods. Casassas et al. [101] were investigated the interactions of  $H^+$  and Cu (II) ions with poly (adenylic acid) (poly A) using FA technique. They detected four spectroscopically different species for poly A. Three of them are the protonated form of Poly A and one for the unprotonated form of Poly A. In this way, they also detected the formation of a new species in the presence of Cu (II) ions by the increase in factor number one. They also proposed this method as the

model free and self-resolving tool for the interaction of metal ions with macromolecular systems.

LPR is also described as polymer assisted ultrafiltration (PAUF), polymer supported ultrafiltration (PSU) polyelectrolyte-enhanced ultrafiltration (PEUF) or polymer filtration (PF) technique [41] allows the binding of metal ions and ultrafiltration at the same time. Since the molecular weight cut-off (MWCO)-pore size of membranes used in ultrafiltration are not proper to separate heavy metal ions, chelating agents are used to form macromolecular complexes by binding metals. These complexes having appropriate molecular weight than will be retained during LPR process. By using LPR or PAUF method, it could be possible to selective separation and recovery of heavy metals [56, 78, 102].

Many kind of polymers can be used in LPR. A long list of water soluble polymers that can be used for LPR can be accessible from Rivas et al.'s literature review [103]. The most popular one of the polymers used in LPR is polyacrylic acid and it was used in binding studies of various metal ions; such as, Cu(II) [104], Cd(II), Pb(II) [105], Zn(II), Ni(II) [106]. Polyethylene imine (PEI) is another influential polymer in recovering Cu(II) [107], Hg(II), Cd(II) [108], Ni(II) [109], Zn(II) [110], Cr(III), Cr(IV) [111], Co(II) [112-114]. Polymer to be used in LPR can be assessed by using many parameters but the most important parameter is the ligand density of the polymer. Low ligand density of the polymer to be used requires high volume of polymer and this could increase the viscosity of the solution that can lead to deteriorating effect on the permeate reflux [115]. PAMAMs are the first dendrimer family to synthesized, characterized and commercialized [15]. High density of nitrogen ligands they carry allow them behave like a container or template for the toxic and heavy metals, which are the main contaminants of the surface water, ground water and coastal water systems that lead to water contamination throughout the world [116]. LPR is an efficient method to recover metal ions from contaminant waters [108, 117-121]. Increasing pH of the solution could be a powerful tool to increase loading capacity of dendrimer. On the contrary, decreasing solution pH make possible the regeneration of heavy metals and recycling usage of dendritic templates. Diallo et al. [122] showed the feasibility of dendrimer enhanced ultrafiltration (DEUF) to recover Cu (II) ions from aqueous solutions by using PAMAMs. In their study, they combined UF with PAUF and developed DEUF [123]. They indicated

that dendrimer-Cu (II) complexes could be effectively separated from aqueous solutions by DEUF and removed Cu (II) ions could easily be regenerated by just decreasing the solution pH 4. In this way, they used DEUF for a cyclic process to removal and regeneration of metal ions from aqueous solutions and they proposed this system for the effective waste water treatment [122].

Jawor and Hoek [124] used nanoparticle-enhanced ultrafiltration to evaluate removal of cadmium ions from water by different type of nanoparticles one of which is carboxyl functionalized PAMAMs. Results of this study revealed that poly (acrylic acid) had the highest binding capacity (180mg/g) and this is followed by PAMAMs (169 mg/g) and zeolite LTA nanoparticles (87 mg/g), respectively.

Rether and Schuster [125] showed that all metal ions can be retained almost quantitatively at pH 9 in recovery of Co(II), Cu(II), Ni(II), Pb(II) and Zn(II) using PSU. In this study, Cu(II) formed the most stable complexes with benzoylthiourea modified PAMAM derivatives. Regeneration of metal ions was accomplished by decreasing solution pH 4.

Dendrimers are used as templates to control size, stability and solubility of nanoparticles in the range of 1nm to up to 4-5 nm [126]. Crooks et al. [126] announced dendrimers as good hosting metal nanoparticles because of their uniform structure that leads to well defined nanoparticles, availability to participate in catalytic reactions, resistance to agglomeration, selectivity to control encapsulation of small substrate molecules, and their surface functionality. Dendrimer encapsulated metal nanoparticles (DEMNs) have gained great interest for use in catalysis [127, 128], optoelectronics [129], and applications areas of semiconductors, noble metals, magnetic dendrimer nanocomposites, environmental cleanup and catalyst [130]. First dendrimer encapsulated nanoparticles (DENs) was reported by Crooks et al. [131] and this was followed parallel by Tomalia [130]. Different types of Pt, Pd, Au, Ag, Cu, Ni, Ru, Mn, and Fe, DEMNs were prepared in the literature [66, 126, 132-135]. Maximum number of metal ions that can be introduced into dendrimer can be calculated by spectroscopic titrations. It was demonstrated by the complexation of Cu<sup>2+</sup> ions interior to PAMAM dendrimer that a strong ligand to metal charge transfer (LMCT) band at 300 nm and 210 nm shift with d-d transition signal [131].

Most common procedure for the synthesis of DENs involves first the complexation of appropriate number of metal ion ratio to be complexed with dendrimer solution under pH

control and then this is followed by an appropriate reducing agent [131]. Appropriate chemical excess of sodium borohydride ( $\text{NaBH}_4$ ) is used as the reducing agent and leads to zerovalent intradendrimer metal nanoparticles. Immediate change of color indicates the reduction. In the case of Cu, LMCT peak at around 300 nm arising from Cu-DENs are replaced with a monotonically increasing absorbance toward shorter wavelength. This indicates the formation of small nanoparticles. Also, an absence of plasmon peak at around 570-590 nm proves that Cu clusters are smaller than 4nm [136, 137]. Transition d-d complex band resulting from the coordination of internal amine groups of ethanol amine terminated PAMAMs were reported at  $\lambda_{\text{max}}$  at 605 nm [131]. This band reported in the range of 600-800 nm depending on surface modification with tris (hydroxymethyl) aminomethane (Tris) [138].

Solubility of dendrimers is greatly influenced by the nature of surface groups of dendrimers. Dendrimers terminated with hydrophobic end groups are soluble in non-polar solvents, while dendrimers having hydrophilic groups are soluble in polar solvents. Furthermore; dendrimers' unique globular shape and the presence of their internal cavities give them the possibility of encapsulating guest molecules in the macromolecular interior. Because of these reasons, there are attempts to use dendrimers in targeted delivery of drugs and other therapeutic agents [139]. Drug molecules can be loaded to the interior and attached the surface groups of dendrimers. Water soluble dendrimers can bind small acidic hydrophobic molecules having antifungal and antibacterial properties. Therefore, bound substrates can be released when they delivered to the target organism while contacting. Such complexes of dendrimers with drugs can be considered as drug delivery systems [140, 141].

Structural properties of PAMAMs with high density of amino groups make them attractive for solubility enhancement applications of drugs with low solubility in aqueous media. Bioactive materials can be delivered by PAMAMs by increasing their solubility and low bioavailability [142]. Inner cavities and inner and surface functionality of PAMAMs are responsible for increased solubility and so they are suitable for drug delivery systems [142]. Designing terminal functional groups of dendrimers gains them to be used as the hydrophilic efficient drug carries, especially for small hydrophobic acidic drugs so that they can be used in many pharmaceutical studies [143, 144]. Encapsulation efficiency of dendrimers increases especially by the increasing generation,

which attributes to dendrimer trapping the drugs by electrostatic, hydrophobic, and hydrogen bond interactions. Nevertheless, the purity of the higher generations are mostly depended on removal of the smaller generations. During higher generation dendrimer synthesis, small traces of unpurified lower generations grow as the dendrimer grows [42]. Water soluble PAMAMs can be host for guest-small hydrophobic acidic molecules by forming inclusion complexes. In the case of inclusion complex, there is no covalent bonding between the host and guest, molecular attractions are generally due to van der Waals forces. Protonation mechanism of PAMAMs can give them to increase steric hindrance with the protonation of surface or inner functional groups, especial for the amine terminated PAMAMs. That is small hydrophobic nonpolar drugs can be trapped in the cavities of PAMAMs so that they can attain the required solubility in polar media [139]. EDA cored PAMAMs used as the solubility enhancers of many drugs; such as ibuprofen [145], cis platin, resveratrol, genistein, curcumin [146], furosemide [147], ketoprofen [148], and vitamins like nicotinic acid [149] and riboflavin [150]. The results of these studies have shown that PAMAMs could be highly efficient possible drug carrier systems due to their controllable structure with branching units and surface groups, protonation mechanisms to behave like a cage, increasing number of ligand units (amino groups) with increasing generation numbers.

Dendrimers are considered as a new class of macromolecules. They differ from many other linear and hyper branched polymers with their monodisperse, highly branched starburst structures [21]. In general, low generation dendrimers have an open structure and they become densely packed and globular in shape as their generation increases. Higher generation of dendrimers are similar in size to many biological structures and they have the ability of mimic proteins [1]. Designing terminal functional groups of dendrimers gains them to be used as the hydrophilic efficient drug carries, especially for small hydrophobic acidic drugs so that they can be used in many pharmaceutical studies [143, 144]. Encapsulation efficiency of dendrimers increases especially by the increasing generation, which attributes to dendrimer trapping the drugs by electrostatic, hydrophobic, and hydrogen bond interactions. Nevertheless, the purity of the higher generations are mostly depended on removal of the smaller generations. During higher generation dendrimer synthesis, small traces of unpurified lower generations grow as the dendrimer grows [42].

The synthesis of higher generation PAMAMs requires quantitative consumptions of the reactants, long time preparations for producing successive generations, and prolonged time consuming and tedious purification steps. Whatever the purity of synthesized crude dendrimer product is, control of the growth of evolving unpurified lower generations could be detected by some instrumental methods like high performance liquid chromatography [151], mass spectroscopy [43] and capillary electrophoresis [152]. However, the instrumental methods could be expensive and often could not be very suitable for routine laboratory analysis. Furthermore, these methods may require long time of sample preparation or pretreatments depending on the sample matrix. Even if the purity of dendrimers can be increased by intensive purification methods like LPR technique [41], a little attention has paid to purity assessment of the dendrimer mixtures by chemometric methods. There are several key factors why the chemist can be more productive if he/she comprehends the fundamental of design. Some of the mains of these key factors are screening, optimization, time efficiency and quantitative modelling. In quantitative modelling, almost in all experiments, a series of simple linear calibration to complex physical processes including a serious observations required to obtain a mathematical model of the system. Multivariate chemometric methods [153-155]; such as, multivariate linear regression (MLR), principal component regression (PCR), and partial least squares (PLS) help to analyze analytical information from full spectra. Moreover, multivariate chemometric techniques have been widely used in the simultaneous qualification and quantification of mixtures in many studies [156-159] and could be an alternative to purity assessment of dendrimers.

## **1.2 Objective of the Thesis**

The studies reported in this dissertation can be divided into two areas. The first involves the MAS method development, synthesis and characterization of higher generation amine, tris, and carboxyl terminated PAMAMs and Cu-DEN metal nanoparticles. The second part concerns the application of dendrimers to the field of investigation of the protonation mechanism of PAMAMs with potentiometric titrations, spectroscopic titrations via the aid of chemometric methods, analysis of metal binding abilities on the removal of metal ions from aqueous solutions, solubility enhancement, and method development for the purity assessment of binary mixtures of PAMAMs with multivariate calibration models.

## **1.3 Hypothesis**

MAS technique to be developed for the amidation step of PAMAM dendrimer synthesis can allow dendrimers to be synthesized in massive amounts in industrial scales. PAMAMs to be synthesized novel type of synthesized water soluble tris and carboxyl surface modified DETA, and Jeffamine<sup>®</sup> T-403 cored could be used in a wide range of field involving, drug delivery systems, electrode cladding material for the detection of trace amount of molecules in urine or blood as sensors, MRI contrasting agents, waste water treatment and many others

In addition, new aspect of view to enlighten protonation mechanism of dendrimers with the integrated use of chemometric techniques; like SPFA, EFA and error analysis with RMSECV can gain better understanding to the researches, who pay extra attention to preliminary characteristic protonation behavior of PAMAMs without using any chemical model or law of mass action. Methods to be developed in this dissertation could be extended for the evaluation other types of dendritic structures in future studies.

### GENERAL INFORMATION

#### 2.1 Introduction: Dendrimer Types and History

Dendritic structures are widely used by nature and human body. Their hyperbranched structures can give them to take special role or advantage in a desired particular function. For example, extraordinary strong adhesion between Geckos foot hair and surface due to multiple Van der Waals forces was attributed to dendritic network of foot hairs of Geckos [160]. Connections between brain cells (Neurons) have maintained by dendritic structures. Likewise, branched structure of dextran, amylopectin and glycogen are formed from the condensation of alcohol groups' reaction with aldehyde groups. Thus, these branched polysaccharides can be used quickly when needed [161, 162].

In Chemistry, the idea of repetitive growth with branching was first emerged in 1978 by Vögtle [163]. Increasing interest in last decades lead dendrimer chemistry to be one of the most popular areas of the current chemistry. In the beginning of the first decades, these architectures were susceptibly avoided to accept as even polymer. Today, many of the predictions of those decades have turned into experimental reality and answered by thousands of paper. Presently, dendrimers are considered as the fourth major class of polymer architecture consisting the subset of linear, cross linked, branched polymers and dendrimers (Figure 2.1) [15]. The word dendrimer is derived from Greek words dendron (tree) and meros (part), and refers to structurally-perfect branched macromolecules. Other common names for dendrimers are known as 'cascade polymers' or 'arboroles'. First paper describing the detailed macromolecular synthesis of true dendrimers was accomplished by Tomalia group [164]. This was followed by Newkome et al. [22]. However, the real interest toward these molecules began and started to be appreciated at

1990s [44]. Afterwards, the number of publications has increased considerably [165]. Wide spread application fields of dendrimer have been attributed to their unique structures [166].

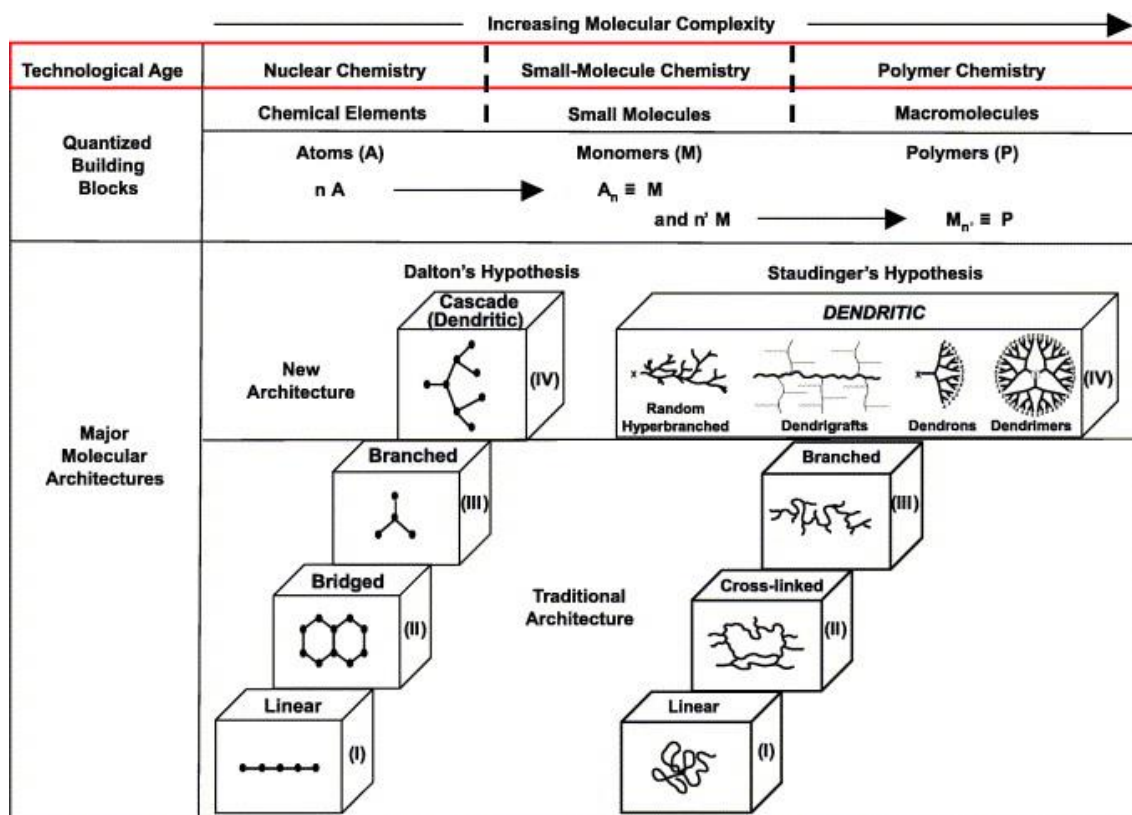


Figure 2.1 A comparison of complexity as a function of molecular architecture, strategy, quantized building blocks, and technological age [167]

When compared with the traditional polymers, despite their large molecular sizes, dendrimers have high monodispersity, high density of functional groups generally on the periphery, small volume compared to linear polymers depended on their semi or globular shape.

Dendrimers are coded with generation numbers depending on their size. Generation numbers are determined by the number of layers between each focal points (cascade points) of dendritic structures (Figure 2.2). There have been confusions on the definite numbering of generations [168]. Generation zero (G<sub>0</sub>) represents sometimes the core and has no focal points. PPIs and PAMAMs are the most common and commercially available dendrimers (Figure 2.2). The core of PPI dendrimers is diamino butane (DAB). In the case of PAMAM dendrimer (Starbust™), EDA core and ammonia core are the most widely used cores and hydrogen substituents to these cores are known as the focal points.

Apart from the PPI dendrimers, intermediates of PAMAMs with carboxylate surface groups called as the half generations and denoted with generations numbers; such as, G1.5 or G2.5. Polyamine linkages and a mix of poly amides and amines made possible to design of PPI [17] and PAMAM [164] dendrimers and there have been growing increase in the design of different type of dendrimer designs based on different subunits; such as poly(aryl ether)[169], carbohydrate [170], calixarene core [171], silicon or phosphorus [172].

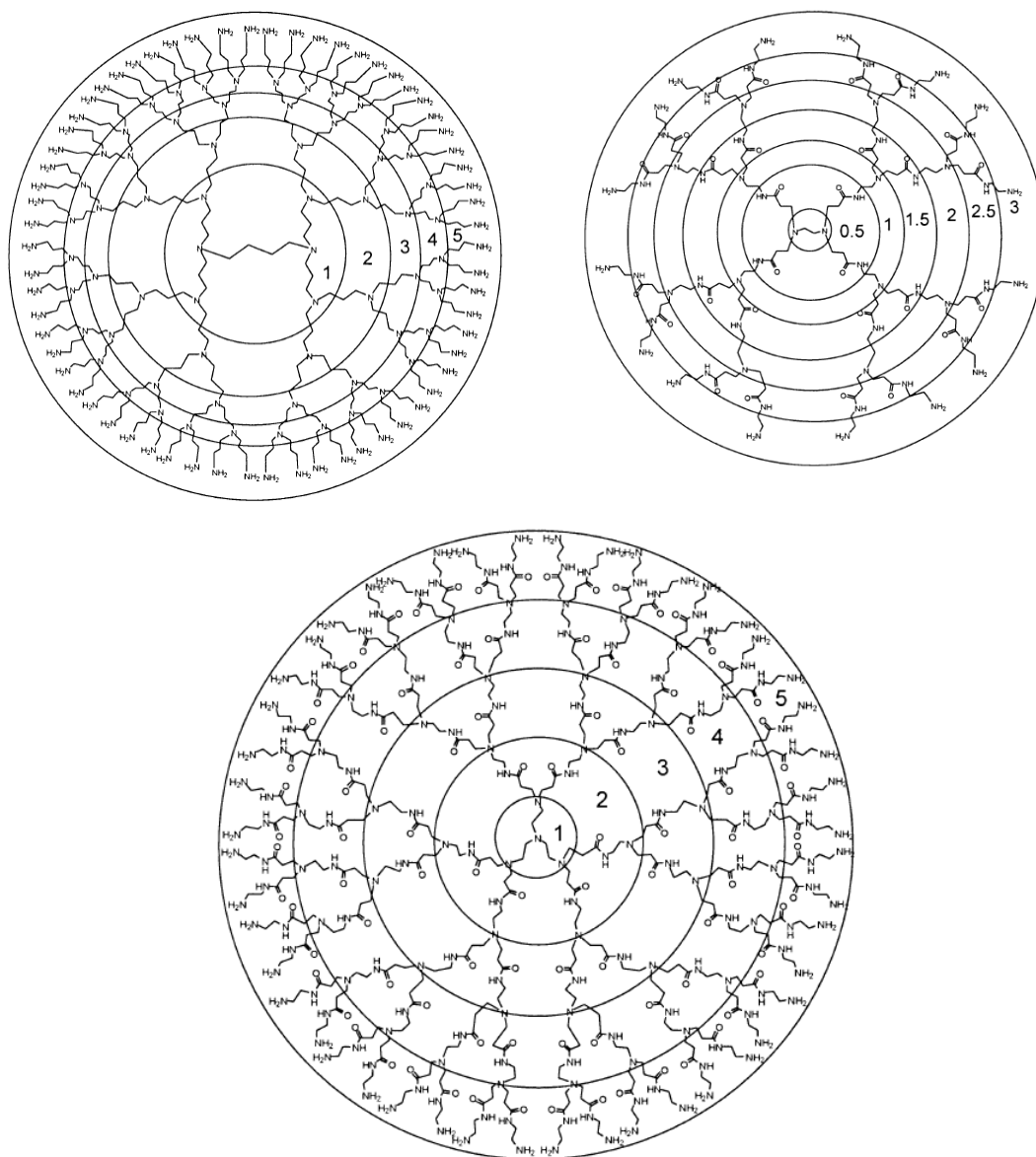


Figure 2.2 Common commercially available dendrimers. Top left: PPI (G5). Top right: PAMAM (G3). Bottom: PAMAM (G5). Each generation is marked with a circle [3]

## 2.2 Chemical Synthesis of Dendrimers

One of the hyperbranched polymer types are dendrimers that they have unique core shell structures with three basic architectural components, namely which are core, repetitive branching units (interior of dendrimer) and terminal functional groups (periphery or outer shell) [173, 174]. Unlike traditional polymers, synthesized by step polymerization or chain polymerization, dendrimers are synthesized either by “divergent” or “convergent” synthesis strategies.

### 2.2.1 Divergent Synthesis

Dendrimers firstly were announced by Vögtle with divergent methodology approach [17]. This method requires the combination of acrylonitrile and reduction chemistry. Molecules reported in that study had small molecular weights (<900 Daltons G=0-2). Vögtle later on declared that higher generation cascade molecules could not be obtained by this method due to synthetic and analytical difficulties [175]. In 1985, Tomalia [164] reported divergent methodology successfully by facile combination of Michael addition and amidation chemistry for high generations (>58000 Daltons G=0-7). Divergent method is an “outside in” method. In this method, starting from a core, dendrimers are built layer by layer. Each layer growth is mentioned as the generation growths. First generation dendrimer is obtained by attaching a branched unit to a core. To synthesize the further generations, periphery surface groups of former generations are reacted with branching building blocks as illustrated in Figure 2.3. This process is repeated until required generation is obtained. In this synthesis method, as the generation increases, the surface functionality also increases. This leads exponential reactions to be performed and this is difficult for even highly efficient reactions. Separation of the byproducts and trailing generations are usually difficult for divergent method as their size, mass and other properties are very close to perfect dendrimer especially in higher generation synthesis [176]. Thus, Hawker and Frechet [177] developed convergent approach.

### 2.2.2 Convergent Synthesis

Convergent synthesis was developed by Hawker and Frechet [177] and followed by Miller and Neenan [178]. Convergent method is an “inside out” method. In this method, firstly dendrons from the small molecules at the surface of the dendrimer sphere are

synthesized and eventually attached to core. In this way, reactions proceed from outside to inward building (Figure 2.3). Unlike the divergent method, small number of possible side reactions emerge in convergent method. Small number of possible side reactions emerge and so purification in each step is easier. Monodispersity of the final generation is expected to be higher compared to divergent synthesis. However, dendrimers synthesized by convergent methods are less than divergent methods due to steric hindrance along the core.

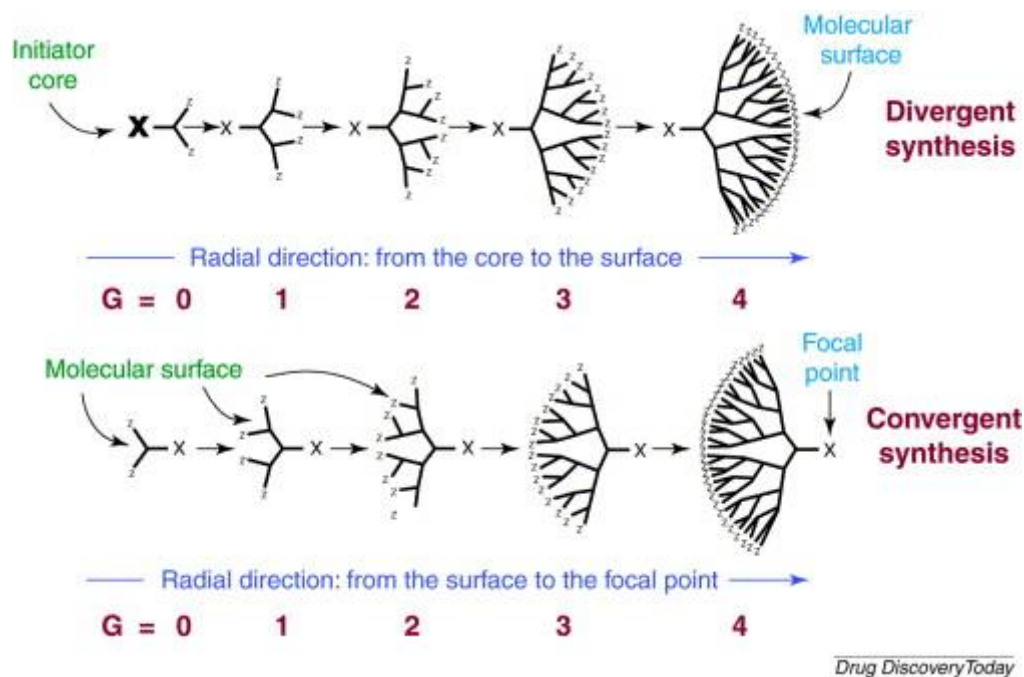


Figure 2.3 Schematically depicted dendrimer synthesis. Top: Divergent strategy. Bottom: Convergent strategy [1]

### 2.3 Properties of Dendrimers

Unlike linear polymers, dendrimers are monodisperse macromolecules. Dendrimers and units of dendrimers, dendrons are highly symmetric and spherical compounds. In nature, classical linear polymerization is seldom. Dendrimers are architectural molecules so that they can be specifically controlled during the synthesis. Due to their molecular structures dendrimers can show improved properties when compared to linear traditional polymers. Properties of dendrimers are mostly determined by the surface functional groups, however, internal functionalities of dendrimers can also be dominant [179-181].

Encapsulation ability of dendrimers allow them to isolate active sites by mimicking just like the biomaterials [165, 182]. By designing the surface functional groups of dendrimers

with charged species or hydrophilic groups, water soluble molecules unlike most polymers can be synthesized. Some of the controllable properties of dendrimers are crystallinity, chirality, toxicity and tecto dendrimer formation [183]

Dendrimers are classified by generations, referring the number of repeating focal point (branching unit) and as the generation number increased they take a globular shape and have internal cavities. By this way, they gain the property of encapsulation guest molecules. In solution, linear chains live as flexible coils; in contrast, dendrimers form a tightly packed ball. This has a great impact on the rheological properties of dendrimers. Molecular mass of dendrimers increases with an exponential manner as the generation increases. However, their intrinsic viscosities goes to a maximum at the fourth generation and then starts to fall. Thus, they have significantly lower viscosity than linear polymers [184, 185]. In classical polymers, intrinsic viscosity increases as the molecular mass increases.

Surface groups of dendrimers has an important role on the physical and chemical properties of dendrimers. Presence of many densely end groups are responsible for the high reactivity, solubility and miscibility [185]. Dendrimers with hydrophobic end groups are soluble in nonpolar solvents, while dendrimers terminated with hydrophilic end groups are soluble in polar solvents.

Globular shape of dendrimers with internal cavities give them opportunity to behave like hosts for the guest molecules in the macromolecular interior. Due to branching units and type, dendrimers can behave like dendritic boxes and be host for the large and small guest molecules (Figure 2.4).

In Biomedical applications, there is a growing interest on dendrimers as the biological properties of dendrimers are crucial. Amine terminated PAMAMs or PPIs are cationic at low pH values and cause hemolysis and so that they are generally cytotoxic. Increasing generation number is deterministic on the toxicity, which increases with number of surface groups [186]. On the contrary, anionic dendrimers with carboxylate surface are not cytotoxic in wide concentration ranges [187]. Jevprasesphant et al. [188] showed in their comparative study on cationic and anionic terminated PAMAMs using Caco-2 cells that amino terminated PAMAMs have a significantly higher cytotoxicity compared to anionic carboxyl functionalized PAMAMs.

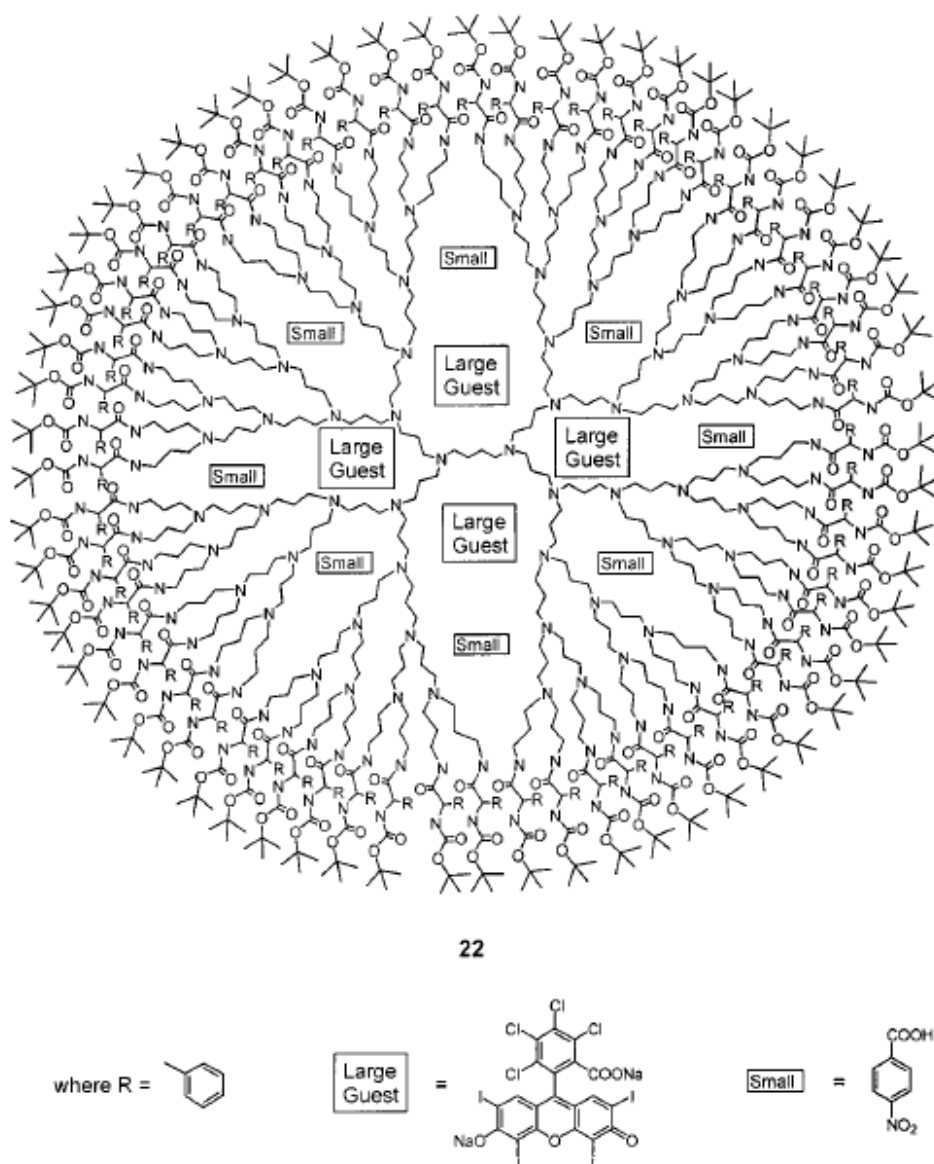


Figure 2.4 The ‘dendritic box’ [189]

## 2.4 Applications of Dendrimers

### 2.4.1 Dendritic sensors

Balzani et al. [190] observed that integrated  $\text{Co}^{2+}$  ions into PPI dendrimer with 32 dansly units on the periphery gives a fluorescent response to very low concentrations of  $\text{Co}^{2+}$  (Figure 2.5). As PPI dendrimer have 30 interior aliphatic amine units, it can make proper coordination with metal ions. When  $\text{Co}^{2+}$  ions integrated into dendrimer, strong fluorescence of the periphery groups are annihilated. In this way, they used low

concentration of dendrimer ( $4.6 \times 10^{-6}$  M) as a sensor for the detection of  $\text{Co}^{2+}$  ions as low as  $4.6 \times 10^{-7}$  M.

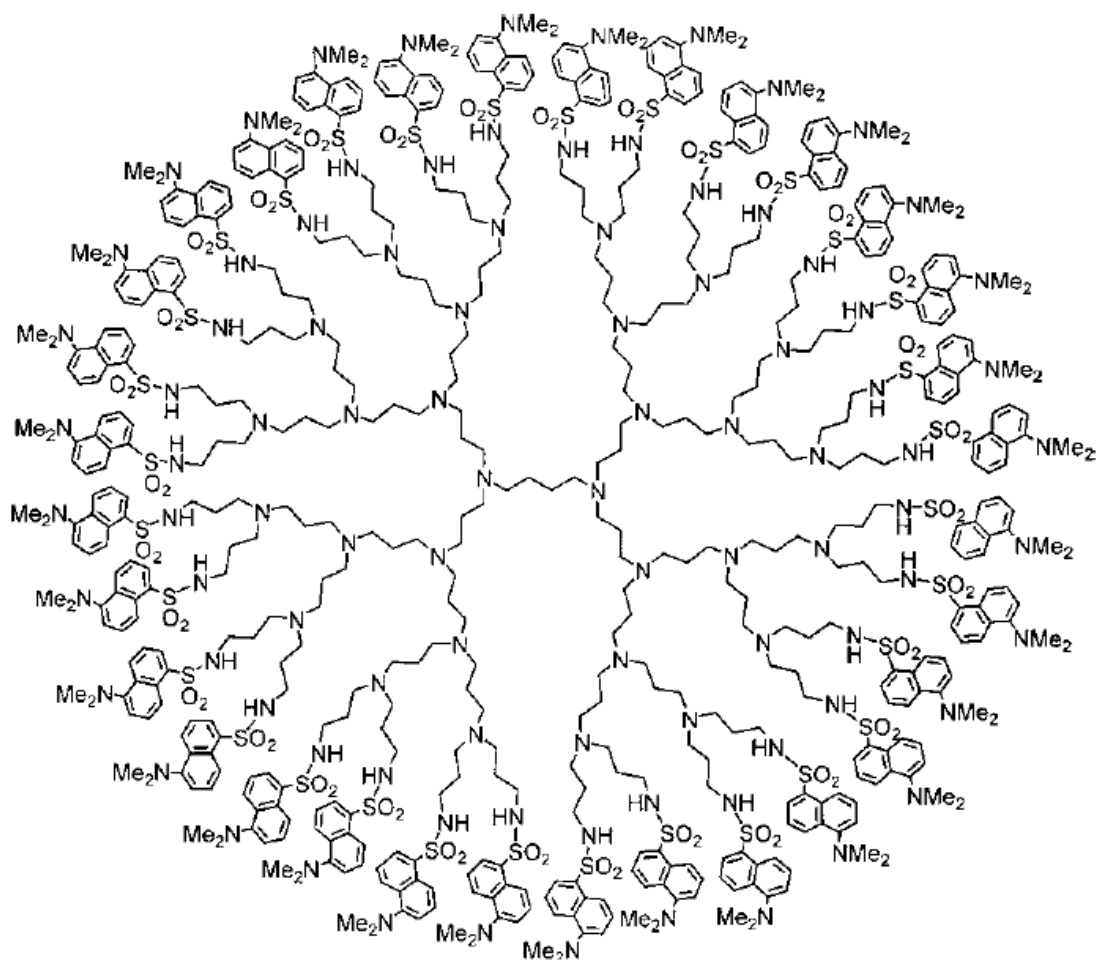


Figure 2.5 PPI dendrimer, containing 32 units at the terminal: fluorescent sensor for the detection of  $\text{Co}^{2+}$  ions [189]

Valerio et al. [191] used ferrocene dendrimers as supramolecular redox sensors for the recognition of small inorganic anions. Redox potential of the ferrocene attached at the periphery of the dendrimer changes in the presence of inorganic anions. They have observed that the ability of dendrimers to sense anions increases as the generation increases.

Dendrimers not only have used as sensors for the detection of inorganic anions but also could be used for the detection of organic molecules. Binding of saccharide molecules were reported by the dendritic sensor with eight boronic acids and eight anthracene groups

(Figure 2.6). Sensing was accomplished by the changes in the fluorescence of anthracene units [192].

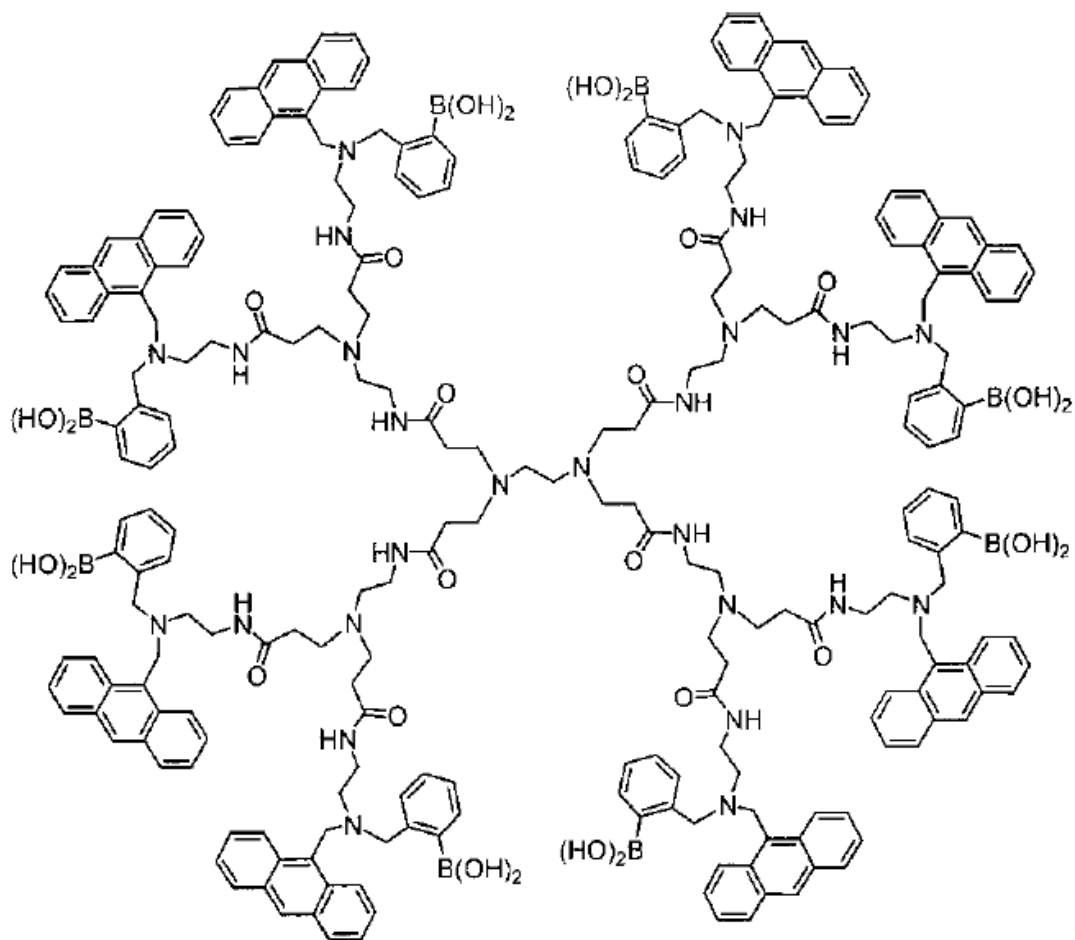


Figure 2.6 PAMAM-based dendritic sensor [192]

#### 2.4.2 Dendrimers as Magnetic Resonance Imaging (MRI) Contrast in Medical Applications

Dendrimers are commercially available polymers and they can be used in wide range of applications including medicine. The most important one of these applications is improved magnetic resonance imaging (MRI) as a powerful medical diagnostic tool. MRI requires the use of contrast agents to observe clearest images especially for soft tissues. Relaxation of hydrogen nuclei in water molecule often accelerated by Gd [193].

After injection to blood vessel, low molecular weight Gd chelates could not be stay in blood vessels for a very long time after injection. So that, they can be used for a short period of time for the imaging of cardiovascular system. Dendritic structures can bind Gd

chelates from their surface. Thus, with the use of high molecular mass dendrimer, proton relaxation times can be accelerated and extended lifetimes can be obtained with the use of lower doses to take quality images [194, 195].

### 2.4.3 Dendrimers-Encapsulated Metal Nanoparticles (DEMNs): Application to Catalysis

Dendrimers are controllably synthesized structures and they can be potentially used as homogenous and heterogeneous catalysis [196] due to their designing property on the size, structure and location of the catalytically active sites [196]. Metallo-dendrimers have been reported as catalyst for a wide range of reactions; such as, Heck reaction [197], hydrogenations [198], oxidation [199], Suzuki coupling [200].

Dendrimers are fairly uniform and yield well defined nanoparticles. Under proper conditions, metal ions can be incorporated into dendrimer inside where tertiary amines are potential chelates. Resulting dendrimer/metal ions are reduced by a reducing agent  $\text{NaBH}_4$  to obtain zerovalent almost monodisperse DEMNs (Figure 2.7)

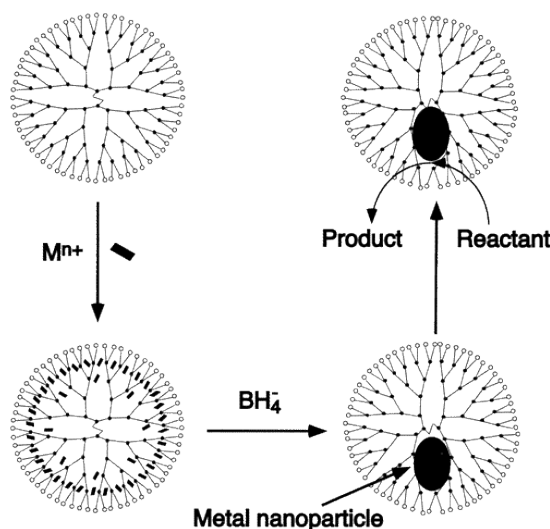


Figure 2.7 Synthesis of DEMNs [126]

#### 2.4.3.1 Intradendrimer Complexes of PAMAMs with $\text{Cu}^{2+}$

First studies on the DEMNs were focused on intradendrimer complexes between PAMAM dendrimer and  $\text{Cu}^{2+}$  as these complexes can be easily characterized by color changes and interpretable from UV-VIS spectra and EPR spectra. In the absence PAMAMs,  $\text{Cu}^{2+}$  ions in aqueous solutions with hexahydrate show a weak absorption band

centered at 810 nm stemming from d-d transition [131, 201]. In the presence of four hydroxyl (ethanol amine) terminated PAMAM dendrimer,  $\text{Cu}^{2+}$  d-d transition band shifts to 605 nm and 300 nm LMCT peak emerges. This peak remains constant even after dialysis against to pure water for 36 hours. The molar ratio of the metal ions to dendrimers can be determined by the spectroscopic titrations. G4-OH dendrimers can sorb up to 16  $\text{Cu}^{2+}$  ions at  $\text{pH} > 7.5$ . At low  $\text{pH} (<3)$ , no binding is observed [126].

#### 2.4.3.2 Reduction of Dendrimer/Metal-Ion Composites

Reduction of  $\text{Cu}^{2+}$  dendrimer metal composites with  $\text{NaBH}_4$  results in the formation of intradendrimer Cu clusters (Cu-DEN) (Figure 2.7). With the sudden addition of excess  $\text{NaBH}_4$  into Dendrimer/ $\text{Cu}^{2+}$  solutions changes the solution color immediately from blue to golden brown. This color change can be detected by the disappearance of d-d 605 nm and LMCT 300 nm peaks and formation of monotonically increasing spectrum of nearly exponential shape toward shorter wavelengths (Figure 2.8). 590 nm plasman band is the beginning signal of the transformation of the Cu clusters. Nearly exponential UV band appearance of the formed Cu clusters is a characteristic of a bandlike electronic structure indicating that reduced Cu atoms exist as a cluster rather than isolated atoms [202]. The absence of Mie plasmon absorption band around 570 nm indicates that Cu clusters are smaller than 4nm [126, 136, 137].

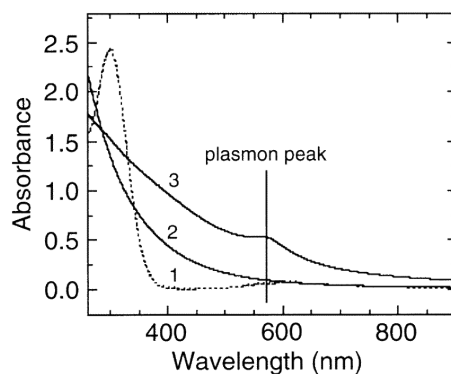


Figure 2.8 UV-VIS monitoring of the synthesis of DEMNs. Dashed line (spectrum 1): G4-OH/ $\text{Cu}^{2+}$  solution; solid line (spectrum 2): reduction with 5-fold molar excess of  $\text{NaBH}_4$ ; solid line (spectrum 3): same condition for G4-NH<sub>2</sub> instead G4-OH [126]

#### 2.4.4 Dendrimers as Drug Delivery Devices

Physical properties of dendrimers like monodispersity, encapsulation efficiency, number and type of surface functional groups, water solubility make them appropriate

macromolecules for evaluation as drug delivery vehicles. Due to these properties of dendrimers, there is an evolving interest on the encapsulation of hydrophobic compounds and for the delivery of anticancer drugs. In drug delivery, dendrimers can be threatened with three methods: first, covalent attachment of drug to the surface of dendrimer as prodrugs, second, coordination of drug to terminal groups with electrostatic interaction or third, encapsulation of pharmaceuticals [203, 204].

Encapsulation of hydrophobic drugs with the use of dendrimers is an outstanding method for the delivery of pharmaceuticals which may not be used in clinically due their low solubility. Controlled delivery of antiretroviral bioactives have been widely explored for dendrimers and observed that they enhance the efficacy of antiretroviral drugs [205-207].

Many therapeutically active drugs are poor water soluble and this is a major problem for the retention and uptake of these molecules. For these reasons, dendrimers are widely investigated as solubility enhancers. Dendrimers may not only increase the solubility of pharmaceuticals but also increase the retention and uptake of compounds within cancer cells. Encapsulation increases with the generation number and so that increasing generation number may be helpful to entrap drugs with a relatively high therapeutic dose. Researches have been constructing new research avenues for the development of dendrimer-drug complexes for cancer and targeting organ systems [208, 209].

#### **2.4.5 Dendrimers: Nanoarchitectures for Solubility Enhancement**

Poor solubility and low bioavailability of bioactive materials and drugs limit the application of them in drug delivery applications and systems. Dendrimers play a role with their unique structures as solubility enhancers depending on their some properties; such as concentration, generation size, core type and terminal functional groups. Solubility properties of dendrimers could be attributed to structure activity relationship in terms of hydrogen bonding, electrostatic interactions, and hydrophobic interactions.

Hydrophobic cored dendrimers with hydrophilic terminal groups can behave like a micelle and display container properties [210]. Dendrimers were firstly proposed as unimoleccular micelles by Newkome in 1985 [211] and emphasized the prominent utilities as solubilizing agents [212]. Use of dendrimers as solubility enhancers could be considered as the following subheadings.

Different generation and type ester and amine terminated PAMAMs were used in the solubility enhancement studies of Nifedipine. Results revealed that aqueous solubility of Nifedipine was increased several times as the generation increased [213]. The possible reasons of the solubility enhancement of Nifedipine were explained by the hydrogen bonding formed between the tertiary amine groups of PAMAMs and hydrogen of the Nifedipine, and hydrophobic cavities.

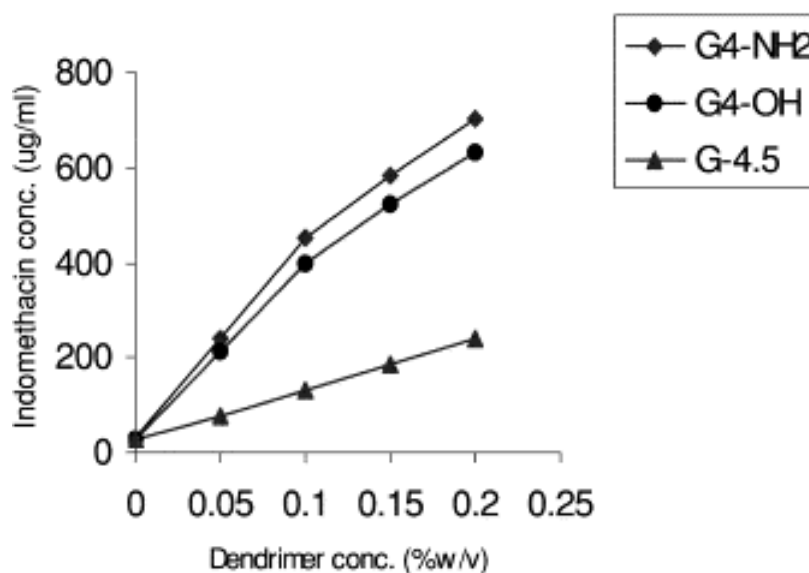


Figure 2.9 Solubility profile of Indomethacin in the presence of differing concentrations of G4-NH<sub>2</sub>, G4-OH, and G-4.5 dendrimers at pH 7.0 [214]

Different surface functionalized fourth generation G4-NH<sub>2</sub>, G4-OH, and G4.5 PAMAMs were used for the solubility enhancement of Indomethacin [214]. It was observed that the solubility of Indomethacin was increased in the order of G4-NH<sub>2</sub> > G4-OH > G4.5 (Figure 2.9).

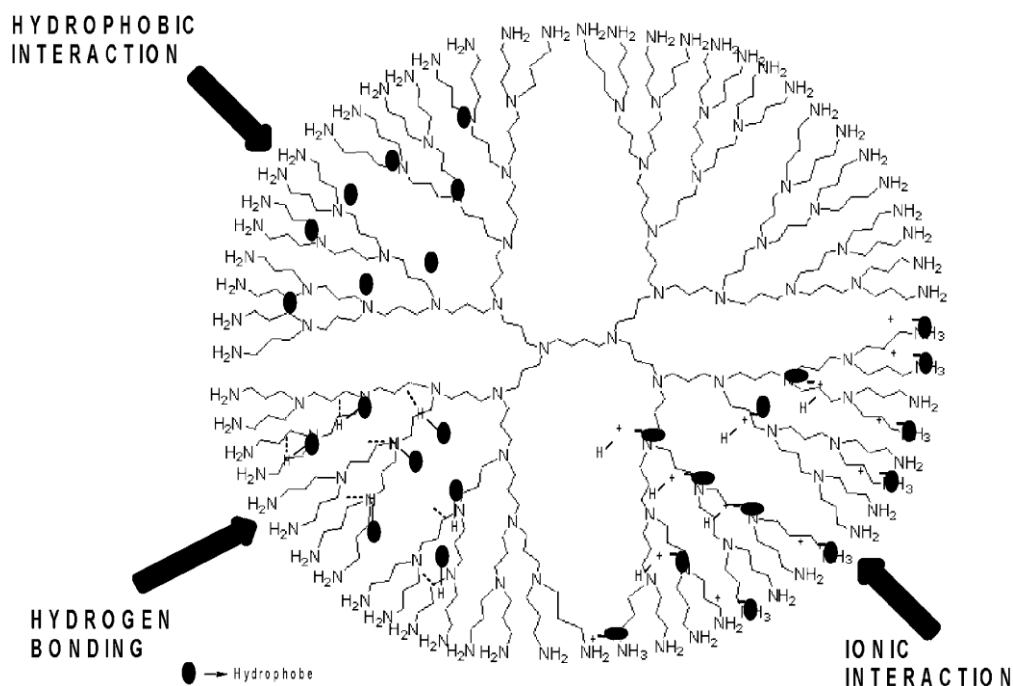


Figure 2.10 Possible mechanisms of dendrimer-mediated solubility enhancement [214]

Solubility enhancement mechanism for Indomethacin was explained by molecular encapsulation and electrostatic interaction between carboxylic groups of Indomethacin and terminal amine groups of G4-NH<sub>2</sub>. Molecular encapsulation were found to be primary interaction for ester terminated dendrimers while hydrogen binding for G4-OH (Figure 2.10).

Protonation mechanism of dendrimers are important as a function of pH as electrostatic interaction of the hydrophobes with tertiary and periphery amine groups of dendrimer can lead to solubility enhancement. Solubility of Nifedipine was investigated by Devarakonda et al. [213] at three different pH (4, 7, 10) for amine terminated G3 PAMAM dendrimer and G0.5, G1.5, G2.5. Results showed that the polarity of inner cavities of amine terminated PAMAMs are higher than ester terminated ones. Thus, the solubility of Nifedipine is higher for ester terminated PAMAMs at pH 4 compared to amine terminated. They also found that the solubility of Nifedipine was higher at pH 7, this was followed by pH 10 and later on pH 4. As the polarity of PAMAMs are related with the protonation of primary and tertiary amines, more polar means the one having more protonated amine groups. At pH 7 (neutral), both the tertiary and primary amine groups are susceptible to protonation compared to pH 4 and 10. This explains why the solubility

higher at pH 7 [213]. Conformational alterations of amine terminated PAMAMs and carboxyl-terminated PPIs were illustrated in Figure 2.11.

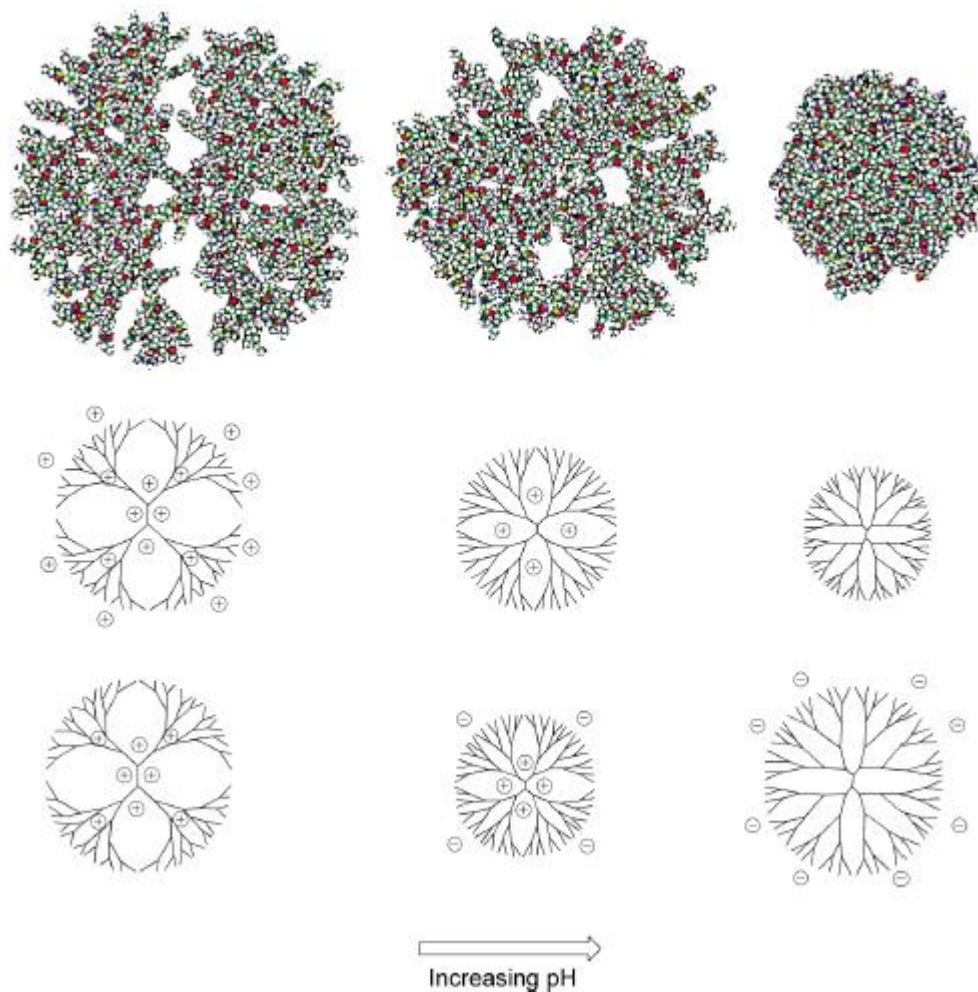


Figure 2.11 Top row: Three dimensional depiction of conformational change of an amino-terminated PAMAM dendrimer at increasing pH[215] Middle row: Two-dimensional depiction of the conformational change of an amino-terminated PAMAM dendrimer upon increasing pH. Bottom row: Two-dimensional depiction of the conformational change of a carboxyl-terminated PPI dendrimer at increasing pH [176, 216]

Likewise, Nifedipine study, application of the G4 PAMAM dendrimer as a solubility enhancer for weakly acidic Flubiprofen revealed that solubility of Flubiprofen is in the decreasing order of pH 10, 7 and 2 [217].

#### 2.4.6 Liquid Phase Polymer Retention (LPR): Dendrimer Enhanced Ultrafiltration (DEUF)

The theory behind the UF is to separate small and dissolved molecules from aqueous solutions. UF can be used to separate molecules differ in magnitude. Molecules having similar sizes cannot be separated by UF. In UF, membrane behaves like a molecular sieve. LPR or PAUF technique is used to separate polymer complexed or trapped molecules from metal ions by the retention of appropriate MWCO UF membranes. Different types of membranes and polymers as template can be used in LPR. A detailed list can be found in literature [103]. UF process is based to interaction between the polymer and metal ions. Interactions are mainly due to coordination bonds, electrostatic interaction but trapping is also possible. Driving force behind the separation of molecules during LPR is known as dead-end UF. That is a source of pressured inert gas like  $N_2$  is used perpendicular to membrane surface over the solution and the elution of the filtrate is maintained (Figure 2.12 and Figure 2.13). Polymer metal ion interaction due to ligand concentration that polymer possess, the nature of functional groups, structure and composition of the polymer, pH of the solution, and type of metal ion, ionic strength, temperature and the dielectric constant of the medium are the variables affecting polymer ion interactions. That is, performance of the UF affected directly from the changes in these variables [218].

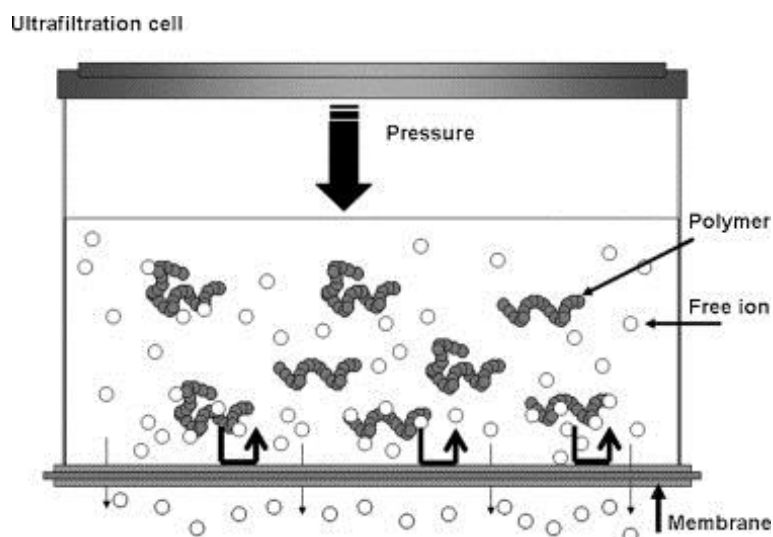


Figure 2.12 Scheme of the process of metal-ion retention by an aqueous soluble polymer in a UF system [218]

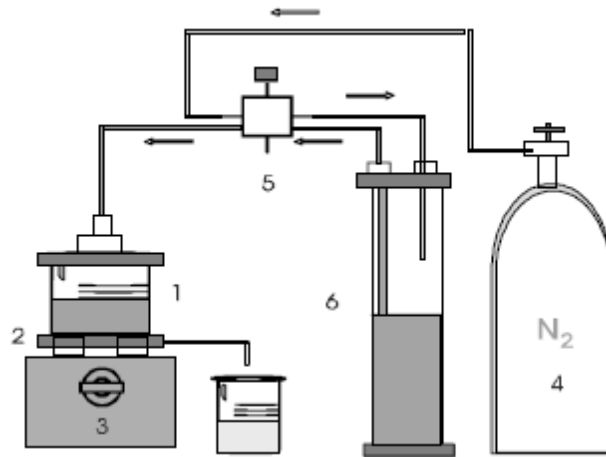


Figure 2.13 Liquid phase retention instrumental arrangement [103]. UF cell with polymeric and / or metal ion solution; (2) membrane filtrate; (3) magnetic stirrer; (4) pressure trap; (5) selector; (6) reservoir with water

PAMAMs are good model templates for LPR. These dendrimers are the first dendrimer family to be synthesized characterized and commercialized. Depending on the generation, tertiary and primary amine groups on the PAMAMs exhibit increasingly potential chelating sites to bind metal ions. High density of these nitrogen groups make PAMAMs high capacity chelating agents for metals, lanthanides and actinides [56, 219]. Diallo et al. [123] combined LPR with PAUF end developed DEUF by evaluating the recovery of Cu (II) ions from aqueous solutions with the polymer template PAMAMs. They used DEUF for a cyclic process to removal and regeneration of metal ions from aqueous solutions and they proposed this system for the effective waste water treatment [122] (Figure 2.14).

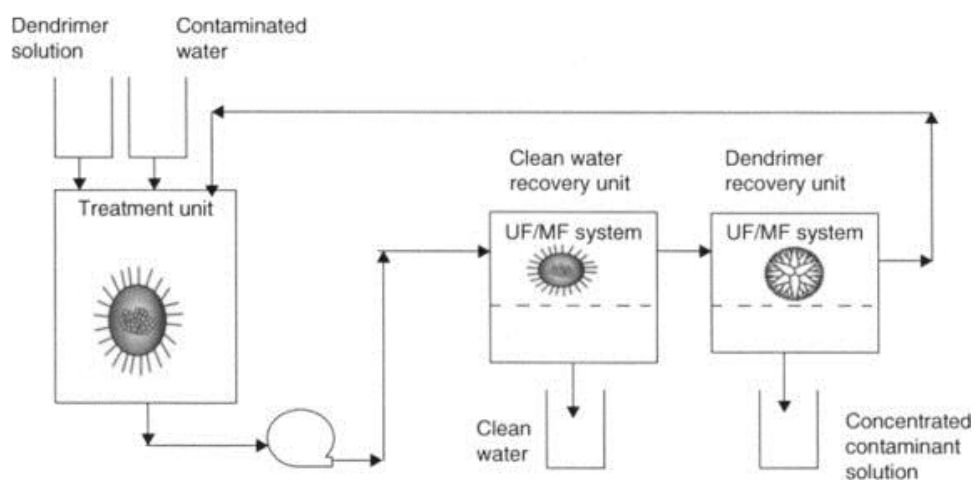


Figure 2.14 Water treatment by DEUF [123]

## **2.5 Microwave Chemistry**

### **2.5.1 Microwave (MW) Theory**

The frequency of MW is defined in the range of 300 to 300,000 megahertz (MHz). For laboratory scale samples MW heating, 2450 MHz has the right penetration depth and so it is preferable [220]. MW energy comprises electric field and magnetic field. However, only electric field transfers energy to heat a substance [221]. Thus, only electric field interactions are considered in chemical synthesis. MW photon energy (0.037kcal/mole) is very low when compared to the energy required to cleave molecular bonds (80-120 kcal/mole). Thus, the role of MW irradiation is only kinetic by rotating the molecules rather than breaking of the chemical bonds [220].

### **2.5.2 Mechanism of Microwave (MW) Heating**

Schematic representation of the sample heating by conventional methods-conduction and MW heating can be seen in Figure 2.15. In traditional methods, heating is performed by an external heat source. Thus, temperature on the outside surface of the reaction vessel and media is greater than the internal temperature and the core of the reaction media. That is, temperature is not conveyed homogeneously through the reaction media. In conventional heating, it takes time to reach an equilibrium temperature between the inside and outside of the solution. Thus, conventional heating is slow, time consuming and inefficient. On the other hand, MW procedure is different. MW heating leads to distribution of temperature homogeneously all over the reaction media with a MW energy source (Figure 2.15) and rapid rise in temperature is observed. As the process is not depended on the thermal conductivity of the vessel, MWs couple directly with the molecules in the reaction solution through dipole rotation or ionic conduction, which are the two fundamentals mechanisms for transferring energy from microwaves to the target substance to be heated. Dipole rotation is an interaction in which polar molecules align themselves with the changing electric field of the MWs. Energy transfer is resulted by the rotational motion of the molecule which try to orient itself with the field. The coupling ability of dipole rotation is connected with the polarity of the molecule and their ability of aligning with the electric field. Thus, the higher the polarity of a molecule, the greater is its ability to couple with MW irradiation [220].

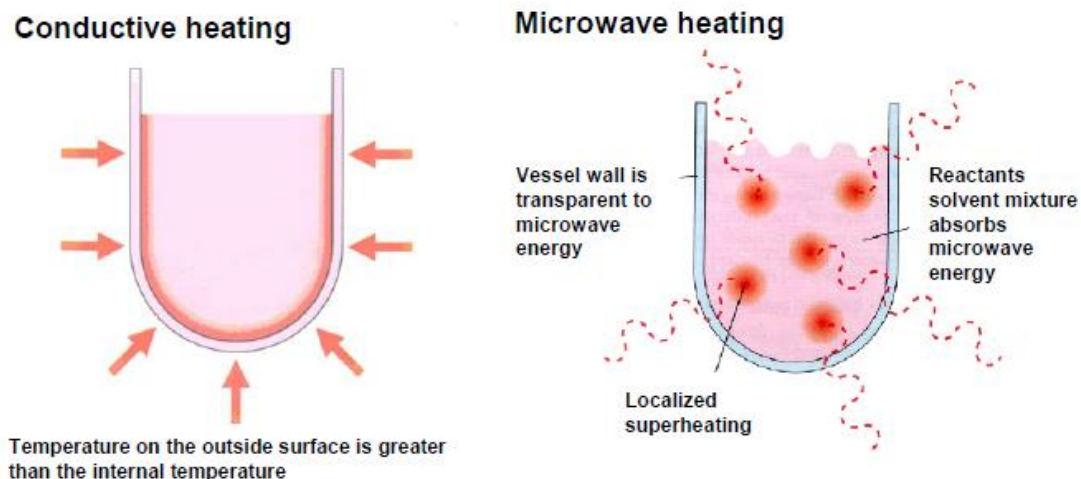


Figure 2.15 Systematic representation of sample heating by conduction and microwaves [220]

Transfer of energy in MW heating is also maintained by ionic conduction, which is due to free ions. Electric field gives rise to ionic motion as the molecules try to orient themselves to the rapidly changing electric field of the MWs. The temperature of the substance has also effect on the ionic conduction. As the temperature increases, ionic conduction increases, too, and the transfer of energy becomes more efficient. Ionic conduction can lead to instantaneous superheating. As a result of dipole rotation and ionic conduction, energy transfers are faster than the molecules can relax. Reaction rate can also be increased in MW heating

$$k = Ae^{-E_a/RT} \quad (2.1)$$

Equation (2.1) is called as the Arrhenius reaction rate equation, where  $k$  is the reaction rate coefficient,  $A$  is a constant,  $E_a$  is the activation energy,  $R$  is the universal gas constant ( $R = 8.314 \times 10^{-3} \text{ kJ mol}^{-1} \text{ K}^{-1}$ ), and  $T$  is the temperature (Kelvin). Collision frequency of the molecules and the fraction of those molecules having higher than activation energy can affect the constant  $A$ . Increase in temperature can increase the reaction rate by increasing the number of collisions as a result of instantaneous super heating. Thus, reactions performed in conventional heating can be performed faster in MW heating [220].

### 2.5.3 Solvent Selection in Microwave Chemistry

The polarity of the solvent in MW chemistry play an important role on the reaction time. Polarity of a solvent can be deterministic on the ability of coupling of a solvent with MW energy. As the coupling efficiency of a solvent with the microwave energy, the temperature of the reaction solution increases faster.

#### 2.5.3.1 Theory

Polarity of a solvent can be characterized by many factors; such as, dielectric constant, dielectric loss and tangent delta. MW absorption characteristic of a solvent is dependent on these three parameters. The dielectric constant ( $\epsilon'$ ) is the ratio of the electrical capacity of a capacitor filled with the solvent to the electrical capacity of the evacuated capacitor ( $\epsilon' = C_{\text{filled}}/C_{\text{evacuated}}$ ). Tangent delta ( $\tan \delta = \epsilon''/\epsilon'$ ) is the dissipation factor.  $\epsilon''$  is the dielectric loss (the amount of input MW energy that is dissipated as heat to the sample). When considering a solvent for a MW assisted organic reactions, boiling points become less important. This is due to fact that 300 W will bypass the boiling points of all solvents in seconds. The dielectric loss while choosing a solvent is most important parameter. The higher the dielectric loss value of a solvent, the more efficiently MW energy converted into thermal energy. Thus, the temperature of a solvent can be increased faster. Table 2.1 shows the values of dielectric constant, tangent delta, and dielectric loss for thirty common solvents, measured at room temperature and at a frequency of 2450MHz [220].

Table 2.1 Dielectric constant ( $\epsilon'$ ),  $\tan\delta$ , and dielectric loss ( $\epsilon''$ ) for 30 common solvents (measured at room temperature and 2450 MHz) [220]

| Solvent (bp °C)                 | Dielectric Constant ( $\epsilon'$ ) | Solvent                   | Tan $\delta$ | Solvent                   | Dielectric Loss ( $\epsilon''$ ) |
|---------------------------------|-------------------------------------|---------------------------|--------------|---------------------------|----------------------------------|
| Water (100)                     | 80.4                                | Ethylene Glycol           | 1.350        | Ethylene Glycol           | 49.950                           |
| Formic Acid (100)               | 58.5                                | Ethanol                   | .941         | Formic Acid               | 42.237                           |
| DMSO (189)                      | 45.0                                | DMSO                      | .825         | DMSO                      | 37.125                           |
| DMF (153)                       | 37.7                                | 2-Propanol                | .799         | Ethanol                   | 22.866                           |
| Acetonitrile (82)               | 37.5                                | 1-Propanol                | .757         | Methanol                  | 21.483                           |
| Ethylene Glycol (197)           | 37.0                                | Formic Acid               | .722         | Nitrobenzene              | 20.497                           |
| Nitromethane (101)              | 36.0                                | Methanol                  | .659         | 1-Propanol                | 15.216                           |
| Nitrobenzene (202)              | 34.8                                | Nitrobenzene              | .589         | 2-Propanol                | 14.622                           |
| Methanol (65)                   | 32.6                                | 1-Butanol                 | .571         | Water                     | 9.889                            |
| NMP (215)                       | 32.2                                | Isobutanol                | .522         | 1-Butanol                 | 9.764                            |
| Ethanol (78)                    | 24.3                                | 2-Butanol                 | .447         | NMP                       | 8.855                            |
| Acetone (56)                    | 20.7                                | 2-Methoxyethanol          | .410         | Isobutanol                | 8.248                            |
| 1-Propanol (97)                 | 20.1                                | <i>o</i> -Dichlorobenzene | .280         | 2-Butanol                 | 7.063                            |
| MEK (80)                        | 18.5                                | NMP                       | .275         | 2-Methoxyethanol          | 6.929                            |
| 2-Propanol (82)                 | 18.3                                | Acetic Acid               | .174         | DMF                       | 6.070                            |
| 1-Butanol (118)                 | 17.1                                | DMF                       | .161         | <i>o</i> -Dichlorobenzene | 2.772                            |
| 2-Methoxyethanol (124)          | 16.9                                | 1,2-Dichloroethane        | .127         | Acetonitrile              | 2.325                            |
| 2-Butanol (100)                 | 15.8                                | Water                     | .123         | Nitromethane              | 2.304                            |
| Isobutanol (108)                | 15.8                                | Chlorobenzene             | .101         | MEK                       | 1.462                            |
| 1,2-Dichloroethane (83)         | 10.4                                | Chloroform                | .091         | 1,2-Dichloroethane        | 1.321                            |
| <i>o</i> -Dichlorobenzene (180) | 9.9                                 | MEK                       | .079         | Acetone                   | 1.118                            |
| Dichloromethane (40)            | 9.1                                 | Nitromethane              | .064         | Acetic Acid               | 1.079                            |
| THF (66)                        | 7.4                                 | Acetonitrile              | .062         | Chloroform                | 0.437                            |
| Acetic Acid (113)               | 6.2                                 | Ethyl Acetate             | .059         | Dichloromethane           | 0.382                            |
| Ethyl Acetate (77)              | 6.0                                 | Acetone                   | .054         | Ethyl Acetate             | 0.354                            |
| Chloroform (61)                 | 4.8                                 | THF                       | .047         | THF                       | 0.348                            |
| Chlorobenzene (132)             | 2.6                                 | Dichloromethane           | .042         | Chlorobenzene             | 0.263                            |
| <i>o</i> -Xylene (144)          | 2.6                                 | Toluene                   | .040         | Toluene                   | 0.096                            |
| Toluene (111)                   | 2.4                                 | Hexane                    | .020         | <i>o</i> -Xylene          | 0.047                            |
| Hexane (69)                     | 1.9                                 | <i>o</i> -Xylene          | .018         | Hexane                    | 0.038                            |

### **2.5.3.2 Choosing a Solvent**

Table 2.1 can be categorized easily into three groups: high, medium and low absorbing solvents. By examining the dielectric loss values of column 3 in Table 2.1, categorization of samples can be detected by bold lines. High absorbing solvents are the ones having dielectric loss value greater than 14. Medium absorbers have the dielectric loss value between 1.00 to 13.99 and low absorbers have the dielectric loss values less than 1.00. High absorbers are like the small chain alcohols (methanol, ethanol, ethylene glycol), dimethyl sulfoxide (DMSO) and nitrobenzene. They all have large dielectric loss, so they heat very quickly in the MW chamber. Medium absorbers are dimethyl formamide (DMF), acetonitrile, butanols, ketones and waters. These are also heat very efficiently, but they need more time to reach desired temperatures. Non polar solvents like hexane, toluene, and benzene are low absorbers. High and medium absorbers are usually used for MAS. These absorbers maintain fast and efficient heating. On the other hand, low absorbers are not used normally in MAS.

Nonpolar solvents (such as hexane, benzene, and toluene) are low absorbers. Low absorbers can be heated above their boiling point, but much longer time is needed to reach the boiling point. Choosing the correct solvent is an important factor for reactions that use MW heating for the formation of metal nanoparticles. High and medium absorbers are normally used as solvents in microwave-assisted reaction due to their efficient and fast heating. Low absorbers (nonpolar solvents) are not normally used in MAS.

In the light of above theory, methanol, ethanol, and ethylene glycol are good solvents for MAS of chemical reactions. They can be also used as the dielectric constants enhancers besides serving as reducing agents [220]. Thus, in this study, methanol was chosen as dielectric constant enhancer for the synthesis of amine terminated PAMAMs and solvent in the surface modification of half generation ester terminated PAMAMs with tris functional groups.

## **2.6 Chemometrics**

### **2.6.1 PCA and Pattern Recognition**

Principal component analysis was invented in 1901 by Karl Pearson [222] and later on method was independently developed by Harold Hotelling in the 1930s [223]. Model is

mostly used for predictive model and as a vehicle in explanatory data analysis, outlier detection, rank (dimensionality) reduction, graphical clustering, classification, and regression. PCA is eigenvalue decomposition of a data covariance (or correlation) matrix or singular value decomposition (SVD) of a data matrix which is usually mean centered [224]. Results of PCA are generally discussed in terms of visualized factor scores and loadings which open up a deeper understanding than what is possible when looking at individual variables alone.

### 2.6.1.1 PCA: Basic Concepts and Master Equations

Data for PCA must be collected in a two-way array or matrix, called  $\mathbf{X}$  (Figure 2.16), in which column vectors represent ‘variables’ (e.g., attributes, wavelengths, retention time, physical/chemical parameters, toxicity values, and biological responses), and row vectors represent ‘objects’ for which these variables are measured, often also called cases, samples, measurements, etc.

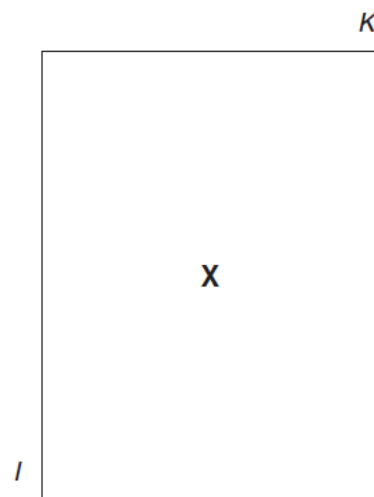


Figure 2.16 Data matrix  $\mathbf{X}$ , consisting of  $I$  rows, ‘objects’, each characterized by  $K$  columns, ‘variables’ [225]

For correlated data, PCA works by projecting the hidden (latent) data structure in a matrix  $\mathbf{X}$  onto two subspaces, termed the ‘score space’ and the ‘loading space’, respectively (Figures 2.16 and 2.17)

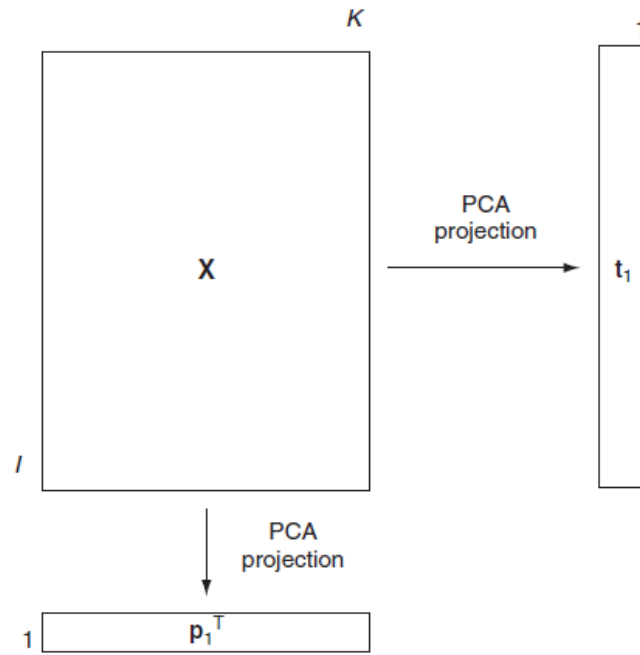


Figure 2.17 PCA projects the columns of  $X$  onto a loading vector  $p_1^T$  and the rows of  $X$  into the complementary score vector  $t_1$ , constituting the ‘first principal component (PC)’ [225]

$$\begin{array}{c}
 \boxed{X} \\
 \\
 \dots + \boxed{t_A}
 \end{array}
 =
 \begin{array}{c}
 \boxed{t_1} \\
 \\
 \dots + \boxed{t_A}
 \end{array}
 \begin{array}{c}
 \overline{p_1^T} \\
 \\
 \overline{p_A^T}
 \end{array}
 +
 \begin{array}{c}
 \boxed{t_2} \\
 \\
 \dots + \boxed{E}
 \end{array}
 \begin{array}{c}
 \overline{p_2^T} \\
 \\
 \dots + \boxed{E}
 \end{array}
 + \dots$$

Figure 2.18 Matrix  $X$  decomposed into a set of rank 1 outer products ( $A$  terms, corresponding to the effective rank,  $A$ ) and the residual matrix,  $E$  [225]

Figure 2.18 shows how PCA projects from a matrix  $X$  into a score vector  $t_1$  and a loading vector  $p_1$ , which together are called the ‘first component’. The process is repeated for obtaining a second component ( $t_2, p_2$ ). Figure 2.18 shows how successive components are formed by the outer product of the vectors  $t_a$  and  $p_a$ . Figure 2.18 also shows that this

process is continued until the number of ‘effective principal components’,  $A$  (see further below), are found, for the component index  $a=1, 2, \dots, A$ . Another important factor is the residual matrix  $\mathbf{E}$ . As the  $\mathbf{E}$  matrix include measurement and sampling noises, this matrix is to be made small in multivariate data analysis [225].

The ‘master equation’ for a properly mean centered and scaled  $\mathbf{X}$  is

$$\mathbf{X} = t_1 \mathbf{p}_1^T + t_2 \mathbf{p}_2^T + \dots + t_A \mathbf{p}_A^T + \mathbf{E} \quad (2.2)$$

or

$$\mathbf{X} = \mathbf{T} \mathbf{P}^T + \mathbf{E} \quad (2.3)$$

$\mathbf{X}$ : data matrix ( $I \times K$ )

$\mathbf{T}$ : score matrix ( $I \times A$ )

$\mathbf{P}$ : loading matrix ( $K \times A$ )

$\mathbf{E}$ : residual matrix ( $I \times K$ )

$t_a$ : a column of  $\mathbf{T}$

$p_a$ : a column of  $\mathbf{P}$

$a=1, \dots, A$ : the principal component (PC) index

The most important properties of this equations are:

- Orthogonality of all scores:  $t_m^T t_n = 0$       $-m \text{ not equal } n; 1 \leq m \leq A; 1 \leq n \leq A$
- Orthogonality of all loadings:  $p_m^T p_n = 0$       $-m \text{ not equal } n$
- Normalization of the  $p_m$ :  $p_m^T p_m = 1$       $- \text{all } m$
- The size of the component  $t_m^T t_m = \lambda_m$       $- \text{all } m$

Master equation drive the important understanding that PC directions are ‘linear combinations’ of all original  $K$  variables.  $\lambda_i$  (Eigenvalue) is the size of component. PCs are calculated, ordered, and indexed according to their size,  $\lambda_i$ . First component PC1 of the models explains the highest possible fraction of this sum. PC2 explains the second largest fraction. Third less than PC2 and goes on this way until the residual SS of  $\mathbf{E}$  is left. The part not contained in the effective number components,  $A$  forms a convenient measure of not modelled fraction of  $\mathbf{X}$ . In this way, the first PC accounts for the largest

variance fraction of  $\mathbf{X}$ , followed by a new, orthogonal PC modeling the second largest variance direction, and so on. Under the ideal assumption that  $\mathbf{E}$  should only describe true noise, one should strive for the size of  $\mathbf{E}$  to be appropriately ‘small’ [225].

The PCA master equation and Figure 2.17 underline that the most challenging issue for PCA is how to choose an appropriate number of PCs ( $A$ ), securing that only true noise ends up in the residual matrix  $\mathbf{E}$ . In other words, how many ‘significant components’ to retain in the PCA model? ‘Significant’ is used here in a somewhat loose way: What is the number of PCA components that carry only systematic structure – meaningful structure – interpretable structure? [225]

The number of PCs can be determined with various approaches. It is a good idea to draw eigenvalues, and root mean square error of cross validation (RMSECV) versus PCs plots as well as evolving factor analysis (EFA) (further discussed). RMSECV shows the predictive residual sum of squares (PRESS) value for the data as function of the number of PCs.

$$\text{RMSECV} = \sqrt{\sum_{i=1}^n \frac{\text{PRESS}}{n}} = \sqrt{\sum_{i=1}^n \frac{(y_i - \hat{y}_i)^2}{n}} \quad (2.4)$$

where  $\hat{y}_i$  contains the values of the Y variable that are estimated by cross-validation (where the value for each object  $i$  is estimated using a model that was built using a set of objects that does not include object  $i$ ). That is, PRESS is calculated via a leave one out cross-validation, i.e. where each sample is left out of the model formulation and predicted once.  $y$  contains the known values of the Y variable, and  $n$  is the total number of objects in the data set. A plot of RMSECV vs. PC plots are useful for determining the optimal number of latent variables to retain in a model that is built using the full set of data (Figure 2.19). RMSECV is the indication of how well the data can be reconstructed from the PCs. Figure 2.19 indicated that minimum reconstruction error is at six PCs. In this instance, the cross-validation suggest that up to six PCs might be best. However, when deciding the number of PCs, there are two rules of thumb with regard to selecting the optimal number of factors: 1. Only choose additional factors when the RMSECV improves by at least 2%, 2. Choose as few factors as possible for the less complexity of the model. Thus, most of the improvement in error is achieved before six PCs and results suggest five PCs for the final model (Figure 2.19). Details of this issue can be seen from the chemometric textbooks [226-229].

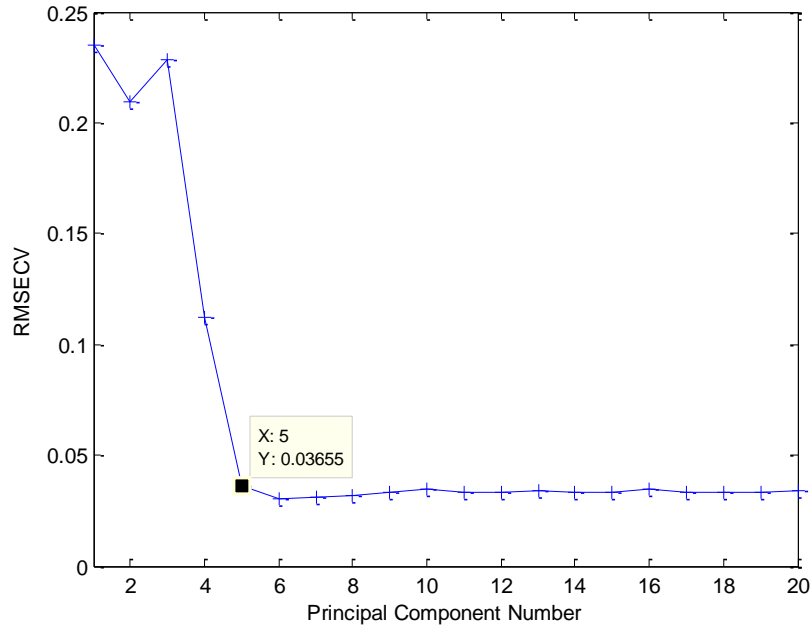


Figure 2.19 A sample Cross validation PRESS curve of P4.NH<sub>2</sub>. 5 PCs.

### 2.6.1.2 PCA NIPALS Algorithm

NIPALS algorithm [226] is one of the common PCA algorithms in chemometrics. PCA analysis of data matrix  $\mathbf{X}$  are processed through the following steps.

1. Take a column of data matrix  $\mathbf{X}$  (often the column with greatest sum of squares) as the first guess of the scores first principal component – call it  $initial\hat{t}$ .
2. Calculate the following:

$$\frac{unnorm\hat{p}}{\sum\hat{t}^2} = \frac{initial\hat{t}}{\sum\hat{t}^2} \quad (2.5)$$

3. Normalize the guess of the loadings, so that:

$$\hat{p} = \frac{unnorm\hat{p}}{\sqrt{\sum unnorm\hat{p}^2}} \quad (2.6)$$

4. Now calculate the new guess of the scores

$$new\hat{t} = \mathbf{X}\hat{p}' \quad (2.7)$$

5. Check if this new guess differs from the first guess; a simple approach is to look at the size of the sum of square difference in the old and new scores, i.e.  $\sum(initial\hat{t} - new\hat{t})^2$ . If this is small the PC has been extracted; set the PC scores

and ( $t$ ) loadings ( $p$ ) for the current PC to  $\hat{t}$  and  $\hat{p}$ . Otherwise return to step 2, substituting the initial scores by the new scores.

6. Subtract the effect of the new PC from the data matrix to get a residual data matrix

$$\text{resid } \mathbf{X} = \mathbf{X} - t\mathbf{p} \quad (2.8)$$

7. If it is desired to compute further PCs, substitute the residual data matrix obtained in step 6 for  $\mathbf{X}$  and go to step 1.

## 2.6.2 EFA

As its understood from the name, EFA is a different version of factor analysis (FA) [230]. One of the important information that can be interfered from EFA is the rank of analyzed data matrix. This rank represents the complexity of the data-number of component in the system. In mathematics, the definition of rank is simple. It is the number of linearly independent rows or columns. On the other hand, in chemistry, there is a considerable variety of situations and no clear and general statements can be made and so that the expression of ‘chemical rank’ is used [231].

By examining the submatrices of complete data matrix to FA, EFA investigates the evolution of the rank of data matrix. Thus, the evolution of the rank is monitored. In general, EFA results are shown graphically conveying useful information about the process under investigation. The main important factor of EFA is the fact that analysis is completely model free and finally the usage of the information for further analyses in secondary model-free analysis methods [231].

### 2.6.2.1 Abstract Factor Analysis

A data matrix for EFA is required. A two and three dimensional array of sample data matrix can be seen in Figure 2.20. In general, FA is often used for the decomposition of a data matrix into a product of orthogonal matrices (2.9):

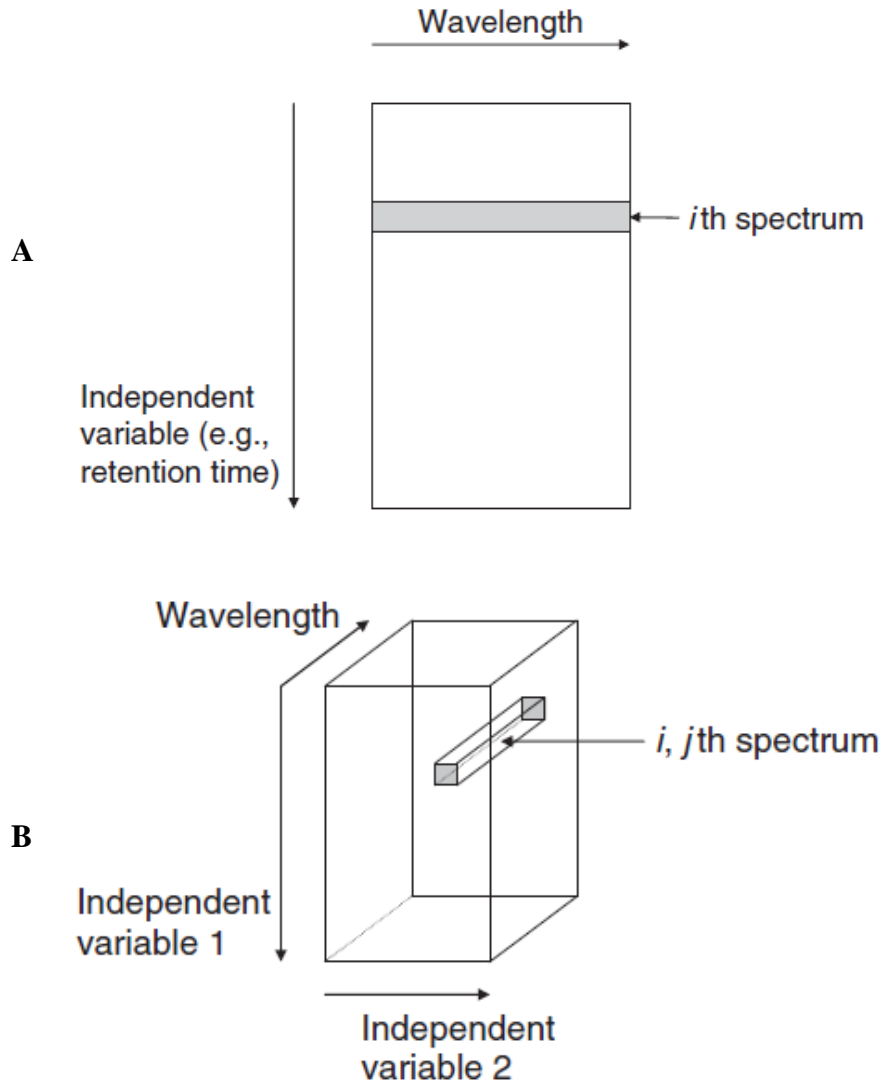


Figure 2.20 (A) Typical structure of data that are subjected to EFA, the rows of the matrix are formed by spectra measured as a function of an independent variable; (B) Hyperspectral data. Spectra are measured as a function of the two coordinates of an image [231]

$$\mathbf{X}=\mathbf{AB} \quad (2.9)$$

where the matrices  $\mathbf{A}$  and  $\mathbf{B}$  are orthogonal. That is, the products of  $\mathbf{A}^T\mathbf{A}$  and  $\mathbf{B}\mathbf{B}^T$  are diagonal matrices. In tradition, Matrix  $\mathbf{A}$  and  $\mathbf{B}$  are called as, score and loading matrices, respectively.

A general and much more suitable way of FA of a matrix  $\mathbf{X}$  that maintains symmetry is the singular value decomposition (SVD).

$$\mathbf{X} = \mathbf{USV}^T \quad (2.10)$$

If the dimensions of  $\mathbf{X}$  are  $(m \times n)$ , with  $m \geq n$ , the dimensions of  $\mathbf{U}$  are  $(m \times n)$  and those of  $\mathbf{S}$  and  $\mathbf{V}^T$  are  $(n \times n)$ . With SVD, the matrices  $\mathbf{U}$  and  $\mathbf{V}^T$  are orthogonal and normalized (orthonormal); therefore,

$$\mathbf{U}^T\mathbf{U} = \mathbf{V}^T\mathbf{V} = \mathbf{I} \quad (2.11)$$

Where  $\mathbf{I}$  is unity matrix of appropriate dimensions and  $\mathbf{S}$  is a diagonal matrix with the singular values arranged in descending order (all singular values are positive). The matrices  $\mathbf{U}$  and  $\mathbf{V}^T$  are the eigenvectors of the square matrices  $\mathbf{X}\mathbf{X}^T$  and  $\mathbf{X}^T\mathbf{X}$  and the singular values are the positive square roots of the eigenvalues. The SVD algorithm is numerically superior to the more traditional algorithms for FA such as vector iteration and NIPALS [231].

Mathematically, the rank of  $\mathbf{X}$  matrix is equal the rank of non-zero singular values and it is equal to the number of linearly independent rows or columns of  $\mathbf{X}$ . The number of rank is usually significantly less than number of rows and columns of  $\mathbf{X}$  Matrix (Figure 2.21)

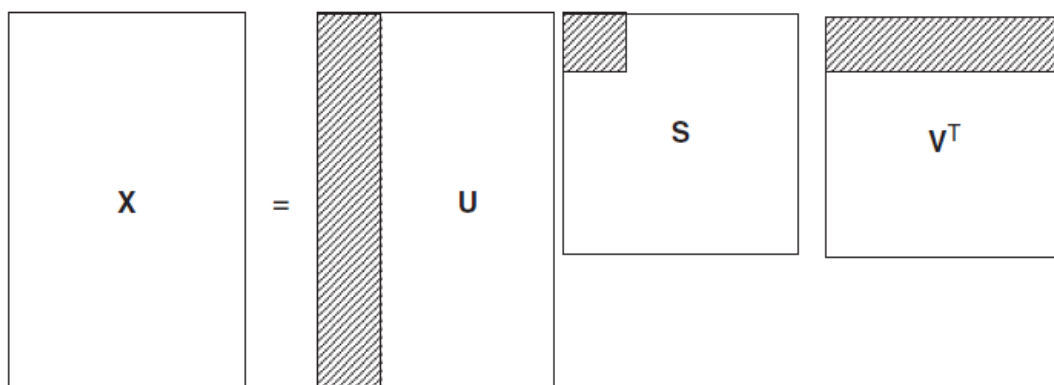


Figure 2.21 The dimensions of  $\mathbf{U}$ ,  $\mathbf{S}$ , and  $\mathbf{V}^T$ . Only the shaded parts are relevant [231]

In Figure 2.21, only the shaded parts of the matrices  $\mathbf{U}$ ,  $\mathbf{S}$ , and  $\mathbf{V}^T$  are relevant as all the others are multiplied by zero (the diagonal elements of  $\mathbf{S}$  outside the shaded area).

From the perspective of chemistry, the relation between the rank of data matrix  $\mathbf{X}$  and the number of chemical components or the system is important. In Beer Lambert law, a data matrix  $\mathbf{X}$  represents absorption measurements and can be decomposed into concentration matrix  $\mathbf{C}$  and matrix  $\mathbf{S}^T$  of molar absorptivities [231].

$$\mathbf{X} = \mathbf{C}\mathbf{S}^T \quad (2.12)$$

The first version of EFA was published in 1985 [232]. In traditional EFA, the series of submatrices that are analyzed is formed by an increasing number of spectra or rows, starting with only the first spectrum, then the first two spectra, the first three, and so on, until all spectra are included. In Figure 2.22A, shaded area of the  $\mathbf{X}$  data matrix is evaluated with SVD and the related singular values are stored in a matrix  $\mathbf{EFA}_f$ . Likewise, EFA is performed in the opposite direction by increasing the number of rows from the end and singular values are stored in a matrix  $\mathbf{EFA}_b$  (Figure 2.22B).

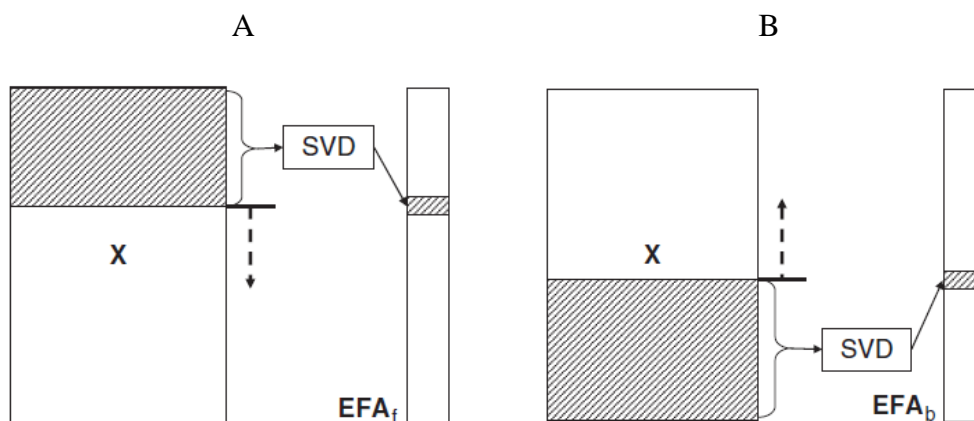


Figure 2.22 Submatrices analyzed by traditional EFA (A) forward EFA; (B) backward EFA [231]

In a sample traditional EFA treatment of spectrophotometric titration data of a tetraprotic acid  $\text{AH}_4^{4+}$  with  $\text{p}K_a$  values of 8, 7, 6, and 3 [231]. Spectra measured between pH 0 and 12 form the rows of  $\mathbf{X}$ . The rank of complete matrix  $\mathbf{X}$  is 5 as it's correlated with the number of species or component present during the spectrophotometric titration. These species are  $\text{AH}_4^{4+}$ ,  $\text{AH}_3^{3+}$ ,  $\text{AH}_2^{2+}$ ,  $\text{AH}^+$  and A. From the forward and backward EFA analysis of  $\mathbf{X}$  in Figure 2.23, it could be seen that  $\text{AH}_4^{4+}$  exist at pH 0, at pH 1,  $\text{AH}_3^{3+}$  starts to form as it's indicated by the appearance of second significant singular value. At pH  $\sim$  4,  $\text{AH}_2^{2+}$  starts to form; at pH 5,  $\text{AH}^+$  and at pH  $\sim$  7, last component, the fully deprotonated A.

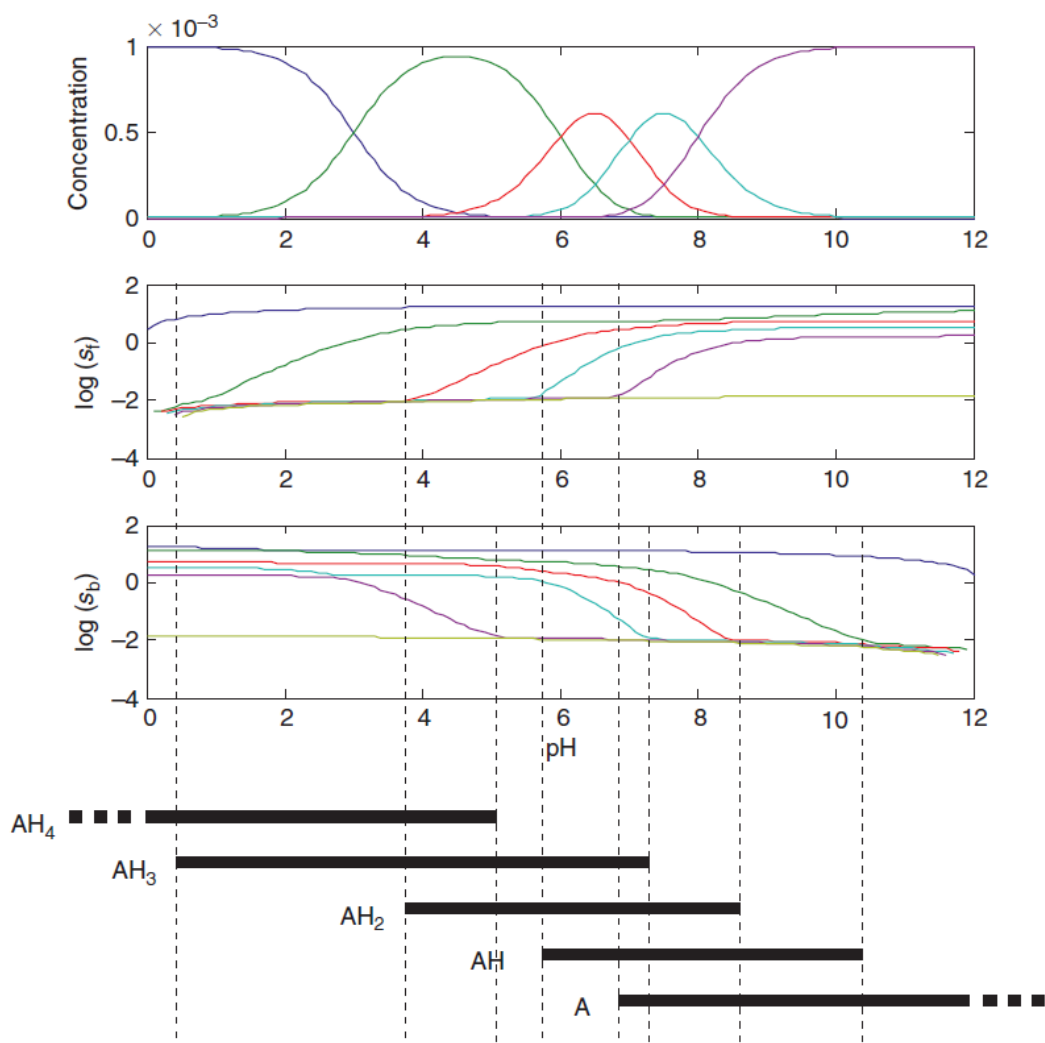


Figure 2.23 The combination of appearance and disappearance of significant singular values results in concentration windows. species distribution curve, forward EFA, backward EFA and species existence range as a function of pH from top the bottom, respectively [231]

Forward and backward EFA analysis can give a good explanation and identification of the chemical rank or the number of chemical species. In Figure 2.23, with a sixth singular value which is the indication of the noise level, it is clearly seen that five significant singular values that are perceptible by their emergence from the noise level. The appearance patterns in EFA clearly visible and often they are used to decide the determination of the number of components or the rank of the matrix. So called concentration windows from the backward and forward EFA analysis, the pH domain and region of the particular species exist can be determined (Figure 2.23). In consecutive protonation equilibria. The connection between the beginnings and endings of concentration profiles is straightforward [231].

### 2.6.3 MCR-Iterative Curve Resolution Methods

Decomposition of the multicomponent information of data matrix  $\mathbf{X}$  stored with the chemically meaningful bilinear models involving the pure contributions of each component can be overcome by curve resolution (CR) methods [233]. Model of CR is expressed generally by

$$\mathbf{X} = \mathbf{C}\mathbf{S}^T + \mathbf{E} \quad (2.13)$$

where  $\mathbf{C}$  is the matrix of pure concentration profiles,  $\mathbf{S}^T$  is the matrix of pure spectra (responses) and  $\mathbf{E}$  is the experimental error. Iterative resolution methods recover the bilinear model through an iterative optimization of  $\mathbf{C}$  and/or  $\mathbf{S}^T$  or through the optimization of a transformation matrix  $\mathbf{R}$ . Thus, the basic bilinear CR model can be written as in equation (2.13) or, in (2.14) [233].

$$\mathbf{X} = (\mathbf{C}_0\mathbf{R})(\mathbf{R}^{-1}\mathbf{S}_0^T) + \mathbf{E} \quad (2.14)$$

where

$$\mathbf{C} = \mathbf{C}_0\mathbf{R} \quad (2.15)$$

$$\mathbf{S}^T = \mathbf{R}^{-1}\mathbf{S}_0^T \quad (2.16)$$

$\mathbf{C}_0$  and  $\mathbf{S}_0^T$  are the initial estimates of  $\mathbf{C}$  and  $\mathbf{S}^T$  and depending on the resolution methods they can be real profiles or abstract profiles. Equations (2.13) and (2.14) can be the basis of many iterative methods. The most widely used methods for the optimization of  $\mathbf{C}$  and/or  $\mathbf{S}^T$  according to (2.13) equation are iterative target transformation factor analysis (ITTFA) [234, 235] and multivariate curve resolution-alternating least squares (MCR-ALS) [92, 236, 237]. On the other hand, the methods resolution factor analysis (RFA) [238, 239] and resolution based on elementary matrix transformations (Gentle)[240] use equation (2.14) as the starting point. The focus of these methods is the determination of the transformation matrix  $\mathbf{R}$  such that the linked concentration profiles ( $\mathbf{C}$ ) and pure spectra ( $\mathbf{S}^T$ ) are chemically meaningful and provide a good reproduction of the original data matrix [233].

All of the iterative resolution methods start the optimization process with the initial estimates of some matrices in the bilinear model  $\mathbf{C}_0$ ,  $\mathbf{S}_0^T$ , or  $\mathbf{R}_0$ . These initial estimates are changed iteratively under the action of constraints. The chemical constraints are as follows:

- *Nonnegativity*: Force response profiles or concentrations to be positive. It is applicable that concentrations and instrumental responses should be positive naturally. Examples are UV absorption and mass spectra.
- *Unimodality*: Profiles should have a single maximum. Concentrations should be related with peak shaped profiles; such as chromatographic peaks, voltametric signals.
- *Closure*: To reach concentration profiles up a certain constant values. In chemistry, it is known as mass balance condition.
- *Hard modelling*: This is a constraint of recent incorporation into multivariate curve resolution (MCR) methods and shapes concentration profiles and responses according to a mathematical function [233].

As the initial estimated profiles are very close the final solution, random initial estimates should be preferably avoided. Because of rotational ambiguity problems, different initial estimates may cause slightly different solutions. However, all the present solutions will be chemically feasible and optimal fit can be maintained. Nonrandom initial estimates of  $\mathbf{C}$  and  $\mathbf{S}^T$  can be developed from the raw data set or by the help of auxiliary chemometric methods. Therefore, selection of a set of columns or rows from the original data set  $\mathbf{X}$ , equal to the number of the components present in the system can provide the initial estimate of the matrices  $\mathbf{C}$  and  $\mathbf{S}^T$ , respectively. On the other hand, under some circumstances, initial background about the chemical problem can be enough to make a selection. For example; in high performance liquid chromatography-diode array detection (HPLCDAD), maxima of observed chromatographic peaks can be used as initial estimates. Besides, if there exist some known pure possible spectra, it can be also possible. EFA can be used for the monitoring of the rank from the emergence and disappearance of a component through a local rank information. In this way, the concentration window of each component can be easily determined and approximate concentration profiles can be generated [233].

#### 2.6.4 MCR-ALS

MCR-ALS was developed and proposed by Tauler's groups [92, 236, 237]. Algorithm of MCR-ALS beyond to basic CR model related with the equation (2.13). That is, MCR-

ALS tries to find the concentration profiles and spectra by optimizing **C**-type and **S<sup>T</sup>**-type estimates by constrained ALS process. The general operating procedure of MCR-ALS as the following [233]:

1. Determination of the number of compounds in **X**.
2. Generation of initial estimates (e.g., **C**-type matrix).
3. Calculation of **S<sup>T</sup>** under constraints.
4. Calculation of **C** under constraints.
5. Reproduction of **X** from the product of **C** and **S<sup>T</sup>**.
6. Go to step (3) until convergence is achieved.

One can now the number of significant components in **X** beforehand or determine it by simple application of PCA.

MCR-ALS method try to solve mainly the following two least square problems under the proper constraints.

$$\min_{\hat{\mathbf{C}}} \|\mathbf{X}_{\text{PCA}} - \hat{\mathbf{C}}\hat{\mathbf{S}}^{\text{T}}\| \quad (2.17)$$

$$\min_{\hat{\mathbf{S}}^{\text{T}}} \|\mathbf{X}_{\text{PCA}} - \hat{\mathbf{C}}\hat{\mathbf{S}}^{\text{T}}\| \quad (2.18)$$

Where  $X_{\text{PCA}}$  is the PCA reproduced data using produced by selecting the number of components;  $\hat{\mathbf{C}}$  and  $\hat{\mathbf{S}}^{\text{T}}$  are the least square estimates of **C** and **S<sup>T</sup>**. The main aim of equation (2.17) and (2.18) is to minimize or keep constant the difference between  $X_{\text{PCA}}$  and ALS reproduced data. Least square solutions of (2.17) is

$$\hat{\mathbf{S}}^{\text{T}} = (\hat{\mathbf{C}}^{\text{T}}\hat{\mathbf{C}})^{-1}\hat{\mathbf{C}}^{\text{T}}\mathbf{X}_{\text{PCA}} \quad (2.19)$$

or

$$\hat{\mathbf{S}}^{\text{T}} = \hat{\mathbf{C}}^+\mathbf{X}_{\text{PCA}} \quad (2.20)$$

where  $\hat{\mathbf{C}}^+$  is the pseudoinverse of the concentration matrix. Similarly, the least square solution of (2.18) is

$$\hat{\mathbf{C}} = \mathbf{X}_{\text{PCA}}\hat{\mathbf{S}}(\hat{\mathbf{S}}^{\text{T}}\hat{\mathbf{S}})^{-1} \quad (2.21)$$

or

$$\hat{\mathbf{C}} = \mathbf{X}_{\text{PCA}}(\hat{\mathbf{S}}^{\text{T}})^+ \quad (2.22)$$

where  $(\hat{\mathbf{S}}^{\text{T}})^+$  is the pseudoinverse of the spectra matrix.

In each iterative cycle, equation (2.17) and (2.18) are solved sequentially. First the  $\mathbf{S}^{\text{T}}$  matrix is calculated and then concentration  $\mathbf{C}$  matrix obtained by using it. Finally the convergence is checked by using the data matrix  $\mathbf{X}$  obtained from PCA. PCA analyzed  $\mathbf{X}$  matrix preserve all the necessary chemical information and discard the noise, so that original data matrix can be evaluated with a more confidential way the convergence of optimized profiles through the sought pure solutions. As a convergence criteria in ALS, a threshold value in the relative difference in fit is used. As a one of the most commonly used criteria, monitoring of the evolution of the profile shapes can be used to stop iterative cycles by setting a maximum iteration number. As long as appropriate constraints is taken into consideration and core bilinear models are followed, MCR-ALS solutions are usually suitable solutions even if intensity ambiguities can still exist due to system under study [233].

## 2.6.5 Classification: Cluster Analysis and Dendrograms

In general, data sets can involve several different groups or classes. There can be many reason of class variations; such as chemical compound type, sample preparation, process control parameter or etc. Methods developed for the classification of samples can be identified in two groups, which are unsupervised pattern recognition (Cluster analysis) and supervised pattern recognition (Classification).

### 2.6.5.1 Distance Measures in Cluster Analysis and Classification

The association of the cluster analysis methods on the sample treatment beyond the assumption that samples close in measurement space are similar and so they exist in the same group. Distance in the space between the samples can be defined in various ways. Most common known one is the Euclidian distance, where the distance  $d_{ij}$  between samples  $\mathbf{x}_i$  and  $\mathbf{x}_j$  is defined as in equation (2.23)

$$d_{ij} = \sqrt{(\mathbf{x}_i - \mathbf{x}_j)(\mathbf{x}_i - \mathbf{x}_j)^{\text{T}}} \quad (2.23)$$

The distance can also be defined by the PCA scores adjusted to unit variance. In this instance, measurement definition is known as a one type of Mahalanobis distance [241] and defined as in the following equation

$$d_{ij} = \sqrt{(\mathbf{t}_i - \mathbf{t}_j)\boldsymbol{\lambda}^{-1}(\mathbf{t}_i - \mathbf{t}_j)^T} \quad (2.24)$$

where,  $\mathbf{t}_i$  and  $\mathbf{t}_j$  are scores ( $\mathbf{t}_i$  and  $\mathbf{t}_j$  are  $1 \times k$  vectors containing the scores on all PCs of the model for samples  $\mathbf{x}_i$  and  $\mathbf{x}_j$ ), and  $\boldsymbol{\lambda}$  is the eigenvalues.

Another approach to measure the distance is Ward's method. Initial cluster distances in Ward method [242] defined as in Euclidian distance by minimum variance criterion as in equation (2.23). Ward's method is a criterion applied in hierarchical cluster analysis (HCA)

### 2.6.5.2 Cluster Analysis and Dendrograms

In cluster analysis, each sample at the beginning is considered as to be a lone cluster. Then, distance between the samples are calculated with one of the methods described in part 2.6.5.1, and smallest distances are found and linked to each other. Again the procedure is repeated and next closest are determined. Result are generally demonstrated by connection dendrograms (Figure 2.24). The results are often displayed as a connection dendrograms. An example of this is shown in Figure 2.24. Here the group of samples (with two measured parameters  $\mathbf{x}_1$  and  $\mathbf{x}_2$ ) are linked together, starting with the closest two, numbers 4 and 5, followed by the next closest samples, 1 and 2. Sample 6 is then linked to sample 5, which is already linked to sample 4, and so on [243].

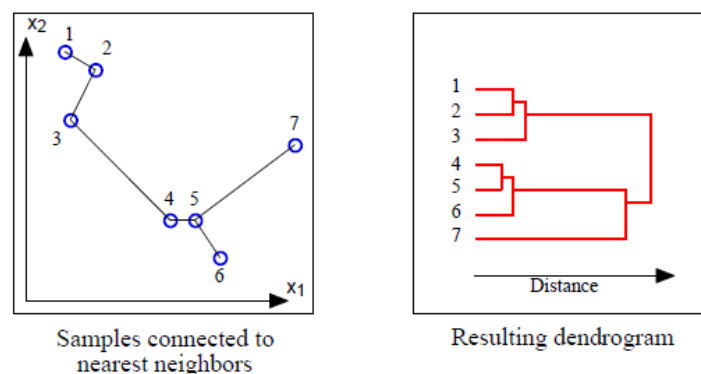


Figure 2.24 Example of linking in cluster analysis and resulting dendrograms [243]

## 2.6.6 Multivariate Regression

### 2.6.6.1 Multivariate Calibration (MLR)

#### Classical Least Squares (CLS)

In CLS model, measurements are the weighted sum of linearly independent signals [244]. In spectroscopy, measured response (spectra) are the sum of pure components weighted by the concentration of the analyte. So, model is

$$\mathbf{x} = \mathbf{p} \mathbf{S} \quad (2.25)$$

where  $\mathbf{x}$  is the measured response vector,  $\mathbf{S}$  is the pure component responses matrix, and  $\mathbf{p}$  is the vector of weights (i.e concentrations) of the analyte. In general, contribution of measurement to overall measurement,  $\mathbf{p}$  can be determined from  $\mathbf{x}$  of vector of measurements by the following equation (2.26)

$$\mathbf{p} = \mathbf{x} \mathbf{S}^+ \quad (2.26)$$

where  $\mathbf{S}^+$  is the pseudoinverse of  $\mathbf{S}$ , defined for CLS as:

$$\mathbf{S}^+ = \mathbf{S}^T (\mathbf{S} \mathbf{S}^T)^{-1} \quad (2.27)$$

To solve equation (2.25), the main drawback is the fact that pure responses of  $\mathbf{S}$  all spectroscopically active components must be known beforehand or estimated using known concentrations of all spectroscopically-active compounds [243]. Given a matrix of concentrations  $\mathbf{C}$  and measured spectra  $\mathbf{X}$ , an estimate of the pure component spectra  $\mathbf{S}_{\text{est}}$  can be obtained from

$$\mathbf{S}_{\text{est}} = (\mathbf{C}^T \mathbf{C})^{-1} \mathbf{C}^T \mathbf{X} \quad (2.28)$$

#### Inverse Least Squares (ILS)

ILS assumes that a regression vector  $\mathbf{b}$  can be used to determine the property of  $\mathbf{y}$  from measured variables  $\mathbf{X}$ . Thus the ILS model is

$$\mathbf{x} \mathbf{b} = \mathbf{y} \quad (2.29)$$

when this inverse model compared with classical model equation (2.25), it could be observable that responses in classical model are expressed as a function of pure component concentration ( $\mathbf{p}$ ), while single concentration ( $\mathbf{y}$ ) as a function of responses. ILS more widely applicable than CLS at least two reasons: 1) it is enough only to know

the property of  $\mathbf{y}$  and 2) there is no obligatory that this property should be a concentration [243].

The regression vector  $\mathbf{b}$  can be determined by means of collection of the measurements  $\mathbf{X}$  and the known values of the property of interest,  $\mathbf{y}$ . Thus,  $\mathbf{b}$  is expressed as the following equation (2.30)

$$\mathbf{b} = \mathbf{X}^+ \mathbf{y} \quad (2.30)$$

where,  $\mathbf{X}^+$  is the pseudoinverse of  $\mathbf{X}$ . It is possible to determine  $\mathbf{X}^+$ , but most probably the most common linear regression model is multiple linear regression (MLR) or with the other name ordinary least squares (OLS) [243]. In this case,  $\mathbf{X}^+$  is defined by

$$\mathbf{X}^+ = (\mathbf{X}^T \mathbf{X})^{-1} \mathbf{X}^T \quad (2.31)$$

In practice, MLR can fail as the some or all columns (response variables) are linear combination of other columns in  $\mathbf{X}$  or there exist fewer rows (samples) in  $\mathbf{X}$  than columns (variables). In both cases,  $(\mathbf{X}^T \mathbf{X})^{-1}$  would not exist. For these reasons, in spectroscopy, MLR model can suffer for the prediction because of insufficient number of representative samples compared the wavelength channels offered.

### 2.6.6.2 Principal Component Regression (PCR)

In MLR, lower number of samples compared to response variables and the possibility of collinearity of the response variables in  $\mathbf{X}$  can lead to weak calibration models in terms of prediction power. One of the regression models to deal with these problems is PCR [228, 245, 246]. In PCR, properties like concentrations are regressed onto PCA scores of measured variables (response). Therefore, the pseudoinverse of the response data matrix,  $\mathbf{X}^+$  estimated as

$$\mathbf{X}^+ = \mathbf{P} (\mathbf{T}^T \mathbf{T})^{-1} \mathbf{T}^T \quad (2.32)$$

Estimation performed by using equation (2.32) is much more stable than that of equation (2.31) because of the orthogonality of PCA scores ( $\mathbf{T}$ ) and loadings ( $\mathbf{P}$ ). Furthermore; the number of PCs are less than response variables and the number of calibration samples which can never be greater than the number of variables. Hence, PCR can be less over fitting compared to MLR. However, the important role of PCR is to predict the property of new samples rather than overfitting which could be possible by increasing the PC number in PCR model. The number PCs are typically determined by cross validation,

which requires a procedure where available data are split wise into a training and a test set. RMSECV error analysis are then determined as a function of the number of PCs retained in the PCR model. These procedure is repeated for several times by using in each time different training and test sets. Finally, a total RMSECV prediction error versus PCs plot is evaluated to decide PCs to be retained in the model to perform best prediction. The crucial point to consider is that as the number of PCs are increased PCR model converges to MLR model. But in real cases, it is the fact that optimal number of PCs to retain in the model is much fewer than the maximum [243].

### 2.6.6.3 Partial Least Squares (PLS)

PLS regression [228, 247-250] is both related with PCR and MLR. This is because of the fact that PCR finds factors that capture the greatest amount of variance in the predictor ( $\mathbf{X}$ ) variables (i.e spectra) and MLR try to find a single regression factor that best correlates predictor ( $\mathbf{X}$ ) variables with predicted ( $\mathbf{Y}$ ) variables (i.e concentration). As thought as to be the combination of MLR and PCR, PLS attempts to find factors which both capture variance and achieve correlation.

There are several ways to calculate PLS model parameters like NIPALS (Non-iterative partial least squares) and SIMPLS. In both methods, there is more than one predicted variable ( $\mathbf{Y}$ ). In the case of multiple  $\mathbf{Y}$  variables,  $\mathbf{U}$  scores and  $\mathbf{Q}$  loading matrices are also calculated for  $\mathbf{Y}$ . Also, a vector of inner relationships coefficients,  $\mathbf{b}$ , which relate the  $\mathbf{X}$  and  $\mathbf{Y}$  block scores, must also be calculated [243]

In NIPALS algorithm for PLS the scores, weights, loadings and inner-coefficients are calculated sequentially. Afterwards, usually one column of  $\mathbf{Y}$  with the greatest variance,  $\mathbf{y}_1$  is selected for the initial estimate of  $\mathbf{u}_1$ . Starting in the  $\mathbf{X}$  data block:

$$\mathbf{w}_1 = \frac{\mathbf{X}^T \mathbf{u}_1}{\|\mathbf{X}^T \mathbf{u}_1\|} \quad (2.33)$$

$$\mathbf{t}_1 = \mathbf{X} \mathbf{w}_1 \quad (2.34)$$

In the y data block:

$$\mathbf{q}_1 = \frac{\mathbf{Y}^T \mathbf{t}_1}{\|\mathbf{Y}^T \mathbf{t}_1\|} \quad (2.35)$$

$$\mathbf{u}_1 = \mathbf{Y} \mathbf{q}_1 \quad (2.36)$$

Convergence of final  $\mathbf{t}_1$  iteration result in Equation (2.34) is checked by comparing the previous iteration. If they are equal within rounding error, algorithm proceeds to equation (2.31). If not, algorithm returns to equation (2.33) by using the  $\mathbf{u}_1$  obtained previously from equation (2.36). If the  $\mathbf{Y}$ -block is univariate, Equations (2.35) and (2.36) can be omitted,  $\mathbf{q}_1$  can be set to 1, and no iteration is required.

The loading values of  $\mathbf{X}$  data block are then calculated, and the process of rescaling scores and weights as the following.

$$\mathbf{p}_1 = \frac{\mathbf{X}^T \mathbf{t}_1}{\|\mathbf{t}_1^T \mathbf{t}_1\|} \quad (2.37)$$

$$\mathbf{p}_{1\text{new}} = \frac{\mathbf{P}_{1\text{old}}}{\|\mathbf{P}_{1\text{old}}\|} \quad (2.38)$$

$$\mathbf{t}_{1\text{new}} = \mathbf{t}_{1\text{old}} \|\mathbf{P}_{1\text{old}}\| \quad (2.39)$$

$$\mathbf{w}_{1\text{new}} = \mathbf{w}_{1\text{old}} \|\mathbf{P}_{1\text{old}}\| \quad (2.40)$$

So then the inner correlation coefficient ( $\mathbf{b}$ ) is calculated

$$b_1 = \frac{\mathbf{u}_1^T \mathbf{t}_1}{\mathbf{t}_1^T \mathbf{t}_1} \quad (2.41)$$

The  $\mathbf{X}$  and  $\mathbf{Y}$  block residuals are then calculated after scores and loadings calculated for the first principal component which is known as latent variable in PLS as the following.

$$\mathbf{E}_1 = \mathbf{X} - \mathbf{t}_1 \mathbf{p}_1^T \quad (2.42)$$

$$\mathbf{F}_1 = \mathbf{Y} - \mathbf{b}_1 \mathbf{t}_1 \mathbf{q}_1^T \quad (2.43)$$

All procedure is then repeated for the next latent variable starting with equation (2.40) by replacing  $\mathbf{X}$  and  $\mathbf{Y}$  with their residuals  $\mathbf{E}_1$  and  $\mathbf{F}_1$  and all subscripts are increased by one.

PLS constructs the matrix inverse as

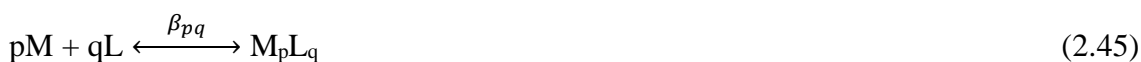
$$\mathbf{X}^+ = \mathbf{W}(\mathbf{P}^T \mathbf{W})^{-1} (\mathbf{T}^T \mathbf{T})^{-1} \mathbf{T}^T \quad (2.44)$$

where the  $\mathbf{W}$ ,  $\mathbf{P}$  and  $\mathbf{T}$  are as calculated above. When  $\mathbf{X}^+$  compared with equations (2.31) and (2.32) in equivalents in MLR and PCR, respectively, it can be seen that scores and loadings calculated in PLS are not the same as those calculated in PCA and PCR. Likewise to PCR, if the number of latent variable increased to maximum, PLS model converges to MLR, as well.

## 2.7 Software Assisted Stability Constant Determination: Hyperquad & HypSpec

A large number of computer programs have been published in order to explain equilibrium of solutions, species distributions and equilibrium constants predominantly from potentiometric, spectroscopic and NMR data. A detailed list of these programs can be found in the literature [83]. Gans et al. [83] have introduced a suite of programs to refine stability constants by means of thermodynamically information collected from different responses; such as potentiometric, spectrophotometric and NMR. They have developed Hyperquad for the evaluation of potentiometric data and HypSpec for the evaluation of spectrophotometric data. Hypsec could be used for the refinement of stability constants of species with titration and batch scale of data involving pH data. Both the Hyperquad and HypSpec use same set of equations and procedures to match experimental data to thermodynamic parameters. In this way, stability constants can be refined.

SUPERQUAD program forms the basis of Hyperquad and Hypspec programs. Gauss Newton or the Newton-Raphson method for the iterative solution of the mass balance equations present in the system were used [83]. For a system with multiple species can be represented by as the following equation (2.45)



System is in both programs are subjected to solve the mass balance equation (2.46) and (2.47) as a constraint.

$$[M]_{total} = [M] + \sum_{p=1, q=1}^{P, Q} p\beta_{p,q} [M]^p [L]^q \quad (2.46)$$

$$[L]_{total} = [L] + \sum_{p=1, q=1}^{P, Q} p\beta_{p,q} [M]^p [L]^q \quad (2.47)$$

where [L] and [M] free reagents; such as ligand and metal, respectively.  $\beta$  is the stability constants. Refinement solves the natural logarithm of  $\ln[M]$  and  $\ln[L]$  instead of solving [L] and [M]. In this way, another constrain which is positive molar concentration is satisfied. This is the main difference of Hyperquad and HypSpec programs from the former programs that allow the negative molar concentrations in the refinement of stability constants [83]. Initial estimated of  $\beta_{p,q}$  parameters can be used to improve to the fit models. Then, the fitted model, calculates the residuals between the model predicted

and experimental results by calculating the sum of square of residuals [83]. Residual calculation is different in each program slightly. In Hyperquad for potentiometric titrations, from the refined free concentrations a predicted pH is calculated and compared with the experimental value. On the other hand, in HypSpec, molar absorptivities are produced by the system by some useful factor analysis and iterations methods mentioned in Part 2.6.2, 2.6.3 and 2.6.4 to predict the spectra of individual pure components and then compared with the sum of experimentally obtained values. Refinement goes on until the sum of squares of fail and stability constants converge.

In Beer's Law,

$$A = l \sum_j \varepsilon_i c_i \quad (2.48)$$

where  $\varepsilon_i$  is a molar absorbance and  $c_i$  is the concentration of a species. If the species is a complex of formula  $M_pL_q$ , the concentration is given by

$$c_{pq} = \beta_{pq} [M]^p [L]^q \quad (2.49)$$

Thus in this example

$$A = \varepsilon_m [M] + \varepsilon_L [L] + \sum (\varepsilon_{pq} \beta_{pq}) [M]^p [L]^q \quad (2.50)$$

$\varepsilon_{pq}$  and  $\beta_{pq}$  are highly correlated because they are multiplied together in the Beer's law expression so that an increase in one can be compensated by a decrease in the other with little effect on the calculated absorbance. This is an inherent property of spectrophotometric data. In HypSpec spectra analysis, equation (2.48) is considered as in equation (2.51), where B represent constant error source origins from baseline.

$$A = l \sum_j \varepsilon_j C_j + B \quad (2.51)$$

Besides to eliminate baseline errors and minimize the collinearity of variables (wavelengths), HypSpec uses a standalone computational module, performing a kind of factor analysis, EFA. The aim of this module is to determine number of significantly absorbing species and estimate the concentration window regions. EFA procedure used by HypSpec is similar to one introduced in part 2.63 by using the SVD. Results of EFA procedure are presented graphically. In these graphics, eigenvectors, driven from SVD and linear combinations of any unit spectra (molar absorptivities) with a corresponding

set of eigenvalues versus wavelengths plots are used. Plots show number of selected eigenvector. Number of non-zero eigenvalues will correspond to number of absorbing species in the analyte.

While interpreting the EFA plots, there are some crucial points originated from experimental errors. Systematic errors will cause one or more additional singular values to be positive, while random errors will cause the singular values to differ slightly from zero. Thus, decision about the number of absorbing species has to be made when a singular value is effectively zero. However, complicated relation between the singular values and experimental error make this difficult.

Selection of the number of absorbing species can be performed via the help of EFA plots. Eigenvectors are the linear combination of unit spectra, but the coefficients of linear combinations are not known. Thus, eigenvectors do not look like a unit spectra. In this case, number of species more than one or two of expected should be entered. By this way, non-zero singular values can be distinguished and the number of absorbing species can be determined from the noisy graph of the outlier eigenvector shape in plots.

## CHAPTER 3

---

### EXPERIMENTAL

#### 3.1 Materials

Jeffamine<sup>®</sup> T-403 Mn 440 was purchased from Aldrich. Methyl acrylate, ethylenediamine, diethylene triamine, methanol, n-butanol, tris(hydroxymethyl) aminomethane were purchased from Merck. NaOH, 37 % HCl, NaH<sub>2</sub>PO<sub>4</sub>, KHP, NaBH<sub>4</sub> were supplied from Merck. All analytical grade divalent nitrate salts of Cd, Zn, Ni, Co, Cu were obtained from Merck and Fluka and used to prepare standard metal solutions. Carvedilol (CAR) was kindly supplied from DEVA Holding. All solutions were prepared by 18.2 MΩ Milli-Q deionized (Millipore) CO<sub>2</sub> free water. pH 4, 7, 11 buffer solutions for the calibration of were supplied from Merck. Dendrimer solutions were stored at 4C<sup>0</sup>. Unless otherwise stated all chemicals were in analytical grade and used without further purification. LPR ultrafiltration membranes, Amicon 8000 Stirred Cell and dialysis membranes having the molecular cut of size (MWCO) 500 and 1000 Da were supplied from Millipore.

#### 3.2 Instrumentation & Software

The CEM Focused Microwave<sup>™</sup> Synthesis System, Model Discover (CEM Corporation, North Carolina, USA) with a continuous microwave power delivery system with operator selectable power output from 0 - 300 watts (+/- 30 watts) programmable in 1-watt increments, infrared temperature control system programmable from 25- 250 °C, and 5-125 mL vessel capacity was used as microwave reactor.

Liquid-phase polymer-based retention (LPR) ultrafiltration membranes, Amicon 8000 Stirred Cell and dialysis membranes having the molecular cut of size (MWCO) 500, 1000, 3000 Da were supplied from Millipore.

Potentiometric titrations were carried out automatically by using TitroLine® 7000 (SI Analytics GmbH, Hattenbergstraße, Germany) autotitrator and thermostated titration vessel under nitrogen media. Temperature was kept at room temperature (25 +/-0.1) using Polysceince ® digital temperature controller circulating bath (Polysceince, Illinois, USA). Titrator was controlled by a personal computer with Schoot Instruments Titrisoft 2.6 software. pH data were collected with IoLine ultra precise glass electrode with iodine/iodide reference system. Glass electrode was calibrated with Merck pH 4, 7, 10 buffer solutions. Driven pH data were transformed to ascII.text format and imported to HYPERQUAD2008 version 5.2.19 software. This software was purchased from Protonic software (peter.gans@hyperquad.co.uk) and used to drive protonation constants from potentiometric data. Hyperquad Simulation and Speciation (HYSS) © 2009 Protonic Software was used to simulation of species distribution curves was performed by.

All spectroscopic data with pH values were evaluated with HypSpec 1.1.33 protonic software computer program (peter.gans@hyperquad.co.uk) to calculate pKa values of dendrimers. Species distribution plots were extracted from HypSpec 1.1.33.

Spectroscopic titrations were carried out automatically by using TitroLine® 7000 (SI Analytics GmbH, Hattenbergstraße, Germany) autotitrator equipped with thermostated titration vessel under nitrogen media and PG TG 70 UV-VIS spectrophotometer equipped with UVWin5 Software v5.0.5, together. PCA, MLR, PCR, PLS analysis were performed with MATLAB interfaced Solo+MIA - Copyright (C) 2007 - 2013 Eigenvector Research, Inc., Release: 7.0.3 software (Solo with Multivariate Image Analysis built-in)

### **3.3 Characterization**

The IR spectra (4000–400  $\text{cm}^{-1}$ , resolution 4  $\text{cm}^{-1}$ ) were recorded with a Perkin Elmer Spectrum One (Serial No: C68739) in ATR. NMR spectra were recorded on a Bruker Avance 400 MHz Spectrometer. Thermo Scientific Flash EA 2000 Series (Organic Elemental Analyzer) CHN/S was used for the determination of main organics. UV vis absorbance spectra were obtained using a PG T 70 Spectrometer (PG Instruments, England) and a quartz cuvette having an optical path length of 1.00 cm. GPC analyses

were performed on a Viscotek TDA302, with a column set Tosoh TSK G3000PWxl, and with buffer (PBS) as eluent.

### 3.4 Microwave Assisted Synthesis of Amine Terminated PAMAMs

#### 3.4.1 General Procedure for the Synthesis of Half Generations (0.5-3.5) of PAMAMs

A solution of MA in methanol was added to a stirred solution of full generation dendrimers (**0-4**) in methanol (2.5 molar eq. per terminal amine). The reaction was stirred at room temperature for 24 hours and excess reagents and methanol were removed under vacuum at 65 °C bath temperature and finally synthesized products were purified by means of LPR in each step. Yields were between 90-100 % depending on each generation (Table 4.1, Table 4.2, and Table 4.3).

##### 3.4.1.1 Synthesis of EDA Cored Half Generations (E0.5-E3.5)

###### Synthesis of E0.5

A well stirred solution of MA (21.49 g, 0.249 mol) in methanol (20 mL) was added to a stirred solution of **EDA** (3.0 g, 49.91 mmol) in methanol (20 mL). The final mixture was stirred at room temperature for 24 hours before being purified as described in general procedure for synthesis of half generation dendrimers. The product was a colorless oil (20.08 g, 99.5 %). Elemental analysis  $C_{18}H_{32}N_2O_8$ : Found: C, 53.75; H, 8.02; N, 7.03. Calc.: C, 53.45; H, 7.97; N, 6.93%. ATR-IR  $\nu_{max}/cm^{-1}$  1730 (C=O).  $^1H$  NMR  $\delta H(300$  MHz;  $D_2O$ ) 2.29 (8H, t,  $NR_2CH_2CH_2COOCH_3$ ), 2.41 (4H, s,  $R_2NCH_2CH_2NR_2$ ), 2.63 (8H, t,  $NR_2CH_2CH_2COOCH_3$ ), 3.61 (12H, s,  $COOCH_3$ ).  $^{13}C$  NMR  $\delta C(400$  MHz;  $CD_3OD$ ) 33.06 ( $CH_2CH_2COOCH_3$ ), 50.38 ( $CH_2CH_2COOCH_3$ ), 51.35 ( $COOCH_3$ ), 52.6 ( $NR_2CH_2CH_2NR_2$ ), 172.06 ( $COOCH_3$ ).

###### Synthesis of E1.5

A well stirred solution of MA (18.30 g, 0.212 mol) in methanol (20 ml) was added to a stirred solution of **E1.NH<sub>2</sub>** (10.99 g, 21.26 mmol) in methanol (20 ml). The final mixture was stirred at room temperature for 24 hours before being purified as described in general procedure for synthesis of half generation dendrimers. The product was a yellowish gel (23.58 g, 92 %). Elemental analysis  $C_{54}H_{96}N_{10}O_{20}$ : Found: C, 54.10; H, 8.07; N, 11.78.

Calc.: C, 53.81; H, 8.03; N, 11.62%. ATR-IR  $\nu_{\max}/\text{cm}^{-1}$  3296 (NH), 1730 (C=O), 1653 (HNC=O), 1535 (HNC=O).  $^1\text{H}$  NMR  $\delta\text{H}$ (300 MHz;  $\text{D}_2\text{O}$ ) 2.34 (16H, bm,  $\text{NR}_2\text{CH}_2\text{CH}_2\text{COOCH}_3$ ), 2.49 (16H, t,  $\text{NR}_2\text{CH}_2\text{CH}_2\text{COOCH}_3$ ), 2.69 (8H, bm,  $\text{CONHCH}_2\text{CH}_2\text{NR}_2$ ), 3.19 (8H, bm,  $\text{CONHCH}_2\text{CH}_2\text{NR}_2$ ), 3.65 (24H, s,  $\text{COOCH}_3$ ).  $^{13}\text{C}$  NMR  $\delta\text{C}$ (400 MHz;  $\text{D}_2\text{O}$ ) 31.42 ( $\text{CH}_2\text{CH}_2\text{COOCH}_3$ ), 47.50 ( $\text{CH}_2\text{CH}_2\text{COOCH}_3$ ), 48.7 ( $\text{CH}_2\text{CH}_2\text{NR}_2$ ), 50.01 ( $\text{COOCH}_3$ ), 171.1 ( $\text{NCH}_2\text{CH}_2\text{CONH}$ ), 171.8 ( $\text{COOCH}_3$ ).

### Synthesis of E2.5

A well stirred solution of MA (18.82 g, 0.218 mol) in methanol (20 ml) was added to a stirred solution of **E2.NH<sub>2</sub>** (15.64 g, 10.93 mmol) in methanol (20 ml). The final mixture was stirred at room temperature for 24 hours before being purified as described in general procedure for synthesis of half generation dendrimers. The product was a yellowish gel (29.16 g, 95%). Elemental analysis  $\text{C}_{126}\text{H}_{224}\text{N}_{26}\text{O}_{44}$ : Found: C, 54.4; H, 8.17; N, 13.12. Calc.: C, 53.91; H, 8.04; N, 12.97%. ATR-IR  $\nu_{\max}/\text{cm}^{-1}$  3294 (NH), 1731 (C=O), 1644(HNC=O), 1544 (HNC=O).  $^1\text{H}$  NMR  $\delta\text{H}$ (400 MHz;  $\text{D}_2\text{O}$ ) 2.37 (32H, bm,  $\text{NR}_2\text{CH}_2\text{CH}_2\text{COOCH}_3$ ), 2.45 (32H, t,  $\text{NR}_2\text{CH}_2\text{CH}_2\text{COOCH}_3$ ), 2.64 (16H, bm,  $\text{CONHCH}_2\text{CH}_2\text{NR}_2$ ), 3.15 (16H, bm,  $\text{CONHCH}_2\text{CH}_2\text{NR}_2$ ), 3.61 (48H, s,  $\text{COOCH}_3$ ).  $^{13}\text{C}$  NMR  $\delta\text{C}$ (400 MHz;  $\text{D}_2\text{O}$ ) 31.96 ( $\text{CH}_2\text{CH}_2\text{COOCH}_3$ ), 47.67 ( $\text{CH}_2\text{CH}_2\text{COOCH}_3$ ), 48.18 ( $\text{CH}_2\text{CH}_2\text{NR}_2$ ), 49.54 ( $\text{COOCH}_3$ ), 170.56, 170.87 ( $\text{NCH}_2\text{CH}_2\text{CONH}$ ), 171.56 ( $\text{COOCH}_3$ ).

### Synthesis of E3.5

A well stirred solution of MA (15.43 g, 0.179 mol) in methanol (20 ml) was added to a stirred solution of **E3.NH<sub>2</sub>** (14.60 g, 4.48 mmol) in methanol (20 ml). The final mixture was stirred at room temperature for 24 hours before being purified as described in general procedure for synthesis of half generation dendrimers. The product was a yellowish gel (25.06 g, 93 %). Elemental analysis  $\text{C}_{270}\text{H}_{480}\text{N}_{58}\text{O}_{92}$ : Found: C, 55.21; H, 8.21; N, 13.76. Calc.: C, 53.95; H, 8.05; N, 13.51%. ATR-IR  $\nu_{\max}/\text{cm}^{-1}$  3271 (NH), 1726 (C=O), 1638 (HNC=O), 1557 (HNC=O).  $^1\text{H}$  NMR  $\delta\text{H}$ (400 MHz;  $\text{D}_2\text{O}$ ) 2.40 (64H, bm,  $\text{NR}_2\text{CH}_2\text{CH}_2\text{COOCH}_3$ ), 2.52 (64H, t,  $\text{NR}_2\text{CH}_2\text{CH}_2\text{COOCH}_3$ ), 2.67 (32H, bm,  $\text{CONHCH}_2\text{CH}_2\text{NR}_2$ ), 3.17 (32H, bm,  $\text{CONHCH}_2\text{CH}_2\text{NR}_2$ ), 3.62 (96H, s,  $\text{COOCH}_3$ ).  $^{13}\text{C}$  NMR  $\delta\text{C}$ (400 MHz;  $\text{D}_2\text{O}$ ) 31.32 ( $\text{CH}_2\text{CH}_2\text{COOCH}_3$ ), 47.41 ( $\text{CH}_2\text{CH}_2\text{COOCH}_3$ ), 48.47 ( $\text{CH}_2\text{CH}_2\text{NR}_2$ ) 50.35 ( $\text{COOCH}_3$ ), 171.02, 171.15, 171.43 ( $\text{NCH}_2\text{CH}_2\text{CONH}$ ), 172.01 ( $\text{COOCH}_3$ ).

### 3.4.1.2 Synthesis of DETA Cored Half Generations (D0.5-D3.5)

#### Synthesis of D0.5

A well stirred solution of MA (18.72 g, 0.217 mol) in methanol (20 mL) was added to a stirred solution of DETA (3.58 g, 34.78 mmol) in methanol (20 mL). The final mixture was stirred at room temperature for 24 hours before being purified as described in general procedure for synthesis of half generation dendrimers. The product was a colorless oil (17.265 g, 96.45 %). Elemental Analysis  $C_{24}H_{43}N_3O_{10}$ : Found: C, 54.30; H, 8.17; N, 7.98. Calc.: C, 54.02; H, 8.12; N, 7.87%. ATR-IR  $\nu_{\max}/\text{cm}^{-1}$  1731 (C=O).  $^1\text{H}$  NMR  $\delta\text{H}$ (300 MHz; DMSO- $d_6$ ) 2.60 (14H, bm,  $\text{CH}_2\text{CH}_2\text{COOCH}_3$  (10H),  $\text{NR}_2\text{CH}_2\text{CH}_2\text{NRCH}_2\text{CH}_2\text{NR}_2$  (4H)), 2.7 (2H, m,  $\text{CH}_2\text{CH}_2\text{COOCH}_3$ ), 2.9 (12H, t,  $\text{NR}_2\text{CH}_2\text{CH}_2\text{NRCH}_2\text{CH}_2\text{NR}_2$  (4H),  $\text{CH}_2\text{CH}_2\text{COOCH}_3$  (8H)), 3.8 (15H,  $\text{COOCH}_3$ ).  $^{13}\text{C}$  NMR  $\delta\text{C}$ (300 MHz; DMSO- $d_6$ ) 32.7, 32.8 (5C,  $\text{CH}_2\text{CH}_2\text{COOCH}_3$ ), 49.8, 50.5 (5C,  $\text{CH}_2\text{CH}_2\text{COOCH}_3$ ), 51.8 (5C,  $\text{COOCH}_3$ ) 52.0 (2C,  $\text{NR}_2\text{CH}_2\text{CH}_2\text{NRCH}_2\text{CH}_2\text{NR}_2$ ), 52.6 (2C,  $\text{NR}_2\text{CH}_2\text{CH}_2\text{NRCH}_2\text{CH}_2\text{NR}_2$ ), 173.1, 173.2 ( $\text{COOCH}_3$ ).

#### Synthesis of D1.5

A well stirred solution of MA (16.35 g, 0.190 mol) in methanol (20 mL) was added to a stirred solution of **D1.NH<sub>2</sub>** (10.24 g, 15.20 mmol) in methanol (20 mL). The final mixture was stirred at room temperature for 24 hours before being purified as described in general procedure for synthesis of half generation dendrimers. The product was a yellowish gel (22.39 g, 96.00 %). Elemental analysis  $C_{69}H_{123}N_{13}O_{25}$ : Found: C, 54.20; H, 8.17; N, 12.02. Calc.: C, 54.00; H, 8.08; N, 11.86%. ATR-IR  $\nu_{\max}/\text{cm}^{-1}$  1730 (C=O).  $^1\text{H}$  NMR  $\delta\text{H}$ (300 MHz; DMSO- $d_6$ ) 2.61 (20H, m,  $\text{NR}_2\text{CH}_2\text{CH}_2\text{COOCH}_3$ ), 2.86 (20H, m,  $\text{NR}_2\text{CH}_2\text{CH}_2\text{COOCH}_3$ ), 2.88 (20H, m,  $\text{CONHCH}_2\text{CH}_2\text{NR}_2$ ), 3.27 (20H, m,  $\text{CONHCH}_2\text{CH}_2\text{NR}_2$ ), 3.78 (30H, s,  $\text{COOCH}_3$ ).  $^{13}\text{C}$  NMR  $\delta\text{C}$ (300 MHz; DMSO- $d_6$ ) 32.66 ( $\text{NR}_2\text{CH}_2\text{CH}_2\text{CONH}$ ), 37.29 ( $\text{CONHCH}_2\text{CH}_2\text{NR}_2$ ), 50.50 ( $\text{NR}_2\text{CH}_2\text{CH}_2\text{CONH}$ ) 51.83 ( $\text{NR}_2\text{CH}_2\text{CH}_2\text{CONH}$ ), 51.87 ( $\text{COOCH}_3$ ), 171.70, 171.70, 173.13, 173.19 ( $\text{COOCH}_3$ ).

#### Synthesis of D2.5

A well stirred solution of MA (8.02 g, 0.093 mol) in methanol (20 mL) was added to a stirred solution of **D2.NH<sub>2</sub>** (6.76 g, 3.72 mmol) in methanol (20 mL). The final mixture was stirred at room temperature for 24 hours before being purified as described in general procedure for synthesis of half generation dendrimers. The product was a yellowish gel (12.642 g, 96.00 %). Elemental analysis  $C_{159}H_{283}N_{33}O_{55}$ : Found: C, 54.49; H, 8.22; N,

13.19. Calc.: 53.99; H, 8.06; N, 13.07%. ATR-IR  $\nu_{\max}/\text{cm}^{-1}$  1730 (C=O).  $^1\text{H}$  NMR  $\delta\text{H}$ (300 MHz; DMSO- $d_6$ ) 2.62 (40H, m,  $\text{NR}_2\text{CH}_2\text{CH}_2\text{COOCH}_3$ ), 2.85 (40H, m,  $\text{NR}_2\text{CH}_2\text{CH}_2\text{COOCH}_3$ ), 2.87 (40H, m,  $\text{CONHCH}_2\text{CH}_2\text{NR}_2$ ), 3.29 (40H, brm,  $\text{CONHCH}_2\text{CH}_2\text{NR}_2$ ), 3.78 (60H, s,  $\text{COOCH}_3$ ).  $^{13}\text{C}$  NMR  $\delta\text{C}$ (300 MHz; DMSO- $d_6$ ) 32.66 (20C,  $\text{NR}_2\text{CH}_2\text{CH}_2\text{COOCH}_3$ ), 37.28 (10C,  $\text{CONHCH}_2\text{CH}_2\text{NR}_2$ ), 50.48 (20C,  $\text{NR}_2\text{CH}_2\text{CH}_2\text{COOCH}_3$ ), 51.83 (10C,  $\text{CONHCH}_2\text{CH}_2\text{NR}_2$ ), 51.87 (20C,  $\text{COOCH}_3$ ), 172.89, 173.13, 173.19 (10C,  $\text{NR}_2\text{CH}_2\text{CH}_2\text{CONH}$ ), 174.84 (20C,  $\text{COOCH}_3$ ).

### Synthesis of D3.5

A well stirred solution of MA (8.53 g, 0.100 mol) in methanol (20 mL) was added to a stirred solution of **D3.NH<sub>2</sub>** (8.12 g, 1.98 mmol) in methanol (20 mL). The final mixture was stirred at room temperature for 24 hours before being purified as described in general procedure for synthesis of half generation dendrimers. The product was a yellowish gel (14.20 g, 95.00 %). Elemental analysis  $\text{C}_{339}\text{H}_{603}\text{N}_{73}\text{O}_{115}$ : Found: C, 55.12; H, 8.27; N, 13.81. Calc.: C, 53.99; H, 8.06; N, 13.56%. ATR-IR  $\nu_{\max}/\text{cm}^{-1}$  1730 (C=O).  $^1\text{H}$  NMR  $\delta\text{H}$ (300 MHz; DMSO- $d_6$ ) 2.60 (80H, m,  $\text{NR}_2\text{CH}_2\text{CH}_2\text{COOCH}_3$ ), 2.86 (80H, brm,  $\text{NR}_2\text{CH}_2\text{CH}_2\text{COOCH}_3$ ), 2.89 (80H, brm,  $\text{CONHCH}_2\text{CH}_2\text{NR}_2$ ), 3.27 (80H, brm,  $\text{CONHCH}_2\text{CH}_2\text{NR}_2$ ), 3.78 (120H, s,  $\text{COOCH}_3$ ).  $^{13}\text{C}$  NMR  $\delta\text{C}$ (300 MHz; DMSO- $d_6$ ) 32.66 (40C,  $\text{NR}_2\text{CH}_2\text{CH}_2\text{COOCH}_3$ ), 37.31 (20C,  $\text{CONHCH}_2\text{CH}_2\text{NR}_2$ ), 51.83 (40C,  $\text{NR}_2\text{CH}_2\text{CH}_2\text{COOCH}_3$ ), 51.87 (40C,  $\text{COOCH}_3$ ), 52.92 (20C,  $\text{CONHCH}_2\text{CH}_2\text{NR}_2$ ), 171.71, 171.77, 171.85 (20C,  $\text{NCH}_2\text{CH}_2\text{CONH}$ ), 173.13 (40C,  $\text{COOCH}_3$ ).

### 3.4.1.3 Synthesis of Jeffamine<sup>®</sup> T-403 Cored Half Generations (P0.5-P3.5)

#### Synthesis of P0.5

A well stirred solution of MA (12.065 g, 0.140 mol) in methanol (20 mL) was added to a stirred solution of amine terminated ether (Jeffamine<sup>®</sup> T-403) (8.2220 g, 18.68 mmol) [trimethylolpropane tris[poly(propylene glycol)] in methanol (20 mL). The final mixture was stirred at room temperature for 24 hours before being purified as described in general procedure for synthesis of half generation dendrimers. The product was a colorless oil (16.62 g, 93 %). Elemental analysis  $\text{C}_{48}\text{H}_{89}\text{N}_3\text{O}_{18}$ : Found: C, 58.21; H, 9.05; N, 4.33. Calc.: C, 57.87; H, 9.00; N, 4.22%. ATR-IR  $\nu_{\max}/\text{cm}^{-1}$  1735 (C=O).  $^1\text{H}$ -NMR  $\delta\text{H}$  (400MHz; DMSO) 2.39 (12H, t,  $\text{CH}_2\text{CH}_2\text{COOCH}_3$ ), 2.75 (12H, t,  $\text{CH}_2\text{CH}_2\text{COOCH}_3$ ), 3.63 (18H, s,  $\text{COOCH}_3$ ).  $^{13}\text{C}$ -NMR  $\delta\text{C}$ (400 MHz; DMSO) 173.06 ( $\text{COOCH}_3$ ), 51.35 ( $\text{COOCH}_3$ ), 55.19 (CNR<sub>2</sub>), 46.38 ( $\text{CH}_2\text{CH}_2\text{COOCH}_3$ ), 34.46 ( $\text{CH}_2\text{CH}_2\text{COOCH}_3$ ).

### Synthesis of P1.5

A well stirred solution of MA (13.74 g, 0.154 mol) in methanol (20 ml) was added to a stirred solution of **P1.NH<sub>2</sub>** (12.00 g, 10.20 mmol) in methanol (20 ml). The final mixture was stirred at room temperature for 24 hours before being purified as described in general procedure for synthesis of half generation dendrimers. The product was a yellowish gel (22.55 g, 98 %). Elemental analysis C<sub>104</sub>H<sub>189</sub>N<sub>15</sub>O<sub>34</sub>: Found: C, 57.12; H, 8.87; N, 9.75. Calc.: C, 56.94; H, 8.68; N, 9.58%. ATR-IR  $\nu_{\max}/\text{cm}^{-1}$  3318 (NH), 1733 (C=O), 1650 (HNC=O), 1535 (HNCO). <sup>1</sup>H-NMR  $\delta\text{H}(400 \text{ MHz; DMSO})$  2.40 (24H, t, CH<sub>2</sub>CH<sub>2</sub>COOCH<sub>3</sub>), 2.72 (24H, t, CH<sub>2</sub>CH<sub>2</sub>COOCH<sub>3</sub>), 3.63 (36H, t, COOCH<sub>3</sub>) ppm. <sup>13</sup>C-NMR  $\delta\text{C}(400 \text{ MHz; DMSO})$  172.91 (COOCH<sub>3</sub>), 75.25 (COOCH<sub>3</sub>), 51.49 (CH<sub>2</sub>CH<sub>2</sub>NR<sub>2</sub>), 49.69 (CH<sub>2</sub>CH<sub>2</sub>COOCH<sub>3</sub>), 32.56 (CH<sub>2</sub>CH<sub>2</sub>COOCH<sub>3</sub>).

### Synthesis of P2.5

A well stirred solution of MA (13.95 g, 0.162 mol) in methanol (20 ml) was added to a stirred solution of **P2.NH<sub>2</sub>** (13.48 g, 5.40 mmol) in methanol (20 ml). The final mixture was stirred at room temperature for 24 hours before being purified as described in general procedure for synthesis of half generation dendrimers. The product was a yellowish gel (23.65 g, 96 %). Elemental analysis C<sub>132</sub>H<sub>245</sub>N<sub>27</sub>O<sub>42</sub>: Found: C, 55.50; H, 8.78; N, 13.25. Calc.: C, 55.00; H, 8.57, N, 13.12%. ATR-IR  $\nu_{\max}/\text{cm}^{-1}$  3291 (NH), 1732 (C=O), 1644(HNC=O), 1535 (HNC=O). <sup>1</sup>H-NMR  $\delta\text{H}(400 \text{ MHz; DMSO})$  2.42 (48H, t, CH<sub>2</sub>CH<sub>2</sub>COOCH<sub>3</sub>), 2.74 (48H, t, CH<sub>2</sub>CH<sub>2</sub>COOCH<sub>3</sub>), 3.65 (72H, s, COOCH<sub>3</sub>). <sup>13</sup>C-NMR  $\delta\text{C}(400 \text{ MHz; DMSO})$  172.86 (COO CH<sub>3</sub>), 75.41 (COOCH<sub>3</sub>), 51.48 (CH<sub>2</sub>CH<sub>2</sub>NR<sub>2</sub>), 49.15 (CH<sub>2</sub>CH<sub>2</sub>COOCH<sub>3</sub>), 32.63 (CH<sub>2</sub>CH<sub>2</sub>COOCH<sub>3</sub>).

### Synthesis of P3.5

A well stirred solution of MA (11.838 g, 0.138 mol) in methanol (20 ml) was added to a stirred solution of **P3.NH<sub>2</sub>** (12.00 g, 2.29 mmol) in methanol (20 ml). The final mixture was stirred at room temperature for 24 hours before being purified as described in general procedure for synthesis of half generation dendrimers. The product was a yellowish gel (19.75 g, 92 %). Elemental analysis C<sub>240</sub>H<sub>437</sub>N<sub>51</sub>O<sub>78</sub>: Found: C, 56.17; H, 8.65; N, 13.81. Calc.: C, 54.54; H, 8.33; N, 13.52%. ATR-IR  $\nu_{\max}/\text{cm}^{-1}$  3291 (NH), 1732 (C=O), 1642 (HNC=O), 1535 (HNC=O). <sup>1</sup>H-NMR  $\delta\text{H}(400 \text{ MHz; DMSO})$  2.42 (96H, t, CH<sub>2</sub>CH<sub>2</sub>COOCH<sub>3</sub>), 2.68 (96H, t, CH<sub>2</sub>CH<sub>2</sub>COOCH<sub>3</sub>), 3.59 (144H s, CH<sub>2</sub>CH<sub>2</sub>COOCH<sub>3</sub>). <sup>13</sup>C-NMR  $\delta\text{C}(400 \text{ MHz; DMSO})$  172.43 (COOCH<sub>3</sub>), 51.15 (CH<sub>2</sub>CH<sub>2</sub>COOCH<sub>3</sub>), 48.87 (CH<sub>2</sub>CH<sub>2</sub>COOCH<sub>3</sub>), 32.00 (CH<sub>2</sub>CH<sub>2</sub>COOCH<sub>3</sub>).

### 3.4.2 General Procedure for the Synthesis of Full Generations (1-4.NH<sub>2</sub>)

An ester branched half generation dendrimers (**0.5-3.5**) dissolved in 1-10 mL of methanol depending on the generation size. 10 molar equivalents of EDA per ester branched half generation (**0.5-3.5**) was added to stirred solution of half generation dendrimer solution. The final mixture was irradiated with CEM Discovery Microwave at 200-250 W between the ranges of 30-80 minutes depending on the synthesis product (1-4) by using open vessel method. Temperature was kept approximately at bulk temperature 120-130 °C during microwave irradiation. The amount of methanol to be added also was determined by considering the preservation of the temperature range between 120 and 130 °C. The final traces of excess EDA, firstly forced to remove under vacuum below the bath temperature 65 °C. Then, the final traces of EDA were removed by using 50 mL of n-butanol as hydrogen competitive reagent for three times. Then product was purified with LPR method. In other words, it was continuously dialyzed with 50 % aqueous methanol solution under 15 psi nitrogen (N<sub>2</sub>) gas pressure for 24 hours by using Millipore ultrafiltration disks having the molecular cut of size 1, 3 kDA depending on full generation product size. Final methanolic solution of retentate product was removed under vacuum below the bath temperature of 65 °C. Yields were between the ranges of 90-97.5 % (Table 4.4, Table 4.5 and Table 4.6).

#### 3.4.2.1 Synthesis of EDA Cored Full Generations (E1-E4.NH<sub>2</sub>)

##### Synthesis of E1.NH<sub>2</sub>

EDA (81.31 g, 1.35 mol) was added to a stirred solution of (13.68 g, 33.81 mmol) **E0.5** in 2 mL methanol. The final mixture was irradiated at 200 W for 60 minutes at 124 °C before being purified as described in the general procedure for the synthesis of full generation dendrimers. The product was a yellowish gel (16.60 g, 95 %). Elemental analysis C<sub>22</sub>H<sub>48</sub>N<sub>10</sub>O<sub>4</sub>: Found: C, 51.30; H, 9.45; N, 27.36. Calc.: C, 51.14; H, 9.36; N, 27.11%. ATR-IR  $\nu_{\max}/\text{cm}^{-1}$  3282 (NH), 1641 (HNC=O), 1548 (HNC=O). <sup>1</sup>H NMR  $\delta\text{H}(400 \text{ MHz}; \text{D}_2\text{O})$  2.25 (8H, bm, NR<sub>2</sub>CH<sub>2</sub>CH<sub>2</sub>CONH), 2.57 (8H, t, NR<sub>2</sub>CH<sub>2</sub>CH<sub>2</sub>CONH), 2.71 (8H, t, CONHCH<sub>2</sub>CH<sub>2</sub>NH<sub>2</sub>), 3.31 (8H, bm, CONHCH<sub>2</sub>CH<sub>2</sub>NH<sub>2</sub>). <sup>13</sup>C NMR  $\delta\text{C}(400 \text{ MHz}; \text{D}_2\text{O})$  33.14 (NCH<sub>2</sub>CH<sub>2</sub>CONH), 40.60 (CONHCH<sub>2</sub>CH<sub>2</sub>NH<sub>2</sub>), 41.10 (CONHCH<sub>2</sub>CH<sub>2</sub>NH<sub>2</sub>), 49.50 (NCH<sub>2</sub>CH<sub>2</sub>CONH), 172.0 (NCH<sub>2</sub>CH<sub>2</sub>CONH).

### Synthesis of E2.NH<sub>2</sub>

EDA (76.253 g, 1.26 mol) was added to a stirred solution of (19.12 g, 15.85 mmol) **E1.5** in 4 mL methanol. The final mixture was irradiated at 200 W for 60 minutes at 128 °C before being purified as described in the general procedure for the synthesis of full generation dendrimers. The product was a yellowish gel (23.97 g, 94.6 %). Elemental analysis C<sub>62</sub>H<sub>128</sub>N<sub>26</sub>O<sub>12</sub>: Found: C, 52.31; H, 9.14; N, 25.68. Calc.: C, 52.08; H, 9.02; N, 25.47%. ATR-IR  $\nu_{\max}/\text{cm}^{-1}$  3280 (NH), 1635 (HNC=O), 1549 (HNC=O). <sup>1</sup>H NMR  $\delta\text{H}(400 \text{ MHz}; \text{D}_2\text{O})$  2.25 (16H, bm, NR<sub>2</sub>CH<sub>2</sub>CH<sub>2</sub>CONH), 2.55 (16H, bm, NR<sub>2</sub>CH<sub>2</sub>CH<sub>2</sub>CONH), 2.66 (16H, bm, CONHCH<sub>2</sub>CH<sub>2</sub>NH<sub>2</sub>), 3.12 (16H, bm, CONHCH<sub>2</sub>CH<sub>2</sub>NH<sub>2</sub>). <sup>13</sup>C NMR  $\delta\text{C}(400 \text{ MHz}; \text{D}_2\text{O})$  33.64 (NCH<sub>2</sub>CH<sub>2</sub>CONH), 40.12 (CONHCH<sub>2</sub>CH<sub>2</sub>NH<sub>2</sub>), 42.32 (CONHCH<sub>2</sub>CH<sub>2</sub>NH<sub>2</sub>), 50.10 (NCH<sub>2</sub>CH<sub>2</sub>CONH), 170.8, 171.12 (NCH<sub>2</sub>CH<sub>2</sub>CONH).

### Synthesis of E3.NH<sub>2</sub>

EDA (68.66 g, 1.14 mol) was added to a stirred solution of (20.05 g, 7.14 mmol) **E2.5** in 3.5 mL methanol. The final mixture was irradiated at 200 W for 60 minutes at 124 °C before being purified as described in the general procedure for the synthesis of full generation dendrimers. The product was yellowish gel (20.93 g, 90 %). Elemental analysis C<sub>142</sub>H<sub>288</sub>N<sub>58</sub>O<sub>28</sub>: Found: C, 52.65; H, 9.05; N, 25.24. Calc.: C, 52.38; H, 8.91; N, 24.95%. ATR-IR  $\nu_{\max}/\text{cm}^{-1}$  3283 (NH), 1639 (HNC=O), 1546 (HNC=O). <sup>1</sup>H NMR  $\delta\text{H}(400 \text{ MHz}; \text{D}_2\text{O})$  2.26 (32H, brm, NR<sub>2</sub>CH<sub>2</sub>CH<sub>2</sub>CONH), 2.58 (32H, brm, NR<sub>2</sub>CH<sub>2</sub>CH<sub>2</sub>CONH), 2.64 (32H, t, CONHCH<sub>2</sub>CH<sub>2</sub>NH<sub>2</sub>), 3.12 (32H, brm, CONHCH<sub>2</sub>CH<sub>2</sub>NH<sub>2</sub>). <sup>13</sup>C NMR  $\delta\text{C}(400 \text{ MHz}; \text{D}_2\text{O})$  32.23 (NCH<sub>2</sub>CH<sub>2</sub>CONH), 39.54 (CONHCH<sub>2</sub>CH<sub>2</sub>NH<sub>2</sub>), 41.02 (CONHCH<sub>2</sub>CH<sub>2</sub>NH<sub>2</sub>), 49.67 (NCH<sub>2</sub>CH<sub>2</sub>CONH), 171.42, 171.54, 171.69 (NCH<sub>2</sub>CH<sub>2</sub>CONH).

### Synthesis of E4.NH<sub>2</sub>

EDA (50.70 g, 0.84 mol) was added to a stirred solution of (15.85 g, 2.63 mmol) **E3.5** in 4 mL methanol. The final mixture was irradiated at 200 W for 60 minutes at 120 °C before being purified as described in the general procedure for the synthesis of full generation dendrimers. The product was a yellowish gel (16.39 g, 90 %). Elemental analysis C<sub>302</sub>H<sub>608</sub>N<sub>122</sub>O<sub>60</sub>: Found: C, 52.85; H, 9.02; N, 24.93. Calc.: C, 52.50; H, 8.87; N, 24.73%. ATR-IR  $\nu_{\max}/\text{cm}^{-1}$  3270 (NH), 1643 (HNC=O), 1550 (HNC=O). <sup>1</sup>H NMR  $\delta\text{H}(400 \text{ MHz}; \text{D}_2\text{O})$  2.24 (64H, brm, NR<sub>2</sub>CH<sub>2</sub>CH<sub>2</sub>CONH), 2.52 (64H, t, NR<sub>2</sub>CH<sub>2</sub>CH<sub>2</sub>CONH), 2.63

(64H, t, CONHCH<sub>2</sub>CH<sub>2</sub>NH<sub>2</sub>), 3.11 (64H, brm, CONHCH<sub>2</sub>CH<sub>2</sub>NH<sub>2</sub>). <sup>13</sup>C NMR δC(400 MHz; D<sub>2</sub>O) 32.02 (NCH<sub>2</sub>CH<sub>2</sub>CONH), 39.43 (CONHCH<sub>2</sub>CH<sub>2</sub>NH<sub>2</sub>), 41.89 (CONHCH<sub>2</sub>CH<sub>2</sub>NH<sub>2</sub>), 48.22 (NCH<sub>2</sub>CH<sub>2</sub>CONH), 170.44, 170.52, 170.58, 170.67 (NCH<sub>2</sub>CH<sub>2</sub>CONH).

### 3.4.2.2 Synthesis of DETA Cored Full Generations (D1-D4.NH<sub>2</sub>)

#### Synthesis of D1NH<sub>2</sub>

EDA (64.68 g, 1.07 mol) was added to a stirred solution of (11.48 g, 21.47 mmol) **D0.5** in 9 mL methanol. The final mixture was irradiated at 250 W for 60 minutes at 124 °C before being purified as described in the general procedure for the synthesis of full generation dendrimers. The product was a yellowish gel (14.075 g, 97 %). Elemental analysis C<sub>29</sub>H<sub>63</sub>N<sub>13</sub>O<sub>5</sub>: Found: C, 51.94; H, 9.51; N, 27.27. Calc.: C, 51.69; H, 9.42; N, 27.02%. ATR-IR ν<sub>max</sub>/cm<sup>-1</sup> 3279(NH), 1639 (HNC=O), 1550 (HNC=O). <sup>1</sup>H NMR δH(300 MHz; DMSO-d<sub>6</sub>) 2.40 (14H, brm, NR<sub>2</sub>CH<sub>2</sub>CH<sub>2</sub>CONH (10), NR<sub>2</sub>CH<sub>2</sub>CH<sub>2</sub>NRCH<sub>2</sub>CH<sub>2</sub>NR<sub>2</sub> (4H)), 2.75 (12H, brm, NR<sub>2</sub>CH<sub>2</sub>CH<sub>2</sub>CONH (8H), NR<sub>2</sub>CH<sub>2</sub>CH<sub>2</sub>NRCH<sub>2</sub>CH<sub>2</sub>NR<sub>2</sub> (4H)), 2.79 (t, 2H, core HR<sub>2</sub>CH<sub>2</sub>CH<sub>2</sub>CONH), 2.88 (10H, t, CONHCH<sub>2</sub>CH<sub>2</sub>NH<sub>2</sub>), 3.23 (10H, m, CONHCH<sub>2</sub>CH<sub>2</sub>NH<sub>2</sub>), 8.15 (5H, bs, CONHCH<sub>2</sub>CH<sub>2</sub>NH<sub>2</sub>). <sup>13</sup>C NMR δC(300 MHz; DMSO-d<sub>6</sub>) 36.71 (1C, NR<sub>2</sub>CH<sub>2</sub>CH<sub>2</sub>CONH), 36.74 (4C, NR<sub>2</sub>CH<sub>2</sub>CH<sub>2</sub>CONH), 42.0 (5C, CONHCH<sub>2</sub>CH<sub>2</sub>NH<sub>2</sub>), 42.81 (5C, CONHCH<sub>2</sub>CH<sub>2</sub>NH<sub>2</sub>), 46.27 (2C, NR<sub>2</sub>CH<sub>2</sub>CH<sub>2</sub>NR<sub>2</sub>), 49.23 (2C, NR<sub>2</sub>CH<sub>2</sub>CH<sub>2</sub>NR<sub>2</sub>), 50.98 (4C, NR<sub>2</sub>CH<sub>2</sub>CH<sub>2</sub>CONH), 52.8 (1C, NR<sub>2</sub>CH<sub>2</sub>CH<sub>2</sub>CONH), 172.1, 172.14 (NCH<sub>2</sub>CH<sub>2</sub>CONH).

#### Synthesis of D2NH<sub>2</sub>

EDA (64.63 g, 1.07 mol) was added to a stirred solution of (16.51 g, 10.75 mmol) **D 1.5** in 10 mL methanol. The final mixture was irradiated at 250 W for 80 minutes at 126 °C before being purified as described in the general procedure for the synthesis of full generation dendrimers. The product was a yellowish gel (19.042 g, 97.50 %). Elemental analysis C<sub>79</sub>H<sub>163</sub>N<sub>33</sub>O<sub>15</sub>: Found: C, 52.52; H, 9.17; N, 25.66. Calc.: C, 52.27; H, 9.05; N, 25.46%. ATR-IR ν<sub>max</sub>/cm<sup>-1</sup> 3283(NH), 1652 (HNC=O), 1594 (HNC=O). <sup>1</sup>H NMR δH(300 MHz; DMSO-d<sub>6</sub>) 2.38 (20H, bm, NR<sub>2</sub>CH<sub>2</sub>CH<sub>2</sub>CONH), 2.73 (20H, bm, NR<sub>2</sub>CH<sub>2</sub>CH<sub>2</sub>CONH), 2.86 (20H, t, CONHCH<sub>2</sub>CH<sub>2</sub>NH<sub>2</sub>), 3.22 (20H, m, CONHCH<sub>2</sub>CH<sub>2</sub>NH<sub>2</sub>), 8.14 (15H, bs, CONHCH<sub>2</sub>CH<sub>2</sub>NH<sub>2</sub>). <sup>13</sup>C NMR δC(300 MHz;

DMSO-d<sub>6</sub>) 36.69 (10C, NR<sub>2</sub>CH<sub>2</sub>CH<sub>2</sub>CONH), 41.96 (10C, CONHCH<sub>2</sub>CH<sub>2</sub>NH<sub>2</sub>), 42.73 (10C, CONHCH<sub>2</sub>CH<sub>2</sub>NH<sub>2</sub>), 52.6 (10C, NR<sub>2</sub>CH<sub>2</sub>CH<sub>2</sub>CONH), 172.11, 172.16 (10C, NCH<sub>2</sub>CH<sub>2</sub>CONH).

#### Synthesis of D3NH<sub>2</sub>

EDA (31.054 g, 0.517 mol) was added to a stirred solution of (9.14 g, 2.58 mmol) **D2.5** in 10 mL methanol. The final mixture was irradiated at 250 W for 80 minutes at 123 °C before being purified as described in the general procedure for the synthesis of full generation dendrimers. The product was a yellowish gel (10.168 g, 96.00 %). Elemental analysis C<sub>179</sub>H<sub>363</sub>N<sub>73</sub>O<sub>35</sub>: Found: C, 52.74; H, 9.09; N, 25.18. Calc.: C, 52.46; H, 8.93; N, 24.95%. ATR-IR  $\nu_{\max}/\text{cm}^{-1}$  3281(NH), 1634 (HNC=O), 1549 (HNC=O). <sup>1</sup>H NMR  $\delta\text{H}$ (300 MHz; DMSO-d<sub>6</sub>) 2.39 (40H, bm, NR<sub>2</sub>CH<sub>2</sub>CH<sub>2</sub>CONH), 2.72 (40H, t, NR<sub>2</sub>CH<sub>2</sub>CH<sub>2</sub>CONH), 2.84 (40H, bm, CONHCH<sub>2</sub>CH<sub>2</sub>NH<sub>2</sub>), 3.09 (40H, brs, CONHCH<sub>2</sub>CH<sub>2</sub>NH<sub>2</sub>), 3.23 (40H, m, CONHCH<sub>2</sub>CH<sub>2</sub>NH<sub>2</sub>), 8.14 (30H, bs, CONHCH<sub>2</sub>CH<sub>2</sub>NH<sub>2</sub>). <sup>13</sup>C NMR  $\delta\text{C}$ (300 MHz; DMSO-d<sub>6</sub>) 36.66 (20C, NR<sub>2</sub>CH<sub>2</sub>CH<sub>2</sub>CONH), 41.94 (20C, CONHCH<sub>2</sub>CH<sub>2</sub>NH<sub>2</sub>), 42.73 (20C, CONHCH<sub>2</sub>CH<sub>2</sub>NH<sub>2</sub>), 52.46 (20C, NR<sub>2</sub>CH<sub>2</sub>CH<sub>2</sub>CONH) 172.17, 172.22 (20C, NCH<sub>2</sub>CH<sub>2</sub>CONH).

#### Synthesis of D4NH<sub>2</sub>

EDA (39.33 g, 0.65 mol) was added to a stirred solution of (12.34 g, 1.63 mmol) **D3.5** in 10 mL methanol. The final mixture was irradiated at 250 W for 80 minutes at 126 °C before being purified as described in the general procedure for the synthesis of full generation dendrimers. The product was a yellowish gel (13.40 g, 94.5 %). Elemental analysis C<sub>379</sub>H<sub>763</sub>N<sub>153</sub>O<sub>75</sub>: Found: C, 52.91; H, 9.06; N, 24.97. Calc.: C, 52.54; H, 8.88; N, 24.73%. ATR-IR  $\nu_{\max}/\text{cm}^{-1}$  3281(NH), 1652 (HNC=O), 1558 (HNC=O). <sup>1</sup>H NMR  $\delta\text{H}$ (300 MHz; DMSO-d<sub>6</sub>) 2.40 (40H, brm, NR<sub>2</sub>CH<sub>2</sub>CH<sub>2</sub>CONH), 2.75 (80H, t, NR<sub>2</sub>CH<sub>2</sub>CH<sub>2</sub>CONH), 2.86 (80H, brm, CONHCH<sub>2</sub>CH<sub>2</sub>NH<sub>2</sub>), 3.28 (80H, brm, CONHCH<sub>2</sub>CH<sub>2</sub>NH<sub>2</sub>), 8.15 (60H, bs, CONHCH<sub>2</sub>CH<sub>2</sub>NH<sub>2</sub>). <sup>13</sup>C NMR  $\delta\text{C}$ (300 MHz; DMSO-d<sub>6</sub>) 36.61 (40C, NR<sub>2</sub>CH<sub>2</sub>CH<sub>2</sub>CONH), 41.91 (40C, CONHCH<sub>2</sub>CH<sub>2</sub>NH<sub>2</sub>), 42.73 (40C, CONHCH<sub>2</sub>CH<sub>2</sub>NH<sub>2</sub>), 52.81 (40C, NR<sub>2</sub>CH<sub>2</sub>CH<sub>2</sub>CONH) 172.03, 172.22 (40C, NCH<sub>2</sub>CH<sub>2</sub>CONH).

### 3.4.2.3 Synthesis of Jeffamine® T-403 Cored Full Generations (P1-P4.NH<sub>2</sub>)

#### Synthesis of P1.NH<sub>2</sub>

EDA (10.80 g, 0.18 mol) was added to a stirred solution of (11.60 g, 10.30 mmol) **P0.5** in 2 mL methanol. The final mixture was irradiated at 200 W for 30 minutes at 129 °C before being purified as described in the general procedure for the synthesis of full generation dendrimers. The product was a yellowish gel (12.55 g, 92 %). Elemental analysis C<sub>54</sub>H<sub>113</sub>N<sub>15</sub>O<sub>12</sub>: Found: C, 56.78; H, 9.87; N, 18.23. Calc.: C, 55.69; H, 9.78; N, 18.04%. ATR-IR  $\nu_{\max}/\text{cm}^{-1}$  3284 (NH), 1643 (HNC=O), 1549 (HNC=O). <sup>1</sup>H-NMR  $\delta\text{H}$ (400 MHz; DMSO) 2.21 (12H, t, NCH<sub>2</sub>CH<sub>2</sub>CONH), 2.69 (12H, t, CONHCH<sub>2</sub>CH<sub>2</sub>NH<sub>2</sub>), 3.05 (12H, t, CONHCH<sub>2</sub>CH<sub>2</sub>NH<sub>2</sub>), 2.56 (12H, t, NCH<sub>2</sub>CH<sub>2</sub>CONH), 7.97 (6H, br s, NCH<sub>2</sub>CH<sub>2</sub>CONH). <sup>13</sup>C-NMR  $\delta\text{C}$ (400 MHz; DMSO) 171.5 (NCH<sub>2</sub>CH<sub>2</sub>CONH), 48.50 (NCH<sub>2</sub>CH<sub>2</sub>CONH), 42.10 (CONHCH<sub>2</sub>CH<sub>2</sub>NH<sub>2</sub>), 41.30 (CONHCH<sub>2</sub>CH<sub>2</sub>NH<sub>2</sub>), 36.14 (NCH<sub>2</sub>CH<sub>2</sub>CONH).

#### Synthesis of P2.NH<sub>2</sub>

EDA (58.078 g, 0.97 mol) was added to a stirred solution of (17.38 g, 8.05 mmol) **P1.5** in 3.5 mL methanol. The final mixture was irradiated at 200 W for 40 minutes at 128 °C before being purified as described in the general procedure for the synthesis of full generation dendrimers. The product was a yellowish gel (18.33 g, 91.2 %). Elemental analysis C<sub>84</sub>H<sub>173</sub>N<sub>27</sub>O<sub>18</sub>: Found: C, 55.18; H, 9.57; N, 20.82. Calc.: C, 54.55; H, 9.43; N, 20.45. ATR-IR  $\nu_{\max}/\text{cm}^{-1}$  3278 (NH), 1636(HNC=O), 1549 (HNC=O). <sup>1</sup>H-NMR  $\delta\text{H}$ (400 MHz; DMSO) 2.21 (24H, t, NCH<sub>2</sub>CH<sub>2</sub>CONH), 2.69 (24H, t, CONHCH<sub>2</sub>CH<sub>2</sub>NH<sub>2</sub>), 3.05 (24H, t, CONHCH<sub>2</sub>CH<sub>2</sub>NH<sub>2</sub>), 2.56 (24H, t, NCH<sub>2</sub>CH<sub>2</sub>CONH), 7.93 (12H, br s, NCH<sub>2</sub>CH<sub>2</sub>CONH). <sup>13</sup>C-NMR  $\delta\text{C}$ (400 MHz; DMSO) 171.47 (NCH<sub>2</sub>CH<sub>2</sub>CONH), 48.55 (NCH<sub>2</sub>CH<sub>2</sub>CONH), 42.05 (CONHCH<sub>2</sub>CH<sub>2</sub>NH<sub>2</sub>), 41.26 (CONHCH<sub>2</sub>CH<sub>2</sub>NH<sub>2</sub>), 35.92 (NCH<sub>2</sub>CH<sub>2</sub>CONH)

#### Synthesis of P3.NH<sub>2</sub>

EDA (44.90 g, 0.75 mol) was added to a stirred solution of (14.20 g, 3,112 mmol) **P2.5** in 4 mL methanol. The final mixture was irradiated at 200 W for 60 minutes at 128 °C before being purified as described in the general procedure for the synthesis of full generation dendrimers. The product was yellowish gel (14.83 g, 91 %).Elemental analysis C<sub>144</sub>H<sub>293</sub>N<sub>51</sub>O<sub>30</sub>: Found: C, 54.02; H, 9.31; N, 22.55. Calc.: C, 53.73; H, 9.17; N, 22.19%. ATR-IR  $\nu_{\max}/\text{cm}^{-1}$  3283 (NH), 1639 (HNC=O), 1547 (HNC=O). <sup>1</sup>H-NMR  $\delta\text{H}$ (400 MHz; DMSO) 2.21 (48H, t, NCH<sub>2</sub>CH<sub>2</sub>CONH), 2.66 (48H, t, CONHCH<sub>2</sub>CH<sub>2</sub>NH<sub>2</sub>), 3.05 (48H,

t, CONHCH<sub>2</sub>CH<sub>2</sub>NH<sub>2</sub>), 2.56 (48H, t, NCH<sub>2</sub>CH<sub>2</sub>CONH), 7.94 (24H, br s, NCH<sub>2</sub>CH<sub>2</sub>CONH). <sup>13</sup>C-NMR δC(400 MHz; DMSO) 171.54 (NCH<sub>2</sub>CH<sub>2</sub>CONH), 48.54 (NCH<sub>2</sub>CH<sub>2</sub>CONH), 42.17 (CONHCH<sub>2</sub>CH<sub>2</sub>NH<sub>2</sub>), 40.99 (CONHCH<sub>2</sub>CH<sub>2</sub>NH<sub>2</sub>), 35.75 (NCH<sub>2</sub>CH<sub>2</sub>CONH).

#### Synthesis of P4.NH<sub>2</sub>

EDA (36.49 g, 0.60 mol) was added to a stirred solution of (11.85 g, 1.26 mmol) **P3.5** in 4 mL methanol. The final mixture was irradiated at 200 W for 60 minutes at 123 °C before being purified as described in the general procedure for the synthesis of full generation dendrimers. The product was a yellowish gel (12.20 g, 90 %). Elemental analysis C<sub>264</sub>H<sub>533</sub>N<sub>99</sub>O<sub>54</sub>: Found: C, 54.12; H, 9.21; N, 23.38. Calc.: C, 53.21; H, 9.02; N, 23.27%. ATR-IR ν<sub>max</sub>/cm<sup>-1</sup> 3281(NH), 1639(HNC=O), 1548(HNC=O). <sup>1</sup>H-NMR δH(400 MHz; DMSO) 2.21 (96H, t, NCH<sub>2</sub>CH<sub>2</sub>CONH), 2.66 (96H, t, CONHCH<sub>2</sub>CH<sub>2</sub>NH<sub>2</sub>), 3.06 (96H, t, CONHCH<sub>2</sub>CH<sub>2</sub>NH<sub>2</sub>), 2.56 (96H, t, NCH<sub>2</sub>CH<sub>2</sub>CONH), 7.94 (48H, br s, NCH<sub>2</sub>CH<sub>2</sub>CONH). <sup>13</sup>C-NMR δC(400 MHz; DMSO) 171.56 (NCH<sub>2</sub>CH<sub>2</sub>CONH), 48.54 (NCH<sub>2</sub>CH<sub>2</sub>CONH), 42.04 (CONHCH<sub>2</sub>CH<sub>2</sub>NH<sub>2</sub>), 41.21 (CONHCH<sub>2</sub>CH<sub>2</sub>NH<sub>2</sub>), 35.90 (NCH<sub>2</sub>CH<sub>2</sub>CONH).

#### 3.4.2.4 LPR Experiment

Appropriate Millipore ultrafiltration membrane disk was equipped with Amicon 8000 Stirred cell. was used for LPR method. (1:1) MeOH:Aqueous solutions of crude product was transferred into the cell. Depending on the expected size of the product, membrane disks were selected in the range of MWCO 1-3 kDA. The solution was diluted to 200 mL inside the cell. Methanol-water mixture was used as feeding solvent. Continuous dialysis was performed under 15 psi nitrogen pressure for 24 hours. Finally methanol water mixture was evaporated under vacuum.

### 3.5 Synthesis of Water Soluble PAMAM Derivatives

#### 3.5.1 General Procedure for the Synthesis of Carboxyl Terminated PAMAMs

A methanolic solution ester terminated half generation PAMAM dendrimer was mixed with 1.5 M equiv. of NaOH per terminal ester. The mixture was stirred for 24 hours and excess amount of solvent was removed under vacuum at bath temperature 65 °C. The

remaining oil was dissolved in methanol and again evaporated in vacuo. Drying under vacuum resulted in a white powder product. Yields were 100 % (Table 4.10 in part 4.2.1)

### 3.5.1.1 Synthesis of E3.COOH

**E2.5** (0.7982 g, 0.28 mmol) and NaOH (0.272 g, 6.8 mmol) was dissolved in 4.5 ml methanol. The mixture was stirred for 24 hours at room temperature. The product was a white powder (0.734 g, 100%). Elemental analysis  $C_{110}H_{192}N_{26}O_{44}$ : Found: C, 51.62; H, 7.62; N, 14.26. Calc.: C, 51.15; H, 7.49; N, 14.10%. ATR-IR  $\nu_{\max}/\text{cm}^{-1}$  3292 (COOH), 1650 (HNC=O), 1569 (HNC=O), 1404 (O-H).  $^1\text{H}$  NMR  $\delta\text{H}$ (400 MHz;  $\text{D}_2\text{O}$ ) 2.71 (32H, t,  $\text{CH}_2\text{CH}_2\text{COOH}$ ), 2.89 (32H, m,  $\text{CH}_2\text{CH}_2\text{COOH}$ ).  $^{13}\text{C}$  NMR  $\delta\text{C}$ (400 MHz;  $\text{D}_2\text{O}$ ) 35.31 ( $\text{CH}_2\text{CH}_2\text{COOH}$ ), 47.61 ( $\text{CH}_2\text{CH}_2\text{COOH}$ ), 48.32 ( $\text{CH}_2\text{CH}_2\text{NR}_2$ ), 177.68 ( $\text{NCH}_2\text{CH}_2\text{CONH}$ ), 183.75, 183.81, 184.21, 184.25 (COOH).

### 3.5.1.2 Synthesis of E4.COOH

**E3.5** (0.6539 g, 0.10 mmol) and NaOH (0.208 g, 5.2 mmol) was dissolved in 4 ml methanol. The mixture was stirred for 24 hours at room temperature. The product was a white powder (0.704 g, 100%). Elemental analysis  $C_{238}H_{416}N_{58}O_{92}$ : Found: C, 52.45; H, 7.69; N, 14.90. Calc.: C, 51.39; H, 7.54; N, 14.61%. ATR-IR  $\nu_{\max}/\text{cm}^{-1}$  3282 (COOH), 1644 (HNC=O), 1564 (HNC=O), 1403 (O-H).  $^1\text{H}$  NMR  $\delta\text{H}$ (400 MHz;  $\text{D}_2\text{O}$ ) 2.41 (64H, bm,  $\text{CH}_2\text{CH}_2\text{COOH}$ ), 2.76 (64H, m,  $\text{CH}_2\text{CH}_2\text{COOH}$ ).  $^{13}\text{C}$  NMR  $\delta\text{C}$ (400 MHz;  $\text{D}_2\text{O}$ ) 35.19 ( $\text{CH}_2\text{CH}_2\text{COOH}$ ), 47.86 ( $\text{CH}_2\text{CH}_2\text{COOH}$ ), 48.09 ( $\text{CH}_2\text{CH}_2\text{NR}_2$ ), 177.50 ( $\text{NCH}_2\text{CH}_2\text{CONH}$ ), 183.86, 183.98, 184.01, 184.05 (COOH).

### 3.5.1.3 Synthesis of D3.COOH

**D2.5** (1.1207 g, 0.31 mmol) and NaOH (0.409 g, 10.22 mmol) was dissolved in 6.8 ml methanol. The mixture was stirred for 24 hours at room temperature. The product was a white powder (1.032 g, 100%). Elemental analysis  $C_{139}H_{243}N_{33}O_{55}$ : Found: C, 51.74; H, 7.66; N, 14.38. Calc.: C, 51.26; H, 7.52; N, 14.19%. ATR-IR  $\nu_{\max}/\text{cm}^{-1}$  3304 (COOH), 1649 (HNC=O), 1574 (HNC=O), 1404 (O-H).  $^1\text{H}$  NMR  $\delta\text{H}$ (300 MHz;  $\text{D}_2\text{O}$ ) 2.62 (40H, m,  $\text{NR}_2\text{CH}_2\text{CH}_2\text{COOH}$ ), 2.85 (40H, brm,  $\text{NR}_2\text{CH}_2\text{CH}_2\text{COOH}$ ), 2.91 (40H, brm,  $\text{CONHCH}_2\text{CH}_2\text{NR}_2$ ), 3.27 (40H, brm,  $\text{CONHCH}_2\text{CH}_2\text{NR}_2$ ).  $^{13}\text{C}$  NMR  $\delta\text{C}$ (300 MHz,

D<sub>2</sub>O) 32.63 (20C, NR<sub>2</sub>CH<sub>2</sub>CH<sub>2</sub>COOH), 37.88 (10C, CONHCH<sub>2</sub>CH<sub>2</sub>NR<sub>2</sub>), 51.07 (20C, NR<sub>2</sub>CH<sub>2</sub>CH<sub>2</sub>COOH), 54.90 (10C, CONHCH<sub>2</sub>CH<sub>2</sub>NR<sub>2</sub>), 181.42, 181.63 (20C, COOH).

#### 3.5.1.4 Synthesis of D4.COOH

**D3.5** (0.7613 g, 0.10 mmol) and NaOH (0.286 g, 7.15 mmol) was dissolved in 4.6 ml methanol. The mixture was stirred for 24 hours at room temperature. The product was a white powder (0.704 g, 100%). ATR-IR  $\nu_{\max}/\text{cm}^{-1}$  3305 (COOH), 1650 (HNC=O), 1574 (HNC=O), 1403 (O-H). Elemental analysis C<sub>299</sub>H<sub>523</sub>N<sub>73</sub>O<sub>115</sub>: Found: C, 52.48; H, 7.67; N, 14.82. Calc.: C, 51.44; H, 7.55; N, 14.65%. ATR-IR  $\nu_{\max}/\text{cm}^{-1}$  3305 (COOH), 1650 (HNC=O), 1574 (HNC=O), 1403 (O-H). <sup>1</sup>H NMR  $\delta\text{H}$ (300 MHz; D<sub>2</sub>O) 2.62 (80H, m, NR<sub>2</sub>CH<sub>2</sub>CH<sub>2</sub>COOH), 2.86 (80H, brm, NR<sub>2</sub>CH<sub>2</sub>CH<sub>2</sub>COOH), 2.89 (80H, brm, CONHCH<sub>2</sub>CH<sub>2</sub>NR<sub>2</sub>), 3.34 (80H, brm, CONHCH<sub>2</sub>CH<sub>2</sub>NR<sub>2</sub>). <sup>13</sup>C NMR  $\delta\text{C}$ (300 MHz, D<sub>2</sub>O) 32.60 (40C, NR<sub>2</sub>CH<sub>2</sub>CH<sub>2</sub>COOH), 37.85 (20C, CONHCH<sub>2</sub>CH<sub>2</sub>NR<sub>2</sub>), 51.06 (40C, NR<sub>2</sub>CH<sub>2</sub>CH<sub>2</sub>COOH), 54.89 (20C, CONHCH<sub>2</sub>CH<sub>2</sub>NR<sub>2</sub>), 181.41, 181.46, 181.61 (40C, COOH).

#### 3.5.1.5 Synthesis of P3.COOH

**P2.5** (1.155 g, 0.25 mmol) and NaOH (0.364 g, 9.1 mmol) was dissolved in 6 ml methanol. The mixture was stirred for 24 hours at room temperature. The product was a white powder (1.070 g, 100%). Elemental analysis C<sub>108</sub>H<sub>197</sub>N<sub>27</sub>O<sub>42</sub>: Found: C, 51.42; H, 7.92; N, 14.99. Calc.: C, 50.95; H, 7.80; N, 14.85%. ATR-IR  $\nu_{\max}/\text{cm}^{-1}$  3270 (COOH), 1641 (HNC=O), 1558 (HNC=O), 1398 (O-H). <sup>1</sup>H NMR  $\delta\text{H}$ (400 MHz; D<sub>2</sub>O) 2.31 (48H, t, CH<sub>2</sub>CH<sub>2</sub>COOH), 2.73 (48H, m, CH<sub>2</sub>CH<sub>2</sub>COOH). <sup>13</sup>C NMR  $\delta\text{C}$ (400 MHz; D<sub>2</sub>O) 30.22 (CH<sub>2</sub>CH<sub>2</sub>COOH), 48.58 (CH<sub>2</sub>CH<sub>2</sub>COOH), 51.14 (CH<sub>2</sub>CH<sub>2</sub>NR<sub>2</sub>), 174.66, 174.73 (NCH<sub>2</sub>CH<sub>2</sub>CONH), 181.03, 181.16 (COOH).

#### 3.5.1.6 Synthesis of P4.COOH

**P3.5** (0.9878 g, 1.033 mmol) and NaOH (0.286 g, 7.59 mmol) was dissolved in 5 ml methanol. The mixture was stirred for 24 hours at room temperature. The product was a white powder (0.704 g, 100%). Elemental analysis C<sub>192</sub>H<sub>341</sub>N<sub>51</sub>O<sub>78</sub>: Found: C, 51.32; H, 7.64; N, 15.72. Calc.: C, 50.00; H, 7.45; N, 15.49%. ATR-IR  $\nu_{\max}/\text{cm}^{-1}$  3274 (COOH), 1641 (HNC=O), 1558 (HNC=O), 1396 (O-H). <sup>1</sup>H NMR  $\delta\text{H}$ (400 MHz; D<sub>2</sub>O) 2.39 (96H,

t,  $\text{CH}_2\text{CH}_2\text{COOH}$ ), 2.65 (96H, t,  $\text{CH}_2\text{CH}_2\text{COOH}$ ).  $^{13}\text{C}$  NMR  $\delta\text{C}$ (400 MHz;  $\text{D}_2\text{O}$ ) 32.67 ( $\text{CH}_2\text{CH}_2\text{COOH}$ ), 48.92 ( $\text{CH}_2\text{CH}_2\text{COOH}$ ), 51.09 ( $\text{CH}_2\text{CH}_2\text{NR}_2$ ), 174.58, 174.73 ( $\text{NCH}_2\text{CH}_2\text{CONH}$ ), 181.21 ( $\text{COOH}$ ).

### 3.5.2 General Procedure for the Synthesis of Tris Terminated PAMAMs

Methanolic solution of ester terminated dendrimer was added to a stirred suspension of Tris (1.2 M equiv. per terminal ester) and anhydrous potassium carbonate (1.2 M equiv. of per terminal ester) in 10-15 mL of MeOH. The final mixture was irradiated with CEM discovery Microwave at 200 W by using open vessel mode. Temperature was kept constant at the bulk temperature range of 70-90  $^\circ\text{C}$  during MW irradiation. The amount of methanol to be added also was determined by considering the preservation of temperature in the range of 70-90  $^\circ\text{C}$ . The final reaction mixture was filtered to remove excess solid reagents, and filtrate collected. Then product was purified with LPR method. In other words, it was continuously dialyzed with 50 % aqueous methanol solution under 15 psi nitrogen ( $\text{N}_2$ ) gas pressure for 24 hours by using Millipore ultrafiltration disks having the molecular cut of size 1 kDA. Final methanolic solution of retentate product was removed under vacuum below the bath temperature of 65  $^\circ\text{C}$ . Yields were between the ranges of 93-96% (Table 4.9 in part 4.2.1)

#### 3.5.2.1 Synthesis of E3.TRIS

Methanolic solution of **E2.5** (1.724 g, 0.61 mmol) was added to a stirred suspension of Tris (1.427 g, 11.77 mmol) and  $\text{K}_2\text{CO}_3$  (2.033 g, 14.71 mmol) in 10 ml methanol. The final mixture was irradiated at 200 W for 120 minutes at 76  $^\circ\text{C}$  before purified as described in the general procedure for synthesis of TRIS terminated dendrimers. The product was opaque oil (2.493 g, 96% ). Elemental analysis  $\text{C}_{174}\text{H}_{336}\text{N}_{42}\text{O}_{76}$ : Found: C, 49.75; H, 8.14; N, 14.10. Calc.: C, 49.37; H, 8.00; N, 13.90%. ATR-IR  $\nu_{\text{max}}/\text{cm}^{-1}$  3263 ( $\text{COH}$ ), 1635 ( $\text{HNC}=\text{O}$ ), 1558 ( $\text{HNC}=\text{O}$ ), 1392 ( $\text{O-H}$ ).  $^1\text{H}$  NMR  $\delta\text{H}$ (400 MHz;  $\text{CD}_3\text{OD}$ ) 2.56 (32H, bm,  $\text{CH}_2\text{CH}_2\text{CONHCR}_3$ ), 2.76 (32H, bm,  $\text{CH}_2\text{CH}_2\text{CONHCR}_3$ ), 3.57 (96H, bs,  $\text{CH}_2\text{OH}$ ).  $^{13}\text{C}$  NMR  $\delta\text{C}$ (400 MHz;  $\text{CD}_3\text{OD}$ ) 32.22 ( $\text{CH}_2\text{CH}_2\text{CONHCR}_3$ ), 48.70 ( $\text{CH}_2\text{CH}_2\text{CONHCR}_3$ ), 49.24 ( $\text{CH}_2\text{CH}_2\text{NR}_2$ ), 56.51 ( $\text{CONHCR}_2\text{CH}_2\text{OH}$ ), 63.26 ( $\text{CONHCR}_2\text{CH}_2\text{OH}$ ), 174.66, 174.82, 180.73, 181.01 ( $\text{NCH}_2\text{CH}_2\text{CONH}$ ).

### 3.5.2.2 Synthesis of E4.TRIS

Methanolic solution of **E3.5** (0.990 g, 0.16 mmol) was added to a stirred suspension of Tris (0.762 g, 6.29 mmol) and  $K_2CO_3$  (1.086 g, 7.85 mmol) in 10 ml methanol. The final mixture was irradiated at 200 W for 140 minutes at 76 °C before purified as described in the general procedure for synthesis of TRIS terminated dendrimers. The product was opaque oil (1.351 g, 93%). Elemental analysis  $C_{366}H_{704}N_{90}O_{156}$ : Found: C, 49.98; H, 8.10; N, 14.40. Calc.: C, 49.60; H, 8.01; N, 14.22%. ATR-IR  $\nu_{max}/cm^{-1}$  3263 (COH), 1641 (HNC=O), 1558 (HNC=O), 1394 (O-H).  $^1H$  NMR  $\delta H$ (400 MHz;  $CD_3OD$ ) 2.52 (64H, bm,  $CH_2CH_2CONHCR_3$ ), 2.70 (64H, bm,  $CH_2CH_2CONHCR_3$ ), 3.65 (192H, bs,  $CH_2OH$ ).  $^{13}C$  NMR  $\delta C$ (400 MHz;  $CD_3OD$ ) 32.62 ( $CH_2CH_2CONHCR_3$ ), 48.88 ( $CH_2CH_2CONHCR_3$ ), 49.02 ( $CH_2CH_2NR_2$ ), 56.37 ( $CONHCR_2CH_2OH$ ), 63.06 ( $CONHCR_2CH_2OH$ ), 174.62, 174.92, 180.93, 181.21 (NCH<sub>2</sub>CH<sub>2</sub>CONH).

### 3.5.2.3 Synthesis of D3.TRIS

Methanolic solution of **D2.5** (0.982 g, 0.27 mmol) was added to a stirred suspension of Tris (0.805 g, 6.64 mmol) and  $K_2CO_3$  (1.146 g, 8.29 mmol) in 15 ml methanol. The final mixture was irradiated at 200 W for 110 minutes at 86 °C before purified as described in the general procedure for synthesis of TRIS terminated dendrimers. The product was opaque oil (1.399 g, 95.00 %). Elemental analysis  $C_{199}H_{383}N_{53}O_{95}$ : C, 47.86; H, 7.77; N, 14.92. Calc.: C, 47.44; H, 7.66; N, 14.73%. ATR-IR  $\nu_{max}/cm^{-1}$  3266 (COH), 1635 (HNC=O), 1554 (HNC=O), 1392 (O-H).  $^1H$  NMR  $\delta H$ (300 MHz;  $CD_3OD$ ) 2.61 (40H, m,  $CH_2CH_2CONHR_3$ ), 2.78 (40H, bm,  $CH_2CH_2CONHR_3$ ), 2.77 (40H, bm,  $CONHCH_2CH_2NR_2$ ), 3.23 (40H, bm,  $CONHCH_2CH_2NR_2$ ), 3.65 (120H, s,  $CH_2OH$ ).  $^{13}C$  NMR  $\delta C$ (300 MHz;  $CD_3OD$ ) 33.67 (20C,  $NR_2CH_2CH_2COOCH_3$ ), 38.23 (10C,  $CONHCH_2CH_2NR_2$ ), 50.33 (20C,  $NR_2CH_2CH_2COOCH_3$ ), 51.22 (10C,  $CONHCH_2CH_2NR_2$ ), 56.47 (15C,  $CONHCCH_2OH$ ), 63.69 (48C,  $CONHCCH_2OH$ ), 174.83, 175.35, 180.48, 181.12 (20C, NCH<sub>2</sub>CH<sub>2</sub>CONH).

### 3.5.2.4 Synthesis of D4.TRIS

Methanolic solution of **D3.5** (1.116 g, 0.14 mmol) was added to a stirred suspension of Tris (0.854 g, 7.04 mmol) and  $K_2CO_3$  (1.217 g, 10.04 mmol) in 13 ml methanol. The final mixture was irradiated at 200 W for 125 minutes at 82 °C before purified as described in

the general procedure for synthesis of TRIS terminated dendrimers. The product was opaque oil (1.461 g, 94.00 %). Elemental analysis  $C_{459}H_{883}N_{113}O_{195}$ : Found: C, 49.96; H, 8.08; N, 14.42. Calc.: C, 49.64; H, 8.01; N, 14.25%. ATR-IR  $\nu_{\max}/\text{cm}^{-1}$  3261 (COH), 1640 (HNC=O), 1554 (HNC=O), 1388 (O-H).  $^1\text{H}$  NMR  $\delta\text{H}$ (300 MHz;  $\text{CD}_3\text{OD}$ ) 2.55 (80H, bm,  $\text{CH}_2\text{CH}_2\text{CONHR}_3$ ), 2.70 (80H, bm,  $\text{CH}_2\text{CH}_2\text{CONHR}_3$ ), 2.82 (80H, bm,  $\text{CONHCH}_2\text{CH}_2\text{NR}_2$ ), 3.29 (80H, bm,  $\text{CONHCH}_2\text{CH}_2\text{NR}_2$ ), 3.71 (240H, s,  $\text{CH}_2\text{OH}$ ).  $^{13}\text{C}$  NMR  $\delta\text{C}$ (300 MHz;  $\text{CD}_3\text{OD}$ ) 33.55 (40C,  $\text{CH}_2\text{CH}_2\text{CONHR}_3$ ), 38.60 (20C,  $\text{CONHCH}_2\text{CH}_2\text{NR}_2$ ), 50.03 (40C,  $\text{CH}_2\text{CH}_2\text{CONHR}_3$ ), 51.10 (20C,  $\text{CONHCH}_2\text{CH}_2\text{NR}_2$ ), 56.37 (30C,  $\text{CONHCR}_2\text{CH}_2\text{OH}$ ), 63.6 (96C,  $\text{CONHCR}_2\text{CH}_2\text{OH}$ ), 174.93, 175.44, 180.4, 181.04 (40C,  $\text{NCH}_2\text{CH}_2\text{CONH}$ ).

### 3.5.2.5 Synthesis of P3.TRIS

Methanolic solution of **P2.5** (0.6867 g, 0.150 mmol) was added to a stirred suspension of Tris (0.525g, 4.33mmol) and  $\text{K}_2\text{CO}_3$  (0.748 g, 5.42 mmol) in 10 ml methanol. The final mixture was irradiated at 200 W for 120 minutes at 80 °C before purified as described in the general procedure for synthesis of TRIS terminated dendrimers. The product was opaque oil (0.910 g, 91 %). Elemental analysis  $C_{204}H_{341}N_{51}O_{90}$ : Found: C, 50.00; H, 7.04; N, 14.66. Calc.: C, 49.52; H, 6.95; N, 14.44%. ATR-IR  $\nu_{\max}/\text{cm}^{-1}$  3275 (COH), 1645 (HNC=O), 1563 (HNC=O), 1393 (O-H).  $^1\text{H}$  NMR  $\delta\text{H}$ (400 MHz;  $\text{CD}_3\text{OD}$ ) 2.58 (48H, bm,  $\text{CH}_2\text{CH}_2\text{CONHCR}_3$ ), 2.77 (48H, t,  $\text{CH}_2\text{CH}_2\text{CONHCR}_3$ ), 3.54 (192H, bs,  $\text{CH}_2\text{OH}$ ).  $^{13}\text{C}$  NMR  $\delta\text{C}$ (400 MHz;  $\text{CD}_3\text{OD}$ ) 32.64 ( $\text{CH}_2\text{CH}_2\text{CONHCR}_3$ ), 48.91 ( $\text{CH}_2\text{CH}_2\text{CONHCR}_3$ ), 52.08 ( $\text{CH}_2\text{CH}_2\text{NR}_2$ ), 56.30 ( $\text{CONHCR}_2\text{CH}_2\text{OH}$ ), 63.12 ( $\text{CONHCR}_2\text{CH}_2\text{OH}$ ) 174.61, 175.53, 181.12 ( $\text{NCH}_2\text{CH}_2\text{CONH}$ ).

### 3.5.2.6 Synthesis of P4.TRIS

Methanolic solution of **P3.5** (0.8408 g, 0.089 mmol) was added to a stirred suspension of Tris (0.626g, 5.16mmol) and  $\text{K}_2\text{CO}_3$  (0.892g, 6.46 mmol) in 10 ml methanol. The final mixture was irradiated at 200 W for 135 minutes at 79 °C before purified as described in the general procedure for synthesis of TRIS terminated dendrimers. The product was opaque oil (1.166 g, 93 %). Elemental analysis  $C_{384}H_{629}N_{99}O_{174}$ : Found: C, 49.62; H, 6.86; N, 14.85. Calc.: C, 48.98; H, 6.73; N, 14.73%. ATR-IR  $\nu_{\max}/\text{cm}^{-1}$  3263 (COH), 1641 (HNC=O), 1558 (HNC=O), 1392 (O-H).  $^1\text{H}$  NMR  $\delta\text{H}$ (400 MHz;  $\text{CD}_3\text{OD}$ ) 2.5 (96H, bm,

$\text{CH}_2\text{CH}_2\text{CONHC}$ ), 2.68 (96H, t,  $\text{CH}_2\text{CH}_2\text{CONHC}$ ), 3.63 (288H, bs,  $\text{CH}_2\text{OH}$ ).  $^{13}\text{C}$  NMR  $\delta\text{C}$ (400 MHz;  $\text{CD}_3\text{OD}$ ) 32.59 ( $\text{CH}_2\text{CH}_2\text{CONHC}$ ), 48.97 ( $\text{CH}_2\text{CH}_2\text{CONHC}$ ), 51.18 ( $\text{CH}_2\text{CH}_2\text{NR}_2$ ), 56.38 ( $\text{CONHCR}_2\text{CH}_2\text{OH}$ ), 63.02 ( $\text{CONHCR}_2\text{CH}_2\text{OH}$ ) 174.65, 175.55, 181.09 ( $\text{NCH}_2\text{CH}_2\text{CONH}$ ).

### **3.6 Determination of the Protonation Constants of PAMAMs by Hyperquad Program**

#### **3.6.1 Potentiometric Titrations and Measurements**

All solutions were prepared by using carbonate free 18.2 m $\Omega$  Milli-Q water. Carbonate free NaOH solutions were used as titrant after standardized with primary grade KHP. Standardized HCl against KHP was used as excess acid in order to adjust initial pH of dendrimer solution to low pH. Acid base titration of dendrimers were conducted according to literature [251, 252]. Both acid and base were standardized against KHP before titration experiments. Analytical grade NaCl was added to a precisely weighed portion of PAMAM solutions to prevent shielding of amine group each other because of interactions, and keep the ionic strength (I) constant in the range of 10-100 mM. Titrations were carried out automatically by using autotitrator and thermostated titration vessel under continuous nitrogen ( $\text{N}_2$ ) stream. Temperature was kept at room temperature ( $25 \pm 0.1^\circ\text{C}$ ). PAMAMs and derivatives (18-22 mg) were dissolved in 20 mL of 0.010-0.1 M NaCl solution to give a final concentration of 0.9-1.1 mg/mL. Dendrimer solution was titrated with standard HCl solution and back titrated with standard NaOH solution, respectively.

The pKa values of PAMAMs were determined by titrating solutions over the pH range of 2-12 with standardized NaOH solutions. Resulting data were analyzed by using HYPERQUAD 2008 computer software program [253].

### **3.7 Spectroscopic Investigation of the Protonation Constants of PAMAMs by Chemometric Approaches and HypSpec Program**

#### **3.7.1 Spectroscopic Titrations and Measurements**

UV-VIS spectrum measurements were performed with PG TG 70 UV-VIS spectrophotometer against to Milli-Q water and all the measurements were taken between the wavelength ranges of 250-350 nm with 10 mm quartz UV cells. Precision of titration was increased  $\pm 0.01$  pH unit by using a TitroLine® 7000 (SI Analytics GmbH, Hattenbergstraße, Germany) autotitrator supported with Titrisoft 2.73 software. After each pH adjustment, dendrimer solution transferred into the cuvette and the absorption spectrum is recorded. The pH meter was calibrated with at least three buffer solutions at pH 4.00, 7.00 and 10.00. Ionic strength was maintained by adding appropriate amount of 0.1 M NaCl.

#### **3.7.2 Protonation Constants**

All solutions were prepared by using carbonate free 18.2 m $\Omega$  Milli-Q water. Carbonate free NaOH solutions were used in initial pH adjustment to  $\sim$ pH 11-12 after standardized with primary grade KHP. Standardized HCl was used as titrant in order to adjust initial pH of dendrimer solution to low pH. Both acid and base were standardized against KHP before titration experiments. Analytical grade NaCl was used to keep ionic strength (I) constant at 100 mM. Titrations were carried out automatically by using autotitrator with thermostated titration vessel under continuous nitrogen (N<sub>2</sub>) stream, and UV-Visible Spectroscopy. Temperature was kept at room temperature ( $25 \pm 0.1$ ). PAMAMs and derivatives (20-100 mg) were dissolved in 20 mL of 0.1 M NaCl solution to give a final concentration of 0.9-5.0 mg/mL. Desired increment of pH was obtained by securely incremental addition of 0.1019 M HCl. The spectral measurements were carried out between 250-350 nm with 5nm intervals with PG TG 70 UV-VIS spectrophotometer. After each pH adjustment, dendrimer solution transferred into the cuvette and the absorption spectrum is recorded. The pKa values of PAMAMs (L) were determined by titrating solutions over the pH range of 2-12 with standardized NaOH solutions. Resulting data were analyzed by using HypSpec 1.1.33 computer software and methodology [253] to calculate the protonation constants and drive species distribution curves.

### **3.7.3 Hierarchical Cluster Analysis (HCA)**

HCA was used to check for pure regions or clusters within data sets. In data mining, HCA is used to build a hierarchy of clusters. In order to determine and decide splitting and merging points of the clusters that refer the pure spectral regions correlated in terms of pH changes from spectroscopic titrations, a measure of dissimilarity between the measurements are required. This was applied by measuring the interpoint distance between all the spectroscopic titration steps with different pH characteristics. Ward's method [242] combined with PCA was used to calculate the matrix of variance weighted distances between cluster centers and defined each point in the data as a separate cluster. Clusters are then merged at this point using linkage method. To achieve the clustering, the data were required to be preprocessed and mined with various options. The Solo+MIA<sup>®</sup> Eigenvector Research 7.0.3 software was used for preprocessing and visualization of the dendrograms for the classification of data. All of the preprocessing methods were applied and best results for HCA analysis of water samples was obtained by using mean-centering.

### **3.7.4 Principal Component Analysis (PCA)**

PCA is an important tool that allows better visualization of data in two (2D) or three-dimensional (3D) environment. Likewise, HCA graphically represents inter-sample and inter-variable relationships. PCA reduces the dimensionality by reducing two or more variables to a single linear combination. These variables are represented by PCs or factors. All the options were tested with Solo-MIA Eigenvector Research 7.0.3 software and optimum results to determine the pure regions on the spectroscopic data were obtained by using mean-centering process. When PCA combined with HCA could be used as a robust chemometric method for the characterization of the pure spectral regions referring the different species form of the aqueous dendrimer solutions. Hence, the number of absorbing species present in the aqueous media can be determined.

### **3.7.5 Data Treatment and Spectral Factor Analysis (SPFA)**

The number of absorbing species in a proton (H) binding dendrimer (L) system were determined by using recent software programs Eigenvector Research 7.0.3 and HypSpec

1.1.33 software together. Data treatment in Eigenvector Research 7.0.3 program was conducted as in the following tasks.

1. After a range of spectrophotometric measurements between the wavelengths 250-350 nm were taken for each pH measurements. A data matrix  $\mathbf{X}$  (NSOLN, NWAVE) where NSOLN, and NWAVE are number of solutions with different pH values and wavelengths analyzed, respectively, were constructed.

2. Data matrix  $\mathbf{X}$  was mean centered and PCA NIPALS algorithm was used. Leave one out Cross validation procedure was applied and RMSECV vs. PCs graphs were plotted. From these plots, PC numbers (absorbing species numbers) were selected where the RMSECV value does not improve more than 2% at the local minima. In this way, it is more reliable to construct a model with less complexity and indicating the number of absorbing species present in the pH range 2-12 where spectroscopic titrations were carried out.

In addition to this, Spectroscopic data were also evaluated with EFA mode of HypSpec Program to determine the number of significant species including cross-validation [236]. In EFA of Hypsec, Eigenvector versus wavelength values were plotted. The plot shows selected eigenvectors. The eigenvectors are the linear combination of the unit spectra. However the coefficients of the linear combinations (absorbing species) are not known. So, the number of eigenvectors where the high level of noise was not present were selected as the number of spectroscopically active species in dendrimer aqueous solutions. It should be emphasized that this analysis does not indicate which species are colored and the eigenvectors cannot be directly assigned to the molar absorbance of any one species. Eigenvector vs. wavelength plots were used to help the number of species that contribute to the observed spectra as a supporting tool the results which are obtained from Eigenvector Research 7.0.3 Software PCs.

### **3.8 Analysis of Co(II)-PAMAM Dendrimer Complexes by UV-VIS Spectroscopy**

#### **3.8.1 Potentiometric Titrations and Measurements**

All solutions were prepared by using carbonate free 18.2 m $\Omega$  Milli-Q water. Carbonate free NaOH solutions were used as titrant after standardized with primary grade KHP. Standardized HCl against was used as excess acid in order to adjust initial pH of

dendrimer solution to low pH. Acid base titration of dendrimers were conducted according to literature [251, 252]. Both acid and base were standardized against KHP before titration experiments. Analytical grade NaCl was added to a precisely weighed portion of PAMAM dendrimer solution to prevent shielding of amine groups and keep the ionic strength (I) constant at 100 mM. Titrations were carried out automatically by using a TitroLine® 7000 (SI Analytics GmbH, Hattenbergstraße, Germany) autotitrator supported with Titrisoft 2.73 software. During titrations temperature was kept at room temperature ( $25 \pm 0.1$ ) by using Polysceince® digital temperature controller circulating bath (Polysceince, Illinois, USA) under continuous nitrogen ( $N_2$ ) stream. P4.NH<sub>2</sub> (18-22 mg) were dissolved in 20 mL of 0.1 M NaCl. The pH meter glass electrode was calibrated with at least three Merck buffer solutions at pH 4.00, 7.00 and 10.00. Ionic strength was maintained by adding appropriate amount of 0.1 M NaCl.

### **3.8.2 UV-VIS Measurements**

UV-VIS spectrum measurements were performed with PG TG 70 UV-VIS spectrophotometer against to Milli-Q water and all the measurements were taken in the wavelength range of 200-750 nm for spectroscopic titration and 450-750 nm for complexation studies with 10 mm quartz UV cells. After complexes of Co (II) to P4.NH<sub>2</sub> at different ratios were prepared, final pH of the solutions were adjusted to 8 and transferred into 10 cm quartz UV cuvette and the absorption spectrum is recorded.

## **3.9 Removal of Metal Ions from Aqueous Solutions by Dendrimer Enhanced Ultrafiltration (DEUF)**

### **3.9.1 Analytical Methods**

The concentration of the metal ions in feed and permeate solutions were measured by Shimadzu AA-6800 AAS as its reported in the literature [41]. The reproducibility of the concentration measurements were in the maximum deviation of % 5 in all cases studies. An automatic titrator, Titroline 7000 were used for the measurement and adjustment of the pH of solutions.

### 3.9.2 Batch Complexation and Polymer Assisted Ultrafiltration (PAUF)

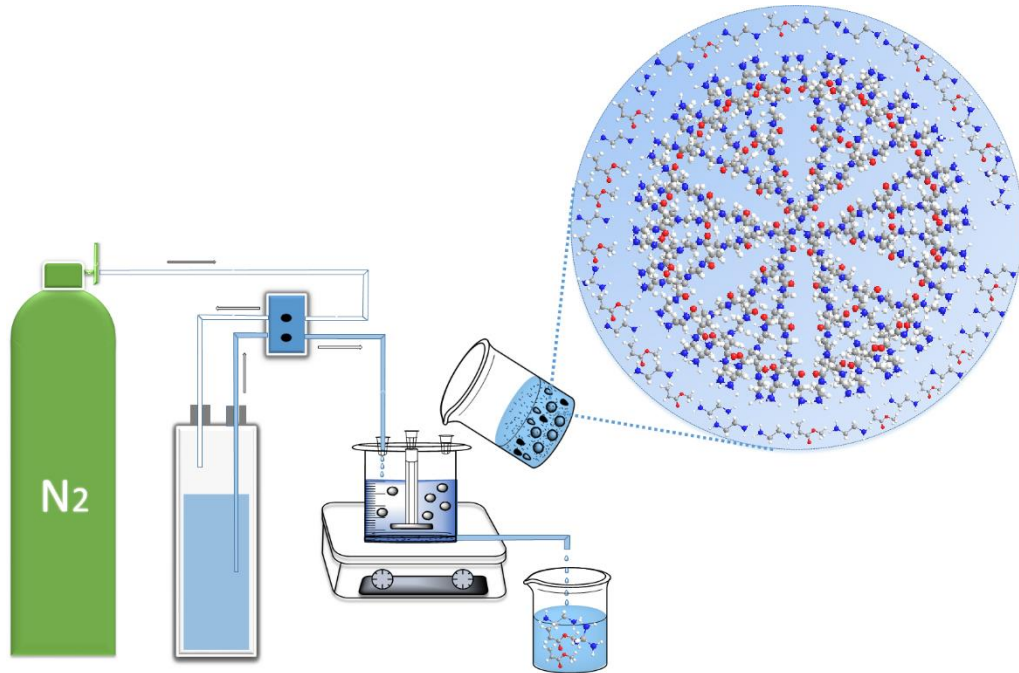


Figure 3.1 Systematic diagram of batch complexation and PAUF

A systematic diagram of batch complexation is shown in Figure 3.1. All complexation experiments were conducted in a stirring 400 mL beaker with a volume of 150 mL. 1:5 molar ratio of standard metal solutions: Cd (II), Zn (II), Ni (II), Co (II), Cu (II) to P3.NH<sub>2</sub> and P4.NH<sub>2</sub> solutions were used for batch complexation. The metal mixture solutions were added to feed solution before the addition of the chelating agent (P4.NH<sub>2</sub>=18.75 mg and P3.NH<sub>2</sub>=18.54 mg) was added to feed solution. pH of the feeding solution was adjusted to the required pH with 0.01 and 0.1 M HCl and NaOH before membrane filtration. The feed solution were mixed for 45 minutes until equilibrium state reached for complexation at room temperature. After the complexation were completed, feed solution transferred in to Amicon 8400 dialysis cell (Figure 3.1). Then, the filtration process was started and followed until 10 permeates with equal masses were collected in time. Commercial membrane YM-1 MWCO was used for the filtrations. During filtration feed solution was stirred gently with magnetic stirrer at 250 rpm. All measurements were conducted by applying an operating pressure 400 kPA. The rejection efficiency for filtration experiments was calculated as the following:

$$Y = \left(1 - \frac{c_p}{c_f}\right) \times 100 \quad (3.1)$$

Where:  $C_f$  is the concentration of metal ion  $[M^{2+}]$  in feed solution (ppm) and  $C_p$  is the concentration of  $[M^{2+}]$  in permeate flux (ppm). Results were shown in the plot of metal retention (%) versus filtration time (hr) figures.

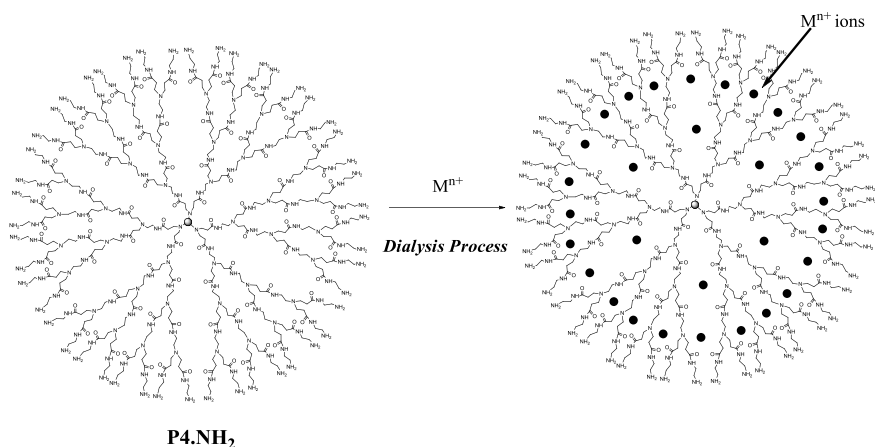


Figure 3.2 Schematic representation of metal complexation of P4.NH<sub>2</sub>

### 3.10 Synthesis and Characterization of Cu-DENs

#### 3.10.1 Binding Studies

Tris and carboxyl surface modified, EDA, DETA and Jeffamine<sup>®</sup> T-403 cored PAMAMs have many metal binding sites (Table 3.2 and Table 3.3). In order to determine the maximum metal loading capacity of each dendrimer; the number of metal ions that can be coordinated with tertiary amine groups were determined by spectroscopic titrations.

#### 3.10.2 Spectroscopic Titration of Dendrimers with Cu<sup>2+</sup> ions

Spectroscopic titration and synthesis of Cu-DENs were adapted from literature [131, 254]. E3-E4, D3-D4, P3-P4 TRIS and COOH PAMAMs were used in this study. Before each titration, the pH of the aqueous unbuffered dendrimer solutions were adjusted to pH ~8.0 and then unbuffered CuSO<sub>4</sub> (pH~4.62) was used to titrate dendrimer solutions.

In General, titration was carried out by the addition of a 10 mL aqueous dendrimer solution to a thermostated vessel at  $25 \pm 0^\circ\text{C}$ . Then, identical aliquots of CuSO<sub>4</sub> solution was added to the vessel each time while a stir bar vigorously stirring the solution. 15~20 seconds were usually allowed to provide sufficient time for Cu<sup>2+</sup> to bind the dendrimers before an absorbance measurement was acquired. UV-VIS spectrum of the solution was

recorded in the wavelength range of 400-900 nm with 5 nm intervals (Table 3.1).  $\lambda_{\text{max}} = 680 \text{ nm}$  was the wavelength, which was associated with the complexation of  $\text{Cu}^{2+}$  ions within the dendrimer with internal tertiary amines of TRIS and carboxyl ended dendrimers (Table 3.2 and Table 3.3). When the excess of  $\text{Cu}^{2+}$  ions was added after the equivalence point, the increase in the absorbance is levelled off, indicating the maximum metal  $\text{Cu}^{2+}$  ions loading capacity of dendrimer. Finally, spectroscopic titration plots, on which absorbance at peak maximum of 680 nm as a function of the  $\text{Cu}^{2+}$  ions per evaluated dendrimers presented were plotted. In order to determine the maximum metal loading capacity of each dendrimer, titration end point was estimated as the extrapolated intersection of the linear regions of the curve before and after the equivalence point. The small absorbance beyond the equivalence point is due to small absorbance contributed by the titrant.

Table 3.1 Concentrations used to titrate aqueous solutions of tris and carboxyl terminated dendrimers with  $\text{Cu}^{2+}$  ions

| <b>Dendrimers</b> | <b>Dendrimer. Conc.(mM)</b> | <b>Conc. of <math>\text{CuSO}_4</math> (mM)</b> | <b><math>\text{CuSO}_4</math> (mM) Increment (<math>\mu\text{L}</math>)</b> |
|-------------------|-----------------------------|---|---|
| E3.TRIS           | 0.441                       | 80.14   | 43  |
| E4.TRIS           | 0.228                       | 81.54   | 37  |
| E3.COOH           | 0.637                       | 80.14   | 44  |
| E4.COOH           | 0.321                       | 80.14   | 44  |
| D3.TRIS           | 0.351                       | 93.12   | 20  |
| D4.TRIS           | 0.202                       | 80.14   | 42  |
| D3.COOH           | 0.549                       | 79.86   | 44  |
| D4.COOH           | 0.268                       | 80.50   | 44  |
| P3.TRIS           | 0.269                       | 81.54   | 35  |
| P4.TRIS           | 0.148                       | 81.54   | 38  |
| P3.COOH           | 0.454                       | 79.86   | 55  |
| P4.COOH           | 0.2                         | 79.86   | 52  |

Table 3.2 Number of amine groups on tris terminated PAMAMs available for binding with Cu<sup>2+</sup> ions

| Dendrimers | Number of surface hydroxyl groups | Number of internal tertiary amine groups |
|------------|-----------------------------------|--|
| E3.TRIS    | 48                                | 14                                       |
| E4.TRIS    | 96                                | 30                                       |
| D3.TRIS    | 60                                | 18                                       |
| D4.TRIS    | 120                               | 38                                       |
| P3.TRIS    | 72                                | 21                                       |
| P4.TRIS    | 144                               | 45                                       |

Table 3.3 Number of amine groups on carboxyl terminated PAMAMs available for binding with Cu<sup>2+</sup> ions

| DENS.   | Number of surface carboxyl groups | Number of internal tertiary amine groups |
|---------|-----------------------------------|--|
| E3.COOH | 16                                | 14                                       |
| E4.COOH | 32                                | 30                                       |
| D3.COOH | 20                                | 18                                       |
| D4.COOH | 40                                | 38                                       |
| P3.COOH | 24                                | 21                                       |
| P4.COOH | 48                                | 45                                       |

### 3.11 P4.NH<sub>2</sub> as Solubility Enhancer of Carvedilol

#### 3.11.1 Phase Solubility Studies

Phase solubility experiments were carried out as per the method described by Higuchi and Connors [255]. 1.87x10<sup>-2</sup>, 3.73x10<sup>-2</sup>, 5.59x10<sup>-2</sup> and 7.46x10<sup>-2</sup> mM P4.NH<sub>2</sub> dendrimer solutions were prepared. Dendrimer solutions were diluted to 5 mL with pH ~7.00 PBS and final pH of the solutions was adjusted to 7.00 by dropwise addition of 0.01-0.1 M NaOH and HCl solutions and transferred to a sealed dark brown glass vessels. Excess

amount of CAR (20 mg) was added to each vessels. Resulting suspensions were shaken with orbital shaker in an incubator at  $24 \pm 01$  °C for 72 hours.

After equilibrium reached, insoluble excess CAR was removed from solutions by using 0.45  $\mu\text{m}$  cellulose acetate filter. The concentration of CAR was determined spectroscopically by using UV-VIS spectrophotometer-PG (Model TG 70 UV-VIS) in the wavelength ranges of 200-350 nm. In lower concentrations of CAR,  $\lambda_{\text{max}}$  absorbans band was observed at 241 nm instead of 249 nm. So, UV measurements were taken at 241 nm (n=4).

### 3.11.2 Drug Binding Constants

The apparent stability constant  $K_{\text{CAR}}$  was calculated from the phase solubility diagram according following Higuchi and Connors equation (3.2) [6]:

$$K_{\text{CAR}} = \frac{\alpha}{S_0(1-\alpha)} \quad (3.2)$$

where,  $S_0$  is the solubility of CAR in the absence of P4.NH<sub>2</sub> at room temperature and  $\alpha$  is the slope of the phase solubility diagram. Encapsulation efficiency of P4.NH<sub>2</sub> (P4.NH<sub>2</sub>EE %) was calculated according to equation (3.3).

$$(\text{P4.NH}_2)\text{EE \%} = \left( \frac{\text{Loaded CAR} - S_0}{S_0} \right) \times 100 \quad (3.3)$$

## 3.12 Determination of Different Generations from Binary Mixtures of Jeffamine® T-403 Cored PAMAMs by UV-VIS Spectroscopy

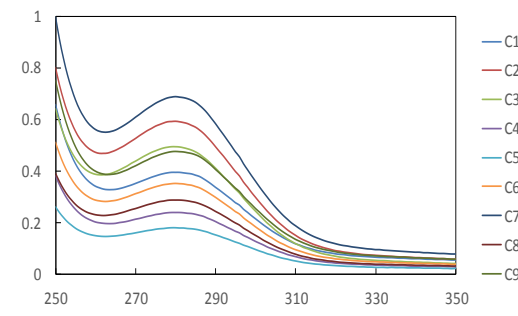
### 3.12.1 UV-VIS Spectroscopy Analysis

#### 3.12.1.1 Design and Analysis of Experiments

A 3<sup>2</sup> full factorial design were used for the design of experiments. The number of independent variables  $Y_1$  and  $Y_2$ , which are P2.NH<sub>2</sub> and P3.NH<sub>2</sub> (k=2), in the mixture were selected as two. The overall absorbance when each component is at a maximum in the mixture were determined within the Beer-Lambert limit (without exceeding 1.2 AU for safety). Variables were evaluated at three levels (l=3) between the range of 3.97 and 15.88 mg for P2.NH<sub>2</sub>, and 3.88 mg and 15.54 mg for P3.NH<sub>2</sub>. Mutually orthogonal

designs were constructed by conducting ( $1^k = 3^2$ ) nine experiments for calibration data. UV-VIS spectra were collected between 250-350 nm as full spectral response to develop multivariate models (Table 3.4).

Table 3.4  $3^2$  Full Factorial Design Layout<sup>a</sup>

| Batch Code   | Variable Levels in Coded Form |                     | Response   |  |
|--------------|-------------------------------|---------------------|--|--|
|              | Y <sub>1</sub> (mg)           | Y <sub>2</sub> (mg) | Full Spectra   |  |
| C1           | -1                            | +1                  |  |  |
| C2           | +1                            | 0                   |  |  |
| C3           | +1                            | -1                  |  |  |
| C4           | -1                            | 0                   |  |  |
| C5           | -1                            | -1                  |  |  |
| C6           | 0                             | 0                   |  |  |
| C7           | +1                            | +1                  |  |  |
| C8           | 0                             | -1                  |  |  |
| C9           | 0                             | +1                  |  |  |
| Coded Values | Actual Values                 |                     |  |  |
|              | Y <sub>1</sub>                | Y <sub>2</sub>      |  |  |
|              | -1                            | 3.97                | 3.89   |  |
|              | 0                             | 9.92                | 9.71   |  |
| +1           | 15.88                         | 15.54               |  |  |

<sup>a</sup>Y<sub>1</sub> indicates the amount of P2.NH<sub>2</sub> (mg) in 10 mL aqueous dendrimer solution. Y<sub>2</sub> indicates the amount of P3.NH<sub>2</sub> (mg) in 10 mL aqueous dendrimer solution

### 3.12.1.2 Preparation of Dendrimer Solutions

Aqueous solutions of intensively purified PAMAMs P2.NH<sub>2</sub> and P3.NH<sub>2</sub> were used in order to prepare the binary mixtures. Sample amount of Y<sub>1</sub> and Y<sub>2</sub> variables for calibration set having the batch code between C1-C9 to form dendrimer mixtures were dissolved in 10 mL of 18.2 mΩ cm double distilled Milli-Q water. No any other sample preparation and treatment were performed before the UV-VIS spectroscopy analysis unless otherwise stated.

### 3.12.2 Data Set

UV-VIS Spectra of P2.NH<sub>2</sub> and P3.NH<sub>2</sub> dendrimer mixtures were collected between the wavelength range of 250-350 nm, which are including the  $\lambda_{max}$  absorbance values of P2.NH<sub>2</sub> and P3.NH<sub>2</sub> (Figure 4.108 in part 4.9.2). Thus, data set including 17 spectrum

was obtained. Spectral evaluation and all preprocessing of data involving centering and normalization were performed by Solo+MIA 7.0.3 (Solo with Multivariate Image Analysis built-in.) Eigenvector Research Software. After the preprocessing, data was divided into a calibration set C1-C9 (nine samples) (Table 3.4) to build the model and a test set (7 samples) to validate the model. Finally, MLR, PCR and PLS regression methods were used to develop multivariate calibration models.

### 3.12.3 Variable Selection

Real reason to build regression models was to make predictions of P2 and P3 quantities of PAMAM dendrimer mixtures, simultaneously. Therefore, before considering the predictive abilities of the models, the first thing to be focused on is the root-mean-square error of calibration (RMSEC). It is defined as

$$\text{RMSEC} = \sqrt{\frac{\sum_{i=0}^C (\hat{y}_i - y_i)^2}{C}} \quad (3.4)$$

where  $\hat{y}_i$  are the values of the predicted variable when all samples are included the model formation and C is the number of calibration samples. RMSEC is a measure of how well the model fits the data.

The ability of model to predict samples that were not used to build model is referred as the root-mean-square error of cross-validation (RMSECV). Equation (3.4) also can be used for the calculation of the RMSECV. In this case,  $\hat{y}_i$  corresponds to predictions for samples that were not included in the model formation. In order to determine the number of factors (k) to be used in PCR and PLS, cross validation procedure was used. In this procedure, ith sample of the data set is left out once, and the remaining samples, PCR and PLS models are formed [256]. RMSECV usually refers to cross validation experiments where the calibration data set is divided into two groups as training and test sets in order to evaluate how a calibration data would perform when applied to a new data. In addition to this, this evaluation can be performed directly by applying a completely independent prediction set of samples which have known Y values. In this point, root-mean square error of prediction (RMSEP) can be calculated when the model is applied to a new data. RMSEP can be calculated as

$$\text{RMSEP} = \sqrt{\sum_{i=0}^{C_t} \frac{(\widehat{y}_i^t - y_i^t)^2}{C_t}} \quad (3.5)$$

where  $C_t$  is the number of test sets;  $\widehat{y}_i^t$  and  $y_i^t$  indicates the measured value and predicted value from the model for  $i$ th sample.

### RESULTS AND DISCUSSION

#### 4.1 Microwave Assisted Synthesis of Amine Terminated PAMAMs

##### 4.1.1 Synthesis of Generation 1-4 PAMAMs

In the conventional synthesis of PAMAM type dendrimers, amidation steps take generally 5-8 days depending on the generation while alkylation steps take 24 hours (Table 4.1, Table 4.2, and Table 4.3) [257]. After the successive alkylations, MAS were performed within 30-80 minutes depending on the PAMAM type and generation (Table 4.4, Table 4.5, and Table 4.6). In the amidation step, important point was the thermal stability. This step was conducted by refluxing ester terminated half generation and EDA mixture in the presence of catalytic amount of methanol in the temperature range of 120-130 °C. The reaction progresses were monitored by ATR to observe the disappearance of esteric peak (1732 cm<sup>-1</sup>) and appearance amide I and amide II peaks (1643 cm<sup>-1</sup> and 1549 cm<sup>-1</sup>) (Figure 4.1). During the reactions, ATR spectra were collected in every 10 minutes through the reaction mixture and observed a decrease in the intensity of esteric peak. After the disappearance of prominent ester peak, MW irradiation was terminated. This was the crucial point, how it was decided and determined the reaction completion. Monitoring the reaction progress by ATR without stopping the reaction was a good advantage. Unlike traditional thin layer chromatography (TLC) monitoring. In ATR monitoring, the reactions were started with MW. During microwave reactions, small identical aliquots of reaction mixture were taken by a micro pipette and their ATRs immediately were measured to monitor the reaction progresses. Removing the excess amount of reagent (EDA) was performed by means of using the n-butanol as a hydrogen competitors followed by LPR. Excess of EDA cannot be removed by simple rotary evaporations even

in the presence of hydrogen competitor such as azeotropic mixture of toluene-methanol or n-butanol. At this point, LPR method provides good purification for the small fractions of undesired dendrimers and excess of EDA.

As a result, series of amine terminated EDA, DETA and Jeffamine<sup>®</sup> T-403 cored PAMAMs (G1-4) were synthesized with a very good yield and purity (Figure 4.3). Complete conversion of amine (P0) to ester (P0.5) and ester to amine (P1.NH<sub>2</sub>) was proven as in ATR spectra in Figure 4.2. These results were also correlated via <sup>1</sup>H NMR and <sup>13</sup>C-NMR spectra.

Polymeric Jeffamine<sup>®</sup> T-403 core allowed to retard the steric hindrance so that Jeffamine cored dendrimers up to four generations could be synthesized without any yield drop. However, this has concluded the final dendrimers not to be perfect monodisperse. As in NMR spectral deconvolution; proton peaks which should arise from primary amino groups were not visible, this could be attributed either too many hydrophilic primary amino groups at the periphery makes densely H-bond or NMR solvents (DMSO-d<sub>6</sub> or CD<sub>3</sub>OD) that can also make H-bond with samples. Same way, the coupling constant of triplet hydrogens couldn't be calculated also, because too many same groups were present at the same positions.

Table 4.1 Preparation of EDA cored ester terminated PAMAMs by conventional method

| <b>Generation</b> | <b>R-Amine<br/>g, (mmol)</b> | <b>MA g,<br/>(mmol)</b> | <b>MeOH<br/>(mL)</b> | <b>Time (h)</b> | <b>Yield (%)</b> |
|-------------------|------------------------------|-------------------------|----------------------|-----------------|------------------|
| E0.5              | 3.00 (49.91)                 | 21.49 (249)             | 40                   | 24              | 99.5             |
| E1.5              | 10.99 (21.26)                | 18.30 (212)             | 40                   | 24              | 92               |
| E2.5              | 15.64 (10.93)                | 18.82 (218)             | 40                   | 24              | 95               |
| E3.5              | 14.60 (4.48)                 | 15.43 (179)             | 40                   | 24              | 93               |

Table 4.2 Preparation of DETA cored ester terminated PAMAMs by conventional method

| Generation | R-Amine<br>g, (mmol) | MA<br>g,(mmol) | MeOH<br>(mL) | Time (h) | Yield (%) |
|------------|----------------------|----------------|--------------|----------|-----------|
| D0.5       | 3.58 (34.78)         | 18.72 (217)    | 40           | 24       | 96.45     |
| D1.5       | 10.24 (15.20)        | 16.35 (190)    | 40           | 24       | 96        |
| D2.5       | 6.76 (3.72)          | 8.02 (93)      | 40           | 24       | 96        |
| D3.5       | 8.12 (1.98)          | 8.53 (100)     | 40           | 24       | 95        |

Table 4.3 Preparation of Jeffamine<sup>®</sup> T-403 cored ester terminated PAMAMs by conventional method

| Generation | R-Amine<br>g, (mmol) | MA<br>g,(mmol) | MeOH<br>(mL) | Time (h) | Yield (%) |
|------------|----------------------|----------------|--------------|----------|-----------|
| P0.5       | 8.22 (18.68)         | 12.06 (140)    | 40           | 24       | 96        |
| P1.5       | 12.00 (10.20)        | 13.74 (154)    | 40           | 24       | 98        |
| P2.5       | 13.48 (5.40)         | 13.95 (162)    | 40           | 24       | 96        |
| P3.5       | 12.00 (2.29)         | 11.84 (138)    | 40           | 24       | 92        |

Table 4.4 Preparation of EDA cored amine terminated PAMAMs by MAS

| Generation         | R-Ester<br>g, (mmol) | EDA <sup>a</sup><br>g,(mol) | MeOH <sup>a</sup><br>(mL) | MW<br>(watt) | Time<br>(min) | Yield (%) |
|--------------------|----------------------|-----------------------------|---------------------------|--------------|---------------|-----------|
| E1.NH <sub>2</sub> | 13.68 (33.81)        | 81.31 (1.35)                | 2                         | 200          | 60            | 95        |
| E2.NH <sub>2</sub> | 19.12 (15.85)        | 76.25 (1.26)                | 4                         | 200          | 60            | 94.6      |
| E3.NH <sub>2</sub> | 20.05 (7.14)         | 68.66 (1.14)                | 3.5                       | 200          | 60            | 90        |
| E4.NH <sub>2</sub> | 15.85 (2.63)         | 50.70 (0.84)                | 4                         | 200          | 60            | 90        |

<sup>a</sup> Methanol as dielectric constant enhancer.

Table 4.5 Preparation of DETA cored amine terminated PAMAMs by MAS

| <b>Generation</b>  | <b>R-Ester<br/>g, (mmol)</b> | <b>EDA<br/>g,(mol)</b> | <b>MeOH<sup>a</sup><br/>(mL)</b> | <b>MW<br/>(watt)</b> | <b>Time<br/>(min)</b> | <b>Yield (%)</b> |
|--------------------|------------------------------|------------------------|----------------------------------|----------------------|-----------------------|------------------|
| D1.NH <sub>2</sub> | 11.48 (21.47)                | 64.68 (1.07)           | 9                                | 250                  | 60                    | 97               |
| D2.NH <sub>2</sub> | 16.51 (10.75)                | 64.63 (1.07)           | 10                               | 250                  | 80                    | 97.5             |
| D3.NH <sub>2</sub> | 9.14 (2.58)                  | 31.05 (0.52)           | 10                               | 250                  | 80                    | 96               |
| D4.NH <sub>2</sub> | 12.34 (1.63)                 | 39.32 (0.65)           | 10                               | 250                  | 80                    | 94.5             |

<sup>a</sup> Methanol as dielectric constant enhancer.

Table 4.6 Preparation of Jeffamine<sup>®</sup> T-403 cored amine terminated PAMAMs by MAS

| <b>Generation</b>  | <b>R-Ester<br/>g, (mmol)</b> | <b>EDA<br/>g,(mol)</b> | <b>MeOH<sup>a</sup><br/>(mL)</b> | <b>MW<br/>(watt)</b> | <b>Time<br/>(min)</b> | <b>Yield (%)</b> |
|--------------------|------------------------------|------------------------|----------------------------------|----------------------|-----------------------|------------------|
| P1.NH <sub>2</sub> | 11.60 (10.30)                | 10.80 (0.18)           | 2                                | 200                  | 30                    | 92               |
| P2.NH <sub>2</sub> | 17.38 (8.05)                 | 58.08 (0.97)           | 4                                | 200                  | 40                    | 91               |
| P3.NH <sub>2</sub> | 14.20 (3.11)                 | 44.90 (0.75)           | 4                                | 200                  | 60                    | 91               |
| P4.NH <sub>2</sub> | 11.85 (11.85)                | 36.49 (0.60)           | 4                                | 200                  | 60                    | 90               |

<sup>a</sup> Methanol as dielectric constant enhancer.

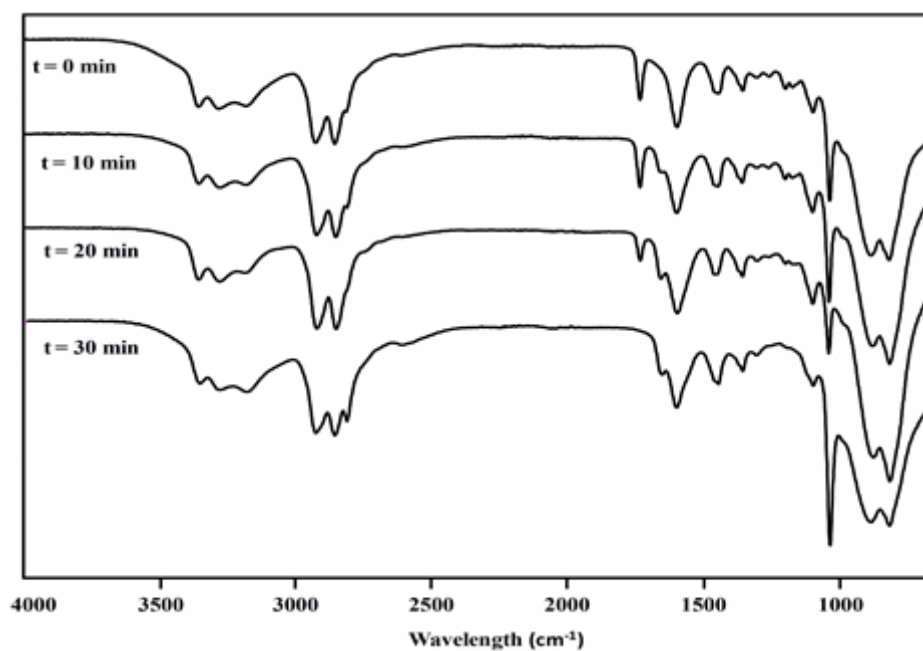


Figure 4.1 ATR monitoring and time dependency from ester to amide (**P0.5** to **P1.NH<sub>2</sub>**) PAMAMs

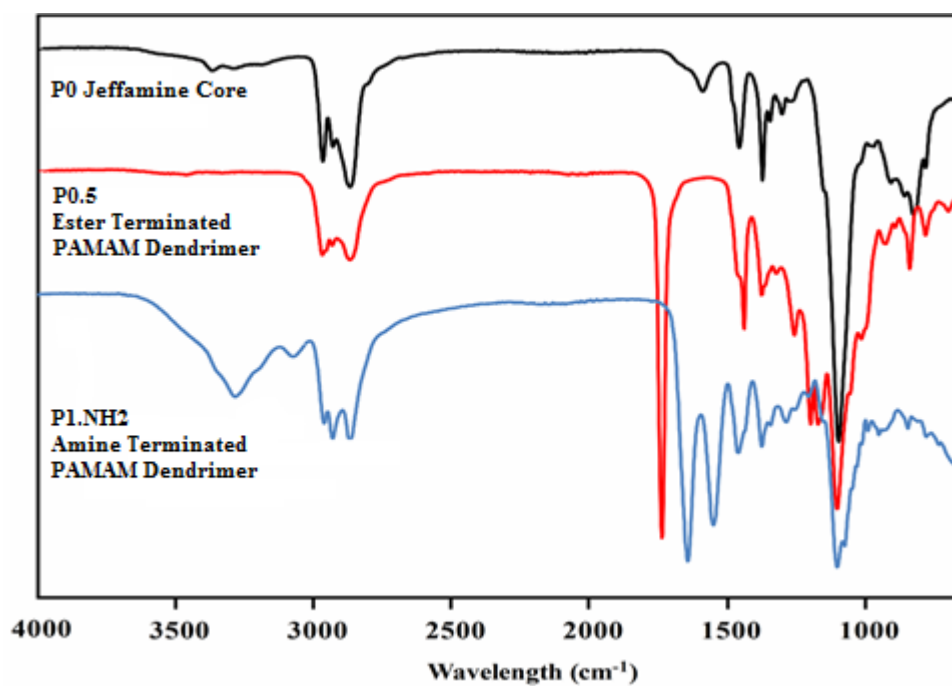


Figure 4.2 ATR spectra of pure, ester, and amine terminated dendrimers respectively

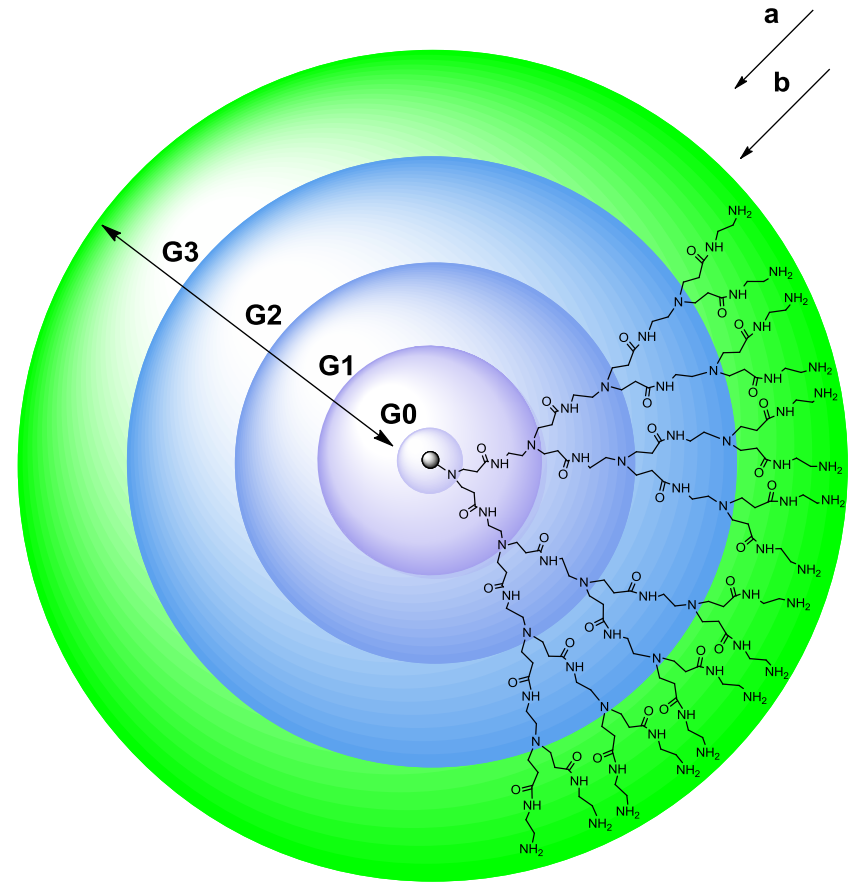
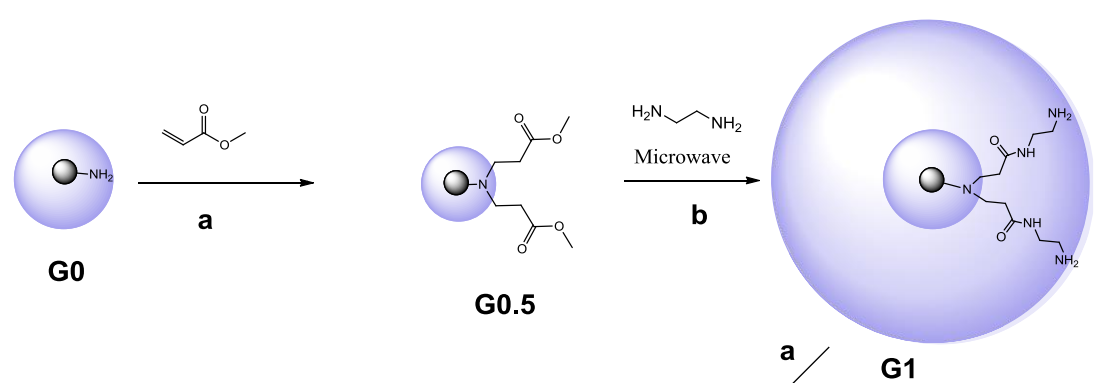
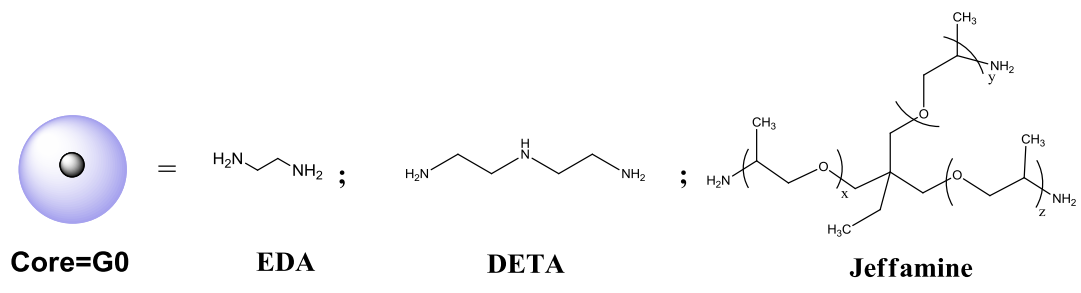


Figure 4.3 Synthesis and structure development of generation (1-4) PAMAMs, a) Alkylation step and b) Amidation step

#### 4.1.2 Comparison of Microwave Assisted Amidation with Conventional Methods

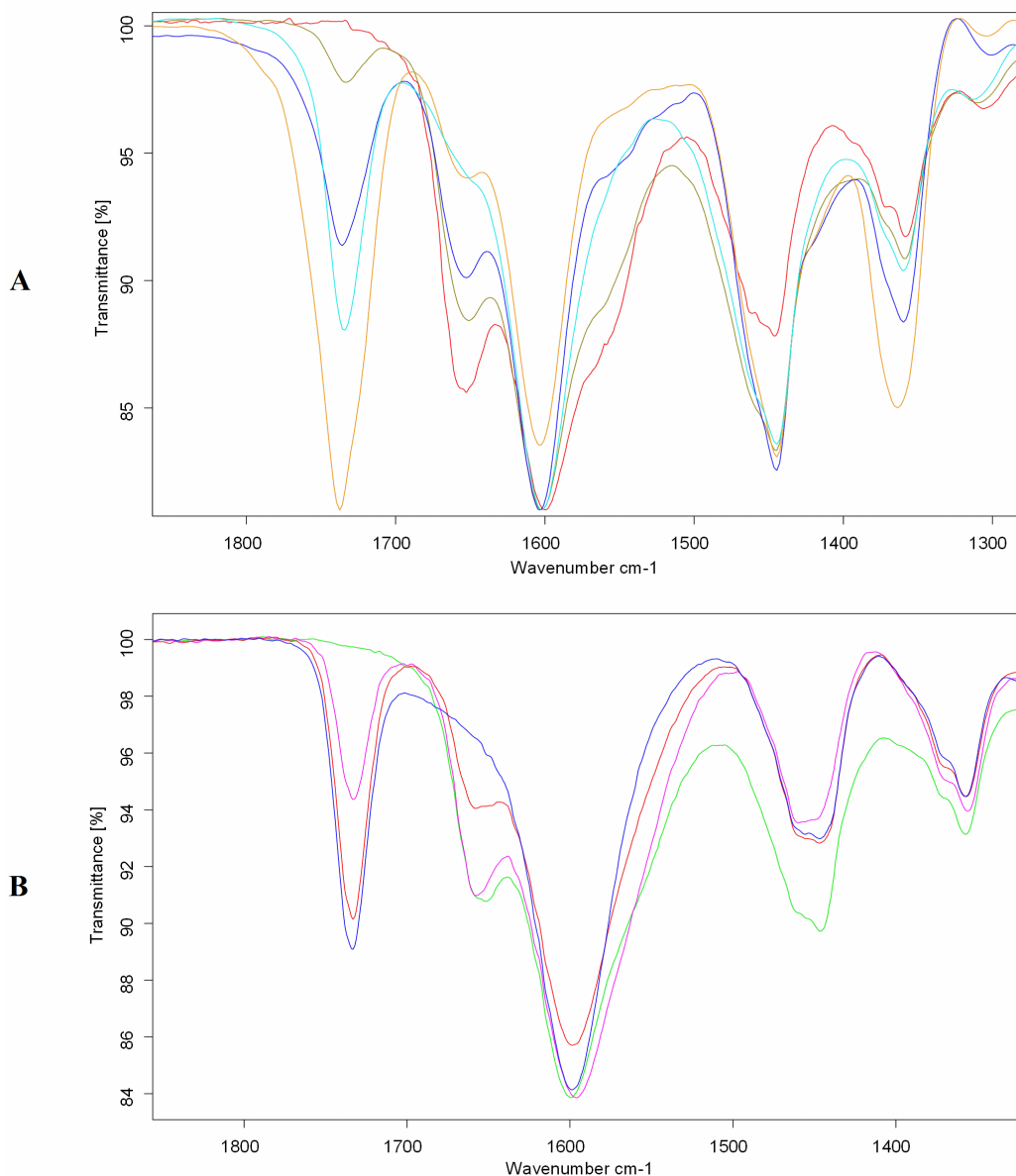


Figure 4.4 ATR monitored conversion spectrum from **P0.5** to **P1.NH<sub>2</sub>** (A) Conventional Conditions: Oil bath, 129<sup>o</sup>C, 150 min. P<sub>0.5</sub> to EDA molar ratio 1:10, 2 mL methanol (B) MW conditions: Open vessel, 200 W, 129 <sup>o</sup>C, 30 min. Dendrimer to EDA ratio: 1:10, 2mL Methanol.

Conversion of **P0.5** to **P1.NH<sub>2</sub>** at 129 <sup>o</sup>C was compared by using conventional method (preheated oil bath) and microwave method (CEM Discover Labmade-Open vessel mode). Conversions were determined by monitoring the disappearance of 1732 cm<sup>-1</sup> ester peak and formation of amide I and II bands (Figure 4.1 and 4.2) by taking identical aliquots at specific time intervals. The conversions achieved by MW were after 10 min. (8.6 %), 20 min. (45.8 %), 30 min (100 %) while 10 min. (12.5 %), 20 min. (24.8 %), 30

min (36.7 %) 60 min. (53.9 %), 90 min. (83.0 %) and 150 min (100 %) by conventional heating in oil bath. These values show that reaction was completed in MW method considerably faster than conventional method. But it could be commented directly whether it is because of MW effect or thermodynamic effect.

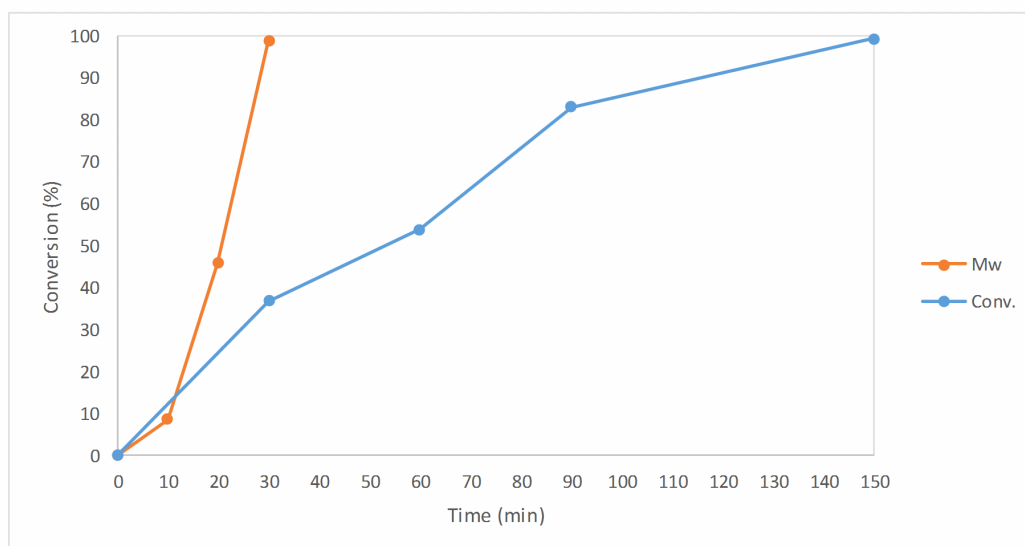


Figure 4.5 Conversion of P0.5 to P1.NH<sub>2</sub> in the presence of 2 mL methanol at 129 °C. Reaction time: 150 min for conventional heating in oil bath and 30 min. under MW. Open vessel mode at 200 W. (Conversion (%) was calculated from the IR spectra (see Figure 4.4)).

In the previous study [258], La Regina has reported open vessel microwave-assisted synthesis by simultaneous cooling while heating under IR sensor temperature control. But, Kappa [259], has strongly criticized this approach by claiming that “when the simultaneous cooling technique is applied, external IR sensors should not be used under any circumstances, since the IR sensor may record a significantly lower temperature (reflecting the vessels surface temperature) than the actual temperature of the reaction mixture inside the reaction vessel”. That is, direct temperature control could not be achieved without using an internal fiber optic (FO) temperature sensor. When accurate reaction temperatures are required, dual systems are recommended. In our case, MAS reactions were performed at bulk temperature (120-130 °C) by using IR temperature controller since simultaneous cooling technique was not applied (Table 4.7).

Table 4.7 Optimization of reaction conditions for the synthesized dendrimers from P1.NH<sub>2</sub> to P4.NH<sub>2</sub>

| Entry | Core | Product            | Heating  | MW (W) <sup>a</sup> | Temp (°C) | Time (min) | Yield <sup>b</sup> (%) |
|-------|------|--------------------|----------|---------------------|-----------|------------|------------------------|
| 1     | P0.5 | P1.NH <sub>2</sub> | Oil bath | -                   | 129       | 150        | 91                     |
| 2     | P0.5 | P1.NH <sub>2</sub> | MW       | 200                 | 129       | 30         | 92                     |
| 3     | P1.5 | P2.NH <sub>2</sub> | Oil Bath | -                   | 128       | 180        | 90                     |
| 4     | P1.5 | P2.NH <sub>2</sub> | MW       | 200                 | 128       | 40         | 91                     |
| 5     | P2.5 | P3.NH <sub>2</sub> | Oil Bath | -                   | 128       | 210        | 91                     |
| 6     | P2.5 | P3.NH <sub>2</sub> | MW       | 200                 | 128       | 60         | 91                     |
| 7     | P3.5 | P4.NH <sub>2</sub> | Oil Bath | -                   | 123       | 210        | 90                     |
| 8     | P3.5 | P4.NH <sub>2</sub> | MW       | 200                 | 123       | 60         | 90                     |

<sup>a</sup> OV: Open vessel mode.

<sup>b</sup> After dialysis.

#### 4.1.3 Gel Permeation Chromatography (GPC) Analysis of Jeffamine<sup>®</sup> T-403 Cored PAMAMs

In the multi-step dendrimer synthesis, there may be some impurities; such as unreacted dendrons, dimerization in the lower generations or dendritic fractals (they are all defects) which may not be identified with simple NMR measurements easily. These fractals may also grow as the desired dendrimer grows and they give very close peaks in the NMR [15, 19]. Poly dispersity index (PDI=Mw (SEC)/Mn (SEC)) interpretations give information about the structural deformation of dendrimers. Increasing PDI value indicates that dendritic fractals and dendrimers have an intermolecular interaction. Dendrimers have relatively high hydrodynamic volume. In order to calculate the Mw of dendrimers with a high accuracy, reference molecule should also maintain the similar property. For this reason, in GPC measurements, selecting suitable reference is very important. In GPC measurements, PS or PEO are generally used as a reference. However, these references are not appropriate for branched molecules like dendrimers, and so, measured molar masses could be smaller than expected molar mass. Therefore; multiangle light scattering

(MALS) detector was selected for GPC measurements of Jeffamine<sup>®</sup> T-403 cored PAMAMs.

Starting core is a polymer and polymers possess average Mw and average PDI (Jeffamine<sup>®</sup> T-403 is quite monodisperse but not perfect (PDI is 1.04). Membrane dialysis was used to purify synthesized **P1-P4.NH<sub>2</sub>** Analysis of dendrimers by GPC showed characteristic PDI values in the range of 1.02-1.09. This indicates that each generation is in unified distribution and the PDI values are quite consistent with the literature to say monodisperse [32, 53, 260, 261]. However, we could not establish any correlation between the PDI values and increasing generations (Table 4.8 and Figure 4.6).

Table 4.8 Molecular weight dependency of different generation of PAMAMs

| Generations        | Mw <sup>a</sup> | Mw (NMR) | Mn (SEC) | Mw(SEC) | PDI  |
|--------------------|-----------------|----------|----------|---------|------|
| P1.NH <sub>2</sub> | 1,124           | 1,135    | 960      | 981     | 1.02 |
| P2.NH <sub>2</sub> | 2,492           | 2,537    | 2,300    | 2472    | 1.09 |
| P3.NH <sub>2</sub> | 5,228           | 5,089    | 4,300    | 4,400   | 1.02 |
| P4.NH <sub>2</sub> | 10,700          | 10,233   | 9,200    | 9,600   | 1.04 |

<sup>a</sup> Mw: Theoretical molecular weight (g/mol)

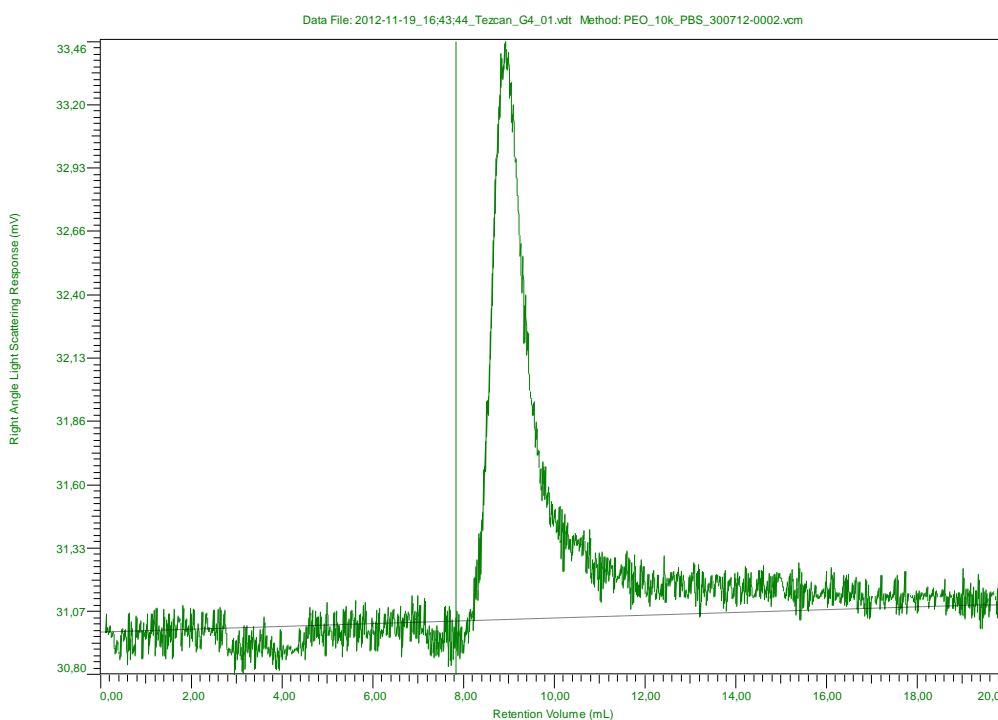


Figure 4.6 GPC of P4.NH<sub>2</sub>

## 4.2 Synthesis of Water soluble PAMAM Derivatives

### 4.2.1 Surface Modification of PAMAMs

The advantage of controllable structures of dendrimers make them suitable for a wide range of applications. Predominantly, terminal groups of dendrimers attain them unique properties. Although, amine terminated dendrimers are water soluble [164], they are mostly at protonated conformation at the pH media of the living cells physiological functions. Thus, when dendrimers come in contact with negatively charged cells, hemolysis of cell occurs. This event makes a negative effect on the future development of clinical applications of amine terminated dendrimers [262].

Drug delivery and toxicity studies on the derivatives of PAMAMs revealed that carboxyl terminated dendrimers are less toxic and their negative charge on the periphery prohibit them to bind or interact with the negatively charged surface of the cells [263]. Thus, in here, different generation and type of water soluble carboxyl and Tris terminated PAMAM derivatives were synthesized (Figure 4.7).

Tris is known as the abbreviation of the common organic compound of tris (hydroxyl methyl) amino methane, which has three surface functional hydroxyl groups. When tris is attached to ester terminated half generation of PAMAMs, the number of resulting terminal hydroxyl groups are three folded. Thus, Tris terminated PAMAMs gain infinitely soluble property and they can be used as drug carrier in many applications [143]. Newkome et al. [173, 264] reported the synthesis of tris terminated PAMAMs from commercially available EDA cored dendrimers previously. By applying the same procedure, Beezer et al. [143] was synthesized three water soluble dendrimers and showed the effect of PAMAMs with Tris surface functionalized on the solubility of a small acidic hydrophobe molecule benzoic acid from 2.9 to 305 mg/mL via inclusion complex formation.

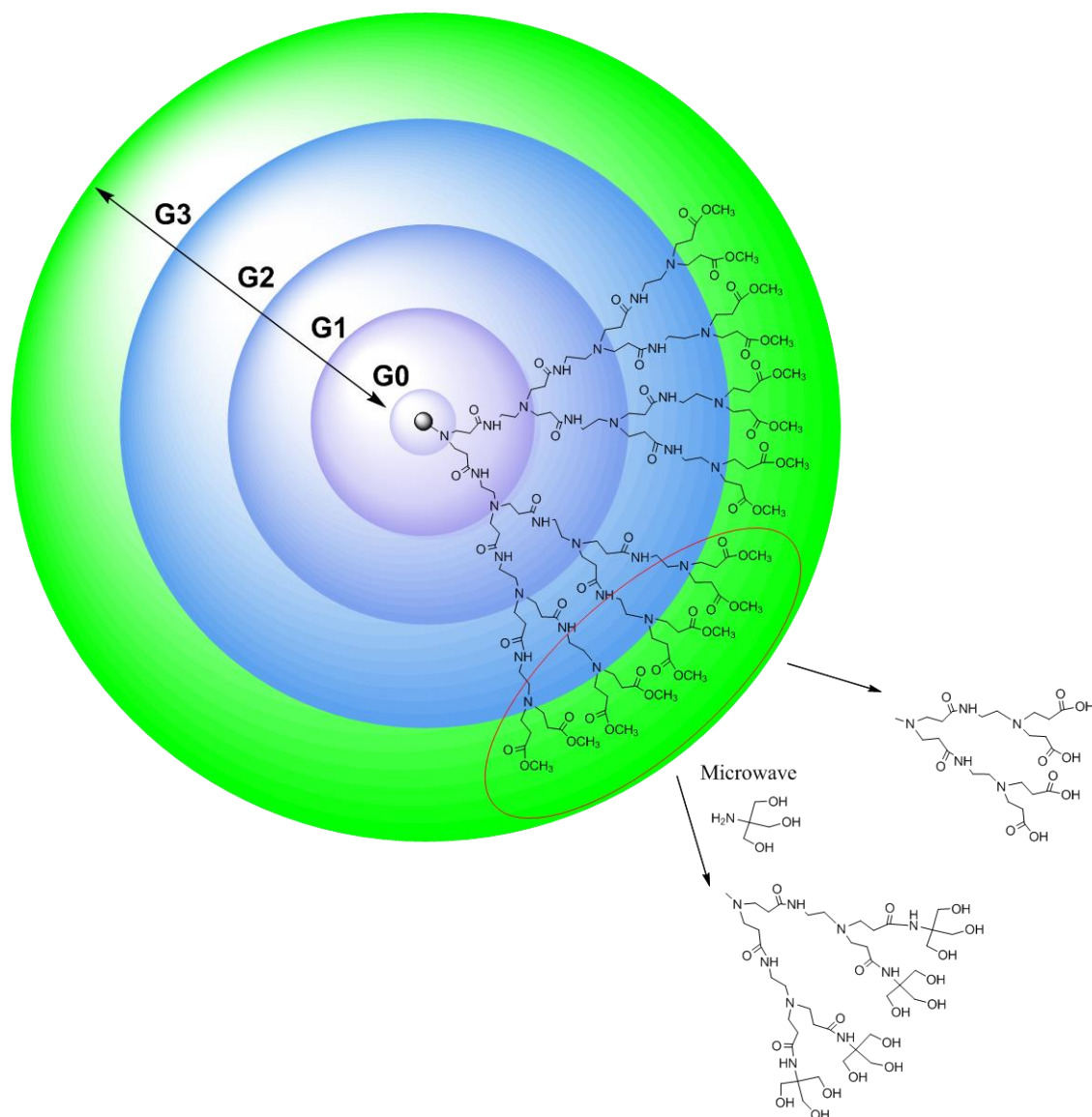


Figure 4.7 Tris and carboxyl surface modification of esteric generations

In this part, synthesis of third and fourth generation EDA, DETA and Jeffamine<sup>®</sup> T-403 core dendrimers with Tris surface functionalized dendrimers were performed with MAS. Monitoring the reaction conditions, deciding the amount of solvent and where to stop were determined with a similar approach used in Part 4.1. Similarly, ATR monitoring of the disappearance of esteric  $1730\text{ cm}^{-1}$  and formation of  $\sim 3260\text{ cm}^{-1}$  broad hydroxyl peak and formation of  $\sim 1635$  and  $\sim 1554\text{ cm}^{-1}$  amide I and amide II peaks were used to decide the completion of reactions. Required MAS conditions for the surface modification of ester terminated half generation PAMAMs were presented in Table 4.9. To sum up, synthesis of tris terminated PAMAMs were shortened up to to 110-135 min. compared to 48 hours in conventional methods [173, 264] (Table 4.9). Furthermore; conversion of half

generation ester terminated PAMAMs to carboxyl terminated PAMAMs were performed by using conventional synthesis method (Table 4.10).

Synthesized water soluble dendrimers could easily be characterized via  $^1\text{H}$  NMR and  $^{13}\text{C}$  NMR. All the expected signals are at the correct intensity and can be seen. In Figure 4.8, the resonances from methyl ester at 3.78 ppm are no longer visible and confirms the complete conversion of ester groups to acids (D4.COOH (middle in Figure 4.8) while formation of a new singlet at 3.71 ppm, resulting from resonances of new methylene protons adjacent to the terminal hydroxyl groups indicates the fully conversion to D4.TRIS (top in Figure 4.8). Moreover, formation of the 181.61, 181.46, 174.86 ppm corresponding to acids and interior amides proves the fully conversion of D3.5 to D4.COOH. Likewise to  $^1\text{H}$  NMR, the strong resonance corresponding to the methyl groups of terminal methyl group at 173.13(C=O), 51.87(COOCH<sub>3</sub>) ppm in the  $^{13}\text{C}$  NMR is no more available. In  $^{13}\text{C}$  NMR of Tris terminated conversions, the formation of 56.67(NHCR<sub>3</sub>), 63.6 (CH<sub>2</sub>OH) ppm bands were indicated the fully formation of tris terminated PAMAMs. Therefore,  $^1\text{H}$  NMR and  $^{13}\text{C}$  NMR spectroscopy evaluations prove a good purity.

In ATR spectroscopy, Figure 4.6 and 4.10 show a representative conversion of D3.5 to water soluble D4.COOH and D4.TRIS dendrimers, respectively. The disappearance of esteric peak  $1730\text{ cm}^{-1}$  and formation of two asymmetrical stretching  $1650\text{-}1550\text{ cm}^{-1}$  and a weaker, symmetrical band near  $1400\text{ cm}^{-1}$  also proves the complete conversion of ester terminated D3.5 to D4.COOH. Similar spectral deconvolutions were observed during the synthesis of EDA, DETA, Jeffamine<sup>®</sup> T-403 cored water soluble dendrimers (Appendix A).

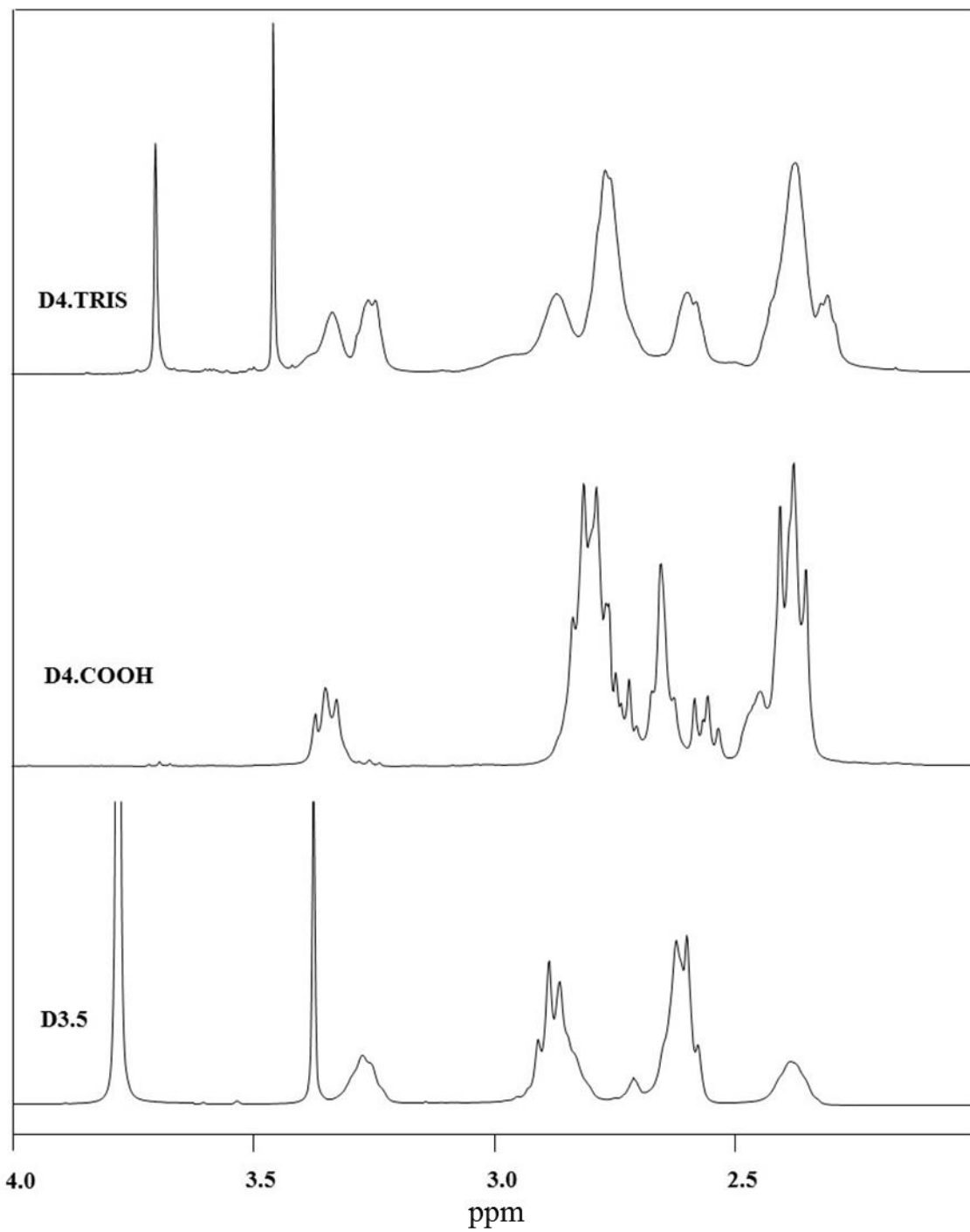


Figure 4.8  $^1\text{H}$  NMR spectrum monitoring of the conversion of D3.5 (bottom) to D4.COOH (middle) and D4.TRIS (Top)

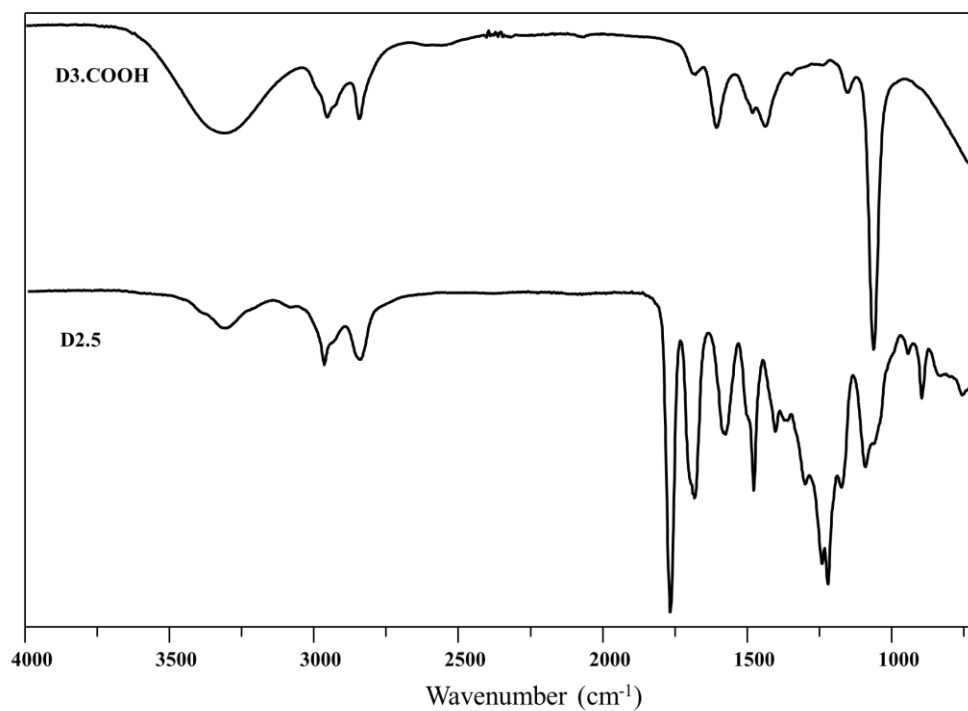


Figure 4.9 ATR monitoring and time dependency from ester to amide (D2.5 to D3.COOH) PAMAMs

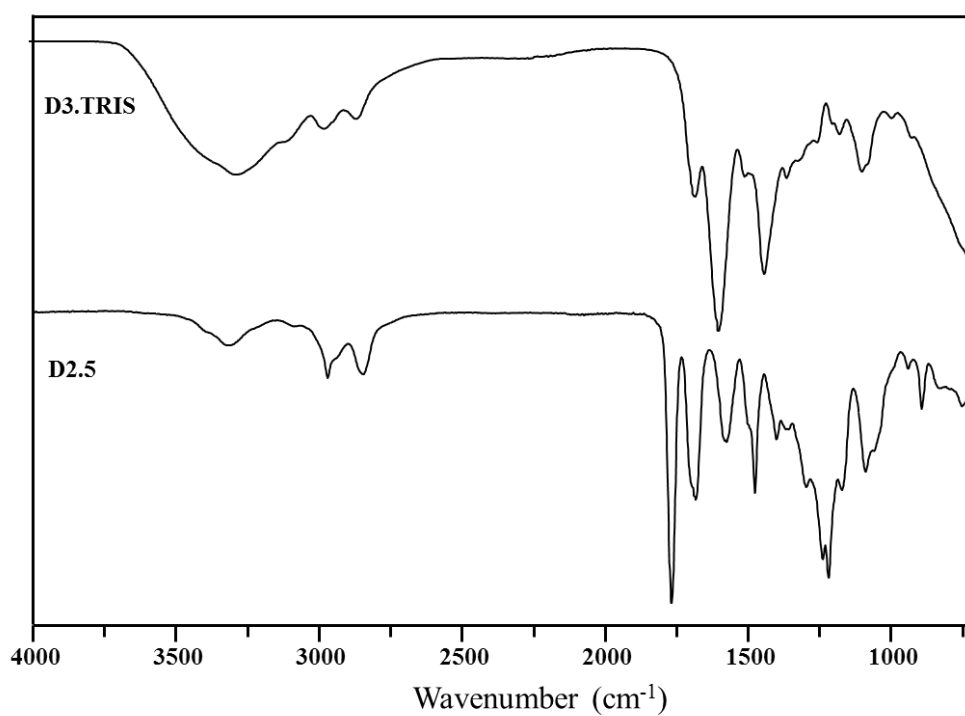


Figure 4.10 ATR monitoring and time dependency from ester to amide (D2.5 to D3.TRIS) PAMAMs

Table 4.9 Preparation of Tris terminated PAMAMs

| <b>G</b> | <b>R-Ester<br/>g, (mmol)</b> | <b>Tris<br/>g, (mmol)</b> | <b>K<sub>2</sub>CO<sub>3</sub><br/>g, (mmol)</b> | <b>MeOH<br/>(mL)</b> | <b>MW<br/>(watt)</b> | <b>Time<br/>(min)</b> | <b>Yield (%)</b> |
|----------|------------------------------|---------------------------|--|----------------------|----------------------|-----------------------|------------------|
| E3.TRIS  | 1.72 (0.61)                  | 1.43 (11.77)              | 2.03 (14.71)                                     | 10                   | 200                  | 120                   | 96               |
| E4.TRIS  | 0.99 (0.16)                  | 0.76 (6.29)               | 1.08 (7.85)                                      | 10                   | 200                  | 140                   | 93               |
| D3.TRIS  | 0.98 (0.27)                  | 0.80 (6.64)               | 1.15 (8.29)                                      | 15                   | 200                  | 110                   | 95               |
| D4.TRIS  | 1.12 (0.14)                  | 0.85 (7.04)               | 1.22 (10.04)                                     | 13                   | 200                  | 125                   | 94               |
| P3.TRIS  | 0.68 (0.15)                  | 0.53 (4.33)               | 0.75 (5.42)                                      | 10                   | 200                  | 120                   | 91               |
| P4.TRIS  | 0.84 (0.09)                  | 0.62 (5.16)               | 0.89 (6.46)                                      | 10                   | 200                  | 135                   | 93               |

Table 4.10 Preparation of carboxyl terminated PAMAMs

| <b>G</b> | <b>R-Ester<br/>g, (mmol)</b> | <b>NaOH<br/>g, (mmol)</b> | <b>MeOH<br/>(mL)</b> | <b>Time<br/>(h)</b> | <b>Yield (%)</b> |
|----------|------------------------------|---------------------------|----------------------|---------------------|------------------|
| E3.COOH  | 0.79 (0.28)                  | 0.27 (6.80)               | 4.5                  | 24                  | 100              |
| E4.COOH  | 0.65 (0.10)                  | 0.21 (5.20)               | 4                    | 24                  | 100              |
| D3.COOH  | 1.12 (0.31)                  | 0.41 (10.22)              | 6.8                  | 24                  | 100              |
| D4.COOH  | 0.76 (0.10)                  | 0.29 (7.15)               | 4.6                  | 24                  | 100              |
| P3.COOH  | 1.15 (0.25)                  | 0.36 (9.1)                | 6                    | 24                  | 100              |
| P4.COOH  | 0.98 (1.033)                 | 0.29 (7.56)               | 5                    | 24                  | 100              |

### 4.3 Determination of the Protonation Constants of PAMAMs by Hyperquad Program

#### 4.3.1 Potentiometric Titrations and Measurements

All potentiometric titrations of PAMAMs were carried out by using TitroLine® 7000 autotitrator with high precise IoLine glass electrode with iodine/iodide reference system. Titrisoft 2.6 software was used to manage titration process over personal computer. Secure mode was used to collect pH data reducing the pH drift error to a minimum with the pH reading error of 0.002 and volume reading error of 0.001 mL. Hence, it was further verified that all titration curves were fully reversible and independent of the dendrimer

concentration within experimental error, indicating that dendrimer-dendrimer interactions are negligible. Observed experimental data were considered first of all in terms of macroscopic constants for modelling of the ligand protonation constants in HYPERQUAD software. However, models have been constructed in terms of microscopic protonation constants as too many protons present in dendrimer and they display common protonation constants in different groups like tertiary amine or primary amine groups' independent protonation behavior.

In this study, potentiometric titrations of amine and tris terminated PAMAMs were performed. Tris ended dendrimers just have the tertiary amines. Thus, experimentally observed tertiary amine numbers of these dendrimer were used as supportive to explain potentiometric titration results of amine terminated dendrimer as just the difference between them surface hydroxyl functional groups. Experimental conditions to perform potentiometric titration of amine and Tris ended PAMAMs can be seen from Table 4.11.

Table 4.11 Experimental potentiometric titration conditions for different PAMAMs<sup>a</sup>

| <b>Dendrimer</b>   | <b>Total weight (mg)</b> | <b>pH range</b> | <b>Initial Volume (mL)</b> | <b>Excess acid (mL)</b> | <b>HCl (mol/L)</b> | <b>NaOH (mol/L)</b> | <b>Data points</b> |
|--------------------|--------------------------|-----------------|----------------------------|-------------------------|--------------------|---------------------|--------------------|
| E3.TRIS            | 19.53                    | 2.78-11.00      | 20                         | 1.325                   | 0.098              | 0.0496              | 148                |
| E4.TRIS            | 21.00                    | 2.77-11.00      | 20                         | 1.700                   | 0.098              | 0.0496              | 167                |
| D3.TRIS            | 19.76                    | 2.47-11.20      | 20                         | 1.125                   | 0.098              | 0.0496              | 248                |
| D4.TRIS            | 19.76                    | 2.47-11.30      | 20                         | 1.950                   | 0.098              | 0.0496              | 246                |
| P3.TRIS            | 18.46                    | 2.81-11.00      | 20                         | 1.425                   | 0.099              | 0.0485              | 152                |
| P4.TRIS            | 21.10                    | 2.79-11.00      | 20                         | 1.300                   | 0.099              | 0.0485              | 146                |
| E3.NH <sub>2</sub> | 20.28                    | 2.40-11.00      | 20                         | 2.5                     | 0.1030             | 0.0493              | 254                |
| E4.NH <sub>2</sub> | 20.50                    | 2.50-11.00      | 20                         | 2.5                     | 0.1030             | 0.0493              | 268                |
| D3.NH <sub>2</sub> | 20.78                    | 2.47-11.00      | 20                         | 2.5                     | 0.1030             | 0.0493              | 255                |
| D4.NH <sub>2</sub> | 20.32                    | 2.50-11.00      | 20                         | 2.5                     | 0.1030             | 0.0493              | 259                |
| P3.NH <sub>2</sub> | 21.71                    | 2.48-11.00      | 20                         | 2                       | 0.1019             | 0.0485              | 232                |

Table 4.11 (cont'd)

|                    |       |            |    |     |        |        |     |
|--------------------|-------|------------|----|-----|--------|--------|-----|
| P4.NH <sub>2</sub> | 19.43 | 2.46-11.50 | 20 | 2.5 | 0.0992 | 0.0484 | 351 |
|--------------------|-------|------------|----|-----|--------|--------|-----|

<sup>a</sup>25  $\mu$ L increments, error in reading is 1  $\mu$ L,  $l=100$  mm at  $25 \pm 0.1$  °C, error in pH reading is 0.002

### 4.3.2 Primary Amine Terminated PAMAMs

Potentiometric titration curves were conducted in order to determine the number of primary and tertiary amine groups. Amines on the dendrimers were determined by using back-titration since this method displays the full protonation state of PAMAMs and their derivatives [251]. PAMAMs exhibit three end points. One is for excess acid stemming from the consumption of excess acid during back titration. Other two are for tertiary (<sup>3</sup>N) and primary (<sup>1</sup>N) amine groups. Thus, the number of tertiary and primary amine groups can be determined from the experimental evaluation of the stoichiometric proportion of the total mmoles of base used as titrant to total mmoles of dendrimer used. Experimentally calculated amine numbers of E4.NH<sub>2</sub>, D4.NH<sub>2</sub>, P4.NH<sub>2</sub> were compared with the theoretical values in Table 4.12.

Table 4.12 Physico-chemical Properties of different generation EX.NH<sub>2</sub>, DX.NH<sub>2</sub>, PX.NH<sub>2</sub> PAMAMs<sup>a</sup>

| Gn.(X) | EX.NH <sub>2</sub> |                |                | DX.NH <sub>2</sub> |                |                | PX.NH <sub>2</sub> |                |                |
|--------|--------------------|----------------|----------------|--------------------|----------------|----------------|--------------------|----------------|----------------|
|        | MW                 | <sup>3</sup> N | <sup>1</sup> N | MW                 | <sup>3</sup> N | <sup>1</sup> N | MW                 | <sup>3</sup> N | <sup>1</sup> N |
| 1      | 516                | 2              | 4              | 674                | 3              | 5              | 1,125              | 3              | 6              |
| 2      | 1,430              | 6              | 8              | 1,816              | 8              | 10             | 2,495              | 9              | 12             |
| 3      | 3,257              | 14             | 16             | 4,100              | 18             | 20             | 5,235              | 21             | 24             |
| 4      | 6,912              | 30             | 32             | 8,667              | 38             | 40             | 10,717             | 45             | 48             |

<sup>a</sup>MW: Molecular weight (g/mol); Gn.(X) is the generation number.

Potentiometric titration studies of E4.NH<sub>2</sub>, D4.NH<sub>2</sub> and P4.NH<sub>2</sub> have revealed two end points (Table 4.13). In titration of E4.NH<sub>2</sub>, experimentally observed amine numbers correspond to tertiary and primary amine numbers [251, 252]. As an evidence, the comparison of experimental average total amine number of E4.NH<sub>2</sub> in Table 4.13 with theoretical value of total amine number 62 which is the sum of <sup>3</sup>N (30) and <sup>1</sup>N (32) in

Table 4.12 indicates that theoretical and experimental values of total amine numbers values are in good agreement with 96.01 %. This value is in connection with the literature [56, 78, 265] and an easy way to enlighten the protonation behavior of tertiary and primary amine groups of PAMAMs distinctively, in addition to the purity assessment of PAMAMs. This is mostly asserted as the result of the low electrostatic interaction of amine groups and supported by the core shell mechanism of the protonation of PAMAMs [65, 266, 267] unlike the onion like protonation mechanism of PPIs [65].

However, situation is a little bit different in the potentiometric studies of D4.NH<sub>2</sub> and P4.NH<sub>2</sub>. For P4.NH<sub>2</sub> which is a polymeric cored dendrimer, only the outer primary amine groups and the outermost tertiary amine groups could be observed (Table 4.12). Theoretical total amine number of P4.NH<sub>2</sub> makes 72, which is the sum of <sup>1</sup>N (48) and outer shell <sup>3</sup>N (24) (See Table 4.12). If it is compared with the experimental average total amine number of P4.NH<sub>2</sub>, 67.25, it could be concluded that there exist 93.40 % convenience. Similarly, D4.NH<sub>2</sub> has the percent of 97.3 with the exception that 2<sup>nd</sup> end point reflects the total amine number of the primary and outer shell tertiary amines while 1<sup>st</sup> end point rest. To sum up, unobservable inner tertiary amine groups or co-observance of outer tertiary amine groups with primary amine groups for P4.NH<sub>2</sub> having polymeric core, and D4.NH<sub>2</sub> with three arm branched core diethylene triamine (DETA) could be attributed to the extent of electrostatic interactions that could be present among the dendrimer core tertiary amine groups, branching tertiary amine groups and periphery amines with each other, and affect the measurements of potentiometric titrations by shielding the theoretically present total amine numbers. In literature, these interactions could only be understood by applying models to fit to potentiometric titration curve and so it is possible to talk about microscopic titration. These interactions have been studied some groups and still under discussion [65, 76] and here is beyond discussion.

Table 4.13 Corresponding amine numbers to 1<sup>st</sup> and 2<sup>nd</sup> end points of the potentiometric titration curves<sup>a</sup>

| Type of Dendrimer  | 1 <sup>st</sup> end point | 2 <sup>nd</sup> end point | Total Amine number |
|--------------------|---------------------------|---------------------------|--------------------|
| E4.NH <sub>2</sub> | 27.69 ± 1.21              | 31.84 ± 1.65              | 59.53 ± 2.54       |
| D4.NH <sub>2</sub> | 19.45 ± 1.38              | 56.48 ± 2.18              | 75.93 ± 2.90       |
| P4.NH <sub>2</sub> | 23.434 ± 0.86             | 44.09 ± 1.18              | 67.25 ± 1.19       |

<sup>a</sup>Five repeated measurements were conducted.

### 4.3.3 Effect of Ionic Strength on Potentiometric Titration Curves of Amine Terminated PAMAMs

Various experiments have been conducted related with the effect of ionic strength on potentiometric titration curves' end points [64, 76]. Results of these studies revealed in general that increasing ionic strength makes end points more sharp. Sharpness of the end point is explained by the reducing electrostatic interaction. That is, the shielding effect of amine groups to each other is lessened and the number of amino groups can be analyzed and determined more clearly. In this study, 0-100 mM range of NaCl were used to investigate the effect of ionic strength on different kind of fourth generation PAMAMs. Results showed that increasing ionic strength, increases the incline of the end points. When a common derivative of the potentiometric titration curves was explored, this increasing incline resulting the sharpness could be easily seen in the same manner in Figure 4.11, 4.12 and 4.13 for E4.NH<sub>2</sub>, D4.NH<sub>2</sub> and P4.NH<sub>2</sub>, respectively.

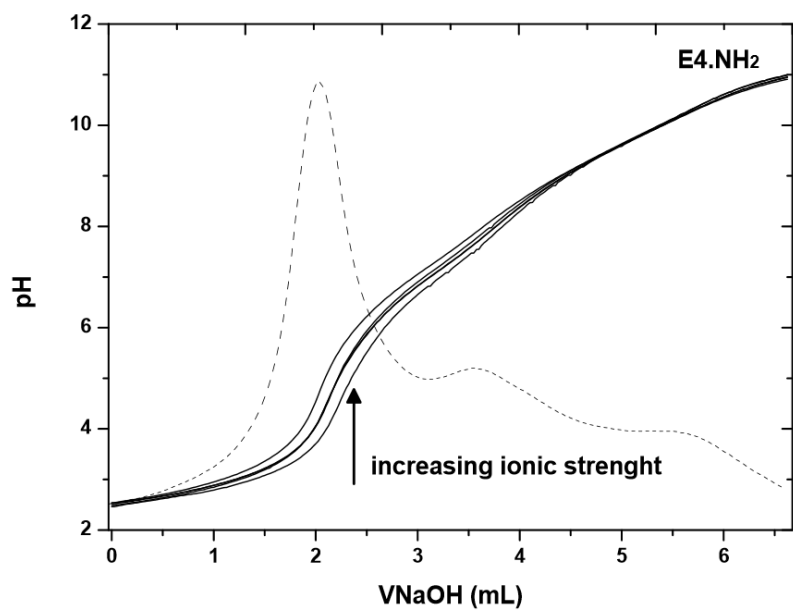


Figure 4.11 Potentiometric pH titration curves for E4.NH<sub>2</sub> at ionic strength of 0, 10, 25, 50, and 100 mM respectively

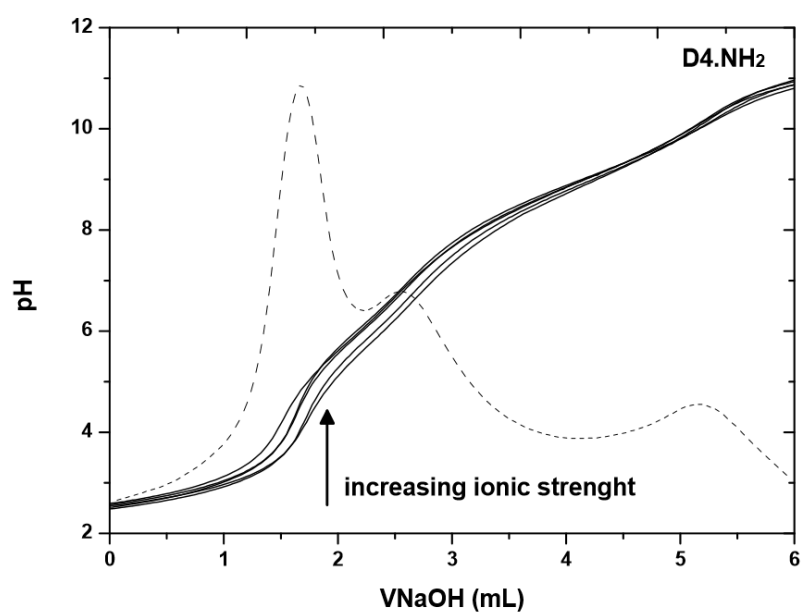


Figure 4.12 Potentiometric pH titration curves for D4.NH<sub>2</sub> at ionic strength of 0, 10, 25, 50, and 100 mM respectively

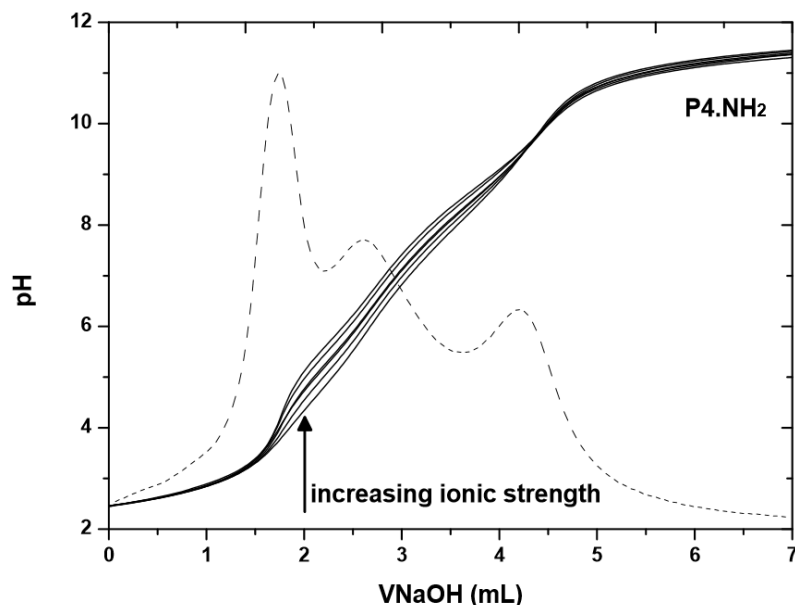


Figure 4.13 Potentiometric pH titration curves for P4.NH<sub>2</sub> at ionic strength of 0, 10, 25, 50, and 100 mM respectively

#### 4.3.4 Tris Terminated PAMAMs

TRIS is the abbreviation of the common known organic compound. Tris (hydroxylmethyl) aminomethane, with the formula (HOCH<sub>2</sub>)<sub>3</sub>CNH<sub>2</sub>. TRIS is widely used in biochemistry and molecular biology and it is highly water soluble. Half generation esteric solutions of PAMAMs are generally water insoluble. Dendrimers are known as designable polymers and they can be used as the building blocks. Surface functionalization of water insoluble half generation ester terminated PAMAMs with Tris functional groups are water soluble because of the high number of surface hydroxyl groups on the periphery.

Potentiometric acid-base titrations allow us to determine average numbers of primary and tertiary amine groups in dendrimers. Initial pH of the aqueous solutions of EX.TRIS, DX.TRIS and PX.TRIS surface modified PAMAMs were in the pH range of 9.7-10.00. According to back titration procedure, initial pH of the solutions were adjusted to pH~2 and back titrated with standardized NaOH (Table 4.11). During potentiometric titration of Tris terminated PAMAMs, two distinctive end points were observed. One of these points is for back titration of excess acid added to initial dendrimer solution while the second one corresponds to total mmoles of the observed tertiary amine groups that dendrimers have. Sample potentiometric titration curves of E4.TRIS, D4.TRIS, and P4.TRIS

PAMAMs can be seen in Figure 4.14, 4.15 and 4.16, respectively. Second derivative of potentiometric titration curves were overlapped in these figures to show end points obviously. These points are accepted as the inflection points and Diallo et al. [56] accept these points as to be pKa values of Tris ended dendrimers. Inflection points of E4.TRIS, D4.TRIS, and P4.TRIS can be seen from Figure 4.14, 4.15 and 4.16. Those of E3.TRIS, D3.TRIS, and P3.TRIS has not shown. According to Diallo's approach, pKa values of the tertiary amine groups of tris ended dendrimers were presented in Table 4.14. It can be seen that the pKa values of tris ended dendrimers increases as the basicity of dendrimer increase in aqueous solutions with increasing number of surface hydroxyl numbers (Table 4.14 and Table 4.15)

Table 4.14 pKa values of the tris terminated PAMAMs at the corresponding inflection point

|                       | <b>E3.TRIS</b> | <b>E4.TRIS</b> | <b>D3.TRIS</b> | <b>D4.TRIS</b> | <b>P3.TRIS</b> | <b>P4.TRIS</b> |
|-----------------------|----------------|----------------|----------------|----------------|----------------|----------------|
| pKa ( <sup>3</sup> N) | 9.71           | 9.81           | 9.75           | 9.79           | 9.63           | 9.78           |

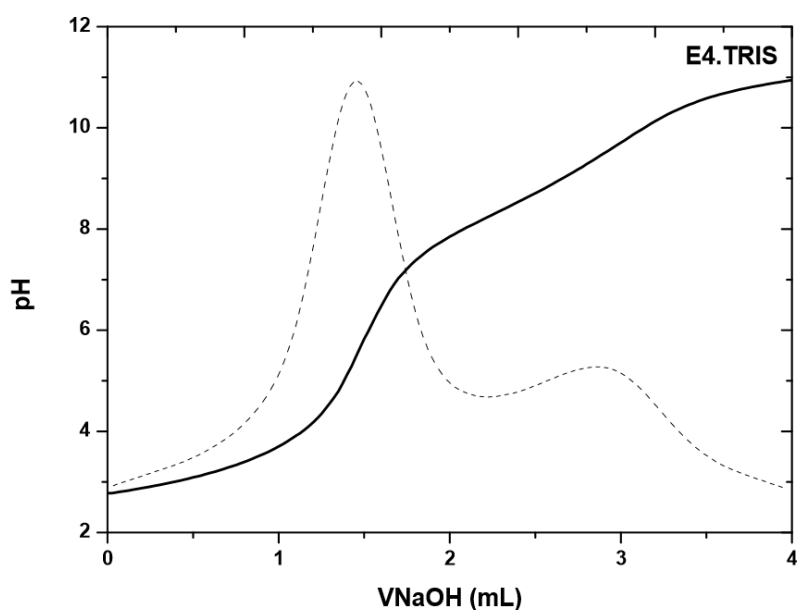


Figure 4.14 Potentiometric pH titration curve for E4.TRIS at ionic strength 100 mM

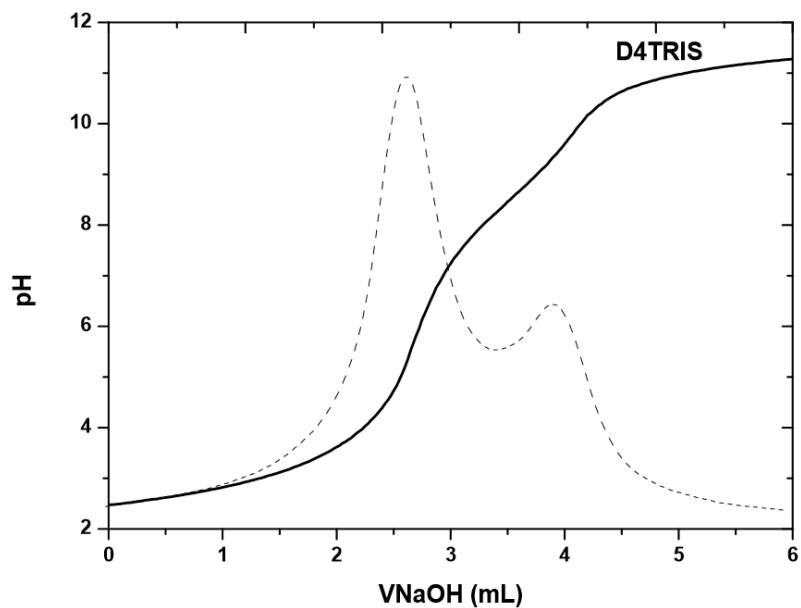


Figure 4.15 Potentiometric pH titration curve for D4.TRIS at ionic strength 100 mM

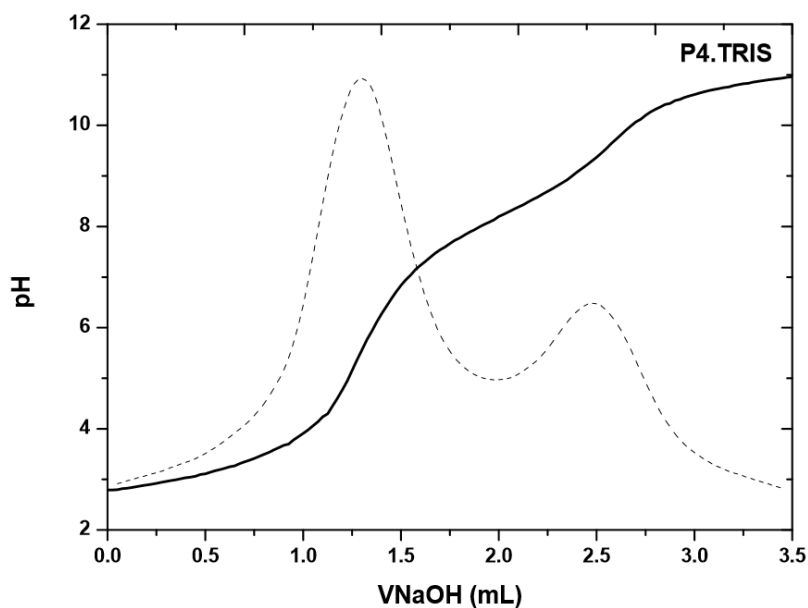


Figure 4.16 Potentiometric pH titration curve for P4.TRIS at ionic strength 100 mM

As it can be seen from Figure 4.14, 4.15 and 4.16, only the tertiary amine groups can be observed from potentiometric studies of tris terminated PAMAMs. Physico-chemical properties and the calculations of present tertiary amine ( $^3\text{N}$ ) numbers were presented in Table 4.15. As it's seen, experimental results are in good agreement with theoretical

values. These results are also important that synthesized dendrimers are almost pure and ideal characteristics.

Table 4.15 Physico chemical properties of some Tris terminated PAMAMs<sup>a</sup>

| Dendrimer | MW (g/mol) | <sup>3</sup> N Theoretical Values | <sup>3</sup> N Practical Values | Terminal hydroxy number | % Correlation |
|-----------|------------|-----------------------------------|---------------------------------|-------------------------|---------------|
| E3.TRIS   | 4234       | 14                                | 13.67 ± 0.32                    | 48                      | 97.64         |
| E4.TRIS   | 8865       | 30                                | 30.82 ± 1.08                    | 96                      | 102.73        |
| D3.TRIS   | 5230       | 18                                | 17.80 ± 0.64                    | 60                      | 98.88         |
| D4.TRIS   | 11109      | 38                                | 37.07 ± 0.67                    | 120                     | 97.55         |
| P3.TRIS   | 6700       | 21                                | 20,74 ± 0.30                    | 72                      | 98.76         |
| P4.TRIS   | 13647      | 45                                | 42.99 ± 1.57                    | 144                     | 95.53         |

<sup>a</sup>Results were calculated from potentiometric titrations for five repeated experiments.

#### 4.3.5 Determination of the Protonation Constants by Hyperquad

pKa values of PAMAMs have been reported [56, 65, 76] between 9-10.5 for the first protonation step (primary amines) and 6.30-6.85 for the second protonation step (tertiary amines) (Table 4.15). These values are mostly for PPI and PAMAMs. These steps reflect the protonation constants for primary and tertiary amines with the different protonation behavior and structures. These structures are mentioned as onion like structure for PPIs and core shell structure for PAMAMs [65, 75]. The idea is claimed for onion like structure is that the rim of PAMAMs that are primary amines are protonated together with the odd shells of the tertiary amines in the first step while even shells of tertiary amine groups protonates together at the following protonation step. Hence two end points from potentiometric titration curves could be observable. The other structure is considered for PAMAMs and the mechanism is simple. The idea is that primary amine groups and tertiary amine groups are protonated independently and tertiary amines go to deprotonation in the order of outer to inner tertiary amine shells and finally the inner core tertiary amines are protonated [65, 75].

#### 4.3.5.1 Protonation Constants of PAMAM E3.NH<sub>2</sub> and E4.NH<sub>2</sub>

Stability constants ( $\log\beta$  values) referring to pKa values for the protonation of E3.NH<sub>2</sub> and E4.NH<sub>2</sub> ligand systems are presented in Table 4.16. Protonated ligands were released only two protonation groups which are corresponding the periphery primary amine groups and inner tertiary amine groups in the pH range of 2-12. Since these steps refers to protonation of all primary and tertiary amine groups, respectively, it is better to mention about the microscopic protonation constants rather than macroscopic protonation constants. A sample potentiometric titration curve of E4.NH<sub>2</sub> reflects that at high pH periphery of dendrimer is protonated and tertiary amines deprotonated, while at low pH all the primary and tertiary amine groups in the pH range of 2-12 (Figure 4.11). From potentiometric data it is difficult to talk about the protonation of the core tertiary amine groups that there have been studies, which have shown that core amine groups protonates in lower pH < 2 values [65, 72]. In Table 4.16, calculated microscopic pKa values of E3.NH<sub>2</sub> and E4.NH<sub>2</sub> by HYPERQUAD 2008 were presented. Results are in good agreement with the literature.

Table 4.16 Stability constants ( $\log\beta$  values, which refer to  $L_q + H_r \rightleftharpoons L_qH_r$ ) of E3.NH<sub>2</sub> and E4.NH<sub>2</sub> PAMAMs at  $25 \pm 0.1$  °C (I = 100 mM NaCl)

| Ligand (L)         | L <sub>q</sub> | H <sub>r</sub> | $\log\beta$ =pK value | Reference $\log\beta$ =pKa value                         |
|--------------------|----------------|----------------|-----------------------|--|
| E3.NH <sub>2</sub> | 1              | 1              | 9.2332 (0.0449)       | 9.90 <sup>a</sup> -9.00 <sup>b</sup> -9.23 <sup>c</sup>  |
|                    | 1              | 2              | 6.9493 (0.0361)       | 6.52 <sup>a</sup> -6.70 <sup>b</sup> -6.30 <sup>c</sup>  |
| E4.NH <sub>2</sub> | 1              | 1              | 9.3215 (0.0446)       | 10.29 <sup>a</sup> -9.00 <sup>b</sup> -9.23 <sup>c</sup> |
|                    | 1              | 2              | 6.7269 (0.0332)       | 6.85 <sup>a</sup> -6.70 <sup>b</sup> -6.30 <sup>c</sup>  |

<sup>a</sup> Data taken from Diallo et al. [56]. <sup>b</sup> Data taken from Cakara et al. [65]. <sup>c</sup> Data taken from Niu et al. [76]

Protonation behavior of E3.NH<sub>2</sub> and E4.NH<sub>2</sub> ligand systems could be seen from speciation distribution curves derived by Hyperquad program in Figure 4.17 and Figure 4.18, respectively. From these figures, it can be seen that at low pH, all dendrimers are protonated fully and predominant species are (E3.NH<sub>2</sub>)H<sub>2</sub> and (E4.NH<sub>2</sub>)H<sub>2</sub>. On the other hand, E3.NH<sub>2</sub> and E4.NH<sub>2</sub> species becomes predominant over pH 9.20. Species (E3.NH<sub>2</sub>)H and (E4.NH<sub>2</sub>)H becomes predominant between the approximate pH range of 6.7-9.00. That is, between these pH ranges, E3.NH<sub>2</sub> and E4.NH<sub>2</sub> polydentate ligands can

have interesting encapsulation efficiencies for many metal ions [78, 135, 268] and the cavities between the globular shaped dendrimer can have the role of dendritic host and behave like drug carriers and so as drug delivery systems [269-271]

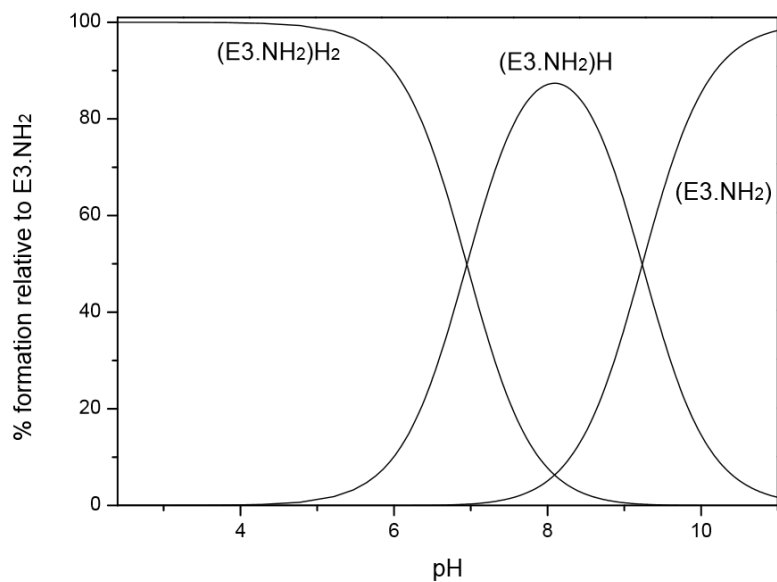


Figure 4.17 Species distribution curves for the E3.NH<sub>2</sub> system vs. pH at  $25 \pm 0.1$  °C,  $I=100$  mM NaCl

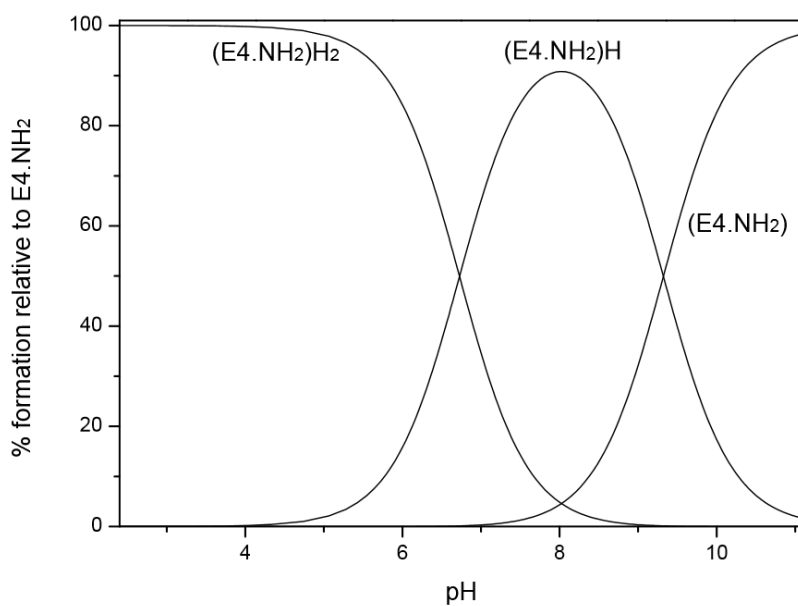


Figure 4.18 Species distribution curves for the E4.NH<sub>2</sub> system vs. pH at  $25 \pm 0.1$  °C,  $I=100$  mM NaCl

#### 4.3.5.2 Protonation Constants of PAMAM D3.NH<sub>2</sub> and D4.NH<sub>2</sub>

Stability constants ( $\log\beta$  values) referring to pKa values for the protonation of D3.NH<sub>2</sub> and D4.NH<sub>2</sub> ligand systems are presented in Table 4.17. Protonated ligands were released only two protonation groups. Table 4.13 shows that D4.NH<sub>2</sub> exhibits two different amine groups from two endpoints. A sample potentiometric titration curve of D4.NH<sub>2</sub> could be seen in Figure 4.12. This protonation behavior was observed different than ethylene diamine cored E4.NH<sub>2</sub> PAMAMs when the protonated amine numbers considered. In the pH range of pH 2-12, average amine number of 56.48 for first protonation step could be representative for the protonation of primary and outer tertiary amine groups together. Similarly average amine number 19.45 could be representative for the total of the rest of inner tertiary amine numbers (Table 4.13). Interaction between the amine groups could be the reason of the different protonation behavior of DETA cored PAMAMs unlike EDA cored PAMAMs. Resulting data in Table 4.13 indicates that experimental total amine number  $75.43 \pm 2.90$  are in good agreement with the theoretical value 78, which is the sum of <sup>3</sup>N and <sup>1</sup>N numbers in Table 4.12.

Since first and second protonation steps are not representative for just the total primary and secondary amine group numbers, they could be attributed to the protonation of last outer tertiary and primary amine groups for the first step and the rest of tertiary amine groups in the second step. Thus, microscopic protonation constants calculated by HYPERQUAD 2008 computer program could be representative these steps and they are presented in Table 4.17.

Table 4.17 Stability constants ( $\log\beta$  values, which refer to  $L_q + H_r \rightleftharpoons L_qH_r$ ) of D3.NH<sub>2</sub> and D4.NH<sub>2</sub> PAMAMs at  $25 \pm 0.1$  °C (I = 100 mM NaCl)

| Ligand (L)         | L <sub>q</sub> | H <sub>r</sub> | Log $\beta$ =pK value |
|--------------------|----------------|----------------|-----------------------|
| D3.NH <sub>2</sub> | 1              | 1              | 9.1267 (0.0429)       |
|                    | 1              | 2              | 6.8256 (0.0356)       |
| D4.NH <sub>2</sub> | 1              | 1              | 9.2587 (0.0483)       |
|                    | 1              | 2              | 6.8921 (0.0390)       |

Protonation behavior of D3.NH<sub>2</sub> and D4.NH<sub>2</sub> ligand systems could be seen from speciation distribution curves driven by Hyperquad program in Figure 4.19 and Figure

4.20, respectively. From these figures, it can be seen that at low pH all dendrimers are protonated fully and predominant species are  $(D3.NH_2)H_2$  and  $(D4.NH_2)H_2$ . On the other hand,  $D3.NH_2$  and  $D4.NH_2$  species are predominant over pH 9.12. Species  $(D3.NH_2)H$  and  $(D4.NH_2)H$  are predominant between the approximate pH range of 6.8-9.12. That is, between these pH ranges,  $D3.NH_2$  and  $D4.NH_2$  polydentate ligands can show interesting encapsulation efficiencies and they can be used as drug carriers or template in many studies.

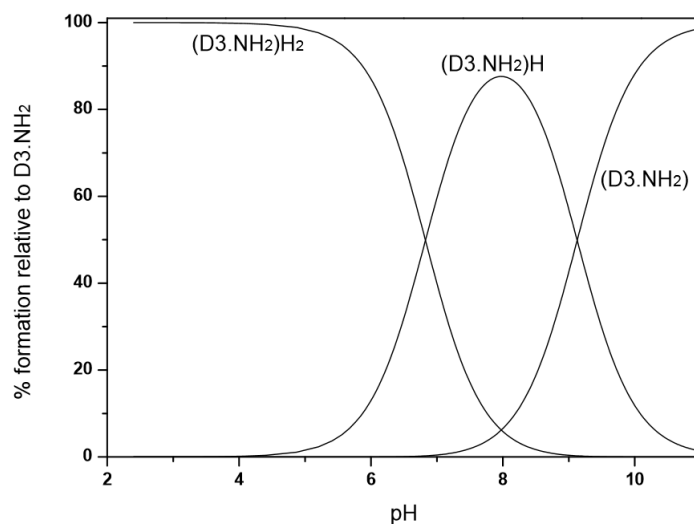


Figure 4.19 Species distribution curves for the  $D3.NH_2$  system vs. pH at  $25 \pm 0.1$  °C,  $I=100$  mM NaCl

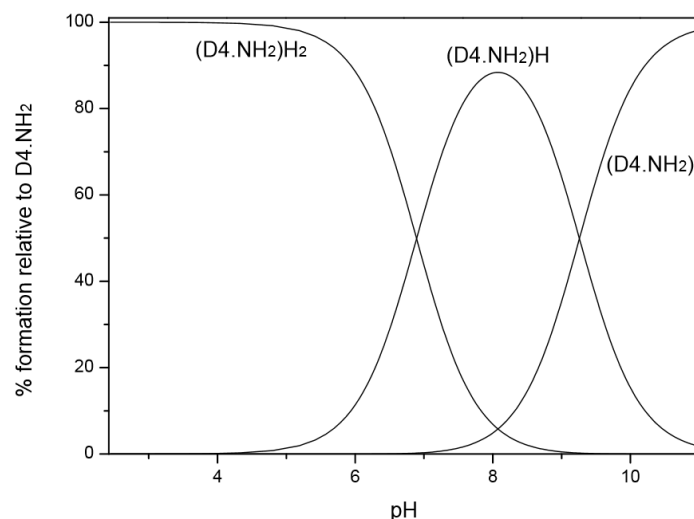


Figure 4.20 Species distribution curves for the  $D4.NH_2$  system vs. pH at  $25 \pm 0.1$  °C,  $I=100$  mM NaCl

#### 4.3.5.3 Protonation Constants of P3.NH<sub>2</sub> and P4.NH<sub>2</sub> PAMAMs

Stability constants ( $\log\beta$  values) referring to pKa values for the protonation of P3.NH<sub>2</sub> and P4.NH<sub>2</sub> ligand systems are presented in Table 4.18. Protonated ligands were released only two protonation groups. Table 4.13 shows that P4.NH<sub>2</sub> exhibits two different amine numbers from two endpoints. A sample potentiometric titration curve of P4.NH<sub>2</sub> reflects that at high pH periphery of dendrimer is protonated and tertiary amines deprotonated, while at low pH all the primary and tertiary amine groups in the pH range of 2-12 (Figure 4.13). This protonation behavior was observed different than EDA cored PAMAMs for Jeffamine<sup>®</sup> T-403 cored ones when the protonated amine numbers considered. In the pH range of pH 2-12, average amine number of 44.09 for first protonation step could be representative for the protonation of primary amine groups. Similarly average amine number of 23.434 could be representative for the outer tertiary amine number (Table 4.13). This could be attributed to hydrophobic polymeric core of P3.NH<sub>2</sub> and P4.NH<sub>2</sub> dendrimers or high electrostatic interaction resulting from the excess acid used to adjust initial concentration of pH 2. In theory, the primary amine number of P4.NH<sub>2</sub> is 48 and the outer tertiary amine number is 24. These values are correlated with the experimental values. Thus, as it's not going to be these values arbitrary, it could be concluded that inner tertiary amine groups are overlapped with the end point of excess acid, which is initially added to media for back titration. In this point, first protonation step of P3.NH<sub>2</sub> and P4.NH<sub>2</sub> PAMAMs reflects the pKa value for primary amine groups and the second one for the outer tertiary amine shell. Calculated pKa values can be seen in Table 4.18.

Table 4.18 Stability constants ( $\log\beta$  values, which refer to  $L_q + H_r \rightleftharpoons L_qH_r$ ) of the proton and P3.NH<sub>2</sub> and P4.NH<sub>2</sub> PAMAMs at 25 ± 0.1 °C (I = 100 mM NaCl)

| Ligand (L)         | L <sub>q</sub> | H <sub>r</sub> | Log $\beta$ =pK value |
|--------------------|----------------|----------------|-----------------------|
| P3.NH <sub>2</sub> | 1              | 1              | 8.7787 (0.0297)       |
|                    | 1              | 2              | 6.0847 (0.0288)       |
| P4.NH <sub>2</sub> | 1              | 1              | 9.1321 (0.0337)       |
|                    | 1              | 2              | 6.1644 (0.0413)       |

Protonation behavior of P3.NH<sub>2</sub> and P4.NH<sub>2</sub> ligand systems can be seen from speciation distribution curves in Figure 4.18 and Figure 4.19, respectively. From these figures, it can be seen that at low pH all dendrimers are protonated fully and predominant species are

$(P3.NH_2)H_2$  and  $(P4.NH_2)H_2$ . On the other hand,  $P3.NH_2$  and  $P4.NH_2$  becomes predominant over pH 8.50. Species  $(P3.NH_2)H$  and  $(P4.NH_2)H$  are predominant between the approximate pH range of 6.00-9.00. That is, between these pH ranges,  $P3.NH_2$  and  $P4.NH_2$  polydentate ligands can have many interesting characteristics.

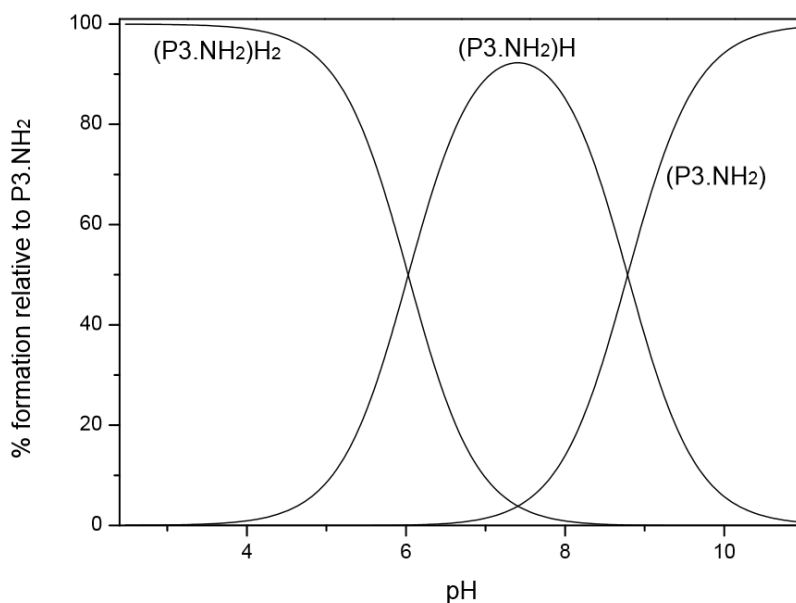


Figure 4.21 Species distribution curves for the  $P3.NH_2$  system vs. pH at  $25 \pm 0.1$  °C,  $I=100$  mM NaCl

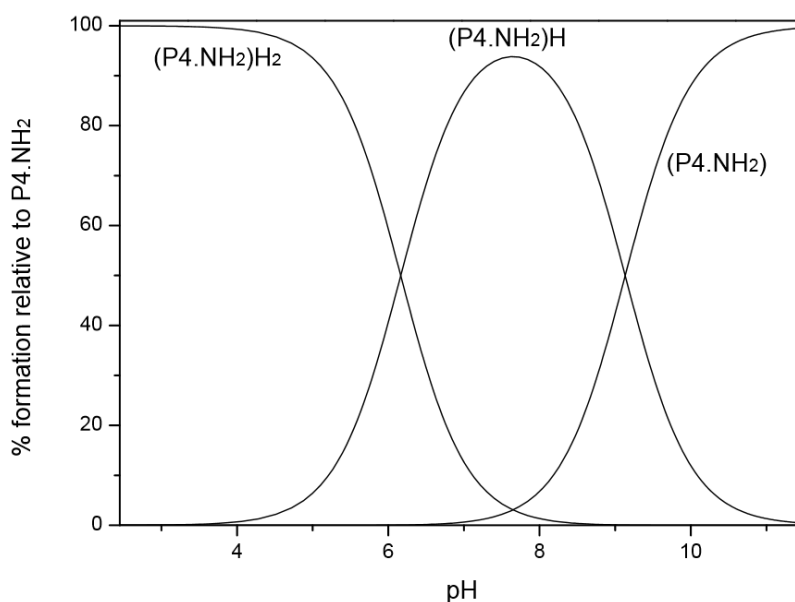


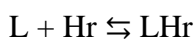
Figure 4.22 Species distribution curves for the  $P4.NH_2$  system vs. pH at  $25 \pm 0.1$  °C,  $I=100$  mM NaCl

#### 4.4 Spectroscopic Investigation of the Protonation Constants of PAMAMs by Chemometric Approaches and HypSpec Program

In this part, interactions of  $H^+$  and macromolecular polydentate ligands PAMAMs are investigated using different factor analysis techniques; such as PCA (NIPALS algorithm) and EFA (SVD algorithm) from data matrix  $\mathbf{X}$ (NSOLN, N WAVE) obtained by several spectroscopic acid base titrations of aqueous solutions of amine, tris and carboxyl terminated different generation PAMAMs. By means of used techniques, model free analysis are performed. The number of absorbing species are determined and unit spectra of spectroscopically active species are detected in the pH range of 2-12. Simultaneous curve resolution techniques; such as ALS, MCR-ALS are used to estimate unitary spectra and concentrations of the protonated species of PAMAM. After detection of the estimation of unit spectra, protonation constants of PAMAMs are calculated by means of HypSpec program.

##### 4.4.1 Determination of the number of UV-VIS Absorbing Species (Pure Components) by PCA and EFA

Data matrices  $\mathbf{X}$  (NSOLN, N WAVE) were constructed from several spectroscopic acid-base titrations of amine (Figure 4.23), tris (Figure 4.25), and carboxyl (Figure 4.27) terminated PAMAMs in the pH range of 2-12. From the changes in UV-VIS absorption spectra, it could be seen that the intensity of absorption band at  $\lambda_{max}$  280-286 decreases as the pH decreases, indicating the protonation of amino groups [72]. That is, depending on the pH of the media, PAMAMs can be found in different protonated conformations (absorbing species). Simply the notation used to show the protonation of a given PAMAM is as the following,



where, for simplicity, H and L represents  $H^+$  and type of PAMAM, respectively. 'r' denotes the protonation of a shell of L. Thus, protonation constant ( $\beta$ ) values to be discussed further are to be micro constants referring the protonation of all the relevant shell.

To talk about the protonation constants, first of all, the rank (number of absorbing species) of the data matrix  $\mathbf{X}$  should be determined. PCA and EFA were comparatively used to

determine number of absorbing species in order to take more accurate results for the determination of the number of absorbing species. Procedure for these methods were explained detailed in part 2.6.1 and 2.6.2. In Summary, during PCA analysis, driven  $\mathbf{X}$  data matrices from spectroscopic titrations have been processed by step 1 to step 7 through the equations (2.5) to (2.8) in part 2.6.1.2 via the help of Eigenvector Software, and RMSECV versus PC numbers were plotted for amine (Figure 4.24), tris (Figure 4.26) and carboxyl (Figure 4.28) terminated PAMAMs. In EFA analysis, SVD algorithm was used to determine eigenvector values, which are the linear combination of singular values and unit spectra. Then, eigenvector vs. wavelength plots were formed by means of HypSpec program (Figure 4.24, 4.26, and 4.28).

As it's mentioned earlier in part 2.6, no one method could be accurately used to decide the number of pure components. In EFA, number of non-zero singular values are expected to be equal to number of pure components or concentration regions. However, in the presence of systematic or random errors, one or two more singular values can be positive. To eliminate the effect of possible errors, common interpretation of PCA and EFA were performed together.

PCA and EFA was used to choose an appropriate number of PCs. PC numbers where RMSECV values make a local minimum and do not improve more than % 2 were selected as the number of absorbing species. Alternatively, the number of eigenvector where the high level of noise is not present was selected as the number of spectroscopically active species in dendrimer solutions. Result were presented in the following subparts.

#### 4.4.1.1 Amine Terminated PAMAMs

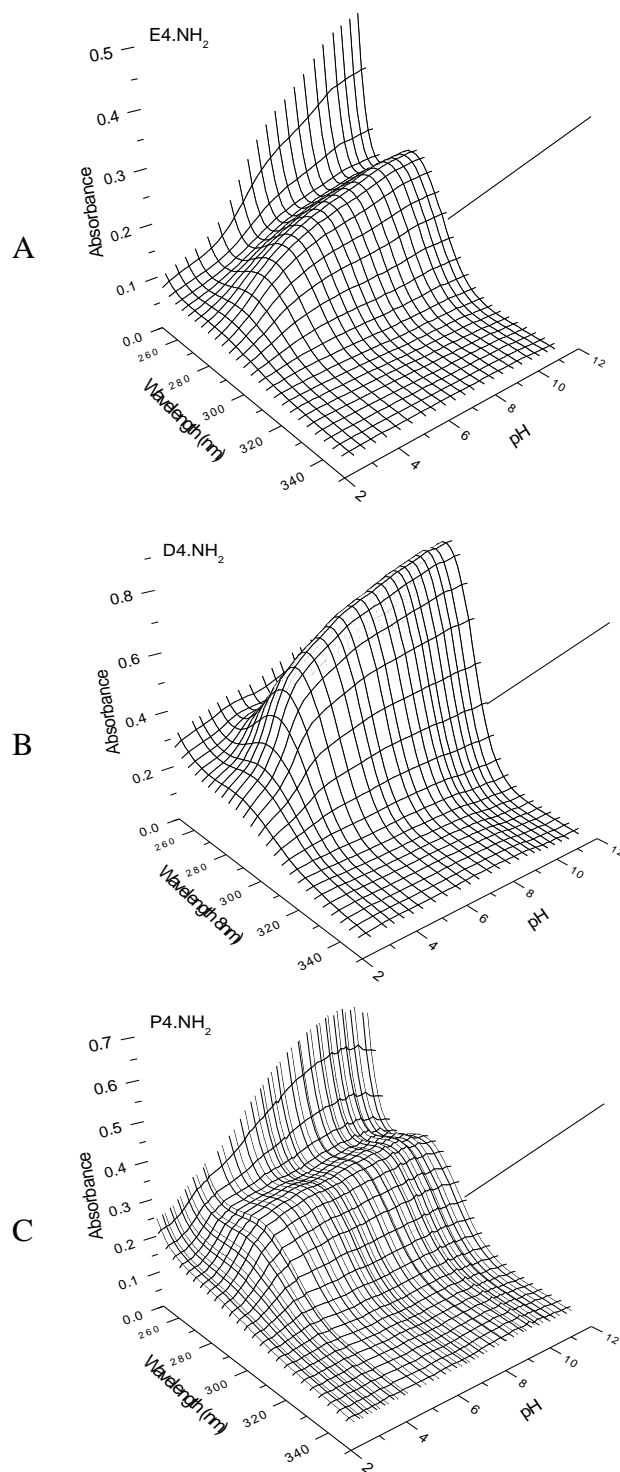


Figure 4.23 3D plots of UV spectroscopic titration of (A) E4.NH<sub>2</sub> ( $1.08 \times 10^{-3}$  M) (B) D4.NH<sub>2</sub> ( $4.98 \times 10^{-4}$  M) (C) P4.NH<sub>2</sub> ( $4.483 \times 10^{-4}$  M) solution with 0.098 N HCl at  $25 \pm 01$  °C,  $I=100$  mM NaCl

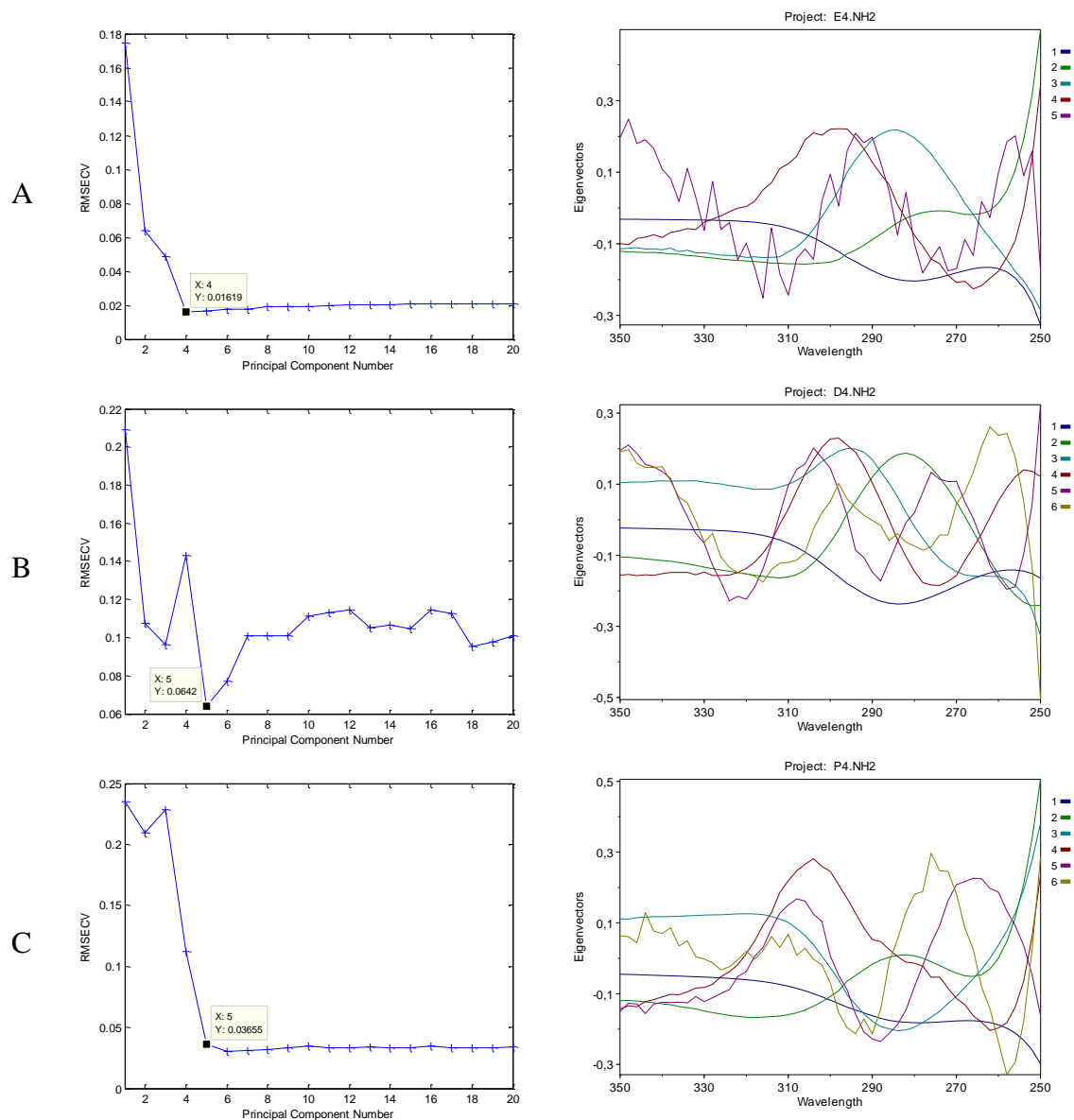


Figure 4.24 Determination of the number of absorbing species (PCs-Factors) by cross validation (left side of (A), (B), (C)) and FA (right side of (A), (B), (C)) for E4.NH<sub>2</sub>, D4.NH<sub>2</sub> and P4.NH<sub>2</sub>, respectively. X is the decision value for the number of PCs in cross validation; High level of noise is deterministic for FA.

Four spectroscopically active species were detected for E4.NH<sub>2</sub> while five for D4.NH<sub>2</sub> and P4.NH<sub>2</sub>. Three of them are the protonated form of E4.NH<sub>2</sub>, and the other is the unprotonated form of E4.NH<sub>2</sub>. For D4.NH<sub>2</sub> and P4.NH<sub>2</sub>, four of them are the protonated form and the other is the unprotonated form of D4.NH<sub>2</sub> and P4.NH<sub>2</sub> (Figure 4.24).

#### 4.4.1.2 Tris Terminated PAMAMs

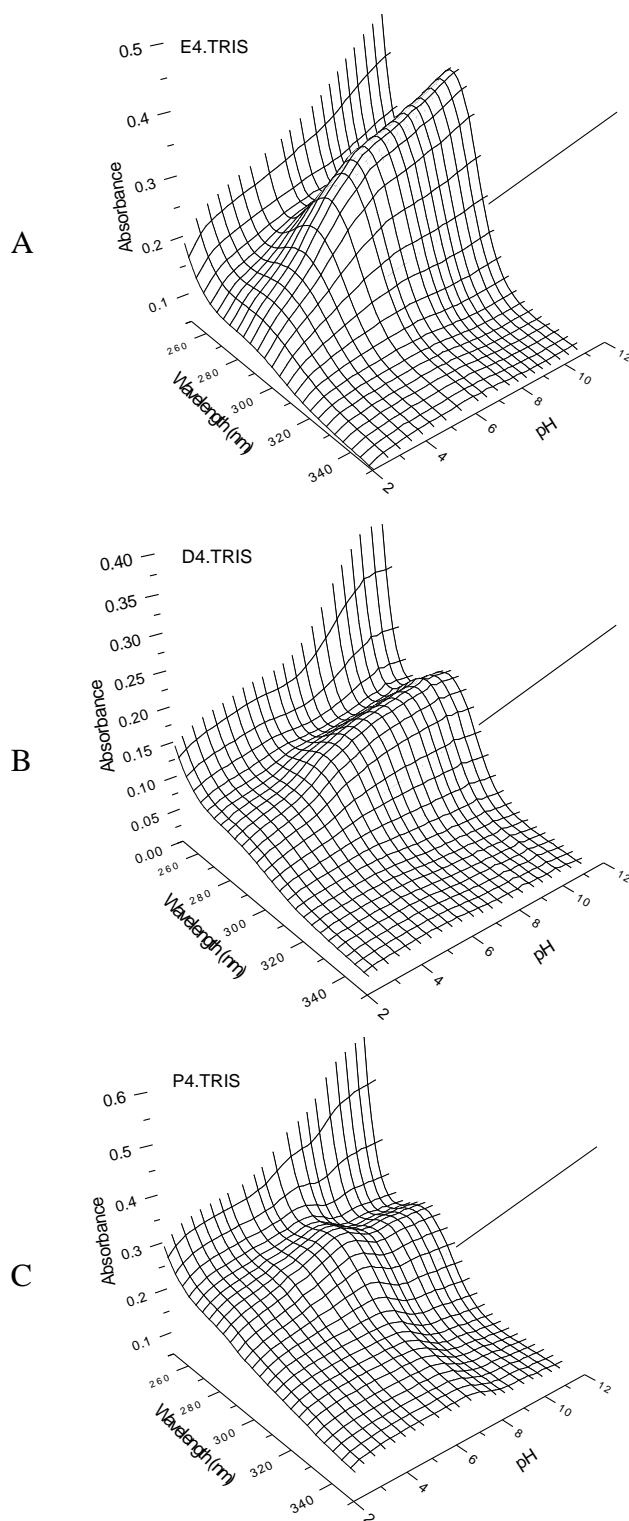


Figure 4.25 3D plots of UV spectroscopic titration of (A) E4.TRIS ( $7.08 \times 10^{-4}$  M) (B) D4.TRIS ( $3.70 \times 10^{-4}$  M) (C) P4.TRIS ( $6.06 \times 10^{-4}$  M) solution with 0.098 N HCl at  $25 \pm 01$  °C,  $I=100$  mM NaCl

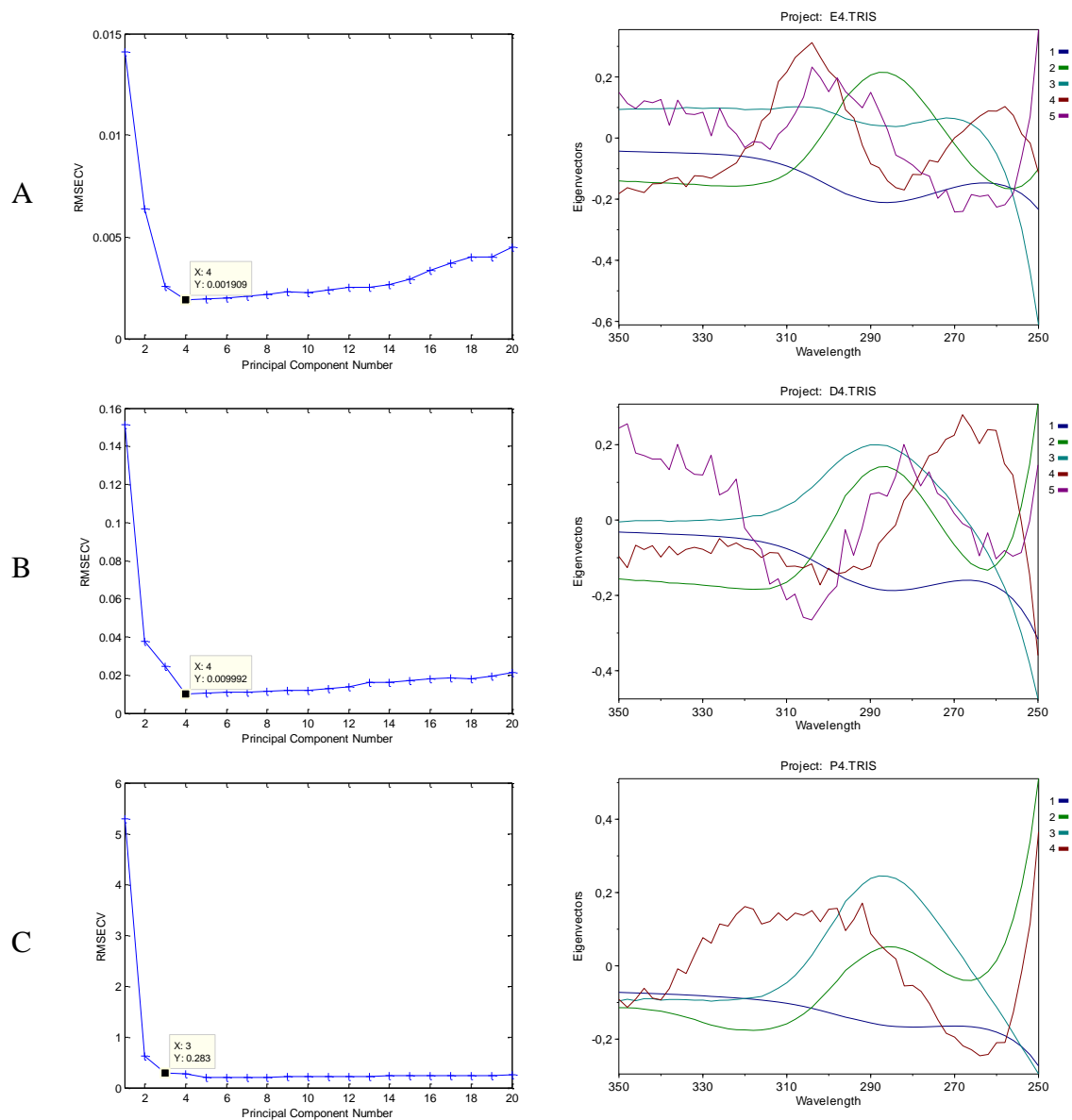


Figure 4.26 Determination of the number of absorbing species (PCs-Factors) by cross validation (left side of (A), (B), (C)) and FA (right side of A), (B), (C) for E4.TRIS, D4.TRIS and P4.TRIS, respectively. X is the decision value for the number of PCs in cross validation; High level of noise is deterministic for FA.

Four spectroscopically active species were detected for E4.TRIS and D4.TRIS while three for P4.TRIS. Three of them are the protonated form of E4.TRIS and D4.TRIS, and the other is the unprotonated form of E4.TRIS and D4.TRIS. For P4.TRIS, two of them are the protonated form and the other is the unprotonated form of P4.TRIS (Figure 4.26).

### 4.4.1.3 Carboxyl Terminated PAMAMs

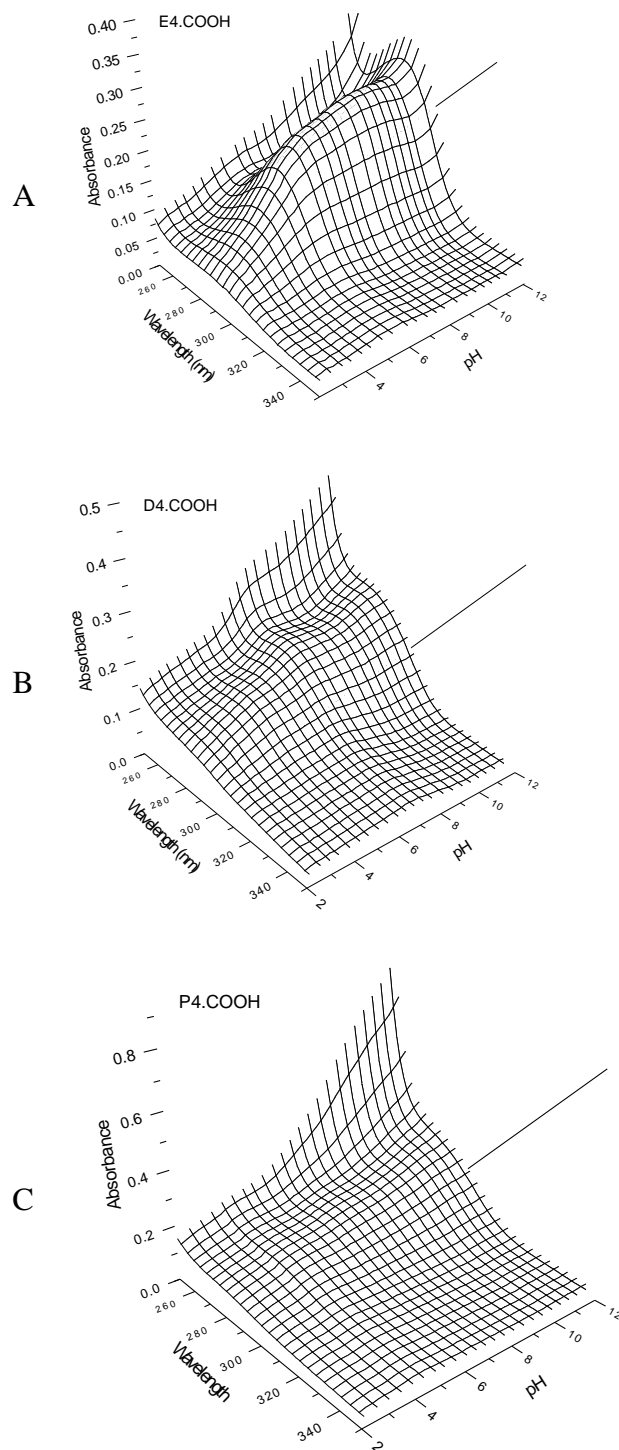


Figure 4.27 3D plots of UV spectroscopic titration of (A) E4.COOH ( $8.24 \times 10^{-4}$  M) (B) D4.COOH ( $8.50 \times 10^{-4}$  M) (C) P4.COOH ( $9.14 \times 10^{-4}$  M) solution with 0.098 N HCl at  $25 \pm 01$  °C,  $I=100$  mM NaCl

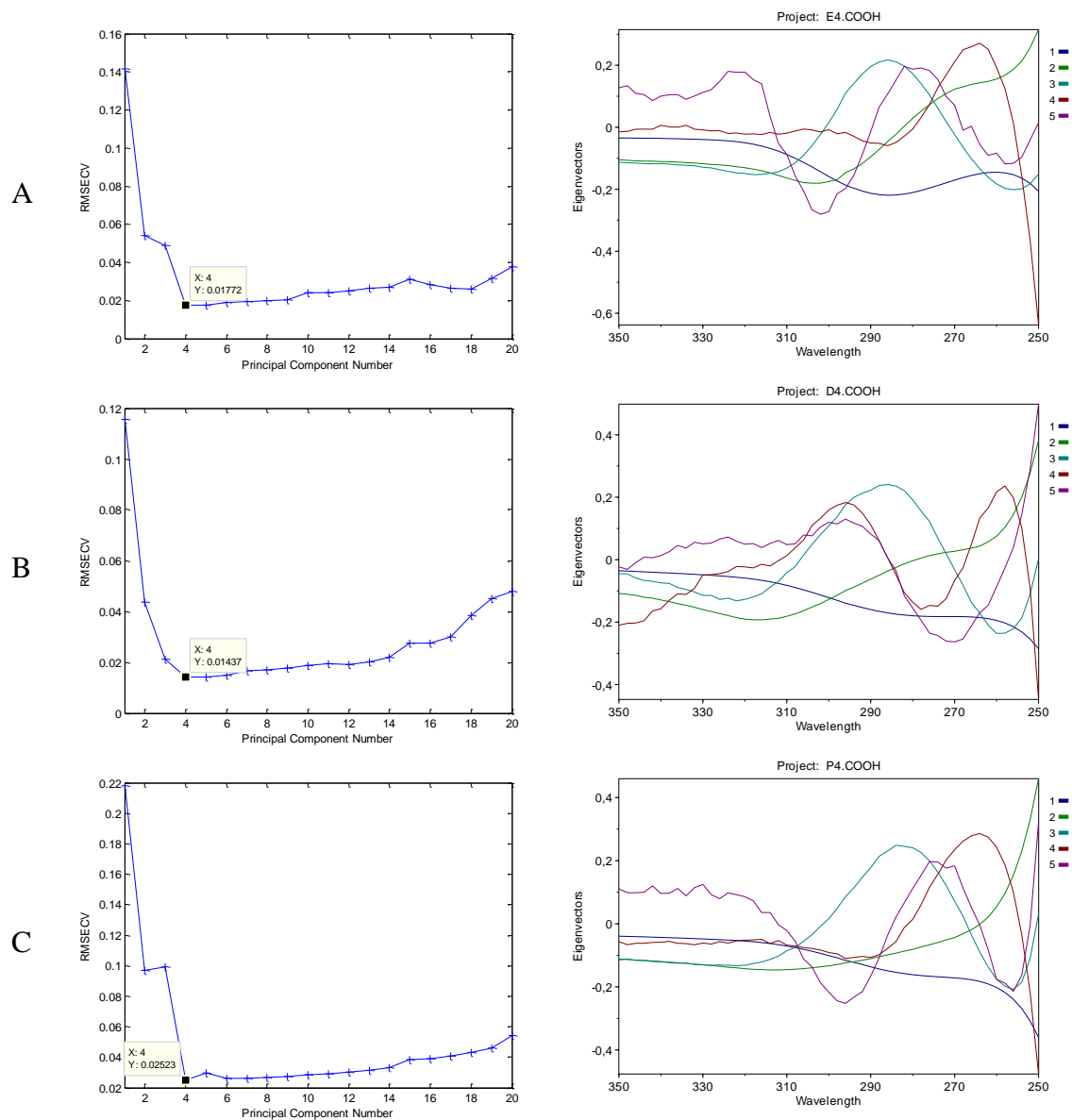


Figure 4.28 Determination of the number of absorbing species (PCs-Factors) by cross validation (left side of (A), (B), (C)) and FA (right side of A), (B), (C) ) for E4.COOH, D4.COOH and P4.COOH, respectively. X is the decision value for the number of PCs in cross validation; High level of noise is deterministic for FA.

Four spectroscopically active species were detected for E4.TRIS, D4.TRIS and P4.TRIS. Three of them are the protonated form of E4.TRIS, D4.TRIS and P4.TRIS, and the other is the unprotonated form of E4.TRIS, D4.TRIS and P4.TRIS. (Figure 4.28).

#### **4.4.2 Exploratory Data Analysis**

In part 4.4.1, the number of absorbing species present in the spectra were determined. In this part, HCA and pattern recognition are used to check for the pure regions or clusters within the data set  $\mathbf{X}$ , where the protonated and unprotonated conformational forms of PAMAMs exist. HCA was used to explain the relation between the variables visually. Background and principles of HCA are explained in part 2.6.5, and application method of experiments are introduced in part 3.7.3.

Pure regions also known as the concentration windows can be used for the initial estimate of concentration values for MCR-ALS. Another method of estimation of the pure regions exist in  $\mathbf{X}$  and so performing the classification of the concentration regions is pattern recognition. One of the ways in chemometrics for pattern recognition is to present score and loading values obtained as a result of PCA in graphically. Concentration profiles which is directly in here related with the pH of the media are presented in part 4.4.2.1 and 4.4.2.2.

##### **4.4.2.1 Hierarchical Cluster Analysis (HCA)**

HCA was performed by means of a recent software Eigenvector Research Solo+MIA 7.0.3 and evaluated results for amine, tris and carboxyl terminated PAMAMs were presented in Figure 4.29 to 4.31, 4.32 to 4.34, and 4.35 to 4.37, respectively. Results are in the form of connection dendrograms. From these figures it could be easily observable the classless (concentration regions) of the protonated and unprotonated conformational forms of PAMAMs.



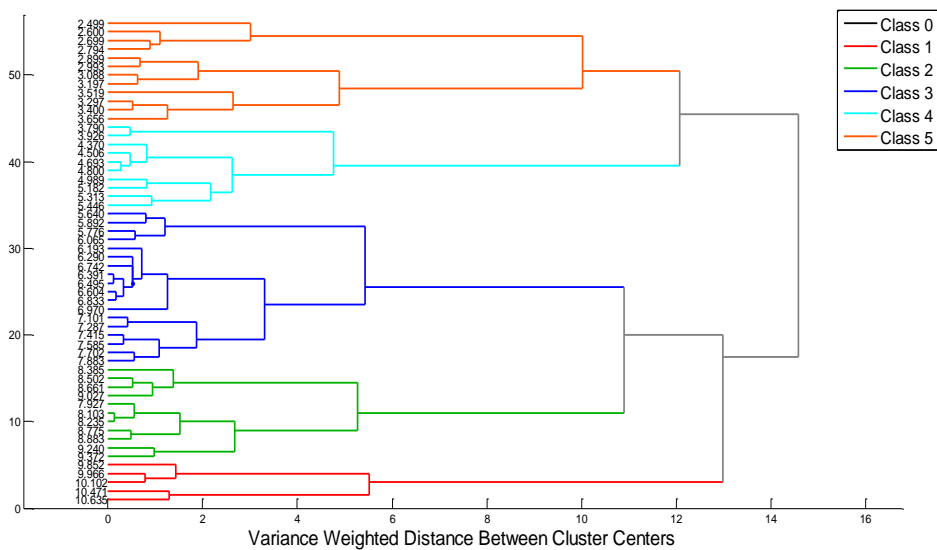


Figure 4.31 Dendrogram for HCA analysis of P4.NH<sub>2</sub> titration data. Cluster identification: Class 1: P4.NH<sub>2</sub>, Class 2: (P4.NH<sub>2</sub>)H, Class 3: (P4.NH<sub>2</sub>)H<sub>2</sub>, Class 4: (P4.NH<sub>2</sub>)H<sub>3</sub>, Class 5: (P4.NH<sub>2</sub>)H<sub>4</sub>

### Tris Terminated PAMAMs

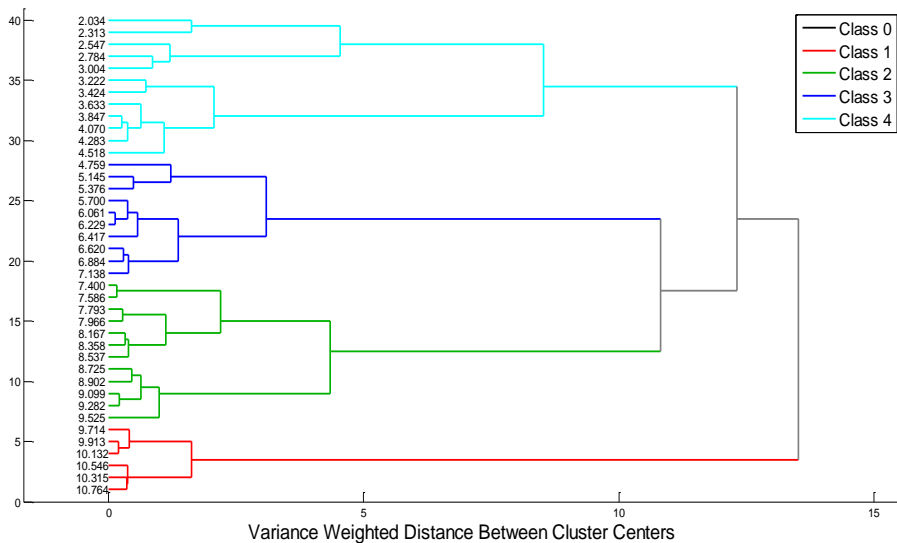


Figure 4.32 Dendrogram for HCA analysis of E4.TRIS titration data. Cluster identification: Class 1: E4.TRIS, Class 2: (E4.TRIS)H, Class 3: (E4.TRIS)H<sub>2</sub>, Class 4: (E4.TRIS)H<sub>3</sub>

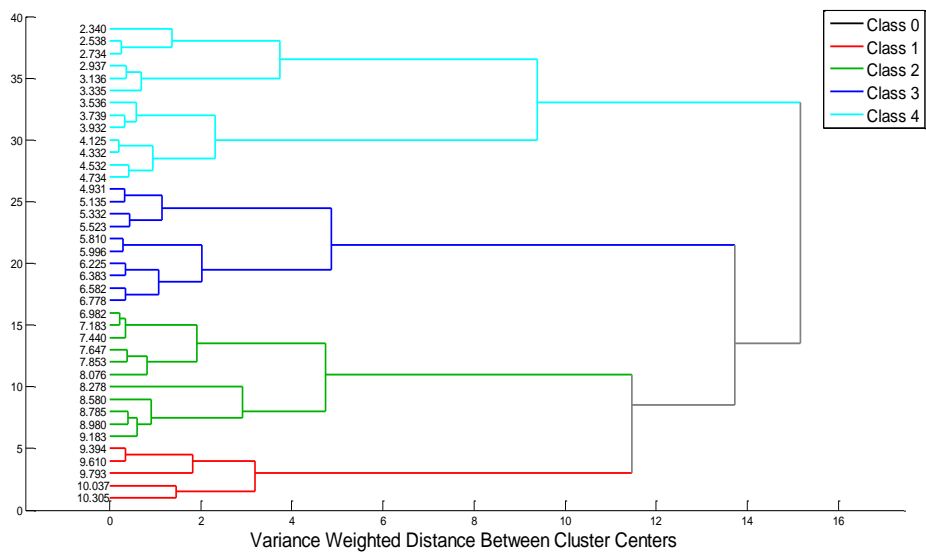


Figure 4.33 Dendrogram for HCA analysis of D4.TRIS titration data. Cluster identification: Class 1: D4.TRIS, Class 2: (D4.TRIS)H, Class 3: (D4.TRIS)H<sub>2</sub>, Class 4: (D4.TRIS)H<sub>3</sub>

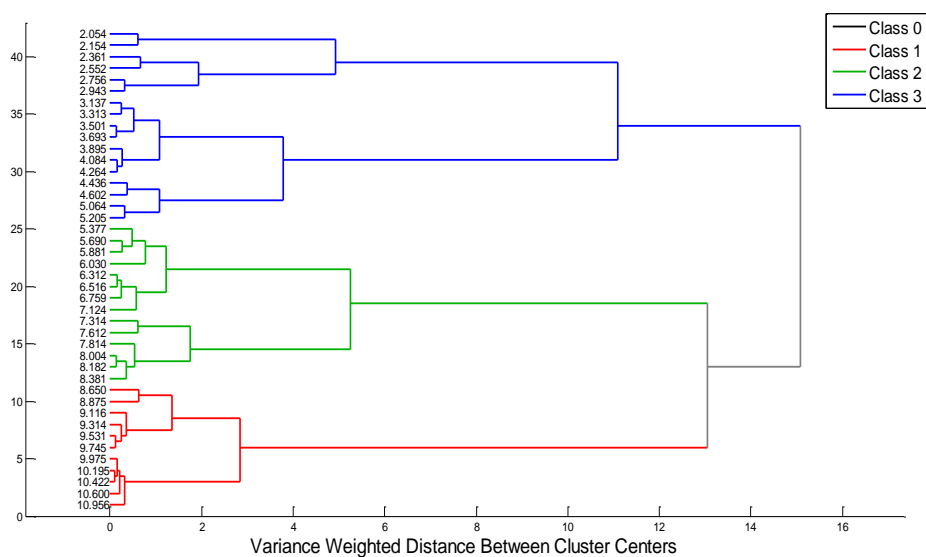


Figure 4.34 Dendrogram for HCA analysis of P4.TRIS titration data. Cluster identification: Class 1: P4.TRIS, Class 2: (P4.TRIS)H, Class 3: (P4.TRIS)H<sub>2</sub>

## Carboxyl Terminated PAMAMs

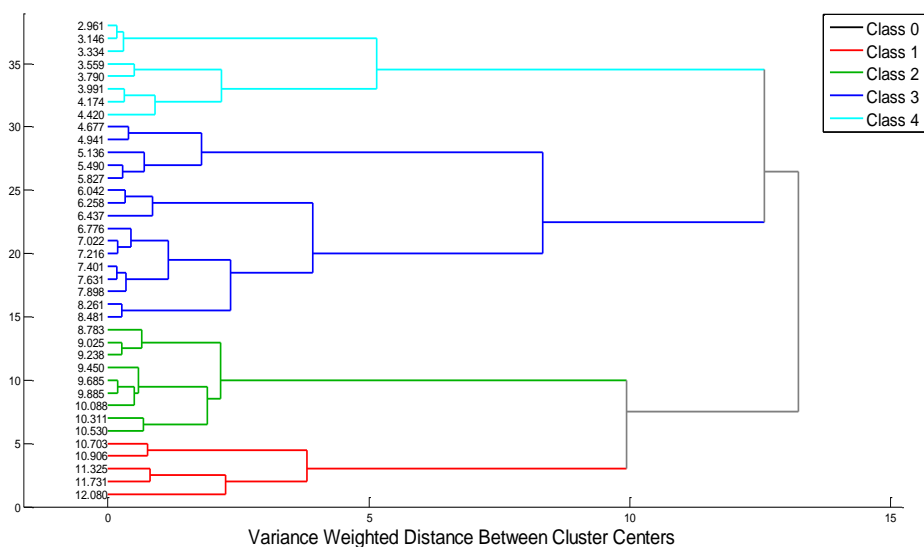


Figure 4.35 Dendrogram for HCA analysis of E4.COOH titration data. Cluster identification: Class 1: E4.COOH, Class 2: (E4.COOH)H, Class 3: (E4.COOH)<sub>2</sub>, Class 4: (E4.COOH)<sub>3</sub>

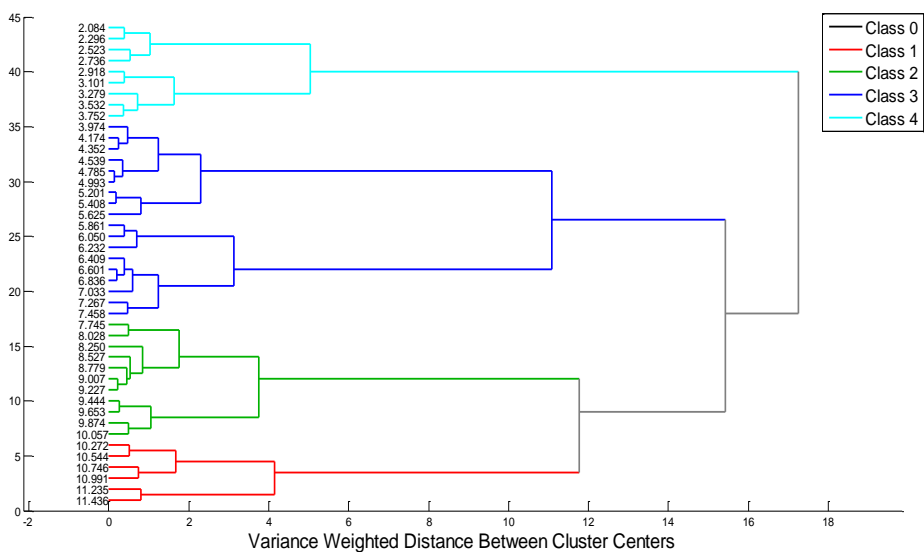


Figure 4.36 Dendrogram for HCA analysis of D4.COOH titration data. Cluster identification: Class 1: D4.COOH, Class 2: (D4.COOH)H, Class 3: (D4.COOH)<sub>2</sub>, Class 4: (D4.COOH)<sub>3</sub>

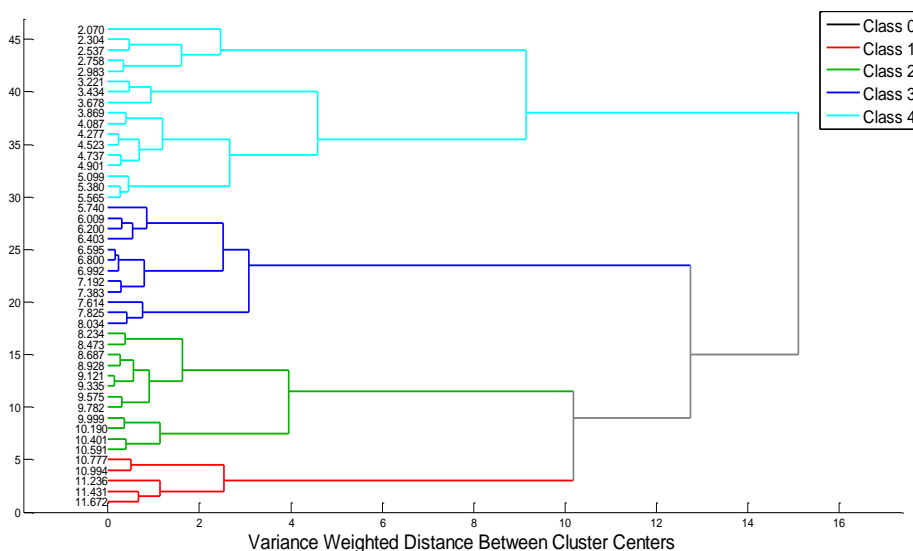


Figure 4.37 Dendrogram for HCA analysis of P4.COOH titration data. Cluster identification: Class 1: P4.COOH, Class 2: (P4.COOH)H, Class 3: (P4.COOH)H<sub>2</sub>, Class 4: (P4.COOH)H<sub>3</sub>

#### 4.4.2.2 Pattern Recognition

As it's mentioned, spectroscopic titrations were stored as  $\mathbf{X}$  data matrix. Rows of  $\mathbf{X}$  are the pH values, while columns of this matrix are absorbance values recorded between the wavelength ranges of 250-350 nm. Mean centering for the preprocessing of data was applied and cross validation procedure was used. Afterwards, PCA was performed and the relation between the pH values having different concentrations were investigated by exploring the score plots. Score plots of amine terminated, tris terminated and carboxyl terminated dendrimers were plotted in Figure 4.38 to 4.40, 4.41-4.43, and 4.44 to 4.46, respectively. In the same figures, it was also shown relation of absorbance as a function of pH, and the classification results of PCA were shown as classes. Classification on the score plots are correlated with the results of HCA analysis performed in part 4.4.2. In this way, it is easier to see and evaluate the relation between the pH values of the pure spectral regions. It was observable from these figures that extreme points could be the points where the component profile changes. In addition, accumulation of the scores at high pH values indicates to the deprotonated form of dendrimers.

## Amine Terminated PAMAMs

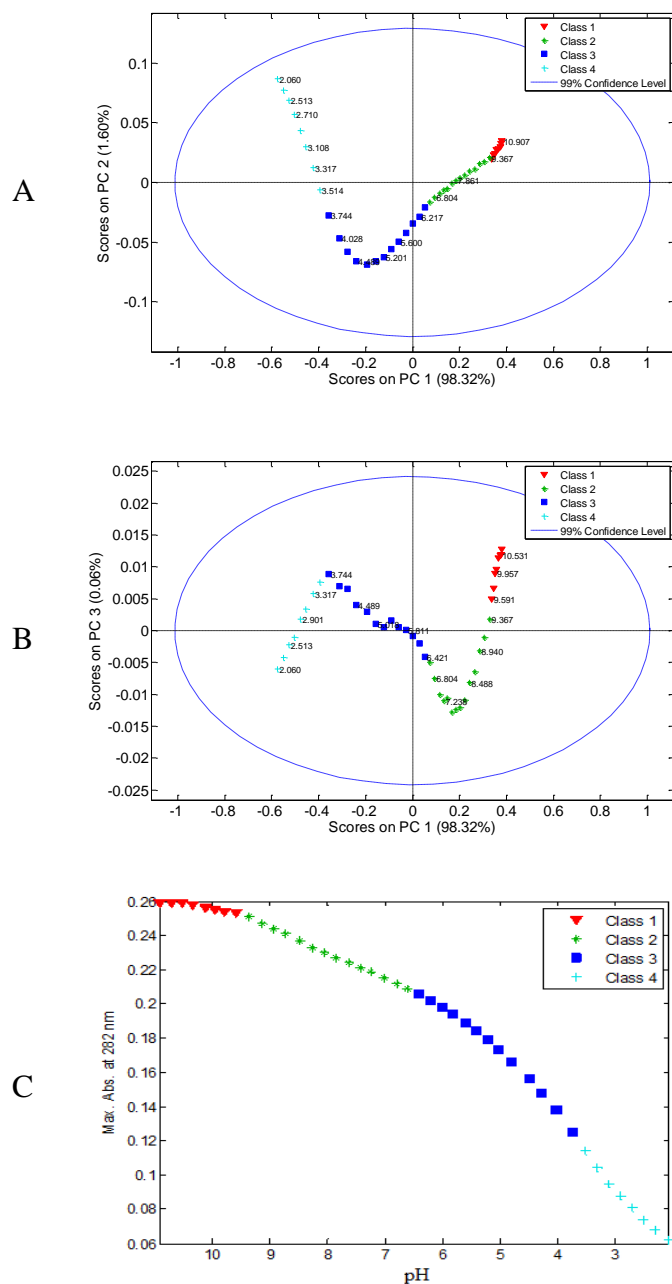


Figure 4.38 Score plots of E4.NH<sub>2</sub> titration data for (A) PC 1 vs. PC 2 (B) PC 1 vs. PC 3 and (C) pattern recognition results on maximum absorbance at 282 nm vs. pH graph for E4.NH<sub>2</sub>. Cluster identification Class 1: E4.NH<sub>2</sub>, Class 2: (E4.NH<sub>2</sub>)H, Class 3: (E4.NH<sub>2</sub>)H<sub>2</sub>, Class 4: (E4.NH<sub>2</sub>)H<sub>3</sub>

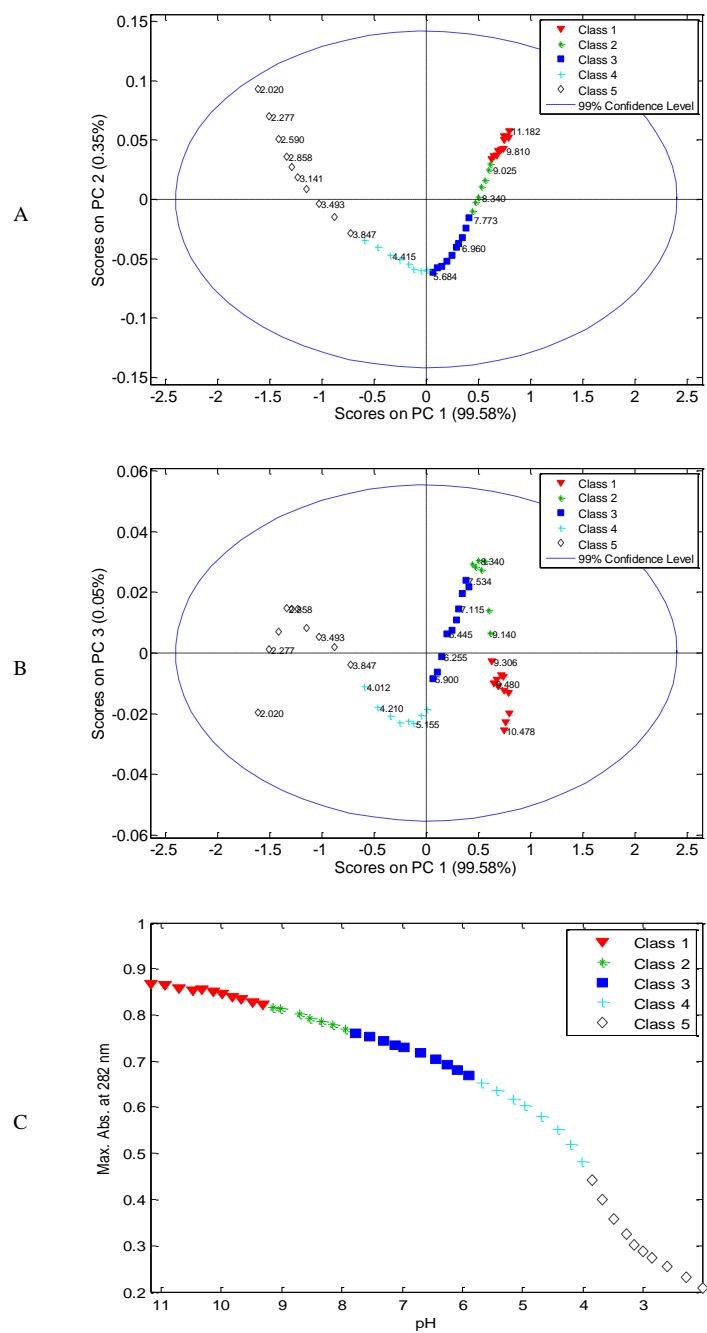


Figure 4.39 Score plots of D4.NH<sub>2</sub> titration data for (A) PC 1 vs. PC2 (B) PC1 vs. PC3 and (C) pattern recognition results on maximum absorbance at 282 nm vs. pH graph for D4.NH<sub>2</sub>. Cluster identification: Class 1: D4.NH<sub>2</sub>, Class 2: (D4.NH<sub>2</sub>)H, Class 3: (D4.NH<sub>2</sub>)H<sub>2</sub>, Class 4: (D4.NH<sub>2</sub>)H<sub>3</sub>, Class 5: (D4.NH<sub>2</sub>)H<sub>4</sub>

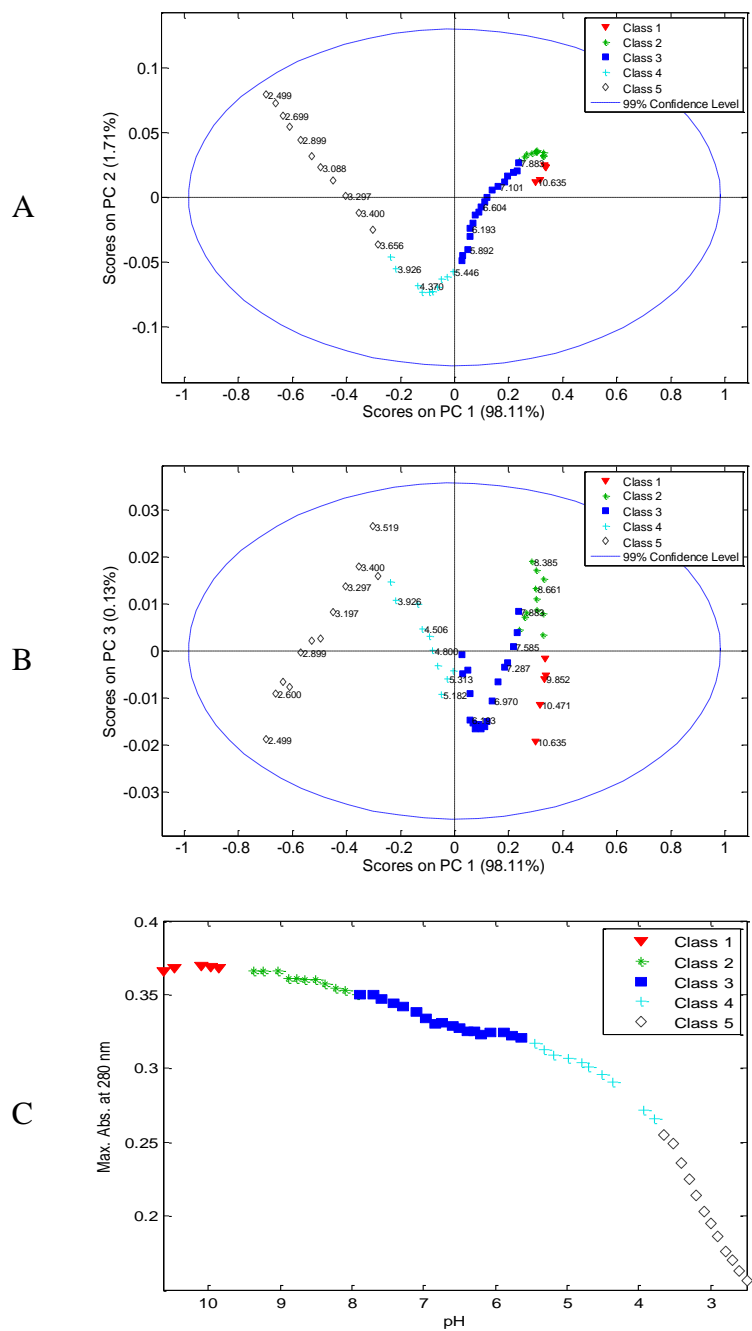


Figure 4.40 Score plots of P4.NH<sub>2</sub> titration data for (A) PC 1 vs. PC2 (B) PC1 vs. PC3 and (C) pattern recognition results on maximum absorbance at 280 nm vs. pH graph for P4.NH<sub>2</sub>. Cluster identification: Class 1: P4.NH<sub>2</sub>, Class 2: (P4.NH<sub>2</sub>)H, Class 3: (P4.NH<sub>2</sub>)H<sub>2</sub>, Class 4: (P4.NH<sub>2</sub>)H<sub>3</sub>, Class 5: (P4.NH<sub>2</sub>)H<sub>4</sub>

## Tris Terminated PAMAMs

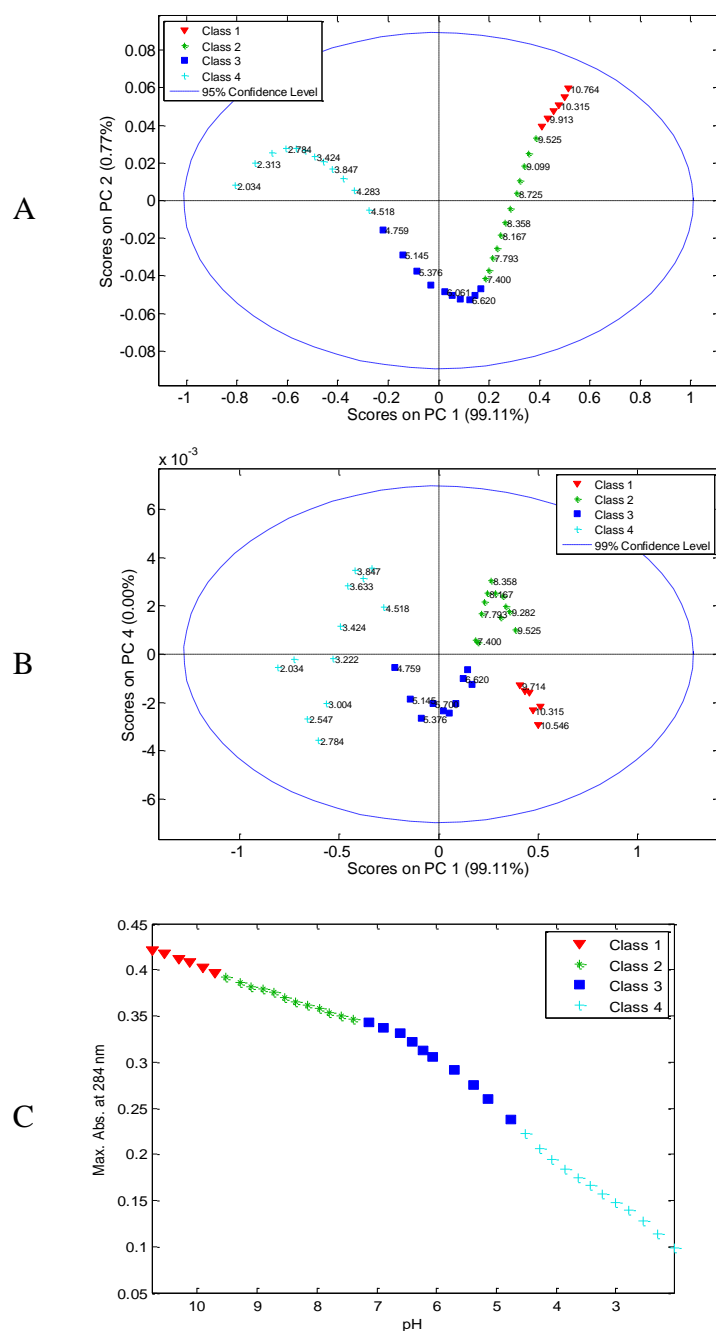


Figure 4.41 Score plots of E4.TRIS titration data for (A) PC 1 vs. PC2 (B) PC1 vs. PC4 and (C) pattern recognition results on maximum absorbance at 284 nm vs. pH graph for E4.TRIS. Cluster identification: Class 1: E4.TRIS, Class 2: (E4.TRIS)H, Class 3: (E4.TRIS)H<sub>2</sub>, Class 4: (E4.TRIS)H<sub>3</sub>

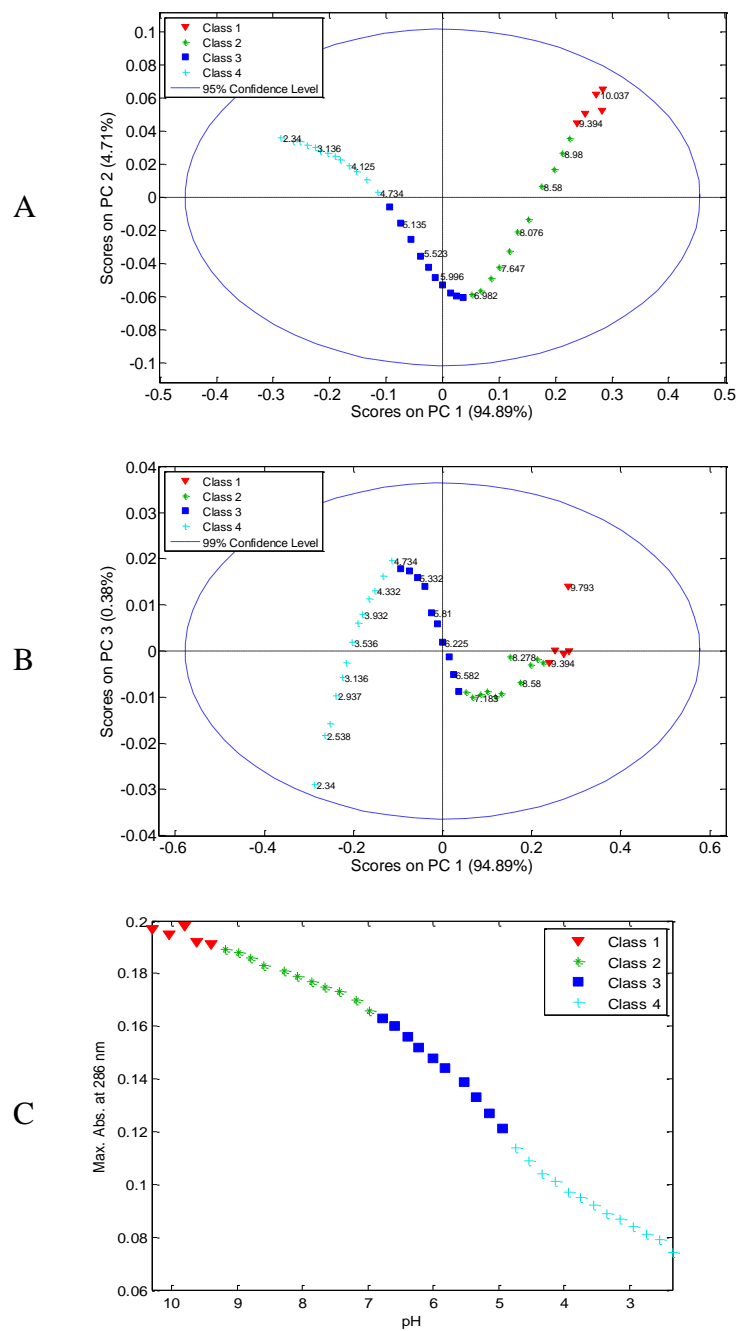


Figure 4.42 Score plots of D4.TRIS titration data for (A) PC 1 vs. PC2 (B) PC1 vs. PC3 and (C) pattern recognition results on maximum absorbance at 286 nm vs. pH graph for D4.TRIS. Cluster identification: Class 1: D4.TRIS, Class 2: (D4.TRIS)H, Class 3: (D4.TRIS)H<sub>2</sub>, Class 4: (D4.TRIS)H<sub>3</sub>

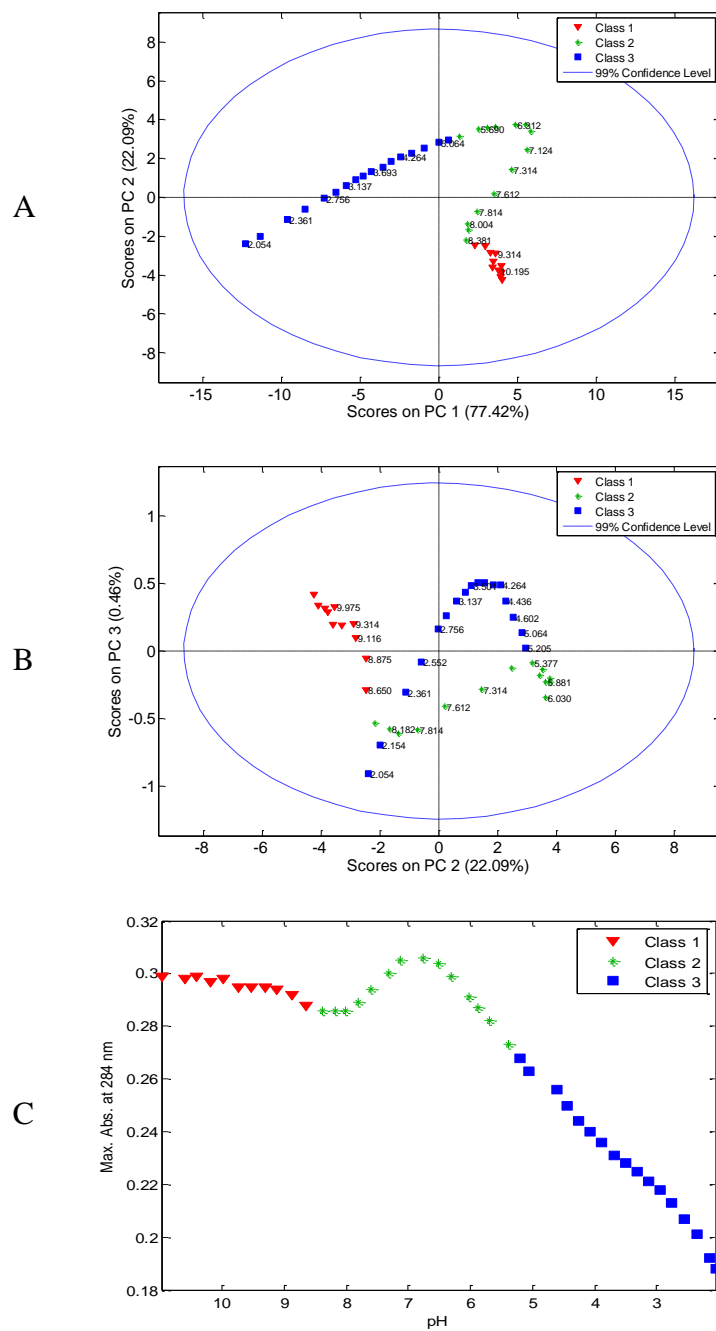


Figure 4.43 Score plots of P4.TRIS titration data for (A) PC 1 vs. PC2 (B) PC1 vs. PC3 and (C) pattern recognition results on maximum absorbance at 284 nm vs. pH graph for P4.TRIS. Cluster identification: Class 1: P4.TRIS, Class 2: (P4.TRIS)H, Class 3: (P4.TRIS)H<sub>2</sub>

## Carboxyl Terminated PAMAMs

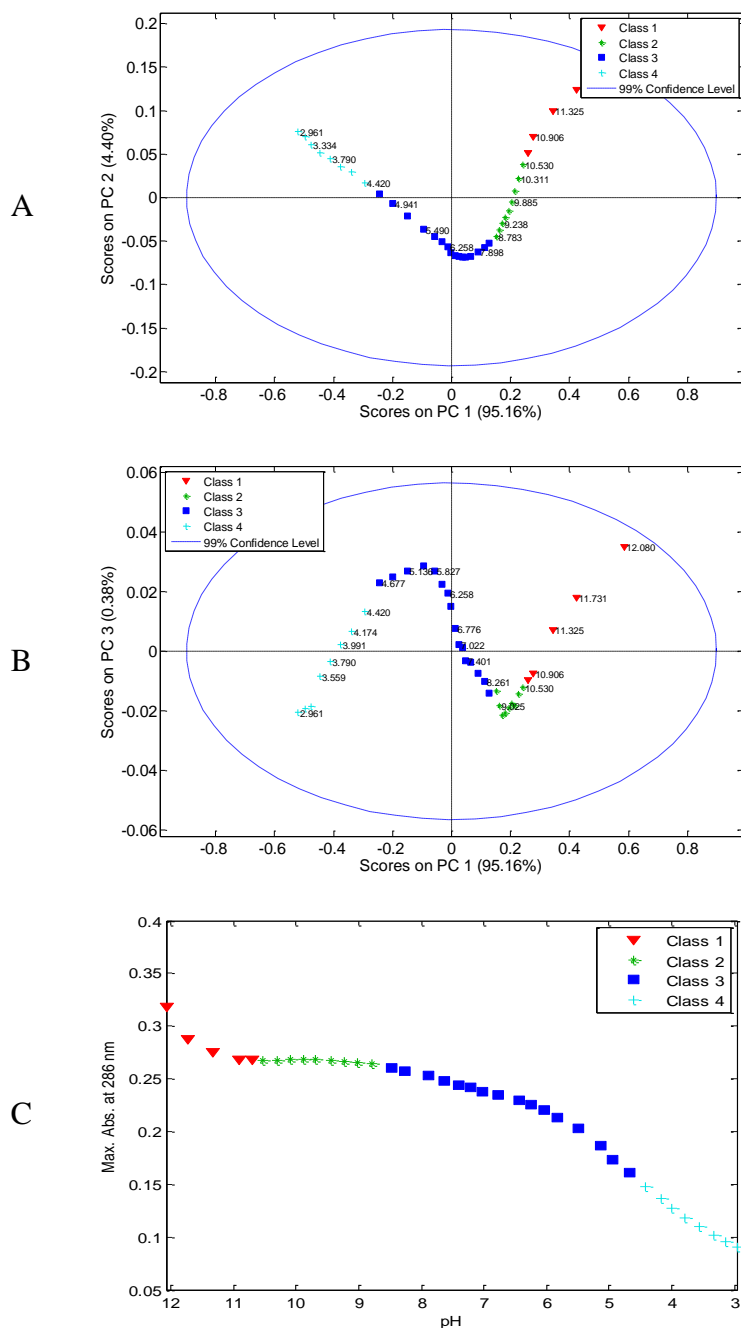


Figure 4.44 Score plots of E4.COOH titration data for (A) PC 1 vs. PC2 (B) PC1 vs. PC3 and (C) pattern recognition results on maximum absorbance at 286 nm vs. pH graph for E4.COOH. Cluster identification: . Class 1: E4.COOH, Class 2: (E4.COOH)H, Class 3: (E4.COOH)<sub>2</sub>, Class 4: (E4.COOH)<sub>3</sub>

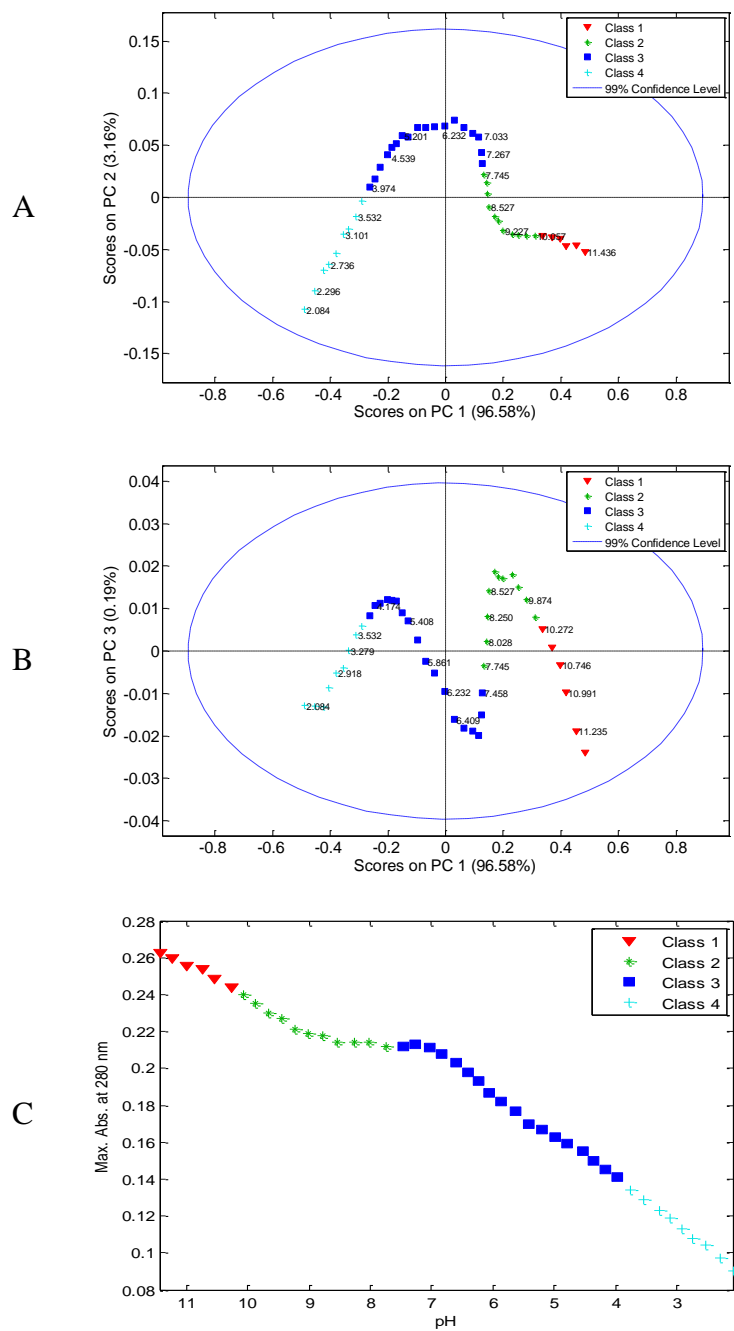


Figure 4.45 Score plots of D4.COOH titration data for (A) PC 1 vs. PC2 (B) PC1 vs. PC3 and (C) pattern recognition results on maximum absorbance at 286 nm vs. pH graph for D4.COOH. Cluster identification: Class 1: D4.COOH, Class 2: (D4.COOH)H, Class 3: (D4.COOH)H<sub>2</sub>, Class 4: (D4.COOH)H<sub>3</sub>

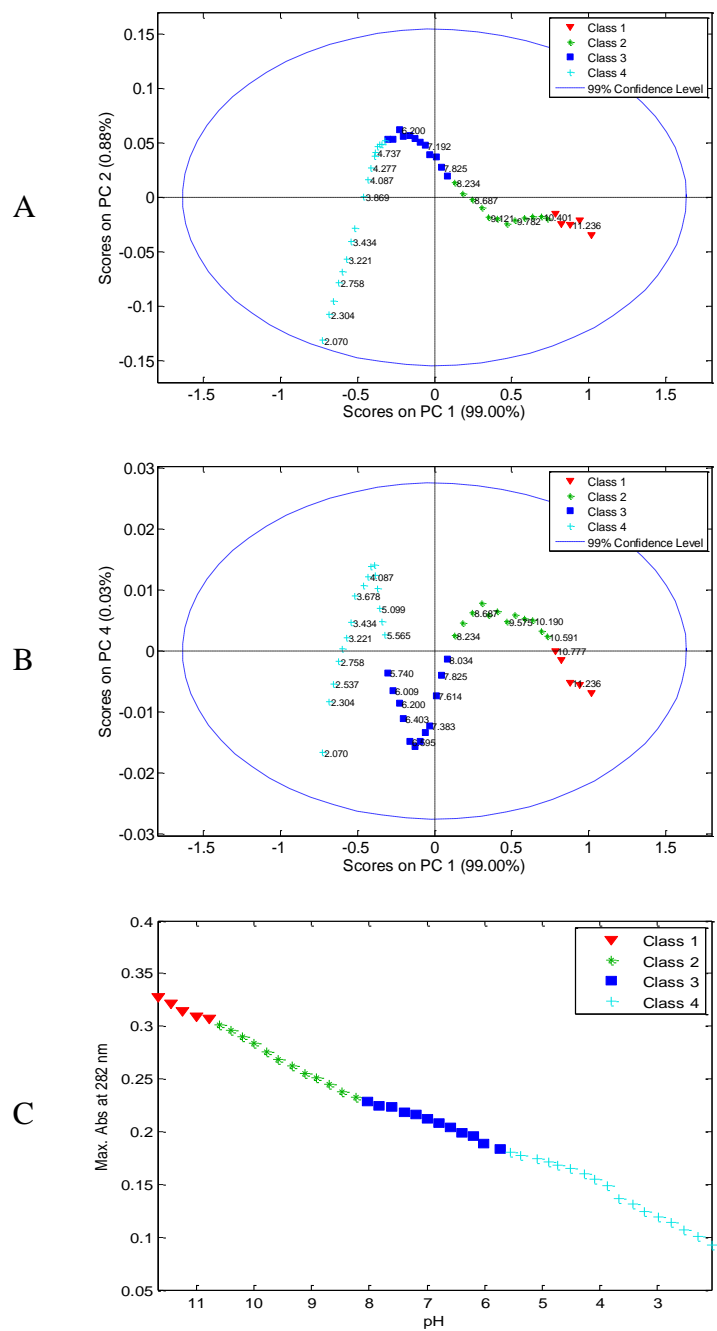


Figure 4.46 Score plots of P4.COOH titration data for (A) PC 1 vs. PC2 (B) PC1 vs. PC4 and (C) pattern recognition results on maximum absorbance at 286 nm vs. pH graph for D4.COOH. Cluster identification: Class 1: P4.COOH, Class 2: (P4.COOH)H, Class 3: (P4.COOH)H<sub>2</sub>, Class 4: (P4.COOH)H<sub>3</sub>

### 4.4.3 MCR-ALS

In part 4.4.1 and 4.4.2, number of absorbing species ( $A$ ) were determined and the relation between the concentrations of the protonated and unprotonated forms of dendrimers were clarified by the model free approach without using any law of mass action and traditional least square methods. In this part, MCR-ALS methods was used to estimate concentration profiles. In other words, the unit spectra of protonated and unprotonated forms of PAMAMs were optimized. The necessary MCR-ALS algorithm was explained in part 2.6.3 and 2.6.4, explicitly. In summary; first of all, the number of absorbing species were determined by PCA or EFA. In general, a data matrix  $\mathbf{X}$ (NSOLN, NWAVE) was obtained by the spectroscopic titrations, a general form of self modelling curve resolution (SMCR) in eqn. (2.13) is as the following

$$\mathbf{X} = \mathbf{C}\mathbf{S}^T + \mathbf{E}$$

where  $\mathbf{C}$  is an  $m \times A$  matrix of pure concentration profiles and  $\mathbf{S}^T$  is  $n \times A$  matrix of pure spectral profiles.

Initial estimation of concentration profile of  $\mathbf{C}$  and  $\mathbf{S}^T$  can be driven by either EFA, HCA and pattern recognition as it's described in part 4.4.2. The basic principle of MCR-ALS is to find a bilinear model that leads to best fit by minimizing the error criteria of sum squared residuals ( $\mathbf{E}$ -SSR) by considering the equation (2.17) as the following

$$SSR = \min_{\hat{\mathbf{C}}} \|\mathbf{X}_{PCA} - \hat{\mathbf{C}}\hat{\mathbf{S}}^T\|$$

MCR-ALS is an algorithm to minimize the SSR with two matrices  $\hat{\mathbf{C}}$  and  $\hat{\mathbf{S}}^T$ . The aim of algorithm is to reach a minimum SSR value (2.17) by iteratively by means of equations (2.19) and (2.21) as the following

$$\hat{\mathbf{S}}^T = (\hat{\mathbf{C}}^T\hat{\mathbf{C}})^{-1}\hat{\mathbf{C}}^T\mathbf{X}_{PCA}$$

$$\hat{\mathbf{C}} = \mathbf{X}_{PCA}\hat{\mathbf{S}}(\hat{\mathbf{S}}^T\hat{\mathbf{S}})^{-1}$$

HypSpec program was used to estimate pure spectra of the protonated and unprotonated concentration profiles of amine, tris and carboxyl terminated PAMAMs. During calculations, HypSpec program is one of the most recent programs that lead to more accurate concentration profiles by considering primarily the negativity constraint and other constraints explained in part 2.6.3 during the derivation of unit spectra [83]. Estimated concentration profiles of protonated and unprotonated concentration profiles

of amine, tris and carboxyl terminated PAMAM can be seen in Figure 4.47 to 4.49, 4.50 to 4.52, and 4.53 to 4.55, respectively in the following subparts.

#### 4.4.3.1 Amine Terminated PAMAMs

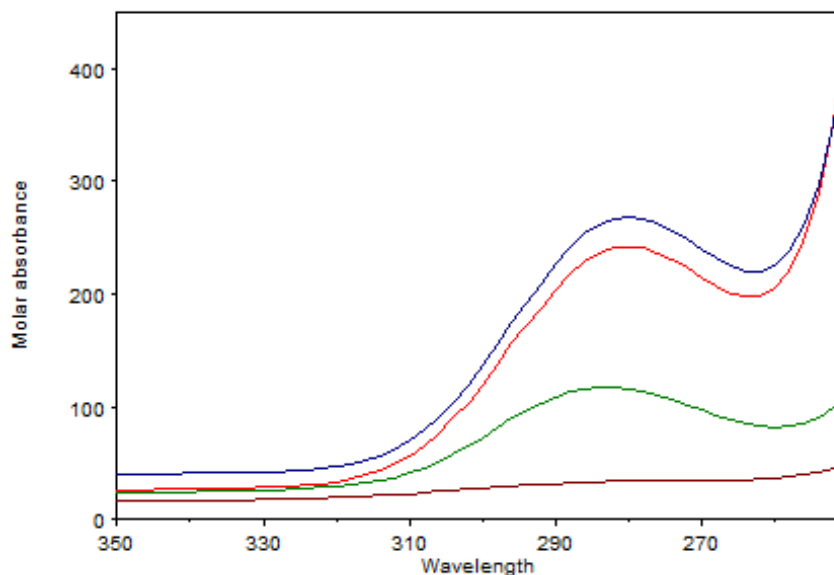


Figure 4.47 Molar absorbance spectrum of E4.NH<sub>2</sub>: Redline, (E4.NH<sub>2</sub>)H: Blue line, (E4.NH<sub>2</sub>)H<sub>2</sub>: Green line, (E4.NH<sub>2</sub>)H<sub>3</sub>: Brown line

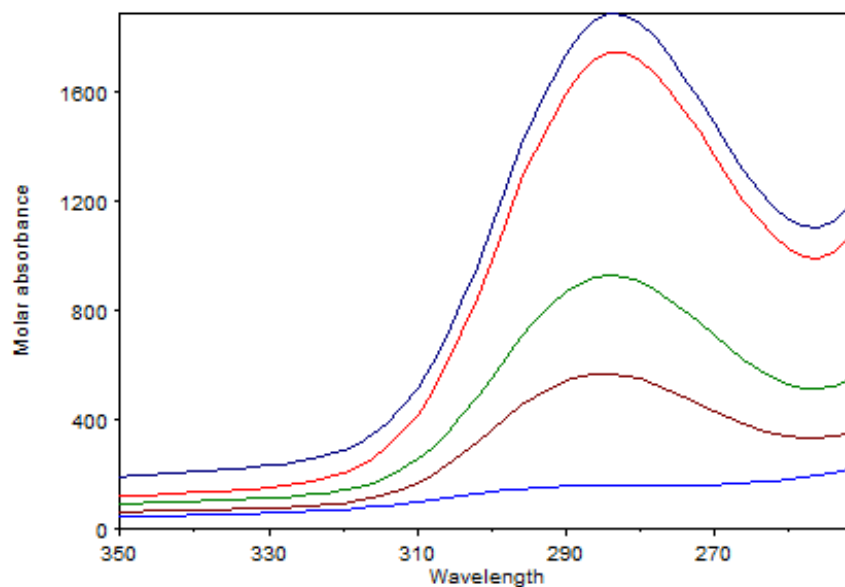


Figure 4.48 Molar absorbance spectrum of D4.NH<sub>2</sub>: Redline, (D4.NH<sub>2</sub>) H: Dark blue line, (D4.NH<sub>2</sub>)H<sub>2</sub>: Green line, (D4.NH<sub>2</sub>)H<sub>3</sub>: Brown line, (D4.NH<sub>2</sub>)H<sub>4</sub>: Light blue line

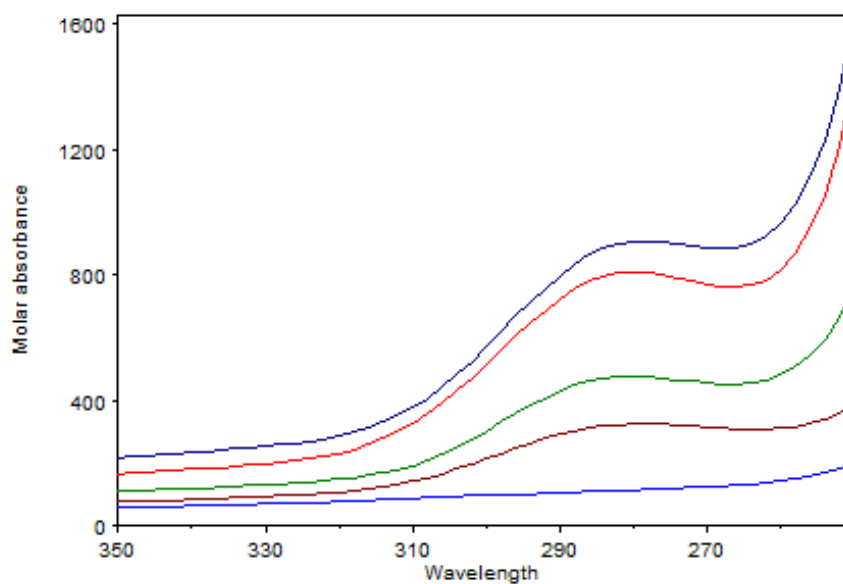


Figure 4.49 Molar absorbance spectrum of P4.NH<sub>2</sub>: Redline, (P4.NH<sub>2</sub>)H: Dark blue line, (P4.NH<sub>2</sub>)H<sub>2</sub>: Green line, (P4.NH<sub>2</sub>)H<sub>3</sub>: Brown line, (P4.NH<sub>2</sub>)H<sub>4</sub>: Light blue line

#### 4.4.3.2 Tris Terminated PAMAMs

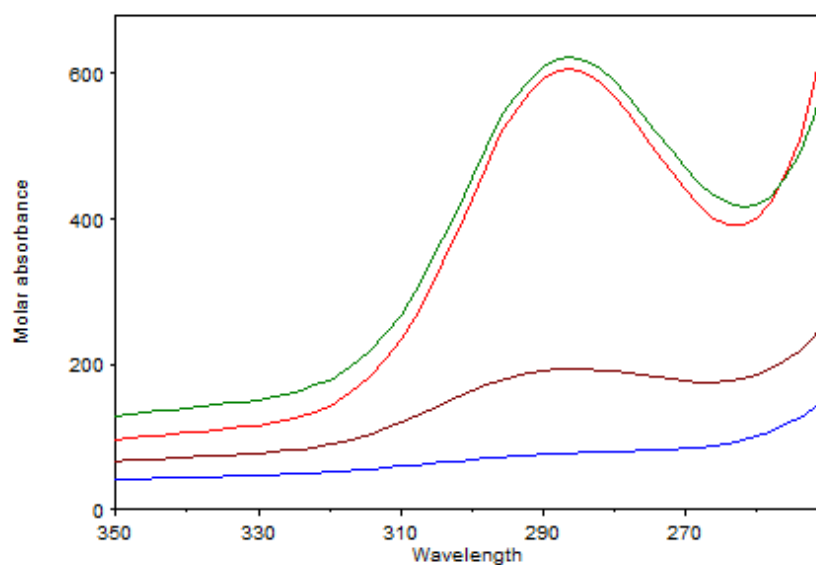


Figure 4.50 Molar absorbance spectrum of E4.TRIS: Redline, (E4.TRIS)H: Green line, (E4.TRIS)H<sub>2</sub>: Brown line, (E4.TRIS)H<sub>3</sub>: Blue line

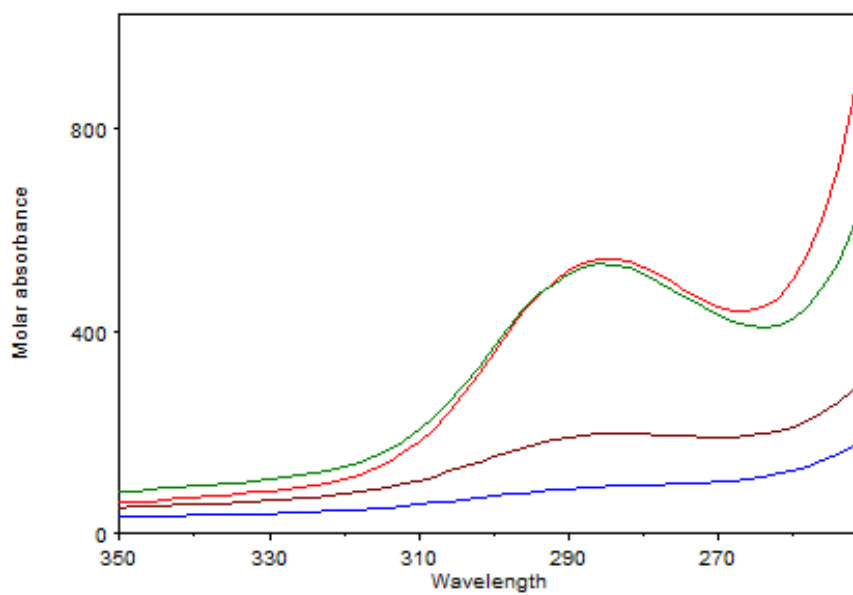


Figure 4.51 Molar absorbance spectrum of D4.TRIS: Redline, (D4.TRIS)H: Green line, (D4.TRIS)H<sub>2</sub>: Brown line, (D4.NH<sub>2</sub>)H<sub>3</sub>: Blue line

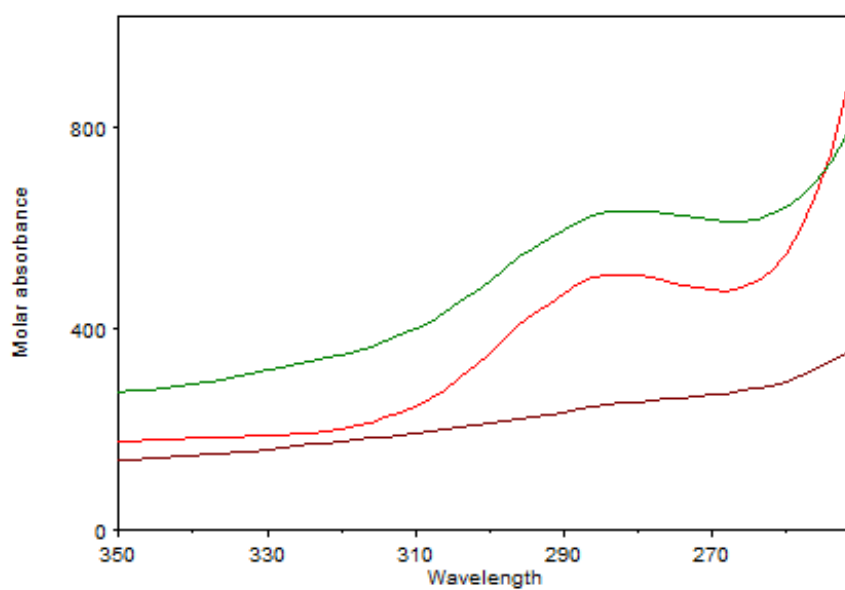


Figure 4.52 Molar absorbance spectrum of P4.TRIS: Redline, (P4.TRIS)H: Green line, (P4.TRIS)H<sub>2</sub>: Brown line

### 4.4.3.3 Carboxyl Terminated PAMAMs

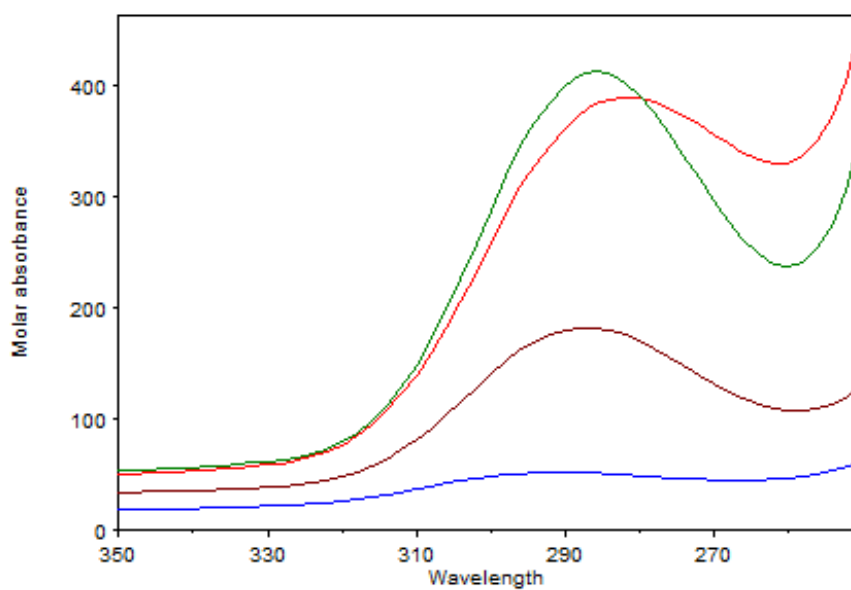


Figure 4.53 Molar absorbance spectrum of E4.COOH: Redline, (E4.COOH)H: Green line, (E4.COOH)H<sub>2</sub>: Brown line, (E4.COOH)H<sub>3</sub>: Blue line

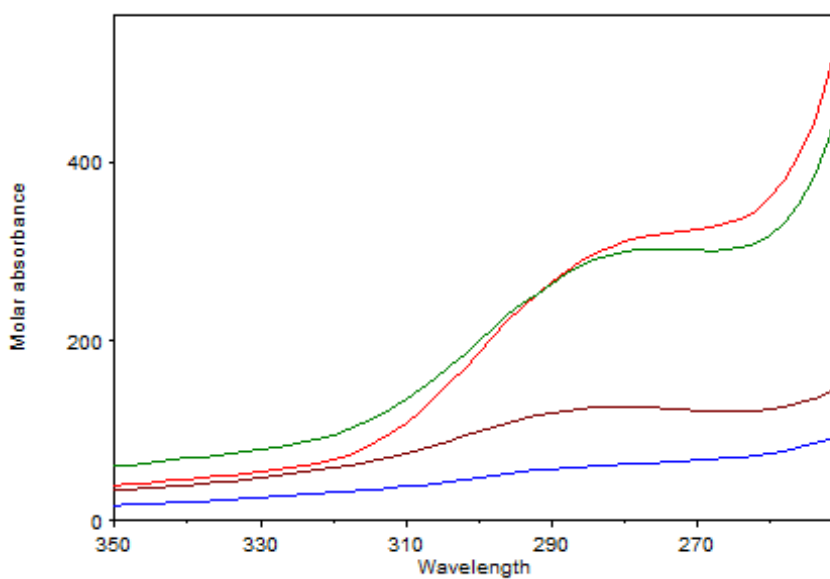


Figure 4.54 Molar absorbance spectrum of D4.COOH: Redline, (D4.COOH)H: Green line, (D4.COOH)H<sub>2</sub>: Brown line, (D4.COOH)H<sub>3</sub>: Blue line

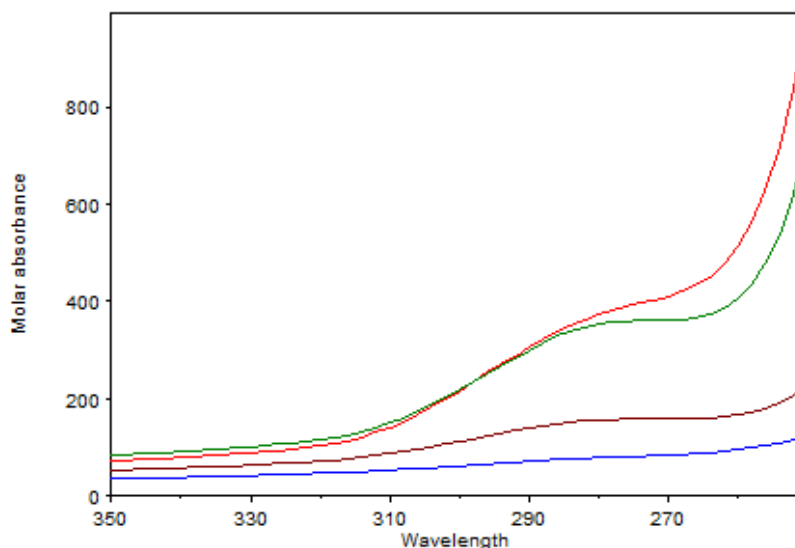


Figure 4.55 Molar absorbance spectrum of P4.COOH: Redline, (P4.COOH)H: Green line, (P4.COOH)H<sub>2</sub>: Brown line, (P4.COOH)H<sub>3</sub>: Blue line

#### 4.4.4 Refinement of Protonation Constants by HypSpec Program

HypSpec program introduces to the user of the program various operation modes. These are titration data with pH value or without pH value, and batch data entry. Spectroscopic titration experiments were conducted at  $25 \pm 0.1$  °C with an ionic strength of  $I = 100$  mM NaCl with pH value present.  $\log\beta$  values calculated in this part were arranged according the representative model  $Lq + Hr \rightleftharpoons LHr$ .

The first thing to do in HypSpec program is to enter data. Recorded absorption spectra at each level of several spectroscopic acid base titration at different pH values are arranged with their pH values in a text file, and entered to the program.

In order to start refinement procedure in HypSpec program, it should have been specified a model to the system. After the process of **X** data matrix through the part 4.4.1 and 4.4.3, it was determined the number of absorbing species present in PAMAM systems. If it is determined the number of species present in the system, the model can be constructed. The model than allows you to enter system which species are expected to absorb by denoting which 'has spectrum'. Once the model has been constructed and project is saved, pure component spectra if available is entered. Finally the wavelengths to be used in the refinement are selected.

In the refinement, process, each species present has an option to hold constant, refined or ignored. The data for refinement of all species are first refined by entering manually a starting stability constant with a best estimates prior to using the automatic refinement. Finally, the refinement is performed by automatically by iteratively and protonation constants for the model are determined.

The refinement is a non-linear process in which stability constant values are optimized. During the refinement three constraints are applied.

- The equations of mass-balance are always satisfied
- The molar epsilon values are those obtained by linear least-squares fitting of the absorbance values according to the Beer-lambert law
- Stability constants must have positive values

The non-linear nature of the process requires that initial estimates be provided for the log beta values. The refinement is protected against divergence by shift-cutting. A refinement will be terminated if shift-cutting does not result in a reduction in the sum of squares. To check that a refinement has not terminated prematurely, the procedure is repeated it with different starting values of the stability constants to be refined. The models of the PAMAM systems and calculated stability constants for the evaluated PAMAMs in this dissertation were presented as the following in Table 4.19 to 4.27. Furthermore, species distribution curves to see the % relative formation and the fit of the model were presented in a separate part 4.4.5

Table 4.19 Stability constants of E3.NH<sub>2</sub> and E4.NH<sub>2</sub>

| LqHr                                | L | Hr | logβ=pKa value  |
|-------------------------------------|---|----|-----------------|
| (E4.NH <sub>2</sub> )H <sub>3</sub> | 1 | 3  | 3.6305 ± 0.0077 |
| (E4.NH <sub>2</sub> )H <sub>2</sub> | 1 | 2  | 5.6597 ± 0.0084 |
| (E4.NH <sub>2</sub> )H              | 1 | 1  | 9.3779 ± 0.0166 |
| (E3.NH <sub>2</sub> )H <sub>3</sub> | 1 | 3  | 3.5702 ± 0.0048 |
| (E3.NH <sub>2</sub> )H <sub>2</sub> | 1 | 2  | 5.8715 ± 0.0174 |
| (E3.NH <sub>2</sub> )H              | 1 | 1  | 8.8828 ± 0.0117 |

Table 4.20 Stability constants of D3.NH<sub>2</sub> and D4.NH<sub>2</sub>

| LqHr                                | Lq | Hr | logβ=pKa value  |
|-------------------------------------|----|----|-----------------|
| (D4.NH <sub>2</sub> )H <sub>4</sub> | 1  | 4  | 3.7300 ± 0.0033 |
| (D4.NH <sub>2</sub> )H <sub>3</sub> | 1  | 3  | 5.9519 ± 0.0320 |
| (D4.NH <sub>2</sub> )H <sub>2</sub> | 1  | 2  | 7.4253 ± 0.0564 |
| (D4.NH <sub>2</sub> )H              | 1  | 1  | 9.0617 ± 0.0121 |
| (D3.NH <sub>2</sub> )H <sub>3</sub> | 1  | 3  | 3.5982 ± 0.0075 |
| (D3.NH <sub>2</sub> )H <sub>2</sub> | 1  | 2  | 5.4848 ± 0.0315 |
| (D3.NH <sub>2</sub> )H              | 1  | 1  | 9.5494 ± 0.0240 |

Table 4.21 Stability constants of P3NH<sub>2</sub> and P4.NH<sub>2</sub>

| LqHr                                | Lq | Hr | logβ=pKa value  |
|-------------------------------------|----|----|-----------------|
| (P4.NH <sub>2</sub> )H <sub>4</sub> | 1  | 4  | 3.2532 (0.0043) |
| (P4.NH <sub>2</sub> )H <sub>3</sub> | 1  | 3  | 5.4212 (0.0173) |
| (P4.NH <sub>2</sub> )H <sub>2</sub> | 1  | 2  | 7.4073 (0.0344) |
| (P4.NH <sub>2</sub> )H              | 1  | 1  | 9.9682 (0.0113) |
| (P3.NH <sub>2</sub> )H <sub>3</sub> | 1  | 3  | 3.5221 ± 0.0076 |
| (P3.NH <sub>2</sub> )H <sub>2</sub> | 1  | 2  | 6.1473 ± 0.0079 |
| (P3.NH <sub>2</sub> )H              | 1  | 1  | 9.7286 ± 0.0347 |

Table 4.22 Stability constants E3.TRIS and E4.TRIS

| LqHr                    | Lq | Hr | $\log\beta=pK_a$ value |
|-------------------------|----|----|------------------------|
| (E4.TRIS)H <sub>3</sub> | 1  | 3  | $3.0532 \pm 0.0157$    |
| (E4.TRIS)H <sub>2</sub> | 1  | 2  | $5.1469 \pm 0.0086$    |
| (E4.TRIS)H              | 1  | 1  | $8.2534 \pm 0.0169$    |
| (E3.TRIS)H <sub>3</sub> | 1  | 3  | $3.6320 \pm 0.0162$    |
| (E3.TRIS)H <sub>2</sub> | 1  | 2  | $5.8877 \pm 0.0084$    |
| (E3.TRIS)H              | 1  | 1  | $8.1859 \pm 0.0125$    |

Table 4.23 Stability constants of D3.TRIS and D4.TRIS

| LqHr                    | Lq | Hr | $\log\beta=pK_a$ value |
|-------------------------|----|----|------------------------|
| (D4.TRIS)H <sub>3</sub> | 1  | 3  | $4.1452 \pm 0.0207$    |
| (D4.TRIS)H <sub>2</sub> | 1  | 2  | $5.8731 \pm 0.0209$    |
| (D4.TRIS)H              | 1  | 1  | $8.2382 \pm 0.0118$    |
| (D3.TRIS)H <sub>3</sub> | 1  | 3  | $4.1473 \pm 0.0137$    |
| (D3.TRIS)H <sub>2</sub> | 1  | 2  | $5.9059 \pm 0.0104$    |
| (D3.TRIS)H              | 1  | 1  | $7.6280 \pm 0.0163$    |

Table 4.24 Stability constants of P3.TRIS and P4.TRIS

| LqHr                    | Lq | Hr | $\log\beta=pK_a$ value |
|-------------------------|----|----|------------------------|
| (P4.TRIS)H <sub>2</sub> | 1  | 2  | $5.1250 \pm 0.0180$    |
| (P4.TRIS)H              | 1  | 1  | $7.7907 \pm 0.0082$    |
| (P3.TRIS)H <sub>2</sub> | 1  | 2  | $4.6748 \pm 0.0190$    |
| (P3.TRIS)H <sub>1</sub> | 1  | 1  | $7.4741 \pm 0.0103$    |

Table 4.25 Stability constants of E3.COOH and E4.COOH

| LqHr                    | Lq | Hr | $\log\beta=pK_a$ value |
|-------------------------|----|----|------------------------|
| (E4.COOH)H <sub>3</sub> | 1  | 3  | $4.3731 \pm 0.0097$    |
| (E4.COOH)H <sub>2</sub> | 1  | 2  | $6.9975 \pm 0.0305$    |
| (E4.COOH)H              | 1  | 1  | $10.5774 \pm 0.0201$   |
| (E3.COOH)H <sub>3</sub> | 1  | 3  | $4.8346 \pm 0.0122$    |
| (E3.COOH)H <sub>2</sub> | 1  | 2  | $8.0864 \pm 0.0220$    |
| (E3.COOH)H              | 1  | 1  | $10.4512 \pm 0.0198$   |

Table 4.26 Stability constants of D3.COOH and D4.COOH

| LqHr                    | Lq | Hr | $\log\beta=pK_a$ value |
|-------------------------|----|----|------------------------|
| (D4.COOH)H <sub>3</sub> | 1  | 3  | $3.7741 \pm 0.0276$    |
| (D4.COOH)H <sub>2</sub> | 1  | 2  | $6.0001 \pm 0.0193$    |
| (D4.COOH)H              | 1  | 1  | $9.1251 \pm 0.0251$    |
| (D3.COOH)H <sub>3</sub> | 1  | 3  | $3.1998 \pm 0.0161$    |
| (D3.COOH)H <sub>2</sub> | 1  | 2  | $6.0884 \pm 0.0161$    |
| (D3.COOH)H              | 1  | 1  | $8.7386 \pm 0.0132$    |

Table 4.27 Stability constants of P3.COOH and P4.COOH

| LqHr                    | Lq | Hr | $\log\beta=pK_a$ value |
|-------------------------|----|----|------------------------|
| (P4.COOH)H <sub>3</sub> | 1  | 3  | $3.7083 \pm 0.0259$    |
| (P4.COOH)H <sub>2</sub> | 1  | 2  | $6.8275 \pm 0.0156$    |
| (P4.COOH)H              | 1  | 1  | $9.1253 \pm 0.0133$    |
| (P3.COOH)H <sub>3</sub> | 1  | 3  | $4.3531 \pm 0.0250$    |
| (P3.COOH)H <sub>2</sub> | 1  | 2  | $7.8330 \pm 0.0185$    |
| (P3.COOH)H              | 1  | 1  | $9.7628 \pm 0.0293$    |

## 4.4.5 Species Distribution Curves

### 4.4.5.1 Amine Terminated PAMAMs

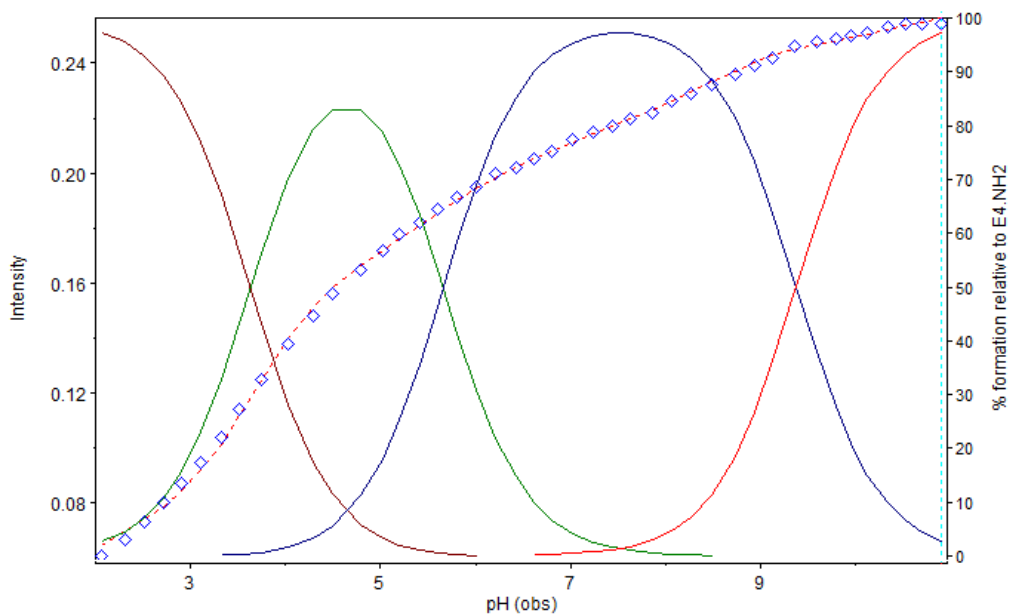


Figure 4.56 Species distribution curve of E4.NH<sub>2</sub> in the pH range of 2-11. % Concentrations of free E4.NH<sub>2</sub>: Redline, (E4.NH<sub>2</sub>)H: Blue line, (E4.NH<sub>2</sub>)H<sub>2</sub>: Green line, (E4.NH<sub>2</sub>)H<sub>3</sub>: Brown line. Blue square mark: Observed intensities and dashed red line: Calculated Intensities at  $\lambda = 284$  nm

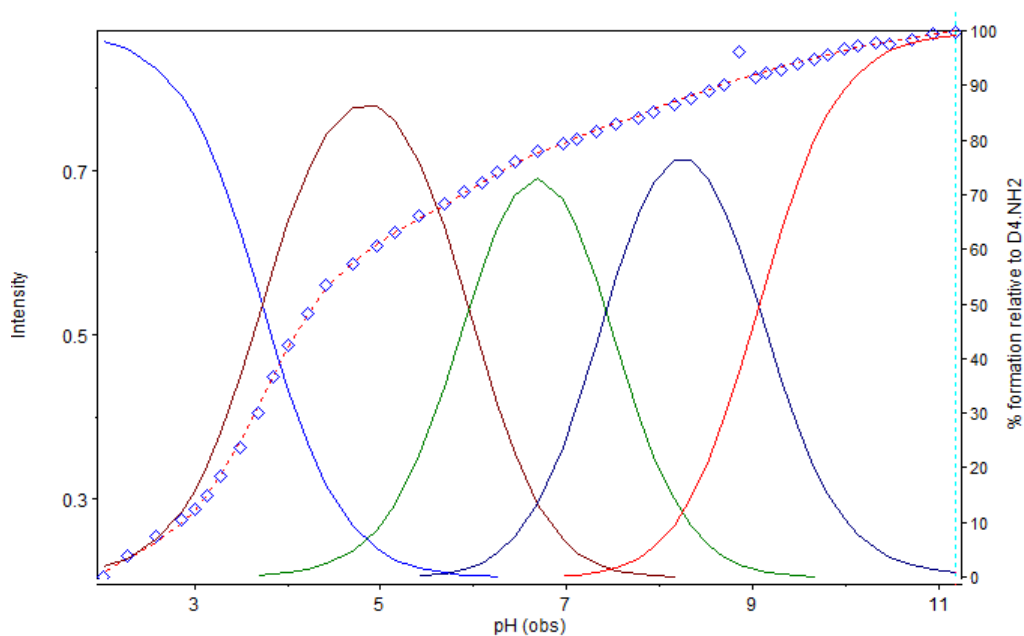


Figure 4.57 Species distribution curve of D4.NH<sub>2</sub> in the pH range 2-11. % Concentrations of free D4.NH<sub>2</sub>: Redline, (D4.NH<sub>2</sub>) H: Dark blue line, (D4.NH<sub>2</sub>)H<sub>2</sub>: Green line, (D4.NH<sub>2</sub>)H<sub>3</sub>: Brown line, (D4.NH<sub>2</sub>)H<sub>4</sub>: Light blue line. Blue square mark: Observed intensities and dashed red line: Calculated Intensities at  $\lambda = 284$  nm

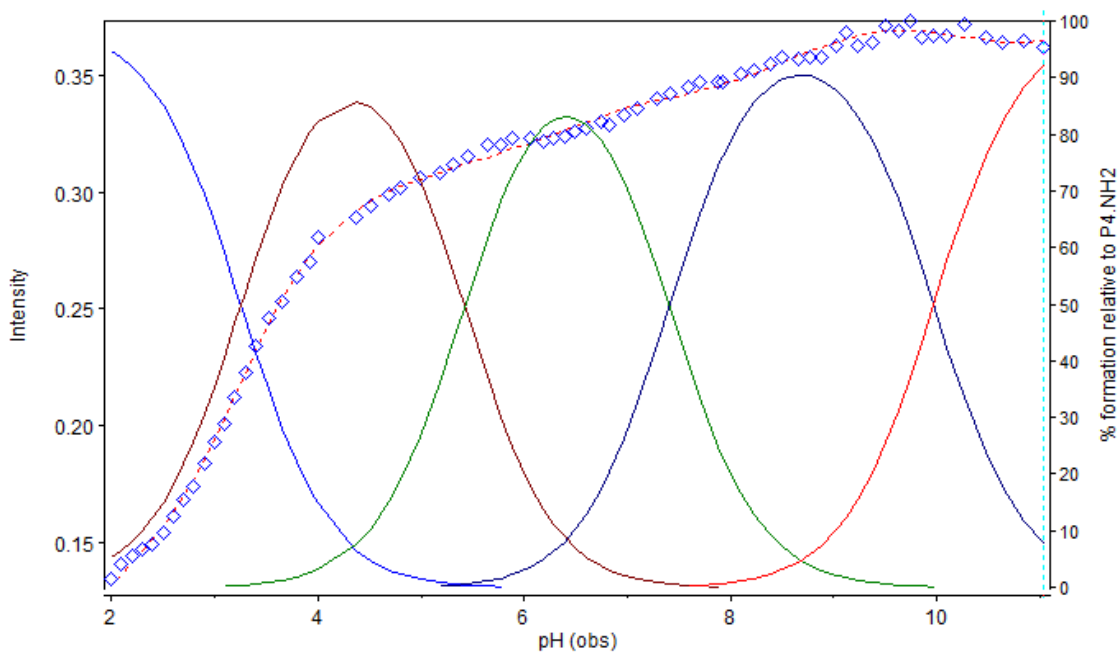


Figure 4.58 Species distribution curve of P4.NH<sub>2</sub> in the pH range 2-11. % Concentrations of free P4.NH<sub>2</sub>: Redline, (P4.NH<sub>2</sub>)H: Dark blue line, (P4.NH<sub>2</sub>)H<sub>2</sub>: Green line, (P4.NH<sub>2</sub>)H<sub>3</sub>: Brown line, (P4.NH<sub>2</sub>)H<sub>4</sub>: Light blue line. Blue square mark: Observed intensities and dashed red line: Calculated Intensities at  $\lambda = 284$  nm

#### 4.4.5.2 TRIS Terminated PAMAMs

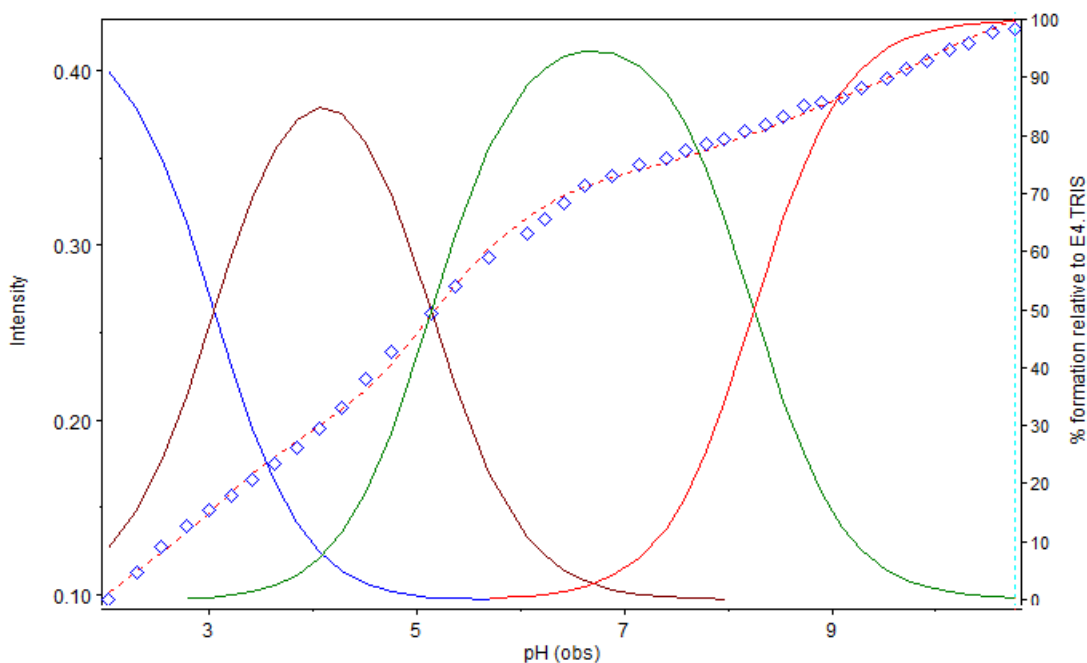


Figure 4.59 Species distribution curve of E4.TRIS in the pH range of 2-11. % Concentrations of free E4.TRIS: Redline, (E4.TRIS)H: Green line, (E4.TRIS)H<sub>2</sub>: Brown line, (E4.TRIS)H<sub>3</sub>: Blue line. Blue square mark: Observed intensities and dashed red line: Calculated Intensities at  $\lambda = 286$  nm

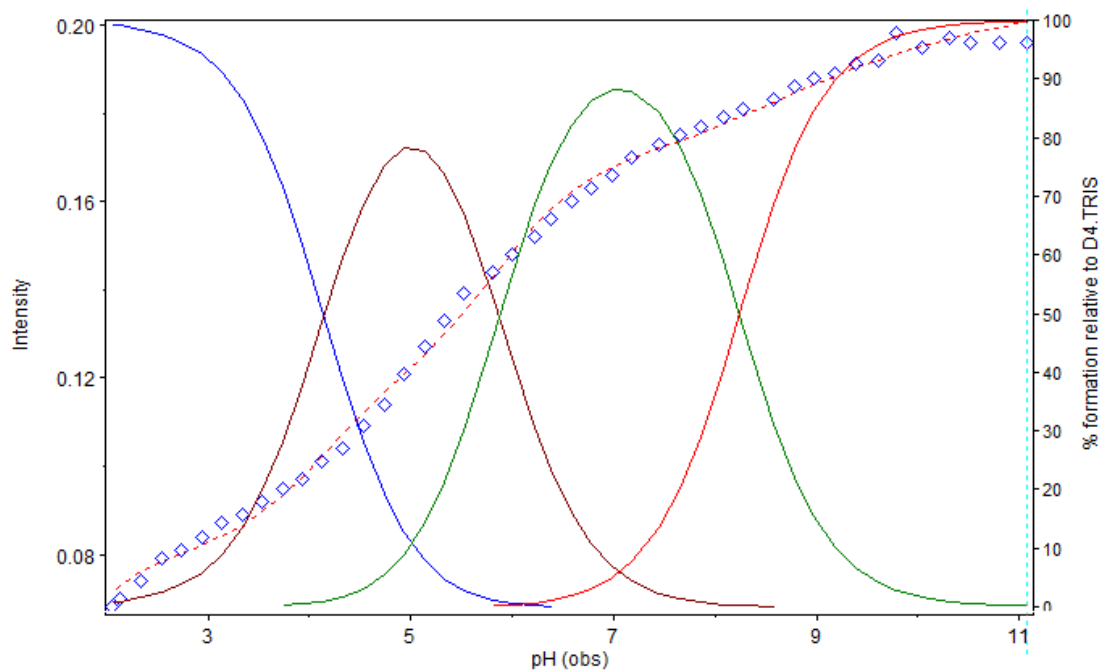


Figure 4.60 Species distribution curve of D4.TRIS in the pH range of 2-11. % Concentrations of free D4.TRIS: Redline, (D4.TRIS)H: Green line, (D4.TRIS)H<sub>2</sub>: Brown line, (D4.TRIS)H<sub>3</sub>: Blue line. Blue square mark: Observed intensities and dashed red line: Calculated Intensities at  $\lambda = 286$  nm

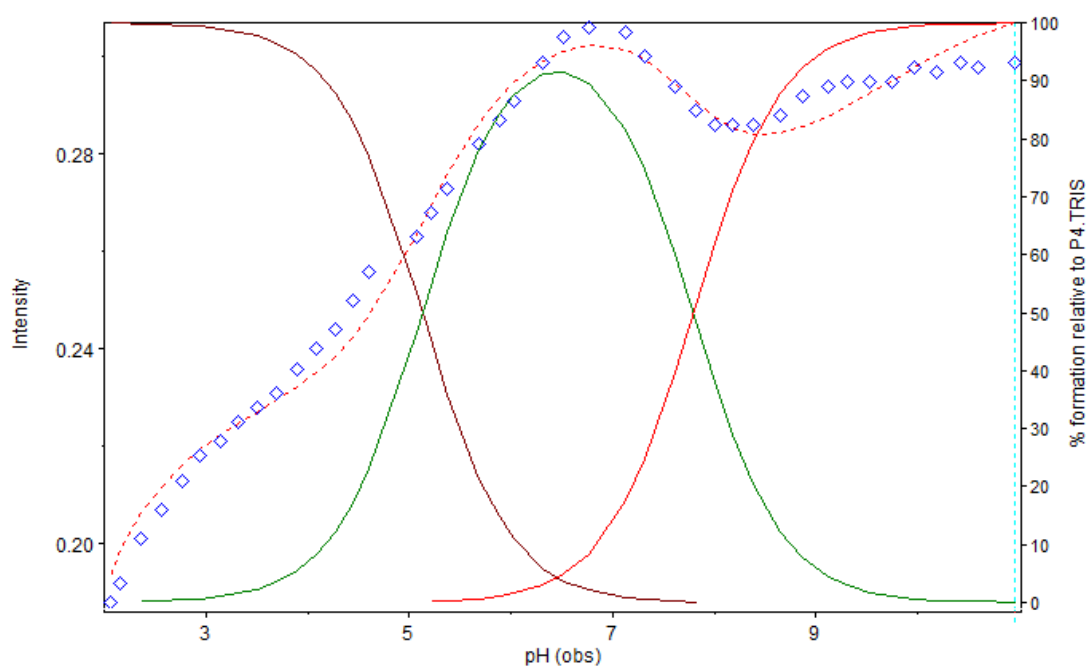


Figure 4.61 Species distribution curve of P4.TRIS in the pH range of 2-11. % Concentrations of free P4.TRIS: Redline, (P4.TRIS)H: Green line, (P4.TRIS)H<sub>2</sub>: Brown line. Blue square mark: Observed intensities and dashed red line: Calculated Intensities at  $\lambda = 284$  nm

### 4.4.5.3 Carboxyl Terminated PAMAMs

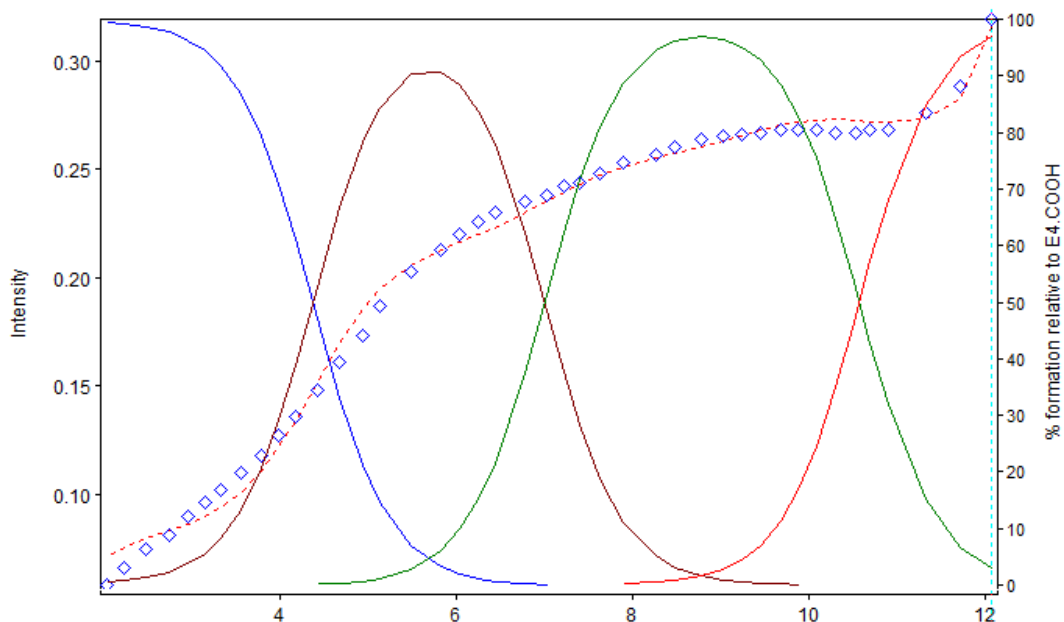


Figure 4.62 Species distribution curve of E4.COOH in the pH range of 2-11. % Concentrations of free E4.COOH: Redline, (E4.COOH)H: Green line, (E4.COOH)H<sub>2</sub>: Brown line, (E4.COOH)H<sub>3</sub>: Blue line. Blue square mark: Observed intensities and dashed red line: Calculated Intensities at  $\lambda = 286$  nm

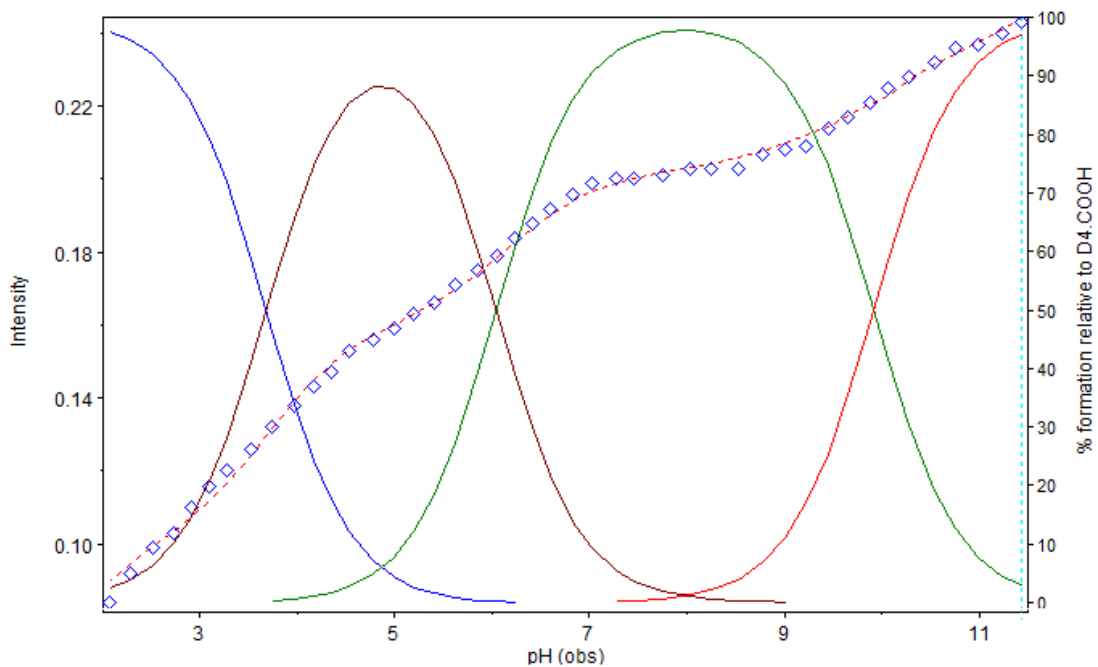


Figure 4.63 Species distribution curve of D4.COOH in the pH range of 2-12. % Concentrations of free D4.COOH: Redline, (D4.COOH)H: Green line, (D4.COOH)H<sub>2</sub>: Brown line, (D4.COOH)H<sub>3</sub>: Blue line. Blue square mark: Observed intensities and dashed red line: Calculated Intensities at  $\lambda = 286$  nm

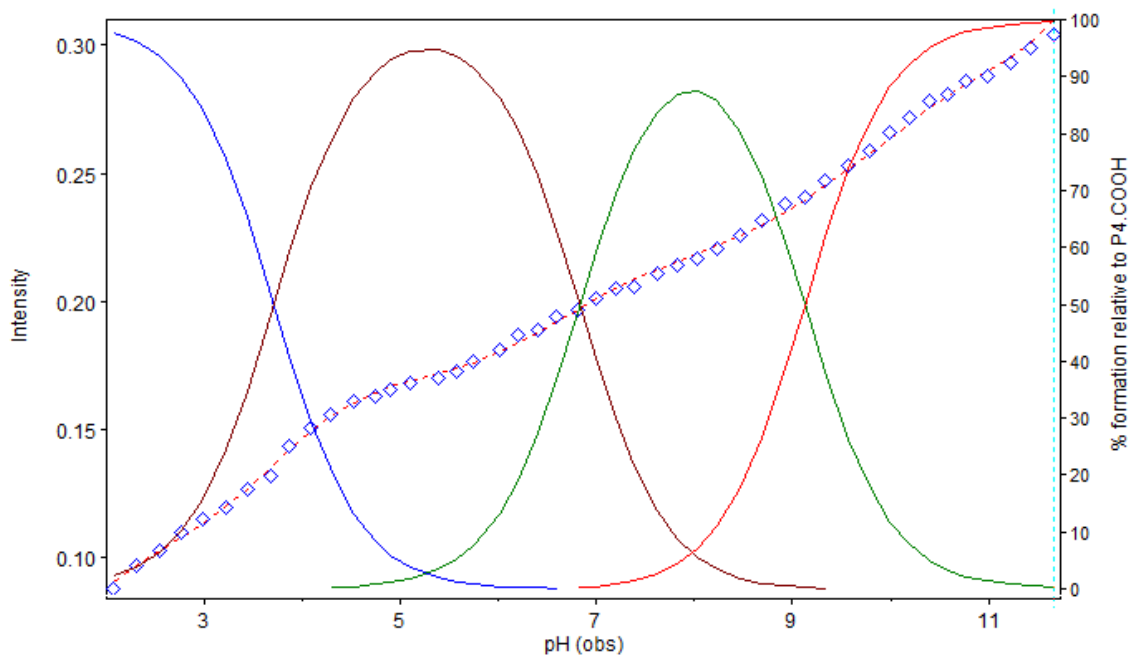


Figure 4.64 Species distribution curve of P4.COOH in the pH range of 2-12. % Concentrations of free P4.COOH: Redline, (P4.COOH)H: Green line, (P4.COOH)H<sub>2</sub>: Brown line, (P4.COOH)H<sub>3</sub>: Blue line. Blue square mark: Observed intensities and dashed red line: Calculated Intensities at  $\lambda = 286$  nm

## 4.5 Analysis of Co(II)-PAMAM Dendrimer Complexes by UV-VIS Spectroscopy

### 4.5.1 Potentiometric Measurements

Tertiary and primary amine groups of PAMAMs are Lewis bases and they can bind most metals simultaneously (Figure 4.65). [174] However, primary amines of dendrimers cannot bind metal ions depending on the pH characteristic of the media. When EOP of amine groups is out of the pH range of metal binding or all amine groups are protonated. Therefore they are not available for metal ion coordination. Forward and back titration of the sample amount of P4.NH<sub>2</sub> supports the existence of two type amino groups, which are tertiary and primary amine groups (Figure 4.66). pK<sub>a</sub> values of the tertiary and primary amine groups of P4.NH<sub>2</sub> were calculated as 9.9682, 7.4073, 5.4212 and 3.2532 for the protonated conformations (P4.NH<sub>2</sub>)H, (P4.NH<sub>2</sub>)H<sub>2</sub>, (P4.NH<sub>2</sub>)H<sub>3</sub>, (P4.NH<sub>2</sub>)H<sub>4</sub>, respectively in part 4.4.4 from spectroscopic titration experiments. It could be observable by the results of potentiometric titration experiments in part 4.3.5.3 and also observable from Figure 4.66 that second end point represents the protonation of outer tertiary amine groups of P4.NH<sub>2</sub>. Thus, pH over the second end point of back titration primary amine

groups of P4.NH<sub>2</sub> starts to protonate as the pH higher. Second point exist in the pH range of 6.1644 and 6.40 (Figure 4.108). However, to attain maximum complexation, we have evaluated the pH of the complexation during Co (II)- P4.NH<sub>2</sub> complexation studies at pH 8.

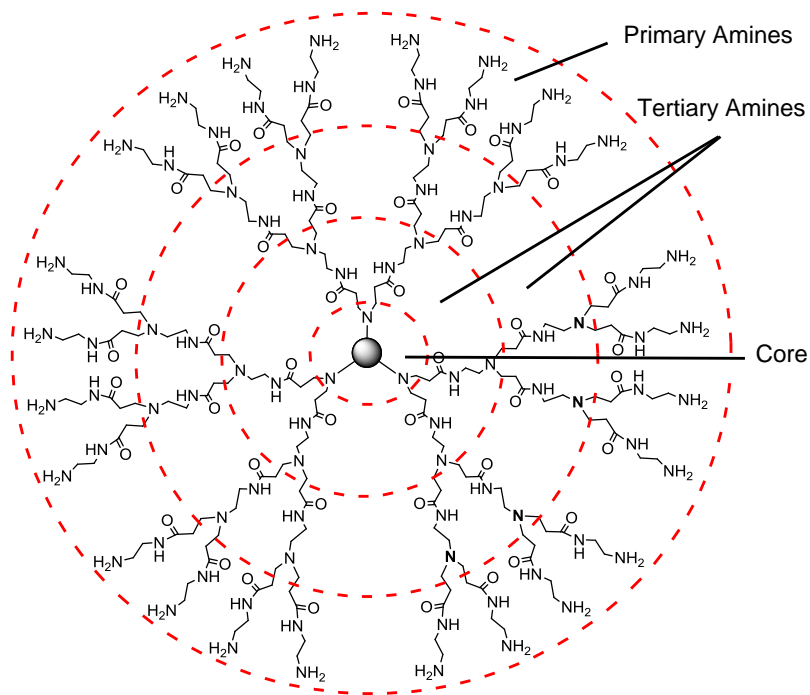


Figure 4.65 A sample structure of Jeffamine<sup>®</sup> T-403 cored PAMAMs. Third generation P3.NH<sub>2</sub> structure

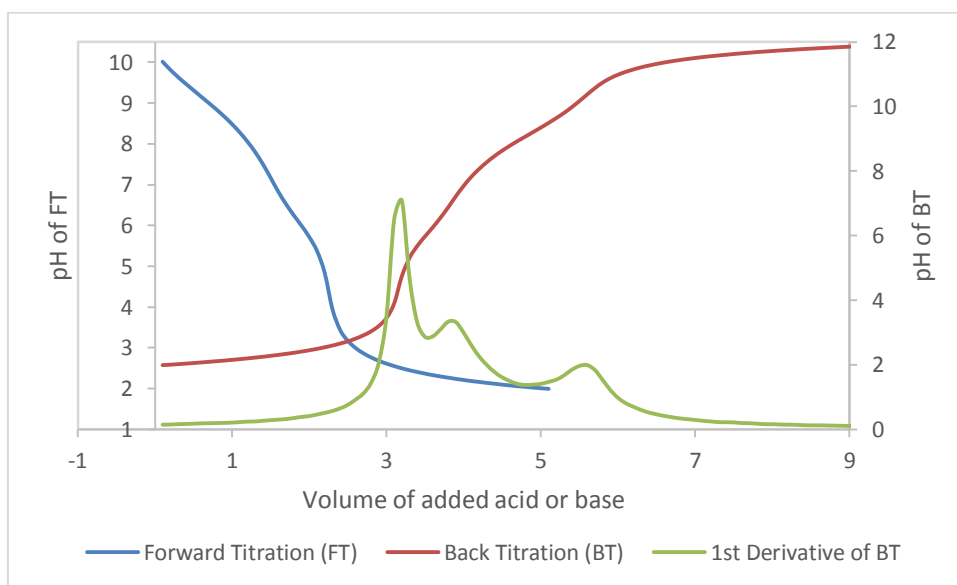


Figure 4.66 Illustration of forward and back potentiometric titration curves of P4.NH<sub>2</sub> with 2<sup>nd</sup> derivative of back titration curve

#### 4.5.2 UV-VIS Characterization of P4.NH<sub>2</sub>

Spectroscopic titration studies of P4.NH<sub>2</sub> revealed a characteristic absorption band in the 280-285 nm region. This band is attributed to internal tertiary amines of PAMAMs as a signal of the monodispersity and purity [72] (Figure 4.67). Figure 4.68 represents the spectra of unbuffered 100  $\mu$ M P4.NH<sub>2</sub> dendrimer. Between the pH ranges 2.03 to 9.97 dendrimer solution displays a characteristic  $\lambda_{\text{max}}$  absorption band ranging between 280-285 nm. This band does not even disappear at lower pH values like pH 2.03. The inset of Figure 4.68 is pH versus absorbance at  $\lambda_{\text{max}}= 280$  nm of P4.NH<sub>2</sub> unbuffered aqueous solution. It can be noted from Figure 4.68 also that disappearance of 280-285 nm absorption band completely depend on the protonation of dendrimer. The investigation of the inset of Figure 4.68 also indicates that P4.NH<sub>2</sub> dendrimer can exhibit interesting ligand properties as chelating agents, especially between the pH ranges 6-8.

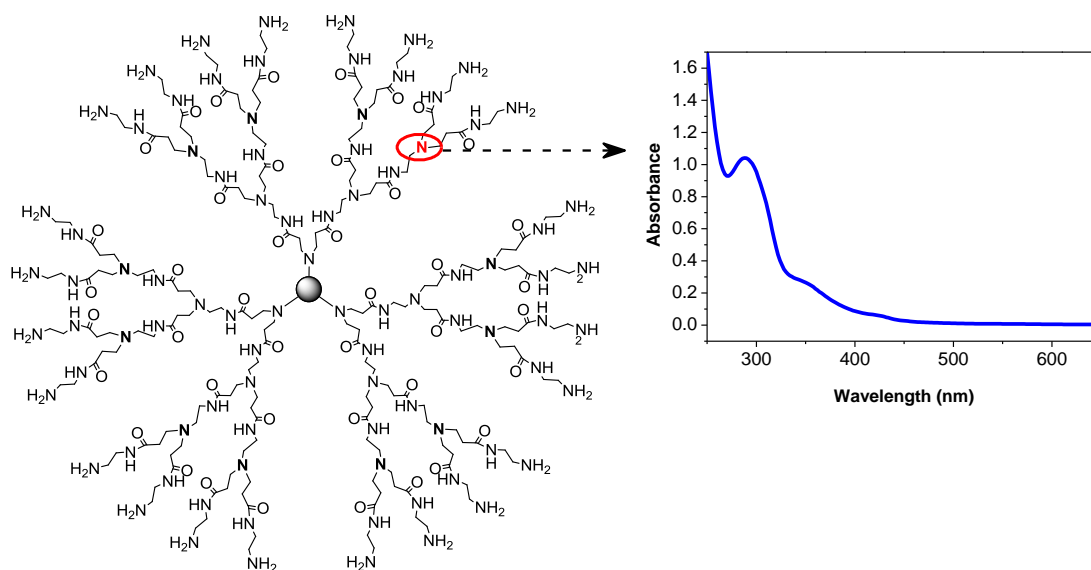


Figure 4.67 PAMAM dendrimer characteristic absorption band in between 280-285 nm

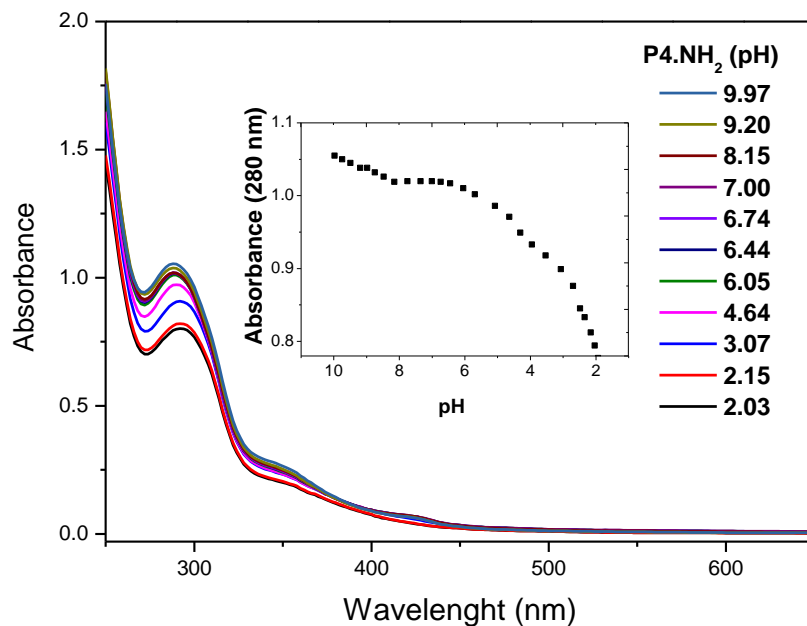


Figure 4.68 Representative absorption spectra of P4.NH<sub>2</sub>. The absorbance band at 288 nm changes as a function of pH. Initial pH of dendrimer was 9.97. The titrant was 0.1015 N HCl. All the spectra were obtained using a 1.00 cm cuvette and all were referenced to water

#### 4.5.3 UV-VIS Characterization of Co (II)-P4.NH<sub>2</sub> Complex

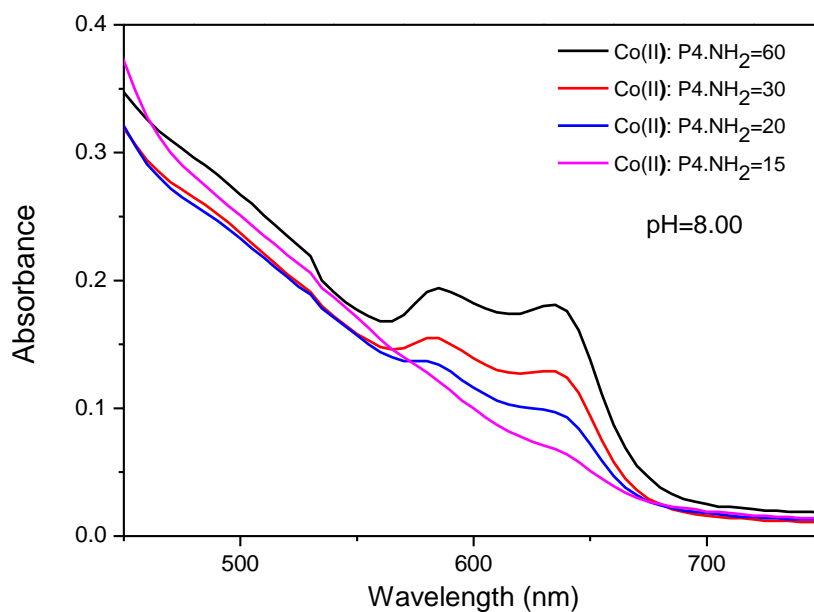


Figure 4.69 Observation of Co(II)-P4.NH<sub>2</sub> complexation bands at 585-635 nm for the alternating concentrations of Co(II):P4.NH<sub>2</sub> ratios

Characterization of the ability of PAMAMs binding Co (II) in aqueous solutions was characterized by UV-VIS spectroscopy. Normally, hexa-coordinated Co(II) aqua complexes in aqueous solutions was observed at  $\lambda_{\text{max}} = 510\text{-}512\text{ nm}$  [272]. UV Measurements were performed between the wavelength ranges of 200-750 nm with 1nm interval against the dendrimer solutions. Displacement of 512 nm band with 585-635 nm d-d transition bands confirmed the formation of Co(II)-P4.NH<sub>2</sub> complexes (Figure 4.69). In addition to this, dendrimer solution color turned immediately to dark green after addition of Co(II) ions to dendrimer solution, which is adjusted to pH 8. This color change and absorption bands could be attributed to formation of tetra amine complexes of Co(II) with dendrimer internal tertiary amine groups (Figure 4.69 and Figure 4.70). Complexation studies were conducted between the pH range of 6-8 and best observations were performed at pH=8 (Figure 4.110 and 4.112).

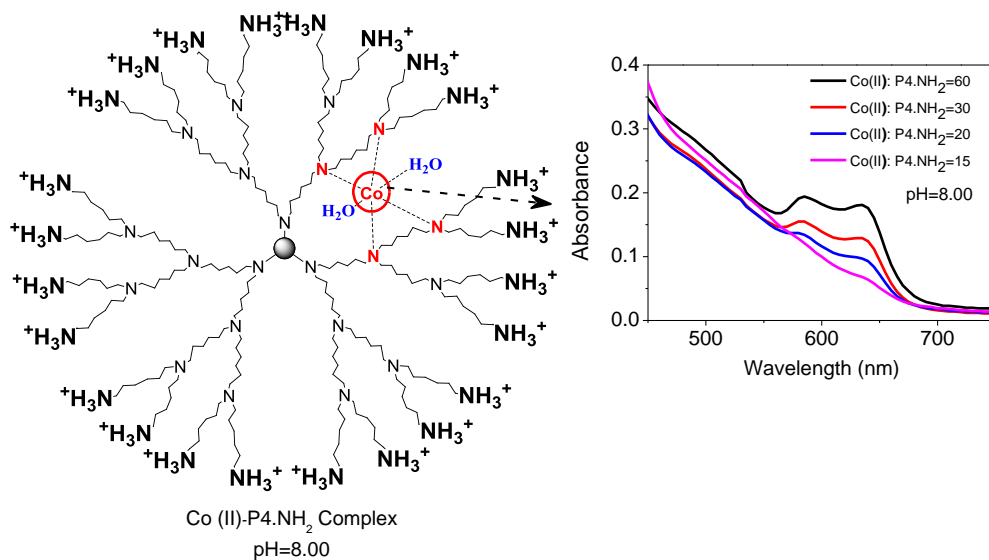


Figure 4.70 Illustration of the complex formation between Co(II) ions and P4.NH<sub>2</sub>

## 4.6 Removal of Metal Ions from Aqueous Solutions by Dendrimer Enhanced Ultrafiltration

### 4.6.1 Generation Effect of P3.NH<sub>2</sub> and P4.NH<sub>2</sub> PAMAMs on the Simultaneous Retention of Cu (II), Co (II), Ni (II), Cd (II), Zn (II)

Polymer assisted ultrafiltration (PAUF) can be a very beneficial way of removing heavy metals from aqueous solutions. The theory behind it is based on ultrafiltration (UF). Normally, UF process is used to separate extremely small particles and dissolved

molecules from solutes. UF is applied in cross-flow or dead-end mode. In dead end mode, a pressure source (usually nitrogen or air) is used to maintain feed flow over a physical barrier-membrane, which allows to pass certain compounds depending on their physical and chemical properties. However, molecules with similar molecular weights could not be separated with UF. On the basis of this theory, macromolecular species can be used to remove some kind of heavy metals from related media. Furthermore, pH characteristic of the media could be deterministic on both removal and recovery of complexed macromolecules. In this part, different generation Jeffamine<sup>®</sup> T-403 cored P3.NH<sub>2</sub> and P4.NH<sub>2</sub> PAMAMs were used as macromolecular templates for the simultaneous removal of the Cu (II), Co (II), Ni (II), Cd (II), Zn (II) divalent heavy metal ions from aqueous solutions by using 1kDa MWCO commercially available regenerated cellulose membranes unlike literaturally common removal of metals with once at a time procedure. Removal studies were conducted in the pH range of 3-9. Results were reported in retention (%) versus time (Figure 4.71-4.75). Retention profiles of the metals were calculated by means of eqn. (3.1). Thus, effect of solution pH and dendrimer generation on the simultaneous removal of metal ions were investigated (Figure 4.76).

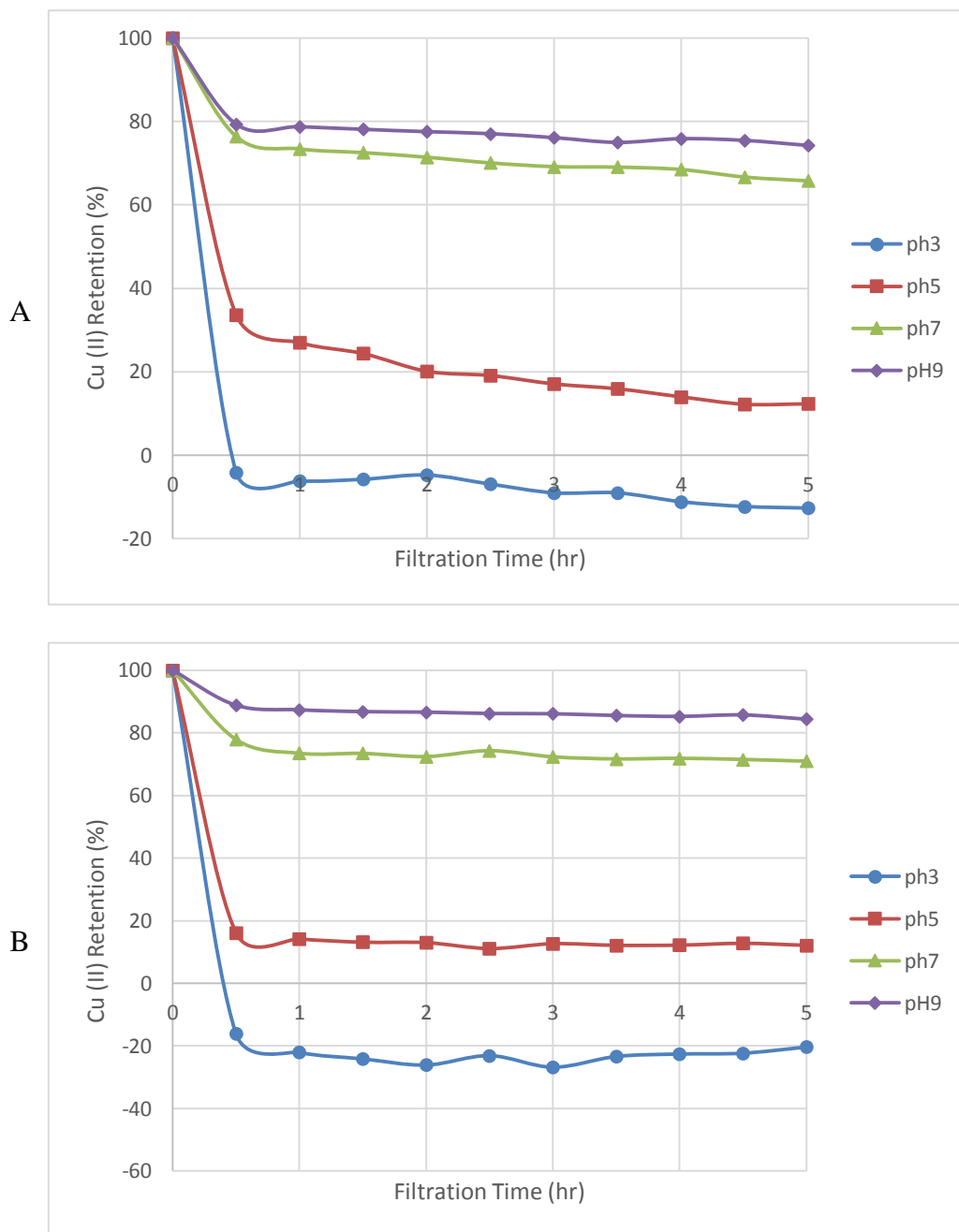


Figure 4.71 Cu (II) retention in aqueous solutions of (A) in P3.NH<sub>2</sub> and (B) in P4.NH<sub>2</sub> solutions as a function of solution pH

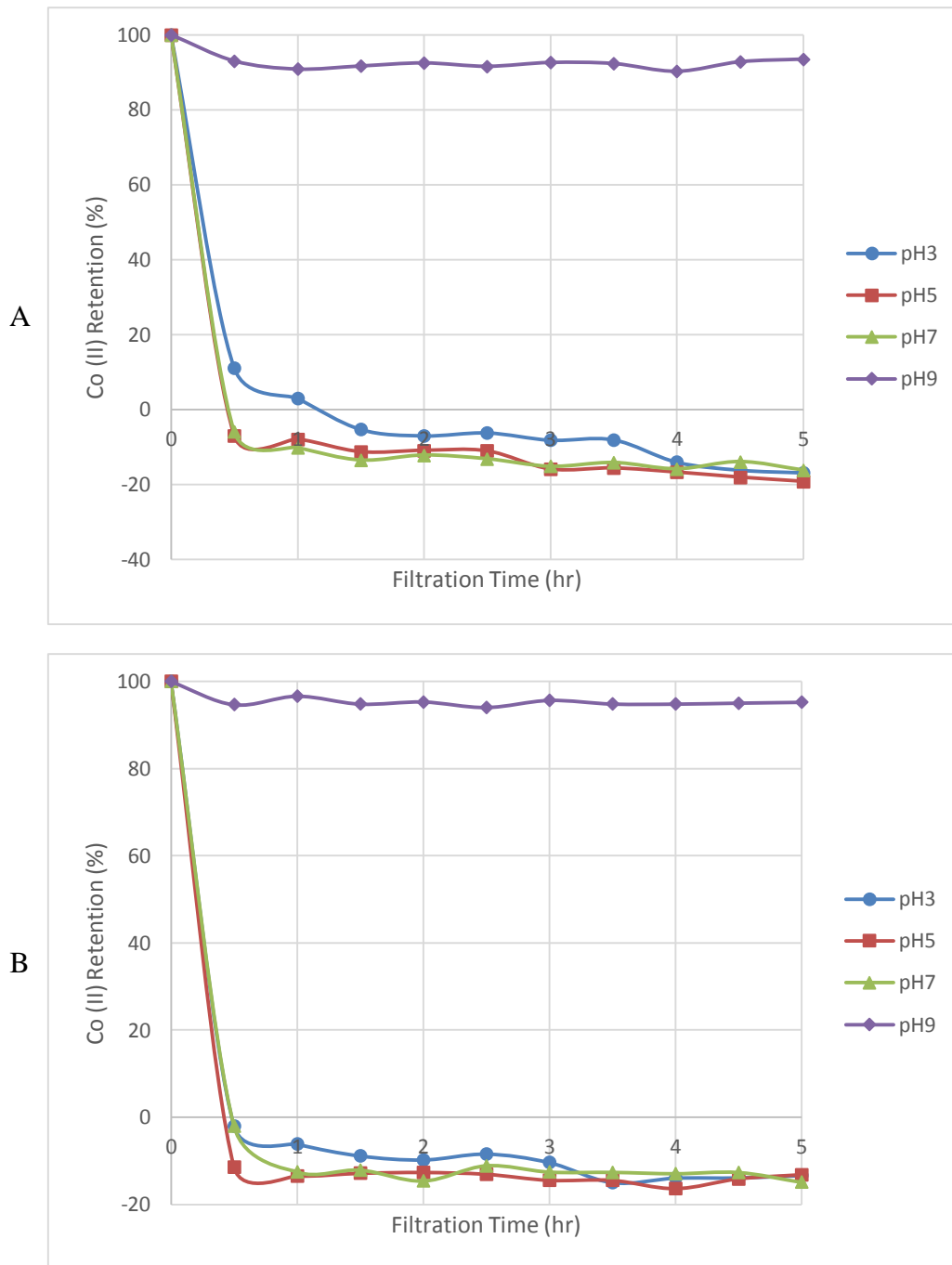


Figure 4.72 Co (II) retention in aqueous solutions of (A) in P3.NH<sub>2</sub> and (B) in P4.NH<sub>2</sub> solutions as a function of solution pH

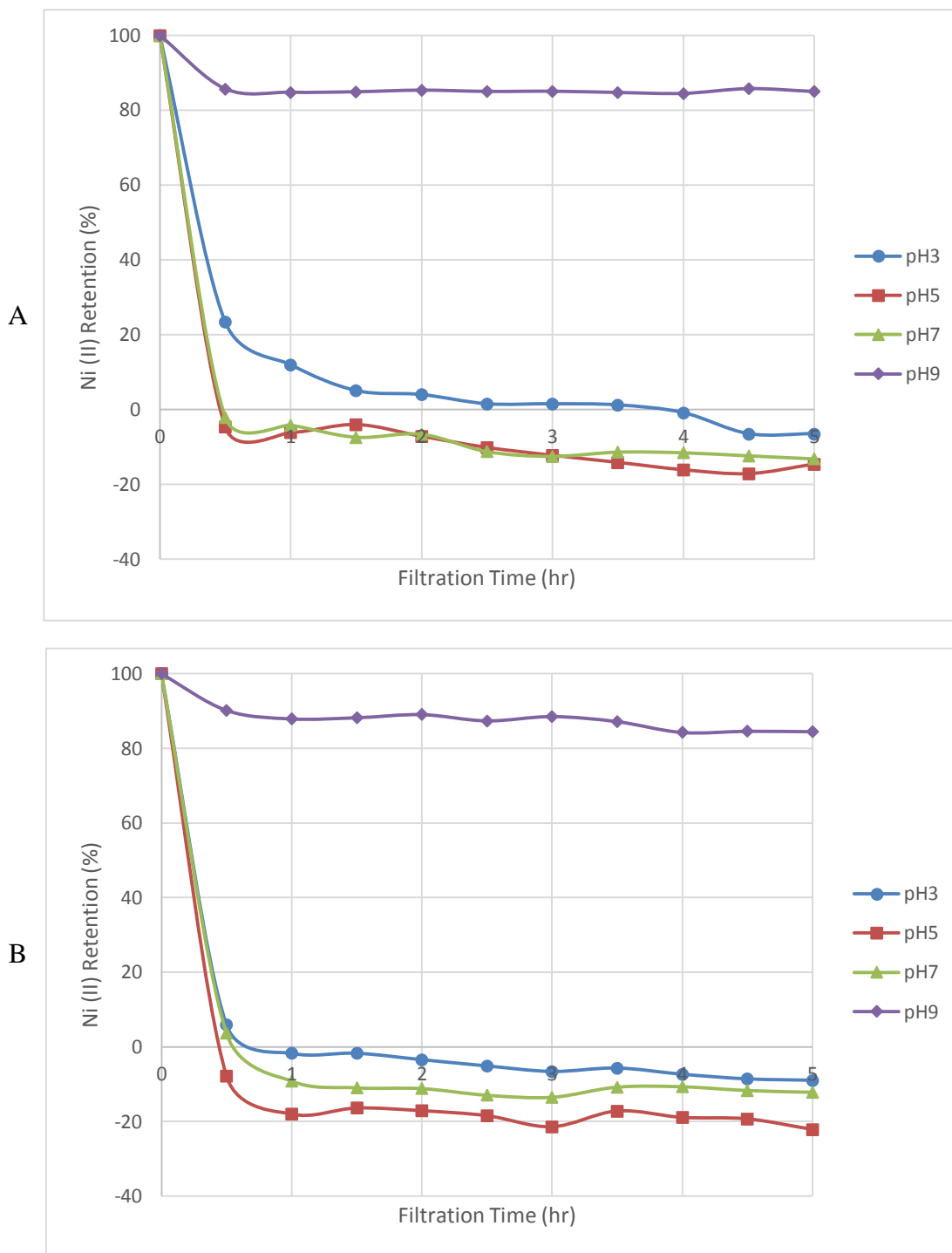


Figure 4.73 Ni (II) retention in aqueous solutions of (A) in P3.NH<sub>2</sub> and (B) in P4.NH<sub>2</sub> solutions as a function of solution pH

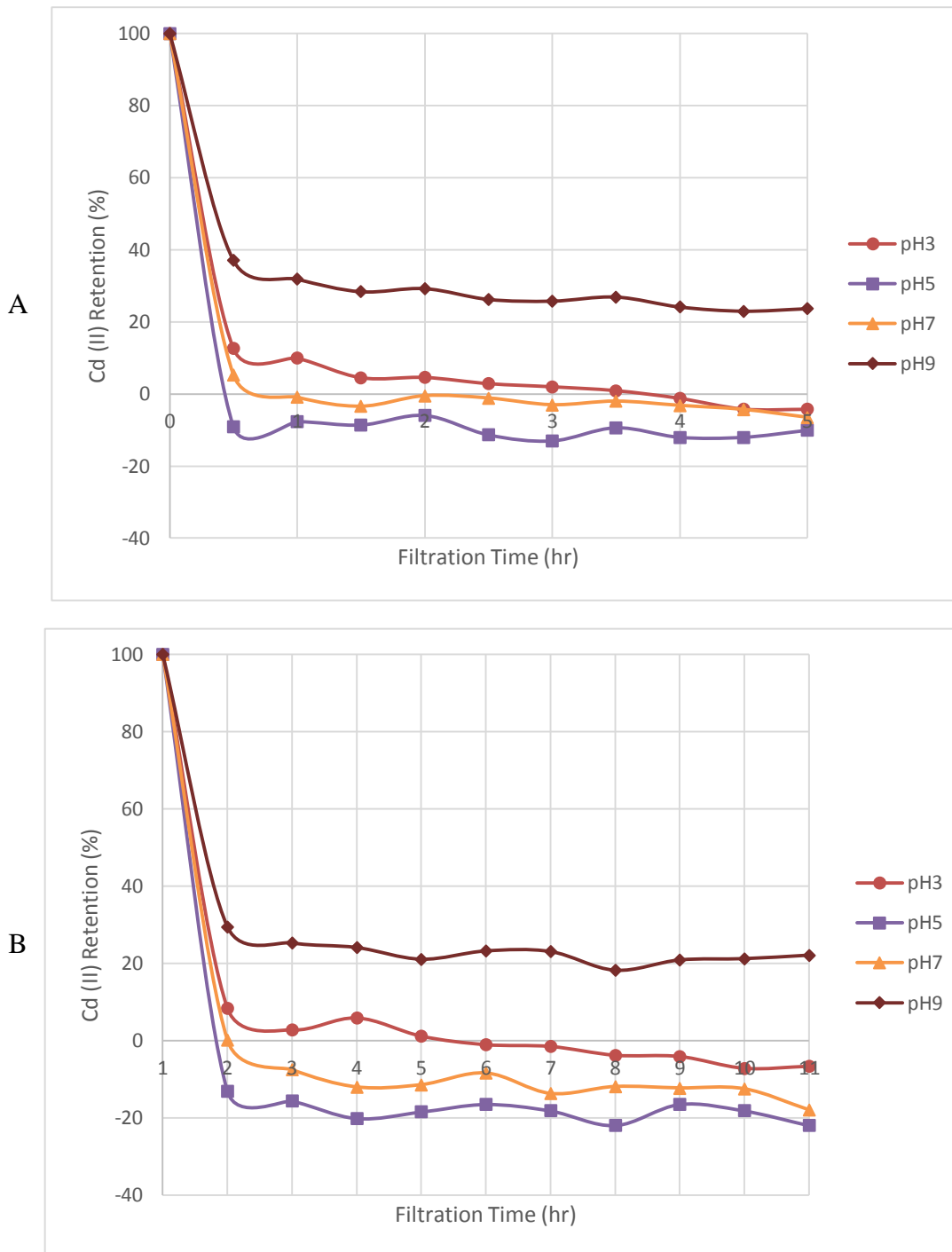


Figure 4.74 Cd (II) retention in aqueous solutions of (A) in P3.NH<sub>2</sub> and (B) in P4.NH<sub>2</sub> solutions as a function of solution pH

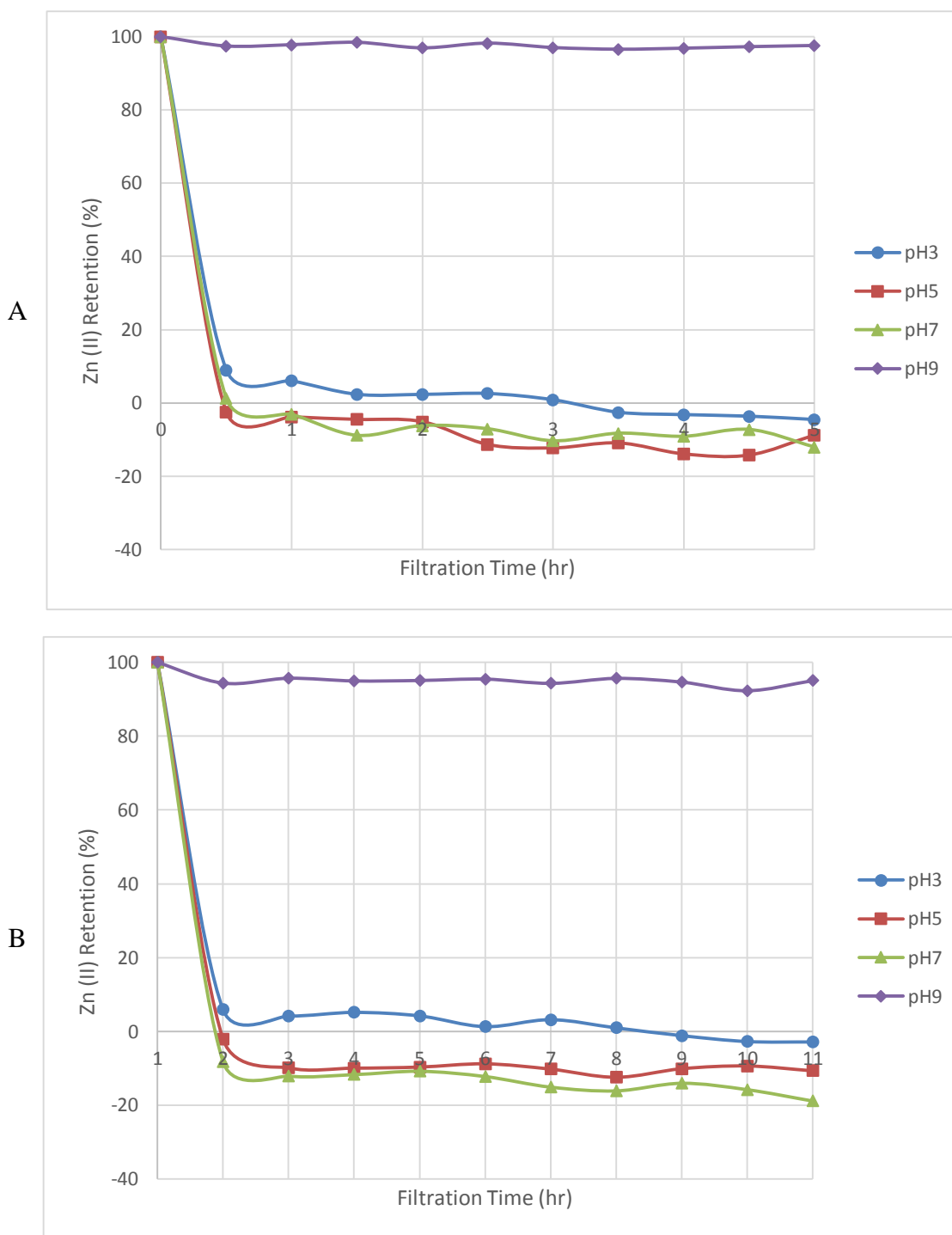


Figure 4.75 Zn (II) retention in aqueous solutions of (A) in P3.NH<sub>2</sub> and (B) in P4.NH<sub>2</sub> solutions as a function of solution pH

P3.NH<sub>2</sub> and P4.NH<sub>2</sub> generations of Jeffamine<sup>®</sup> T-403 cored PAMAMs can be deterministic on selectivity towards metal ions. Thus, selectivity of generations towards metal ions were investigated at four different pH, which are pH 3, 5, 7, and 9. In this way,

low, neutral and high pH values were evaluated for the efficiency of simultaneous removal of metal ions from aqueous solutions by different generations.

At low pH 3, all of the metal ions Cu (II), Co (II), Ni (II), Cd (II), and Zn (II) were released by the P3.NH<sub>2</sub> and P4.NH<sub>2</sub>. This could be observed by the negative retention profiles in Figure 4.76.

At neutral pH 7 and low pH 3, both of the generations were observed as selective towards Cu (II). But, only more than 50 % of Cu (II) retained at neutral pH while this is lowered to 12.32 % for generation P3.NH<sub>2</sub> and 12.12 % for generation P4.NH<sub>2</sub> at pH 5 (Figure 4.76).

At high pH 9, the affinity of P3.NH<sub>2</sub> towards metal ions are in the decreasing order of Zn (II) > Co (II) > Ni (II) > Cu (II) > Cd (II) with more than 74 % except Cd (II) 23.68 %. Similarly, the affinity of P4.NH<sub>2</sub> towards metal ions are in the decreasing order of Zn (II) > Co (II) > Ni (II) ≥ Cu (II) > Cd (II) with more than 84 % except Cd (II) 22.13 % (see Figure 8.). Zn (II) and Co (II) were retained over 90 % by both generations in the presence of other metals. This indicates that P3.NH<sub>2</sub> and P4.NH<sub>2</sub> are highly selective towards Zn (II) and Co (II) at higher pH 9 and almost no generation effect can be observable for Zn (II), Co (II) and Cd (II) (Figure 4.76). On the other hand, Cu (II) retention increases as the generation increases at pH 9.

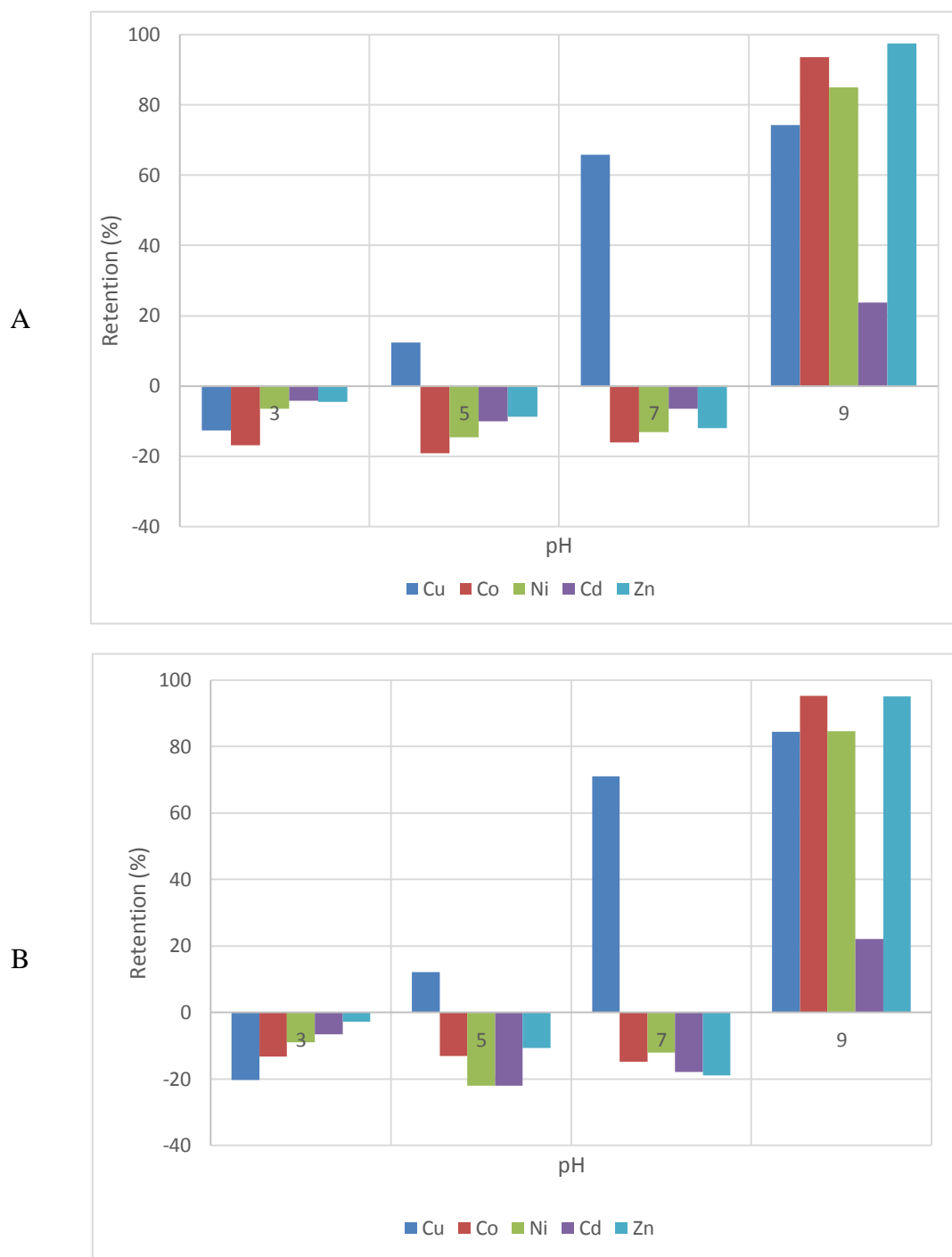


Figure 4.76 Cu (II), Co (II), Ni (II), Cd (II), Zn (II) retention profiles in aqueous solutions of (A) P3.NH<sub>2</sub> and (B) P4.NH<sub>2</sub> as a function of solution pH

#### 4.6.2 Effect of EOP on Metal Binding Abilities of P3.NH<sub>2</sub> and P4.NH<sub>2</sub>

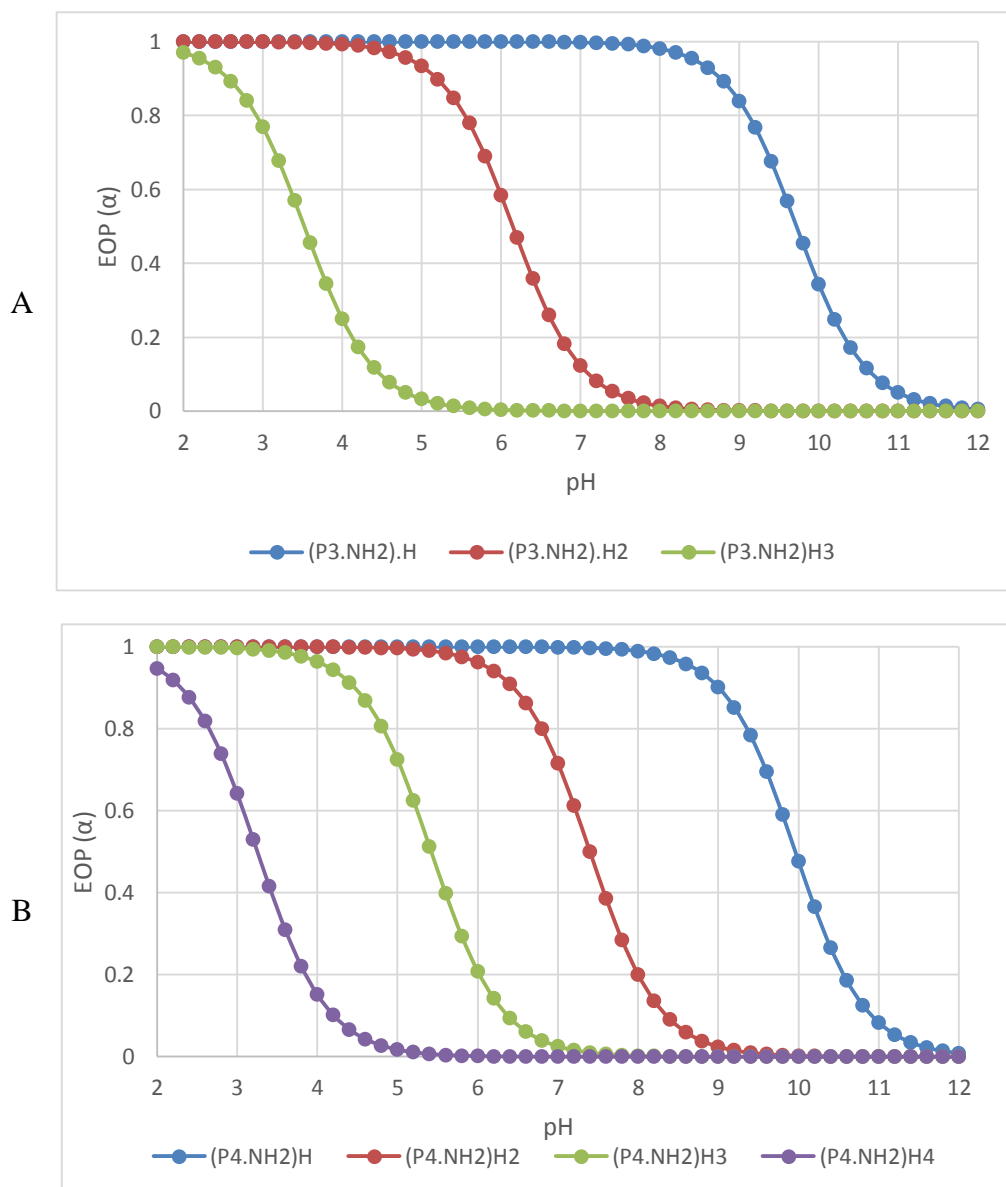


Figure 4.77 Extend of Protonation ( $\alpha$ ) of primary and tertiary amine groups of (A) P3.NH<sub>2</sub> and (B) P4.NH<sub>2</sub> dendrimer

Table 4.28 shows the predicted EOP ( $\alpha$ ) of amino groups of P3.NH<sub>2</sub> and P4.NH<sub>2</sub> as metal binding sites (Figure 4.77). These EOP values were calculated by executing calculated pK<sub>a</sub> values from spectroscopic titration data in Part 4.4.1.4 with Henderson-Hasselbech equation (4.1) [273] (Table 4.28A and 4.28B). EOP predictions indicate that all amine groups of P3.NH<sub>2</sub> and P4.NH<sub>2</sub> dendrimers become almost protonated at low pH ( $\leq 5$ ) while at higher pH 9 only the tertiary amine groups remain deprotonated. That is, almost all primary amine groups are protonated, and (P3.NH<sub>2</sub>)H and (P4.NH<sub>2</sub>)H conformations

become predominant (Table 4.28). These conformations are the most favorable conformations so that metal binding capacities of these generations are higher at that pH (Figure 4.76).

$$\log \frac{\alpha}{1-\alpha} = \text{pKa} - \text{pH} \quad (4.1)$$

where,  $\alpha$  is extend of protonation, pKa is the acidity constants for tertiary and primary amine groups. pH is the measurement of the hydronium ion concentration of the aqueous media.

Table 4.28 Extent of protonation of (A) tertiary amines and (B) primary amines of evaluated P3.NH<sub>2</sub> and P4.NH<sub>2</sub>

**A. Fraction ( $\alpha$ ) of protonated amine groups<sup>a</sup>**

| Dendrimers                          | pKa             | pH 3  | pH 5  | pH 7  | pH 9  |
|-------------------------------------|-----------------|-------|-------|-------|-------|
| (P3.NH <sub>2</sub> )H <sub>2</sub> | 6.1473 ± 0.0079 | 0.999 | 0.933 | 0.123 | 0.000 |
| (P3.NH <sub>2</sub> )H <sub>3</sub> | 3.5221 ± 0.0076 | 0.768 | 0.032 | 0.000 | 0.000 |
| (P4.NH <sub>2</sub> )H <sub>2</sub> | 7.4073 ± 0.0344 | 0.999 | 0.996 | 0.715 | 0.025 |
| (P4.NH <sub>2</sub> )H <sub>3</sub> | 5.4212 ± 0.0173 | 0.996 | 0.725 | 0.025 | 0.000 |
| (P4.NH <sub>2</sub> )H <sub>4</sub> | 3.2532 ± 0.0043 | 0.641 | 0.017 | 0.000 | 0.000 |

**B. Fraction ( $\alpha$ ) of protonated primary amine groups<sup>a</sup>**

| Dendrimers                          | pKa             | pH 3  | pH 5  | pH 7  | pH 9  |
|-------------------------------------|-----------------|-------|-------|-------|-------|
| (P3.NH <sub>2</sub> )H <sup>b</sup> | 9.7286 ± 0.0347 | 0.999 | 0.999 | 0.999 | 0.839 |
| (P4.NH <sub>2</sub> )H <sup>c</sup> | 9.9682 ± 0.0113 | 0.999 | 0.999 | 0.998 | 0.901 |

<sup>a</sup>Data obtained from the EOP graphs of P3.NH<sub>2</sub> and P4.NH<sub>2</sub> (Figure 4.77)

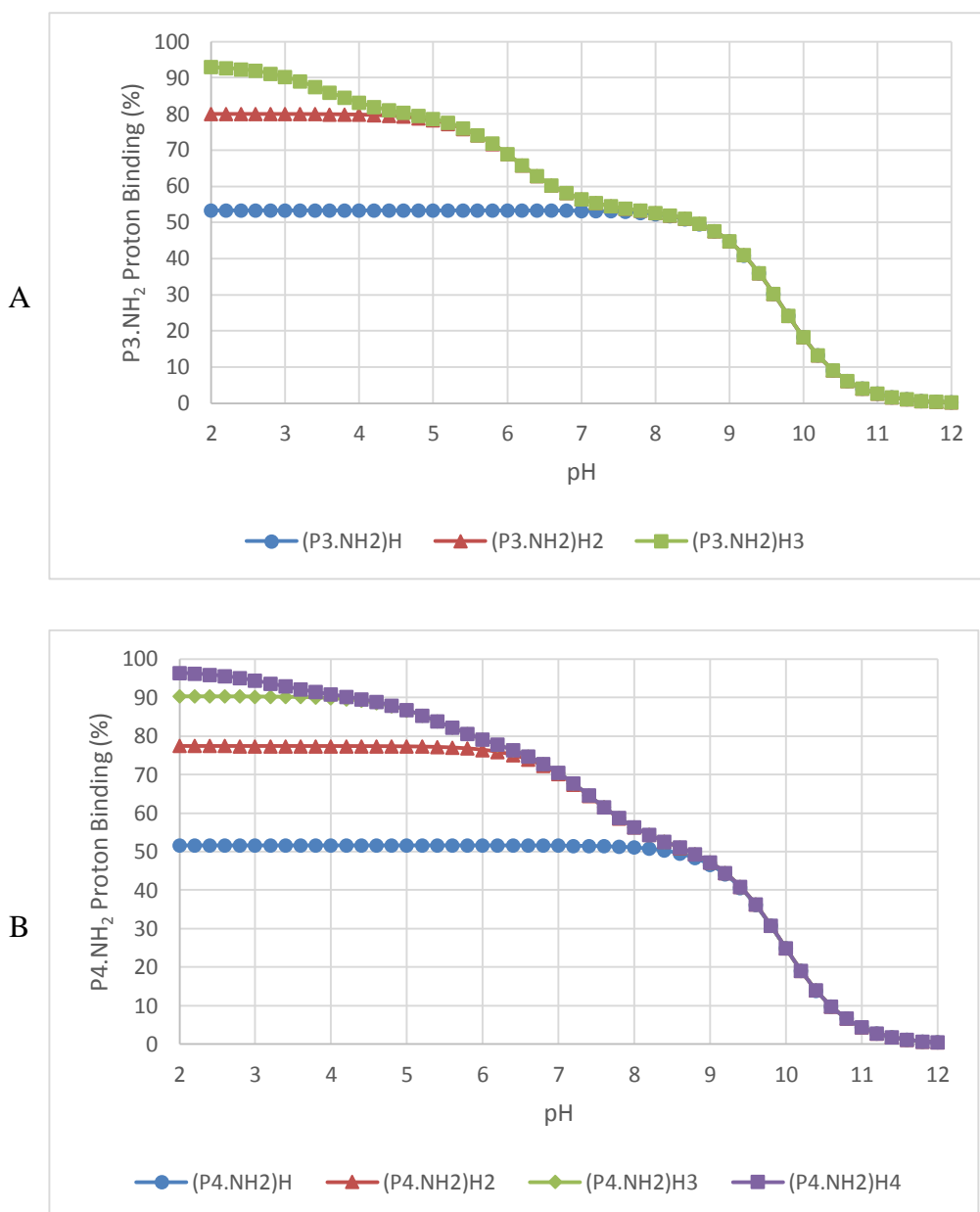


Figure 4.78 % proton binding curve for (A) P3.NH<sub>2</sub> and (B) P4.NH<sub>2</sub>.

Structures of dendrimer can be controllable and mass of dendrimers increases as the generation increases. Selected properties of P3.NH<sub>2</sub> and P4.NH<sub>2</sub> can be seen in Table 4.29 Figure 4.78 shows P3.NH<sub>2</sub> and P4.NH<sub>2</sub> proton binding percent values in different pH values. These values were driven from EOP values present in Figure 4.77. In Figure 4.78, it could be easily seen that all tertiary amines are almost deprotonated at pH 9 while almost all primary amine groups are protonated at pH 9 and P3.NH<sub>2</sub> and P4.NH<sub>2</sub> are in the species form of (P3.NH<sub>2</sub>)H and (P4.NH<sub>2</sub>)H. These species are the most favorable conformations that P3.NH<sub>2</sub> and P4.NH<sub>2</sub> could behave like hosts to many metal ions with

the deprotonated inner tertiary amine groups. Figure 4.78 shows the proton binding ability of P3.NH<sub>2</sub> and P4.NH<sub>2</sub> in the pH range of 2-12. According to these profiles, all amine groups of P3.NH<sub>2</sub> and P4.NH<sub>2</sub> become almost protonated at low pH 2 with 92.94 %, 96.24 % for P3.NH<sub>2</sub> and P4.NH<sub>2</sub>, respectively. During derivation of these values, it was benefited from core shell protonation methodology [65, 266, 267] of PAMAMs. This methodology asserts that dendrimers starts to protonate at higher pH and continue to protonate as the pH decreases. During this protonation, amino groups present in each core protonates together (Table 4.29 and Figure 4.78).

Table 4.29 Selected properties of Jeffamine<sup>®</sup> T403 cored PAMAMs

| Generation         | MW (g/mol) | Tertiary Amine number | Primary Amine Number |
|--------------------|------------|-----------------------|----------------------|
| P1.NH <sub>2</sub> | 1,125      | 3                     | 6                    |
| P2.NH <sub>2</sub> | 2,495      | 9                     | 12                   |
| P3.NH <sub>2</sub> | 5,235      | 21                    | 24                   |
| P4.NH <sub>2</sub> | 10,717     | 45                    | 48                   |

#### 4.6.3 Effect of Initial Free Metal Ion Concentration on Dendrimer Metal Complexation

Table 4.30 shows the solubility products of some metal hydroxides. P3.NH<sub>2</sub> and P4.NH<sub>2</sub> complexation studies with the mixture of metal solutions were evaluated to assess their metal ions removal from aqueous solutions. In this point, free metal ion concentration [M<sup>2+</sup>] has a critical importance. If the solubility of metal is not proper for complexation at the studied pH. Then, sudden metal hydroxide formation is expected. Thus, it could not be mentioned about a successful dendrimer-multi metal complexation process. In complexation studies, it was not observed any precipitations of metal hydroxides between the pH ranges of 3-9. Precipitation was observed above the pH 9.20. For this reason, Batch complexation experiments were conducted between the pH ranges of pH 3-9 as aligned with the literature [56]. Thus, higher percent rejection (%R) values were observed at pH 9. This can be attributed to low extend of protonation of behavior of amine groups (4.77). The relation between the pH and free metal concentration on the precipitation of metal hydroxides can be seen from Figure 4.79.

Table 4.30 Solubility Products of metal hydroxides at 25 °C [274]

| Compound            | K <sub>sp</sub> (Solubility Products) |
|---------------------|---------------------------------------|
| Cd(OH) <sub>2</sub> | 4.5 x 10 <sup>-15</sup>               |
| Co(OH) <sub>2</sub> | 1.3 x 10 <sup>-15</sup>               |
| Cu(OH) <sub>2</sub> | 4.8 x 10 <sup>-20</sup>               |
| Ni(OH) <sub>2</sub> | 6.0 x 10 <sup>-16</sup>               |
| Zn(OH) <sub>2</sub> | 3.0 x 10 <sup>-16</sup>               |

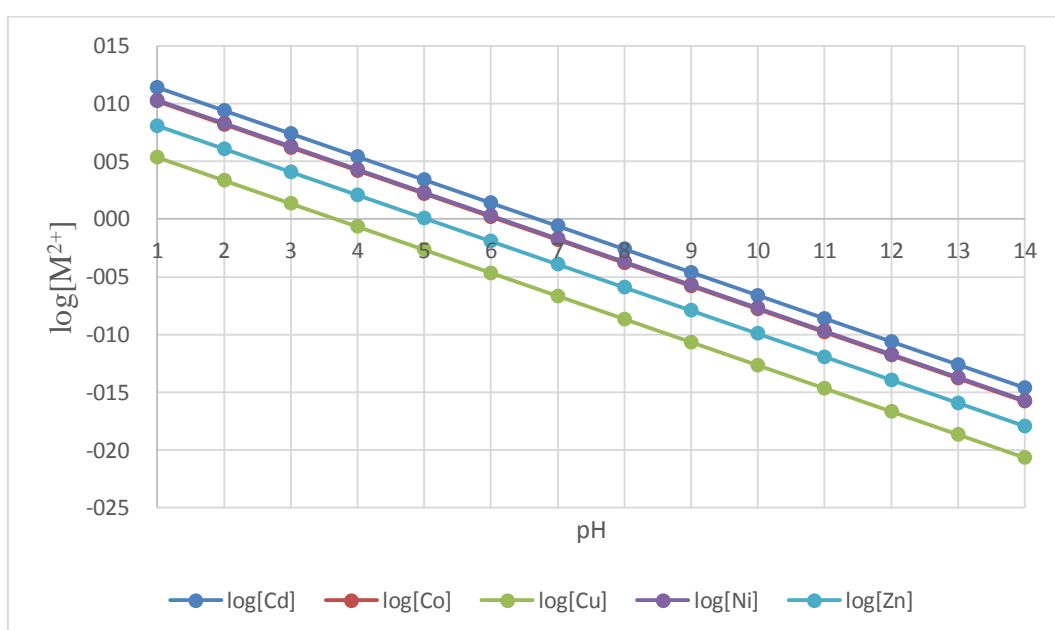


Figure 4.79 Precipitation diagram of metal hydroxides at 25 °C. Initial free metal ion concentration [M<sup>2+</sup>] in batch complexation study plays an important factor to prevent metal hydroxide formation

## 4.7 Synthesis and Characterization of Cu-Dendrimer Encapsulated Nanoparticles

### 4.7.1 Spectroscopic Titrations of Tris and Carboxyl Terminated Dendrimers

Crooks et al. [131, 254] have shown that Cu<sup>2+</sup> ions coordinate with the maximum number of four tertiary amine numbers. Addition of Cu<sup>2+</sup> ions to Tris terminated E4.TRIS, D4.TRIS, P4.TRIS, and carboxyl terminated E4.COOH, D4.COOH and P4.COOH in aqueous solutions immediately resulted in a deep blue color change. This color change

due to intradendrimer metal dendrimer complexes was characterized with UV-VIS spectroscopy with a broad absorption band at  $\lambda_{\text{max}} = 680 \text{ nm}$  for EDA, DETA and Jeffamine<sup>®</sup> T-403 cored and tris (Figure 4.80-4.82) and carboxyl terminated (Figure 4.83-4.85) PAMAMs. This band belonging the copper *d-d* transition indicates the complex formation between the two species at 1:4 dendrimer to tertiary amine ratio [138]. The maximum number of internal tertiary amine numbers of dendrimers evaluated in this study were shown in Table 4.15 in part 4.3.4.

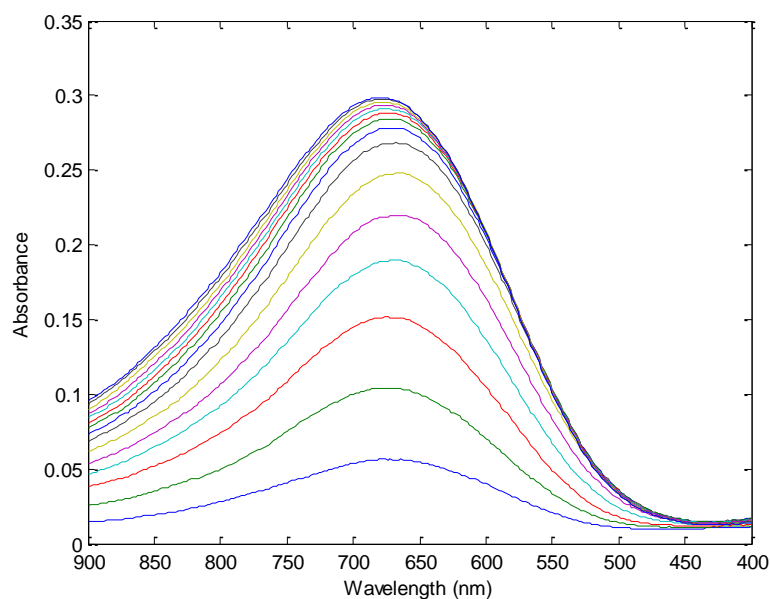


Figure 4.80 Absorption spectra of E4.TRIS dendrimer (0.228 mM) solution titrated with  $\text{Cu}^{2+}$  (81.54 mM) at 680 nm

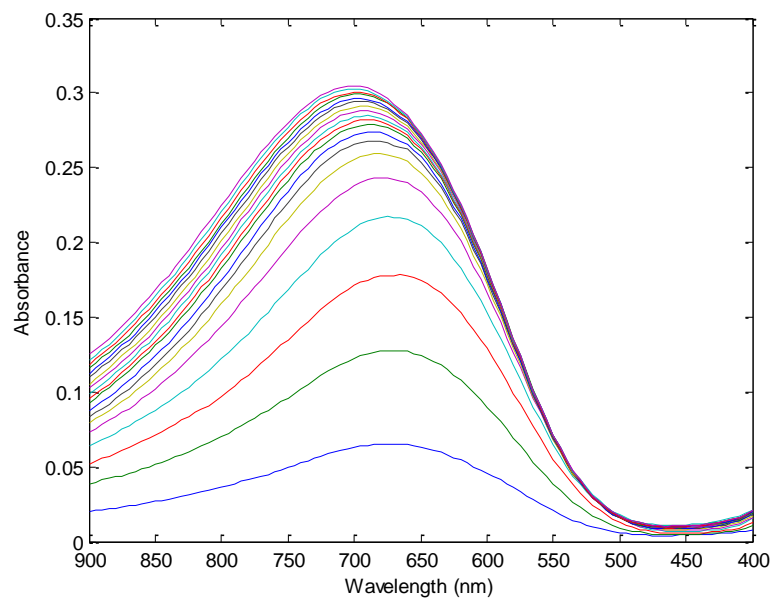


Figure 4.81 Absorption spectra of D4.TRIS dendrimer (0.202 mM) solution titrated with Cu<sup>2+</sup> (80.14 mM) at 680 nm

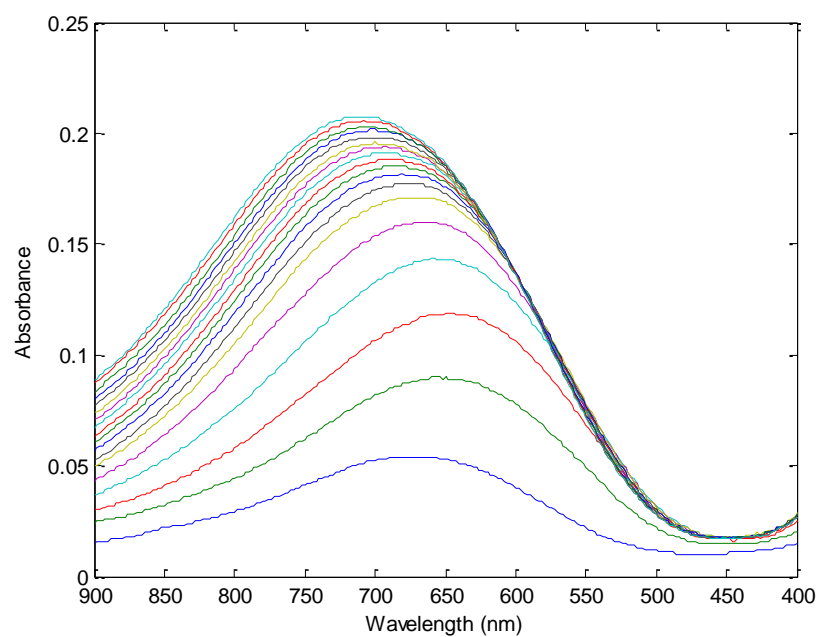


Figure 4.82 Absorption spectra of P4.TRIS dendrimer (0.148 mM) solution titrated with Cu<sup>2+</sup> (81.54 mM) at 680 nm

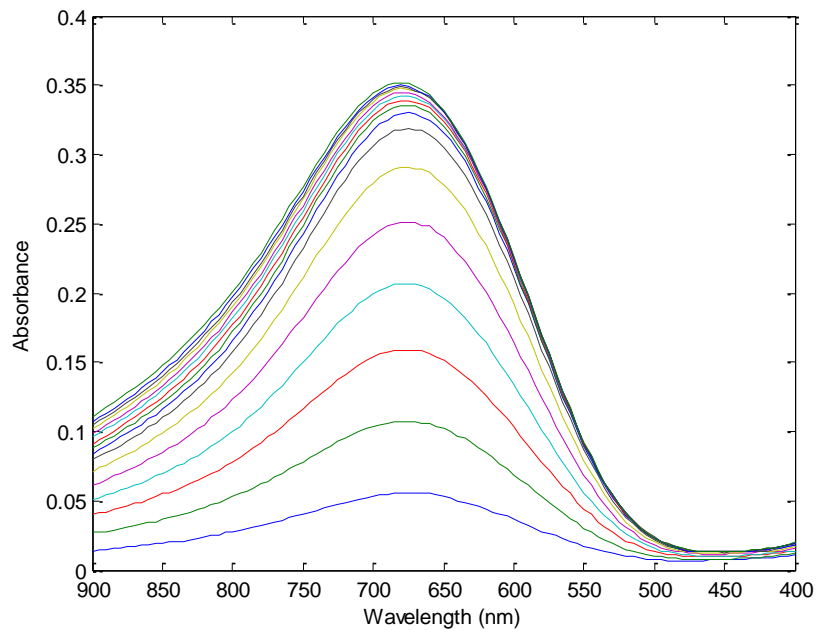


Figure 4.83 Absorption spectra of E4.COOH dendrimer (0.321 mM) solution titrated with  $\text{Cu}^{2+}$  (80.14 mM) at 680 nm

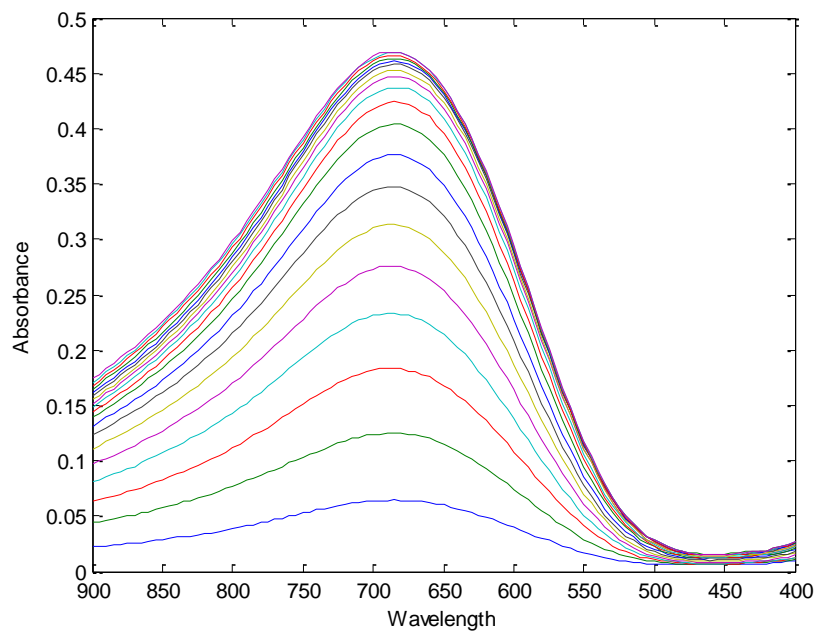


Figure 4.84 Absorption spectra of D4.COOH dendrimer (0.268 mM) solution titrated with  $\text{Cu}^{2+}$  (80.50 mM) at 680 nm

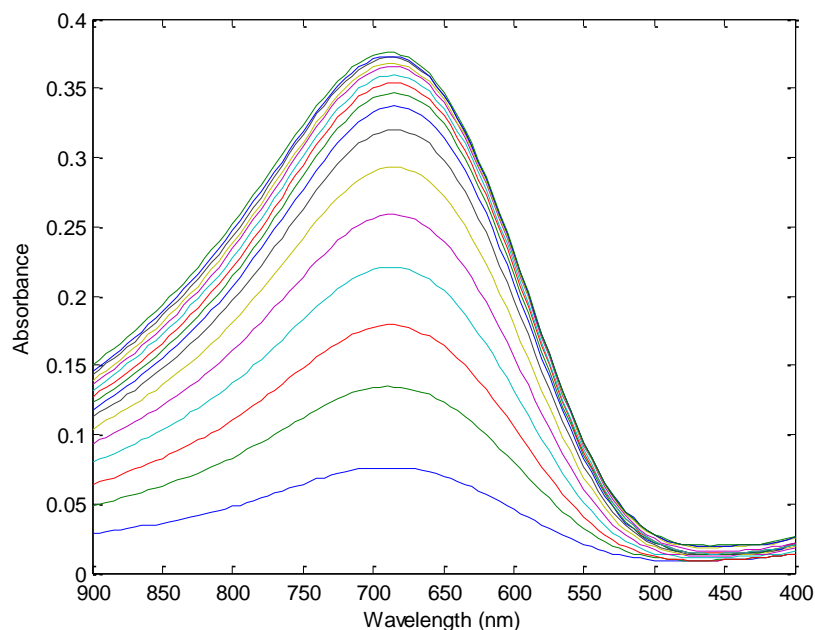


Figure 4.85 Absorption spectra of P4.COOH dendrimer (0.200 mM) solution titrated with  $\text{Cu}^{2+}$  (79.86 mM) at 680 nm

In order to learn about  $\text{Cu}^{2+}$  binding capacity of different generation tris and carboxyl terminated EDA, DETA and Jeffamine<sup>®</sup> T-403 cored PAMAMs, spectroscopic titration studies were performed. Sample spectroscopic titration spectra of tris terminated E4.TRIS, D4.TRIS, P4.TRIS can be seen from Figure 4.80, 4.81, and 4.82 while carboxyl terminated E4.COOH, D4.COOH, P4.COOH can be seen from Figure 4.83, 4.84 and Figure 4.85, respectively.

Absorbance at  $\lambda_{\text{max}}=680$  nm versus  $\text{Cu}^{2+}$ /DENs molar ratio plots were used to determine experimental end points at where dendrimer could bind maximum number of  $\text{Cu}^{2+}$  ions. That is, maximum molar excess of  $\text{Cu}^{2+}$  that can be loaded to dendrimer was calculated from these plots (Figure 4.86-4.97). The maximum molar excess of  $\text{Cu}^{2+}$  ions tris and carboxyl terminated PAMAMs can bind were shown on spectroscopic titration curves (Figure 4.86-4.97) and also summarized in Table 4.31. Results revealed that the number of tertiary amine numbers observed from spectroscopic titration data were correlated with the calculated ones (Table 4.32). That is, Tris and carboxyl ended dendrimers evaluated in this study absorb the number of  $\text{Cu}^{2+}$  ions equivalent the number of tertiary amine numbers. This correlation also indicates the structure of PAMAMs are almost monodisperse and at desired monodispersity. Thus, it could be concluded that each  $\text{Cu}^{2+}$  ion is coordinated by four tertiary amine groups.

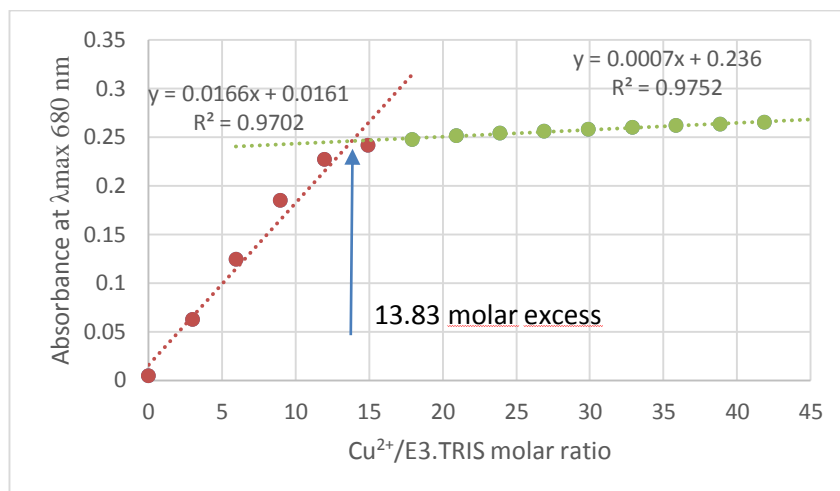


Figure 4.86 Spectroscopic titration curve of the E3.TRIS dendrimer with  $\text{Cu}^{2+}$  ions

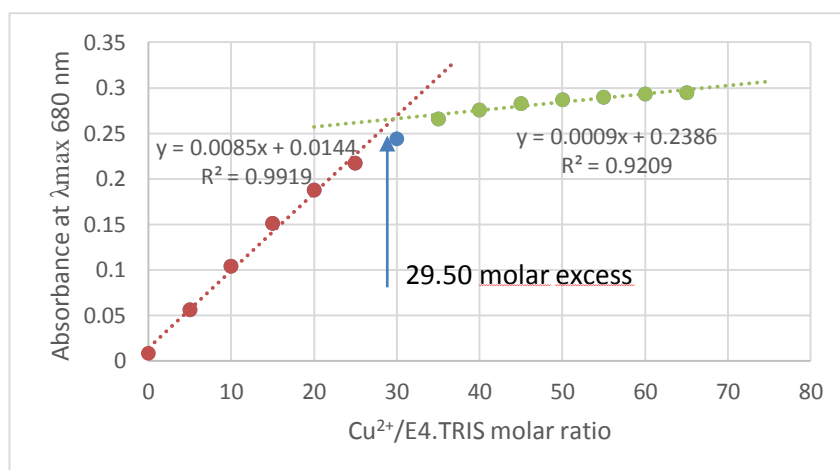


Figure 4.87 Spectroscopic titration curve of the E4.TRIS dendrimer with  $\text{Cu}^{2+}$  ions

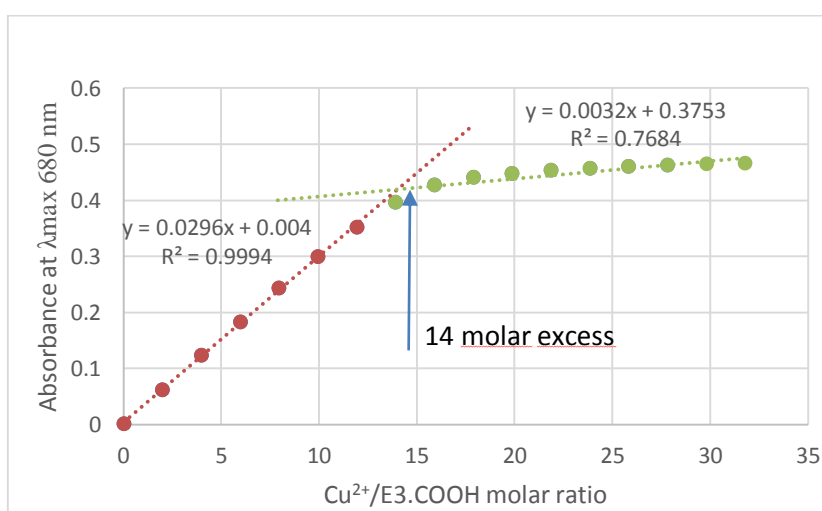


Figure 4.88 Spectroscopic titration curve of the E3.COOH dendrimer with  $\text{Cu}^{2+}$  ions

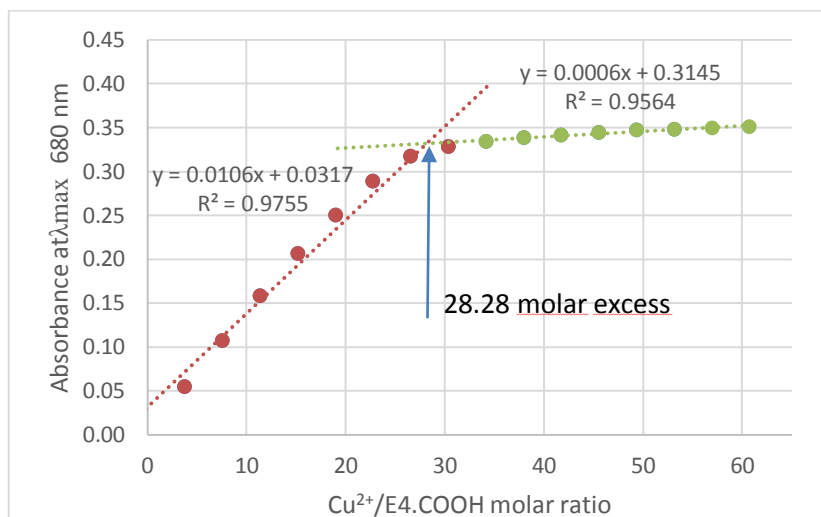


Figure 4.89 Spectroscopic titration curve of the E4.COOH dendrimer with  $\text{Cu}^{2+}$  ions

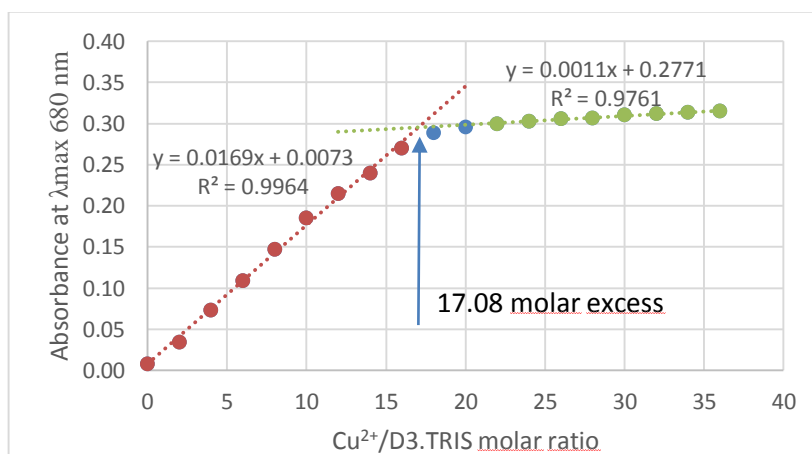


Figure 4.90 Spectroscopic titration curve of the D3.TRIS dendrimer with  $\text{Cu}^{2+}$  ions

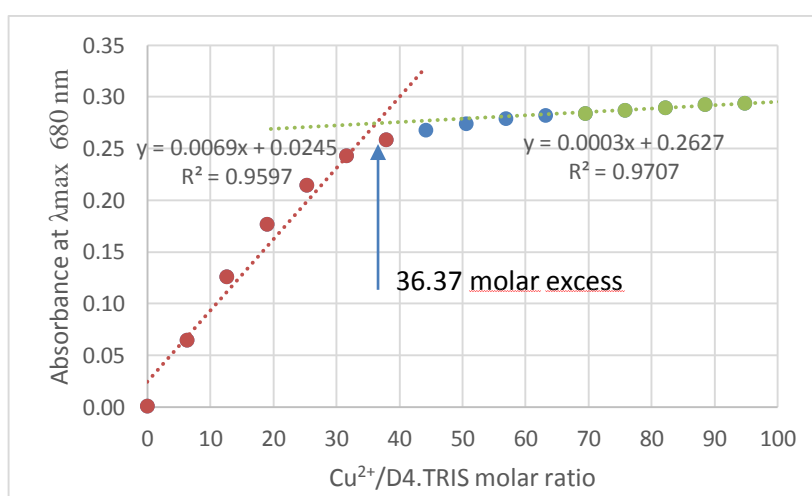


Figure 4.91 Spectroscopic titration curve of the D4.TRIS dendrimer with  $\text{Cu}^{2+}$  ions

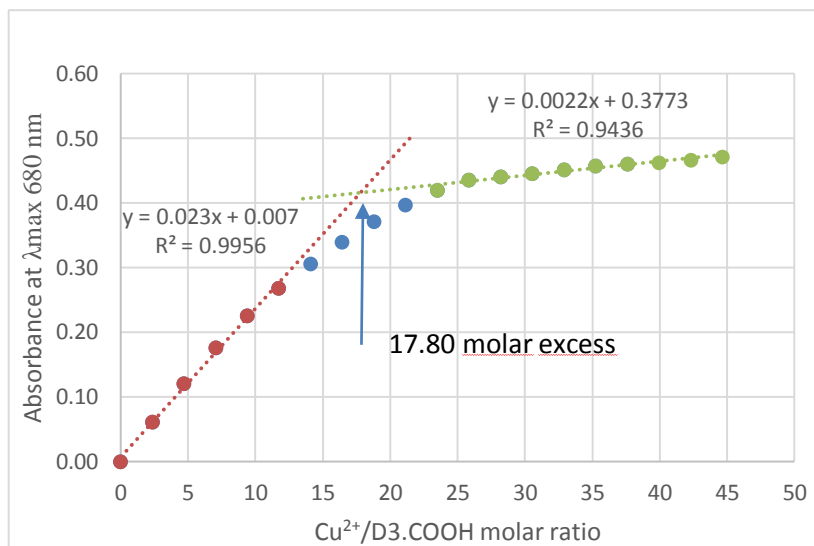


Figure 4.92 Spectroscopic titration curve of the D3.COOH dendrimer with  $\text{Cu}^{2+}$  ions

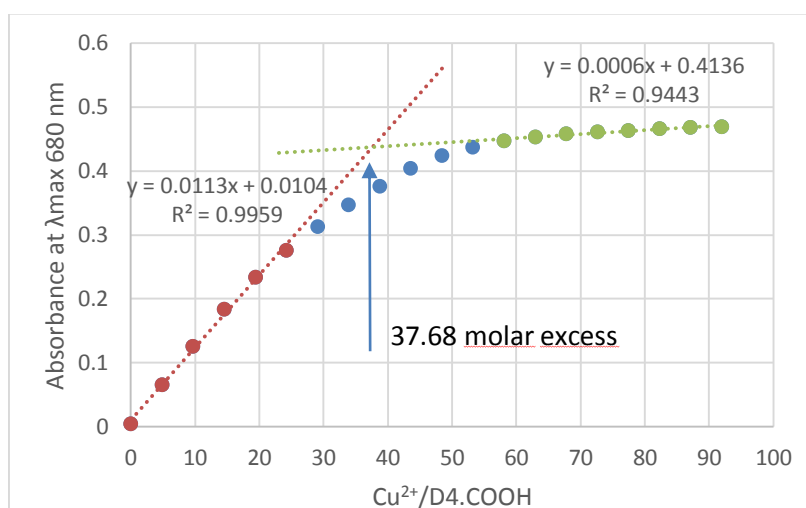


Figure 4.93 Spectroscopic titration curve of the D4.COOH dendrimer with  $\text{Cu}^{2+}$  ions

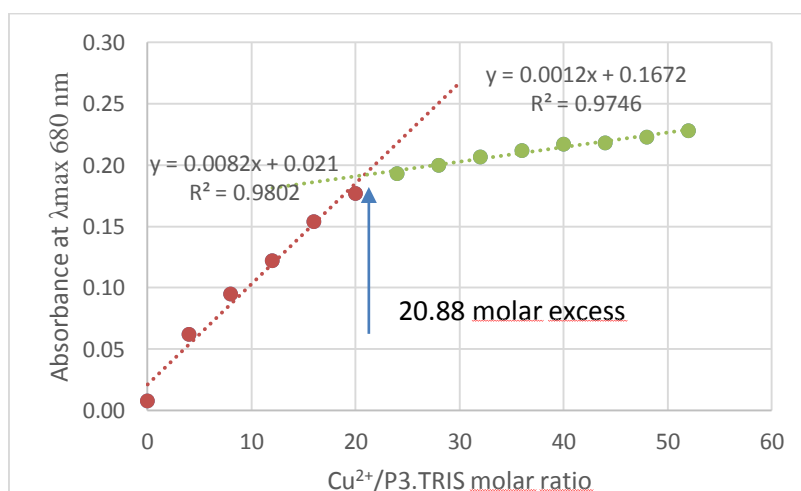


Figure 4.94 Spectroscopic titration curve of the P3.TRIS dendrimer with  $\text{Cu}^{2+}$  ions

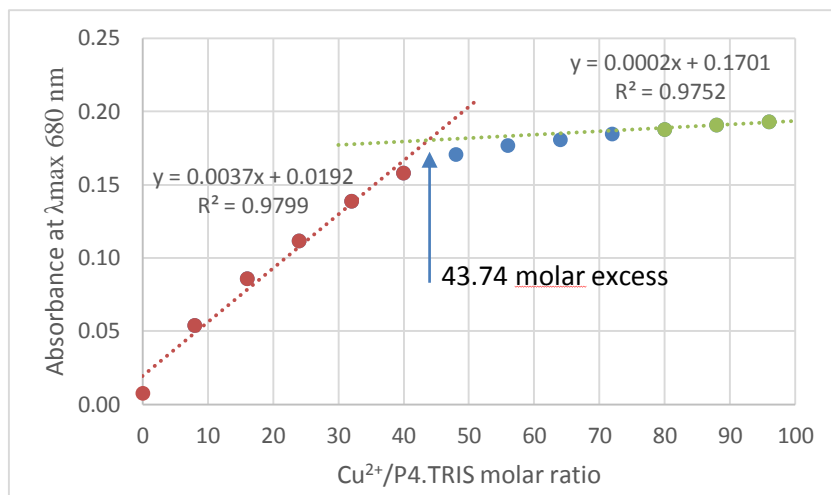


Figure 4.95 Spectroscopic titration curve of the P4.TRIS dendrimer with  $\text{Cu}^{2+}$  ions

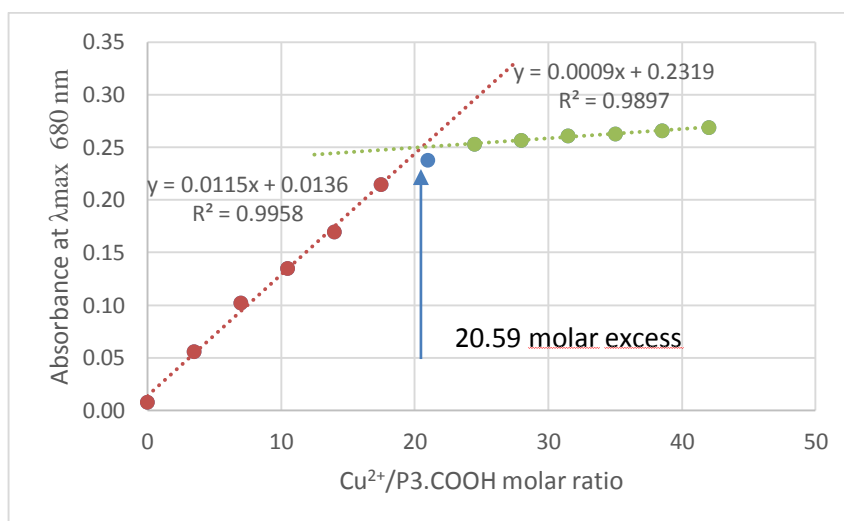


Figure 4.96 Spectroscopic titration curve of the P3.COOH dendrimer with  $\text{Cu}^{2+}$  ions

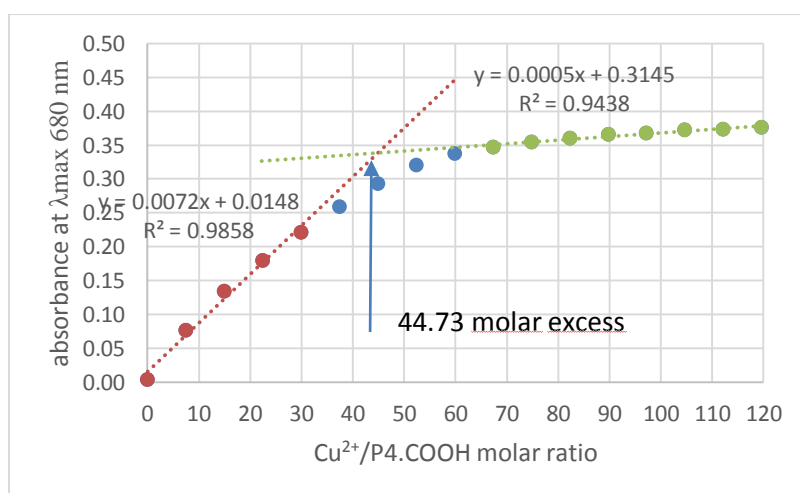


Figure 4.97 Spectroscopic titration curve of the P4.COOH dendrimer with  $\text{Cu}^{2+}$  ions

Table 4.31 Number of amine groups on TRIS terminated DENs available for binding with Cu<sup>2+</sup> ions

| Dendrimer | Calculated end point | Experimentally obtained end point <sup>a</sup> |
|-----------|----------------------|--|
| E3.TRIS   | 14                   | 13.83  |
| E4.TRIS   | 30                   | 29.50  |
| D3.TRIS   | 18                   | 17.08  |
| D4.TRIS   | 38                   | 36.37  |
| P3.TRIS   | 21                   | 20.88  |
| P4.TRIS   | 45                   | 43.74  |
| E3.COOH   | 14                   | 14.00  |
| E4.COOH   | 30                   | 28.28  |
| D3.COOH   | 18                   | 17.80  |
| D4.COOH   | 38                   | 37.68  |
| P3.COOH   | 21                   | 20.59  |
| P4.COOH   | 45                   | 44.73  |

<sup>a</sup>Each end point has been calculated as an average value of three experimental runs

#### 4.7.2 Synthesis and UV-VIS Characterization of Cu-DENs

From binding studies in part 4.7.1, the number of Cu<sup>2+</sup> that can be loaded to tris and carboxyl ended EDA, DETA and Jeffamine<sup>®</sup> T-403 cored PAMAMs were determined. Similar synthetic procedures were applied for all of the evaluated dendrimers. Generally, 10 mL of 5μM aqueous dendrimer solutions were prepared. This concentration kept constant for all dendrimer solutions. The pH of the aqueous dendrimer solution was adjusted to pH~8. Correct amount of aqueous CuSO<sub>4</sub> (pH~4.62) (Table 4.31) was added to each dendrimer solution. The final pH of the solution was about pH ~5. The solution than stirred for 30 minutes to allow complexation of Cu<sup>2+</sup> ions with the inner tertiary amines of dendrimers. Chemical reduction of Tris and carboxyl terminated, Cu<sup>2+</sup> loaded Cu<sup>2+</sup>/dendrimers with 20 molar excess NaBH<sub>4</sub> in 0.1 M NaOH was resulted in

intradendrimer Cu-Dens. A straightforward evidence of this comes from the change in solution color from blue to golden brown immediately as aligned with the literature [131, 254] (Figure 4.98). Then pH was adjusted to pH ~8 at where dendrimer solutions are most stable with a negligible amount of dropwise addition of 0.01-0.1 HCl and NaOH solutions. The formation of Cu-DENs were also monitored with UV-VIS spectroscopy. Upon the addition of the appropriate molar ratio of calculated  $\text{CuSO}_4$  solutions to aqueous dendrimer solutions, a strong band at around 270-280 nm for carboxyl and 280-300 nm for Tris terminated PAMAMs were occurred, respectively. These bands are assigned to LMCT bands [275-277]. In addition, *d-d* copper transition band at around 680 nm for all  $\text{Cu}^{2+}$ /DEN complex solutions were observed (Figure 4.99-4.104.). This band could not be observable for low concentrations. After the addition of excess reducing agent  $\text{NaBH}_4$ , LMCT peak at around 300 nm and *d-d* transition band at 680 nm in all  $\text{Cu}^{2+}$ /DENs were disappeared immediately and replaced with a nearly exponentially monotonically increasing spectrum towards to shorter wavelengths (Figure 4.99-4.104). Moreover, the size of Cu clusters can be understood from the absence of a Mie plasman peak at around 570 nm in UV-VIS spectra (Figure 4.99 to Figure 4.104). The absence of this band indicates that Cu clusters are smaller than 5nm. [131] Results of UV characterizations are in good agreement with the previously reported Cu-DENs [131, 254].

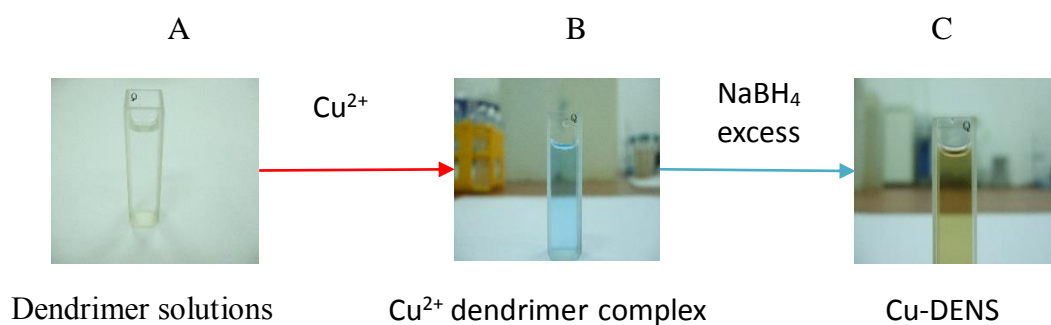


Figure 4.98 Change in color during the synthesis of Cu-DENs (A) aqueous dendrimer solutions (B)  $\text{Cu}^{2+}$  dendrimer complex solution (C) Cu-DENs solution

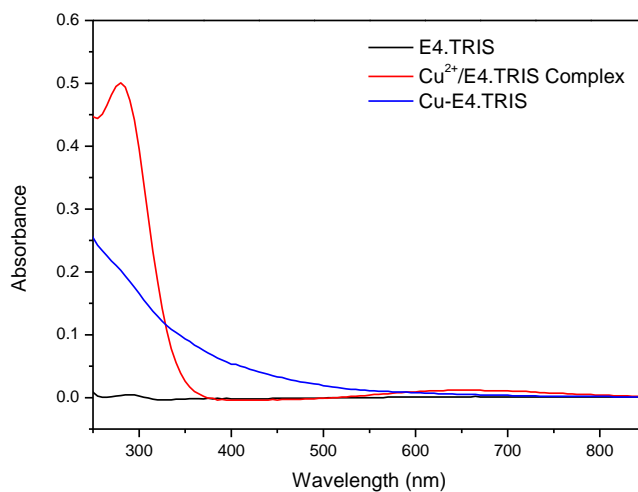


Figure 4.99 UV-VIS absorption spectra of the formation of Cu-E4.TRIS

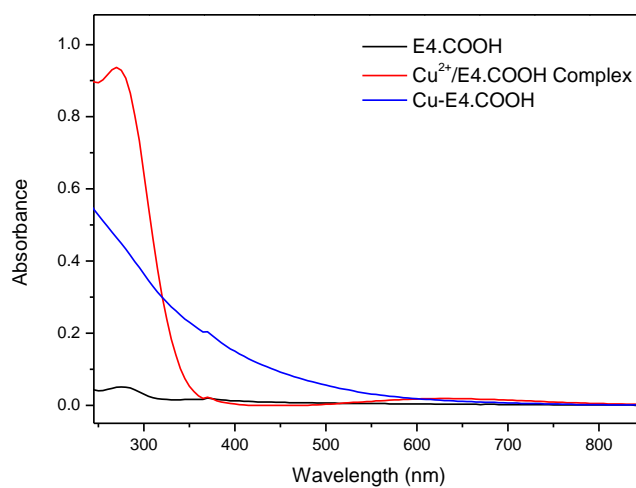


Figure 4.100 UV-VIS absorption spectra of the formation of Cu-E4.COOH

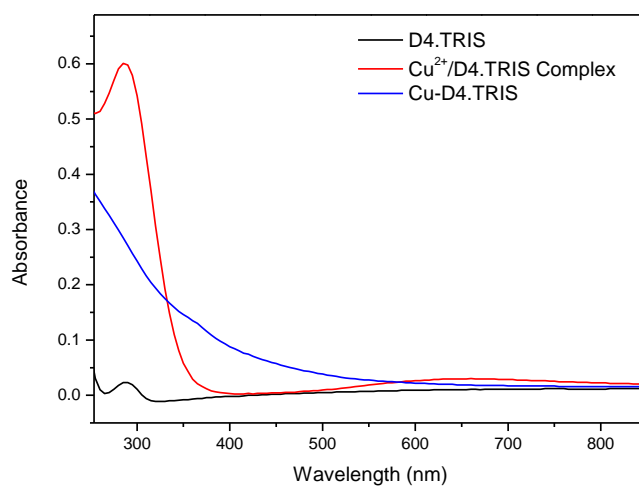


Figure 4.101 UV-VIS absorption spectra of the formation of Cu-D4.TRIS

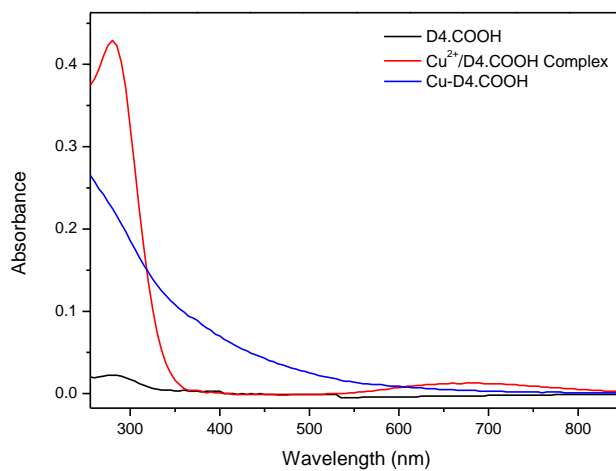


Figure 4.102 UV-VIS absorption spectra of the formation of Cu-D4.COOH

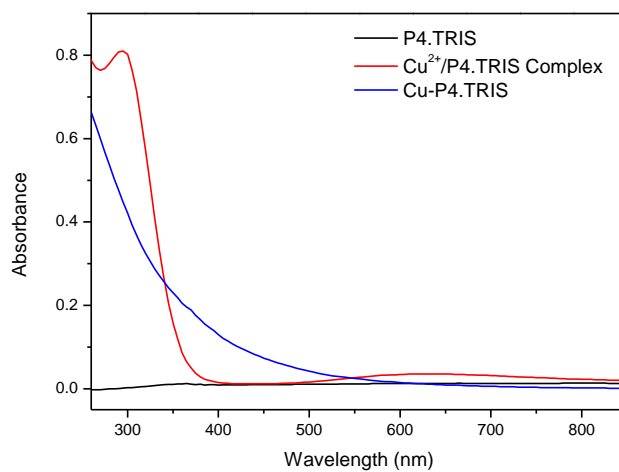


Figure 4.103 UV-VIS absorption spectra of the formation of Cu-P4.TRIS

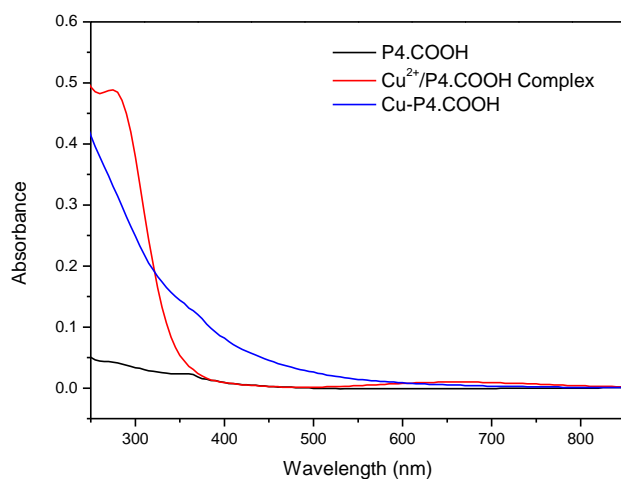


Figure 4.104 UV-VIS absorption spectra of the formation of Cu-P4.COOH

## 4.8 P4.NH<sub>2</sub> as Solubility Enhancer of Carvedilol

### 4.8.1 Effect of PAMAM Concentration on Solubility of Carvedilol

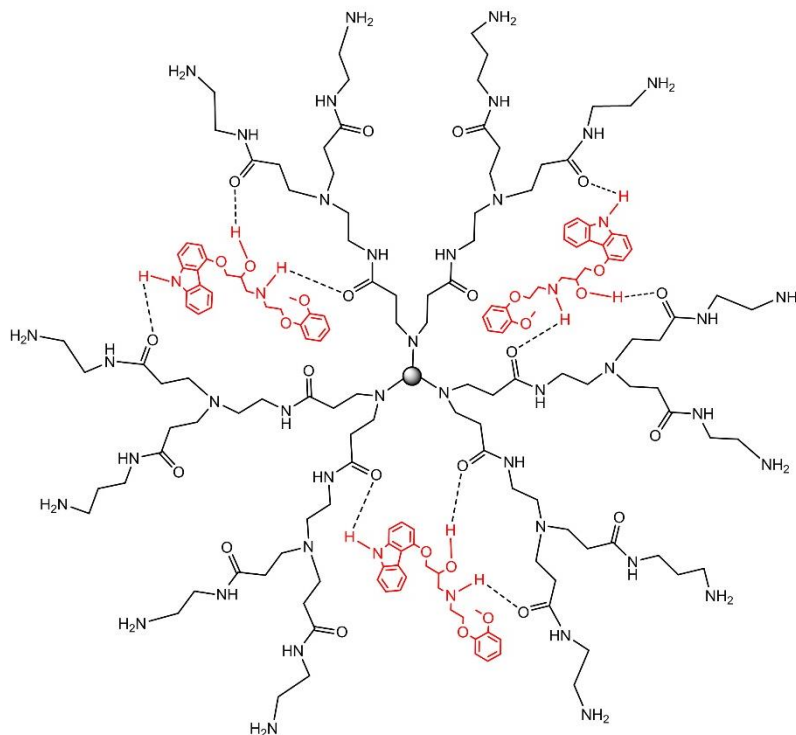


Figure 4.105 Representative illustration of the CAR-dendrimer inclusion complex

As it can be seen in Figure 4.106, the solubility of CAR increases as the dendrimer concentration increases with a good linearity,  $R^2 = 0.9937$ . From the aspect of host-guest molecule interactions, inner cavities of PAMAMs can be host for the guest molecules like drug active ingredient CAR (Figure 4.105).

When the dendrimer drug complexation occurs via covalent binding, it is expected to be observed a new complexation band in the UV-VIS spectrum resulting from the electronic transitions between the dendrimer and drug. However, it can be clearly seen in Figure 4.107 that no such kind of a complexation peak exists. In Figure 4.107, UV spectrum revealed that a hypsochromic increase occurred as aligned with the increasing dendrimer concentration. This could be driven from the hydrogen bond formation between the inner cavity of P4.NH<sub>2</sub> and CAR, and indicates the inclusion complex formation by encapsulation of CAR inside the dendrimer. In this case, it could be concluded that the solubility of CAR increases as the dendrimer concentration increases depending on the

dendrimer drug inclusion complex formation. This formation could be supported by the phase solubility diagram in Figure 4.106 and seen from the increase of absorbance of CAR in Figure 4.107A and 4.107B.

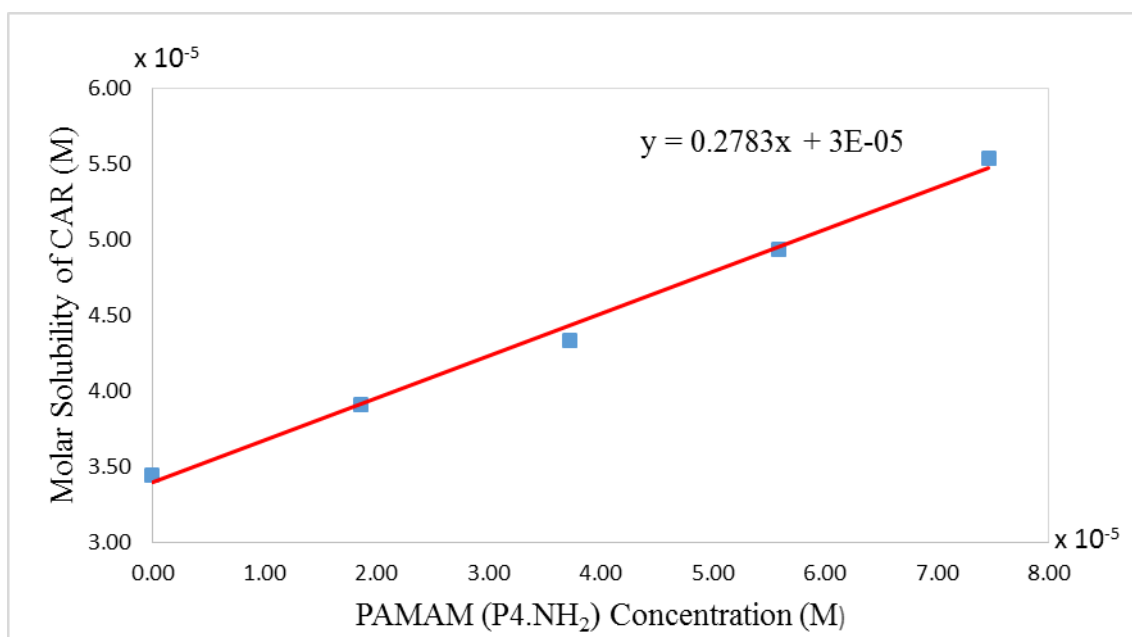


Figure 4.106 Phase solubility diagram of P4.NH<sub>2</sub>. Change in molar solubility of CAR as a function of increasing PAMAM (P4.NH<sub>2</sub>) dendrimer concentration

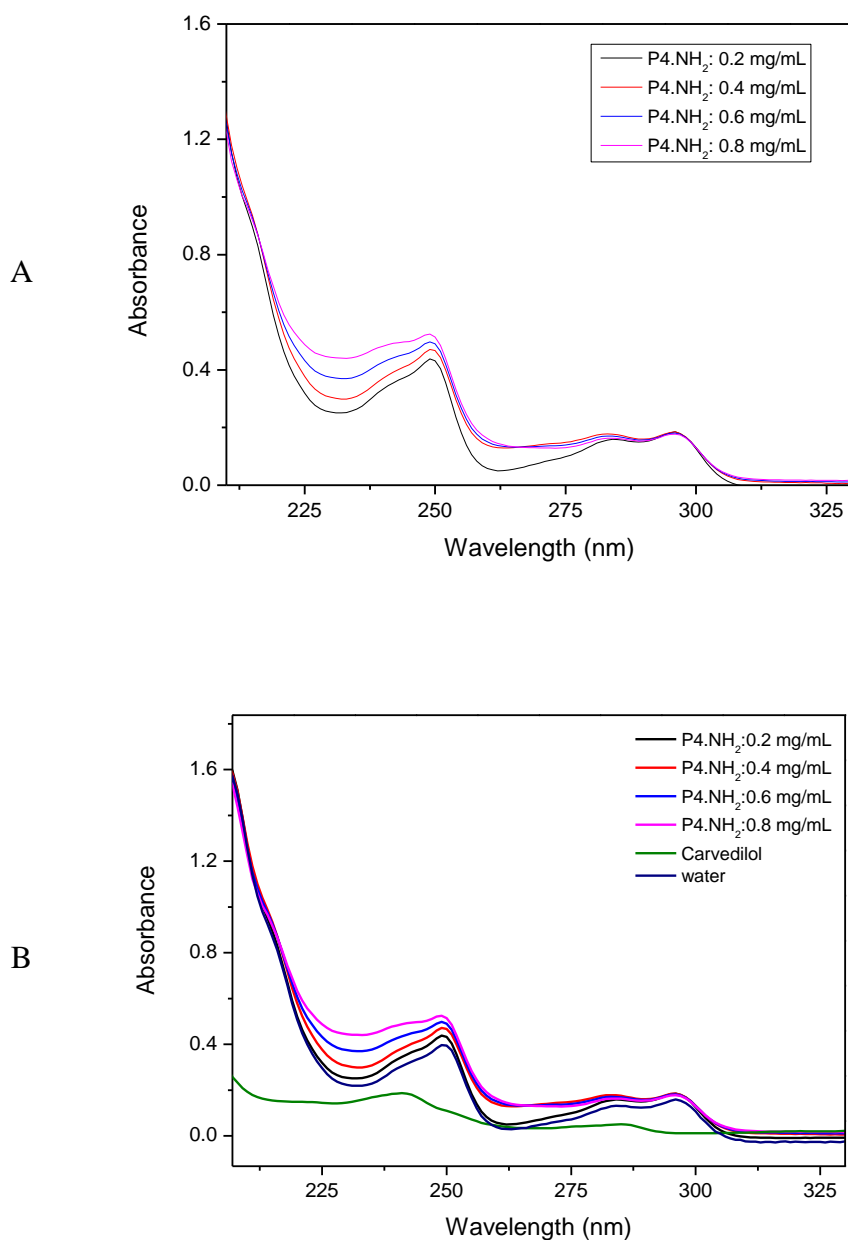


Figure 4.107 Increase in the absorbance of CAR by increasing P4.NH<sub>2</sub> concentration and hypsochromic shift

#### 4.8.2 Drug Binding Constants and Encapsulation Efficiency of P4.NH<sub>2</sub>-CAR Complexes

In the region where the linearity is observed in phase solubility diagram, a linear regression analysis was performed and the following equation (4.2) was obtained for P4.NH<sub>2</sub>-CAR system.

$$y = 0.2783x + 0.00003 \quad (4.2)$$

In the equation (4.2),  $x$  is the molar concentration of P4.NH<sub>2</sub> and  $y$  is the molar concentration of CAR; the correlation constant is 0.9937. Since the slope of the phase solubility diagram is less than 1, the stoichiometry of these complexes were assumed to be 1:1, A<sub>L</sub> type (linear) [6]. Thus, the apparent stability constant  $K_{CAR}$  was calculated from the straight line portion of the phase solubility diagram [6] according to the equation (3.2) in part 3.11.2.

In equation (3.2),  $S_0 = 3.45 \times 10^{-5}$  M is the experimentally obtained solubility of CAR in water and  $\alpha = 0.2783$  [150]. By using these values, the apparent stability constant (drug binding constant)  $K_{CAR}$  was calculated as 11,177.31 M<sup>-1</sup>. This indicates that the CAR binding ability of P4.NH<sub>2</sub> is ~50 times higher compared to 227 M<sup>-1</sup> of  $\beta$ -cyclodextrin drug carrier [278].

Dendrimer encapsulation efficiencies for the increasing  $1.87 \times 10^{-2}$ ,  $3.73 \times 10^{-2}$ ,  $5.59 \times 10^{-2}$  and  $7.46 \times 10^{-2}$  mM dendrimer concentrations were calculated as 13.37%, 25.87%, 43.02%, and 60.75% from equation (3.3) in part 3.8.2. Results indicate that as the P4.NH<sub>2</sub> concentration increases (P4.NH<sub>2</sub>)EE % increases (Figure 4.106,  $R^2 = 0.9937$ ). Thus, Jeffamine<sup>®</sup> T-403 polymeric cored PAMAMs can be used as drug delivery systems or carriers for low bioavailable small hydrophobic acidic molecules.

## **4.9 Determination of Different Generations from Binary Mixtures of Jeffamine<sup>®</sup> T-403 Cored PAMAMs by UV-VIS Spectroscopy**

### **4.9.1 UV-VIS Spectroscopy Analysis of PAMAMs**

Dendrimers can show maximum UV absorption bands depending on their internal tertiary amines and these bands can be observed in different wavelength ranges according to generations. Pande and Crooks [72] were first reported these bands between the wavelengths of 280-285 nm. As it's seen from Figure 4.108, in this part, it was observed these characteristic absorption bands indicating the presence of free tertiary amines of P<sub>2</sub>.NH<sub>2</sub> and P<sub>3</sub>.NH<sub>2</sub> PAMAMs at 280 nm and 285 nm, respectively. Although the maximum absorption band difference is 5nm between P<sub>2</sub>.NH<sub>2</sub> and P<sub>3</sub>.NH<sub>2</sub>, and so the identification, screening and quantification of the binary mixtures of dendrimers seem to

be difficult, it could be possible to develop multivariate calibration models based on the experimental designs like full factorial designs.

Full UV-Vis spectra of the binary mixtures can have the large scale of information. Chemometric models can interpret and evaluate this full spectra as a response matrix and models to predict P2.NH<sub>2</sub> and P3.NH<sub>2</sub> concentrations from the binary mixtures of PAMAMs could be developed. UV-visible spectral range (250-350 nm) characteristic to PAMAMs were observed successfully as aligned with the literature from the intensively purified with LPR method and characterized P2.NH<sub>2</sub> and P3.NH<sub>2</sub> dendrimer generations successfully. Later, these range was used in a good agreement to model calibration data (C1-C9), which is designed with 3<sup>2</sup> full factorial design (Table 3.4 in part 3.12.1 ).

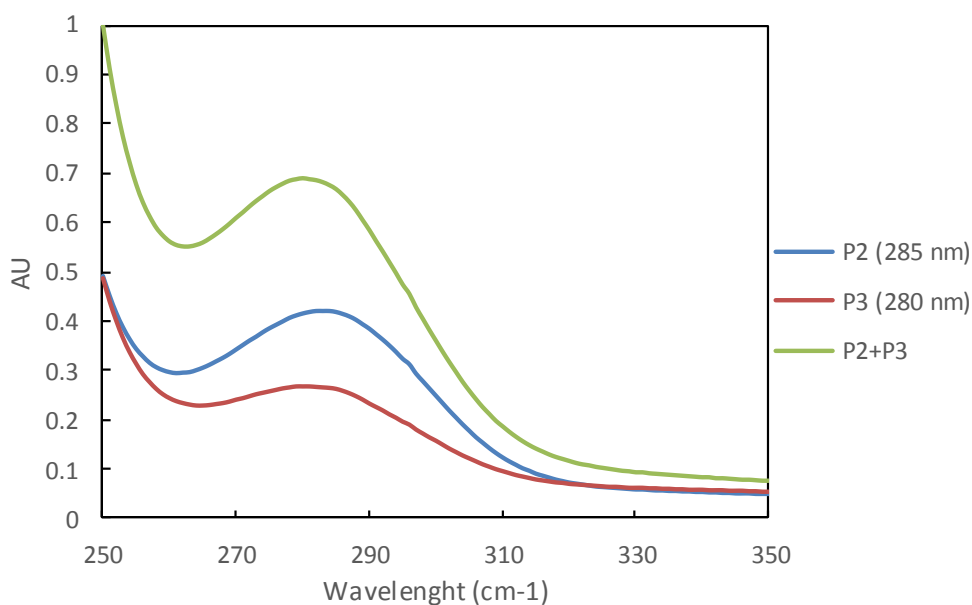


Figure 4.108 UV-VIS spectra of different generation PAMAMs and their mixtures at  $\lambda$  maximum

#### 4.9.2 Design of Experiments and Data Processing

Spectroscopic data can be designed in  $m \times n$  data matrix  $\mathbf{X}$ , where  $m$  refers the number of calibration experiments (C1-C9) and  $n$  indicates the number of variables (wavelengths: 250-350 nm). Calibration experiments were designed by applying 3<sup>2</sup> full factorial design. Thus, nine experiments were conducted at three levels for the simultaneous determination of P2.NH<sub>2</sub> and P3.NH<sub>2</sub> from binary dendrimer mixtures (Table 3.4 in part 3.12.1). UV-VIS spectra of each calibration experiments were collected between 250-350 nm and

absorbance values at each wavelength was used to construct  $X_{m \times n}$  data matrix (Response-full spectra matrix.). On the other hand,  $Y_{m \times 2}$  concentration matrix was constructed by using actual values instead of coded values of  $Y_1$  and  $Y_2$  variables illustrated in Table 3.4 in part 3.12.1. Precision and prediction ability of chemometric models can be influenced by preprocessing. Hence, preprocessing of normalization and column centering were applied to both the X and Y matrix by Solo MIA 7.0.3 Eigenvector Software auto scale function.

### **4.9.3 Determination of the Number of Variables**

The optimum number of PCs or latent variables (LVs) were determined by applying cross validation procedure [227]. In this procedure, ith sample of the data is leave one out once and PCR and PLS models have been built. Then, RMSECV is computed from equation (2.4) in part 2.6.11 with different number of components to form PCR and PLS models. PCR and PLS models require the optimal number of PCs or LVs when the local minimal level of RMSEC is reached. That is, a good rule to decide number of components is not to include additional factors improve the RMSECV at least 2 %. It can be obviously seen from Figure 4.109 that PCs and LVs in PCR and PLS models do not improve more than 2% at the local minima of three PCs or LVs for both P2.NH<sub>2</sub> and P3.NH<sub>2</sub>. In addition, it is more reliable to construct a model with less complexity. For these reasons, PCs and LVs to build the PCR and PLS models were selected as three (Figure 4.109).

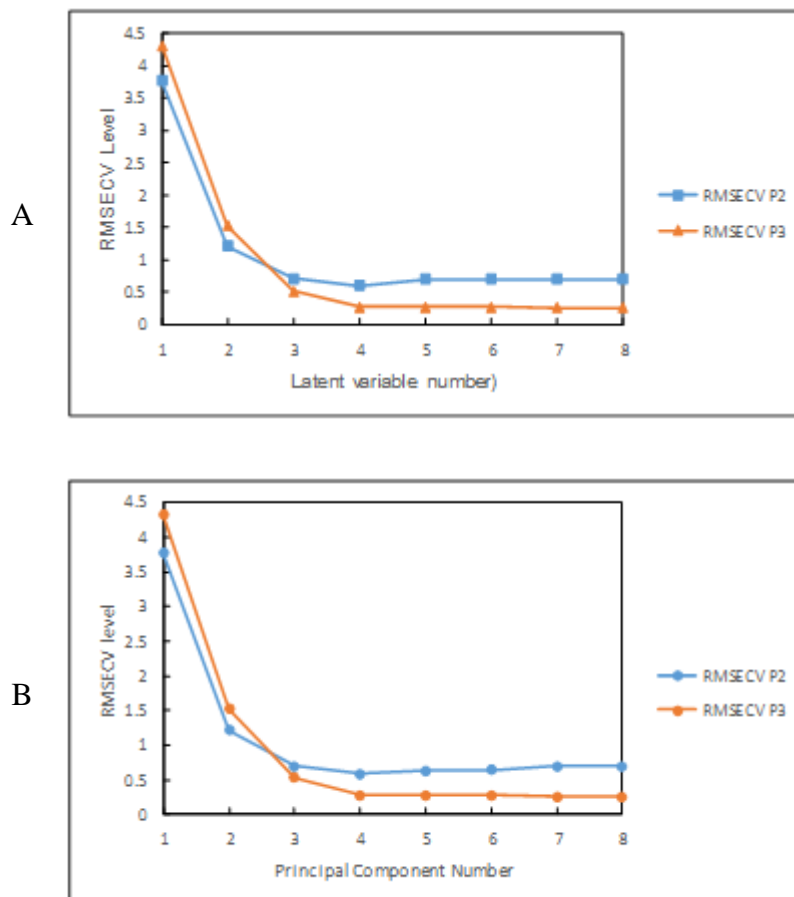


Figure 4.109 RMSECV levels of P2.NH<sub>2</sub> and P3.NH<sub>2</sub> for (a) PLS (b) PCR model

#### 4.9.4 Multivariate Models: MLR, PCR and PLS

##### 4.9.4.1 Comparison of Models

In the divergent synthesis of PAMAMs, core monomer or polymer are reacted with successive addition of excess MA and EDA for the synthesis of higher generation dendrimers. Insufficient or improper purification of synthesized dendrimers result in non-ideal lower generation growth [42]. In this point, multivariate calibration models could be used as a purity or ideal structural growth screening tools for dendrimers. Therefore, the components of the dendrimers solutions can be determined quantitatively. In Table 4.32, it could be clearly seen that MLR model shows the smallest RMSEC, the error of calibration, values for P2.NH<sub>2</sub> and P3.NH<sub>2</sub>. This means that, MLR model fits the calibration data best, as its expected (MLR:  $R^2=1$ ). However, it could be observable from Table 4.32 that RMSECV values for P2.NH<sub>2</sub> is not a distinguishable value to infer which

model is predicts best as they are almost have the same RMSECV values. On the other hand, one can see from RMSECV values of P3.NH<sub>2</sub> that MLR has the smallest RMSECV and it is expected to predict best with the original calibration data. This is followed by PLS model and second closely by PCR model. Nevertheless, for the prediction of new samples: validation data (RMSEP), PLS model outperforms the other models and this is followed closely by PCR for P2.NH<sub>2</sub>. On the other hand, PCR and PLS could predict new sample generally in same performance as it can be seen the P3.NH<sub>2</sub> RMSECV values in Table 4.32. In practice, it could be evident from the comparison of models that fit and prediction are totally different aspects of model's performance. If prediction is the goal, investigation of RMSEP values for MLR, PCR and PLS in Table 4.32 reveals that PLS almost predicts better the P2.NH<sub>2</sub>-P3.NH<sub>2</sub> binary dendrimer mixtures with just the 5 nm maximum absorbance wavelength difference (Figure 4.108) in contrast to MLR and PCR.

Table 4.32 Comparison of RMSEC, RMSECV and RMSEP on MLR, PCR and PLS models

| Model | P2.NH <sub>2</sub> |        |       |                |
|-------|--------------------|--------|-------|----------------|
|       | RMSEC              | RMSECV | RMSEP | R <sup>2</sup> |
| PLS   | 0.29               | 0.71   | 0.23  | 0.9965         |
| PCR   | 0.28               | 0.70   | 0.47  | 0.9968         |
| MLR   | 0.00               | 0.69   | 1.99  | 1.0000         |
| Model | P3.NH <sub>2</sub> |        |       |                |
|       | RMSEC              | RMSECV | RMSEP | R <sup>2</sup> |
| PLS   | 0.25               | 0.50   | 0.32  | 0.9974         |
| PCR   | 0.28               | 0.54   | 0.35  | 0.9966         |
| MLR   | 0.00               | 0.26   | 2.31  | 1.0000         |

#### 4.9.4.2 Validation

Validation of MLR, PCR and PLS models were conducted by selecting seven independent validation test data. Predictive abilities of these models on both calibration, and validation data were investigated. Y measured and Y predicted concentration values for MLR, PCR and PLS models were shown in (a), (b) and (c) at Figure 4.110 and Figure

4.111, respectively. % Residual Error of prediction values of models were calculated. Then, these values were plotted against the total sample number (nine for full factorial calibration data and seven for validation data) (Figure 4.110 and 4.111.). Furthermore, 1:1 line and fitting line corresponding to calibration and validation data respectively were shown on Figure 4.110 and Figure 4.111. It can be easily seen and distinguished from % residual versus sample plots in both Figure 4.110 and Figure 4.111 that MLR model predicts best the calibration data as its expected and evidenced from Table 4.32 ( $R^2=1$ ). This can also be understood from 0 % residual error for calibration data. However, it fails to predict validation data with different than calibration data. % Residual error for the prediction of MLR model is present between 10-35 % for P2.NH<sub>2</sub> (see Figure 4.110. (a)) while it is between 15-25 % for P3.NH<sub>2</sub> (Figure 4.110 (a) and Figure 4.111 (b)). This also explains that why there exists a huge gap between the 1:1 and fitting lines visually (MLR: P2.NH<sub>2</sub> ( $R^2=0.912$ ); P3.NH<sub>2</sub> (0.922)). These results are also correlated with the results presented in Table 4.32 that calibration data fit the MLR model best but this model is not as much as predictive as PCR and PLS Model. That is, it has the highest root-mean-square error of prediction values (RMSEP=1.99 (P2.NH<sub>2</sub>), 2.31 (P3.NH<sub>2</sub>)).

In contrast to MLR results, if PCR and PLS models' predictive abilities are investigated from Figure 4.110 and 4.111, it could be seen that they have the higher regression coefficients (PCR: P2.NH<sub>2</sub> ( $R^2=0.993$ ), P3.NH<sub>2</sub> ( $R^2=0.995$ ); PLS: P2.NH<sub>2</sub> ( $R^2=0.995$ ), P3.NH<sub>2</sub> ( $R^2=0.995$ )) representing both the calibration and validation data than those of MLR model (MLR: P2.NH<sub>2</sub> ( $R^2=0.912$ ); P3.NH<sub>2</sub> (0.922)). In addition, it could be easily interpreted from visual data presented in Figure 4.110 and 4.111 for PCR and PLS models that 1:1 lines and fitting lines are almost overlapped. That is, PCR and PLS models can both predict the calibration data and validation data in reasonable % Residual Errors. While PCR model predicts binary mixtures of PAMAMs between % Residual errors of  $\pm 8$  % (RMSEP: P2.NH<sub>2</sub>=0.698; P3.NH<sub>2</sub>=0.535), PLS predicts between those of  $\pm 6$  % (RMSEP: P2.NH<sub>2</sub>=0.470; P3.NH<sub>2</sub>=0.347). These prediction parameter values are beyond the prediction values of MLR (Figure 4.110, 4.111: (a), (b), (c)). To sum up, PLS predicts better, but the PCR is second close, than MLR and could be successfully used for the quantitative determination of the binary mixtures of PAMAMs

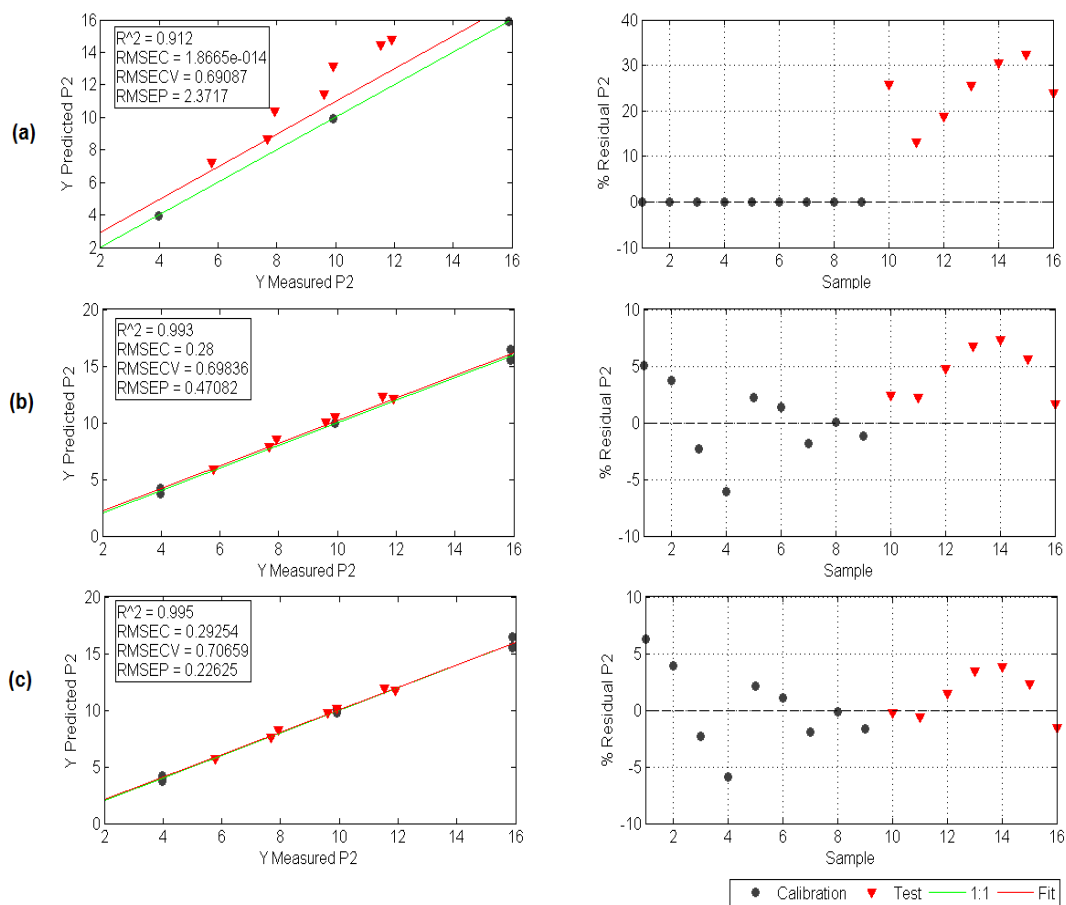


Figure 4.110 Y measured and Y predicted values of (a) MLR model (b) PCR model (c) PLS model for P2.NH<sub>2</sub> component. Units of Y Measured and Y Predicted values are mg in 10 mL aqua

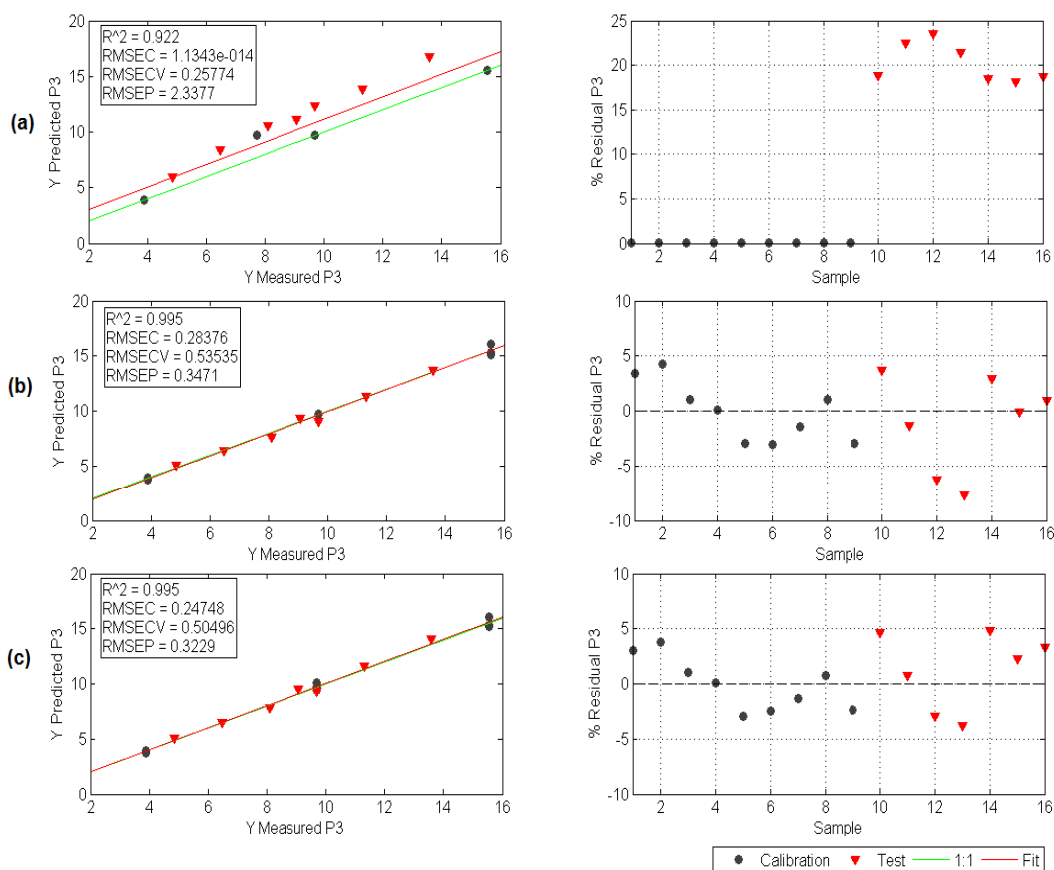


Figure 4.111 Y measured and predicted values of (a) MLR model (b) PCR model (c) PLS model for P3.NH<sub>2</sub> component. Units of Y Measured and Y Predicted values are mg in 10 mL aqua

#### 4.10 General Results and Summary

A new microwave assisted amidation method for the synthesis of EDA, DETA and Jeffamine<sup>®</sup> T-403 cored PAMAMs up to fourth generations was developed. Synthesis of higher generation PAMAMs in a short time have significant limitations by mostly depending on the amidation step. Studies performed on the amidation of ester terminated half generation Jeffamine<sup>®</sup> T-403 cored PAMAMs showed that amidation step was accelerated 3-5 times by using MAS technique compared to conventional heating in oil bath. That is, amidation step was shortened up to 60 minutes for higher generation PAMAM synthesis compared to 5-8 days performed in traditional ways at room temperature [15].

In the amidation step, it has been paid extra attention to the temperature which was controlled by MW IR sensor. Reaction proceedings were monitored by ATR without final

purification. With the growth of dendrimer, it was not possible to move the molecules on TLC, so ATR has provided a big advantage to follow the appearance and disappearance of ester and amine peaks respectively. It has been observed that current technique has accelerated the reaction time, minimized the excessive use of reagents and solvents, increased the yield, decreased the byproducts without using any coupling reagent or special catalysts and allow the massive production of amine terminated PAMAMs. In order to increase the purity of synthesized products, LPR technique was used in each step. Surface modification of esteric generations of PAMAMs were performed by tris and carboxyl functionalization. The synthesis of tris terminated PAMAMs also were performed by specifically new developed other microwave assisted methodology. This method allows the synthesis of tris terminated PAMAMs in 110-130 minutes rather than two days [173, 264].

Synthesis of amine and tris terminated PAMAMs were performed by new developed MAS methods while carboxyl terminated PAMAMs were synthesized with conventional methods. In fact, even if the synthesis of EDA cored and amine, tris terminated PAMAMs were synthesized before, they were synthesized with new developed MAS methods first time, the other series of PAMAM and derivatives synthesized in this thesis show the characteristic of novel molecules. Furthermore, all the molecules synthesized are water soluble except ester terminated ones. Tris and carboxyl terminated dendrimers are infinitively soluble.

Synthesized dendrimers were purified by liquid-phase polymer-based retention (LPR) technique and characterized by  $^1\text{H-NMR}$ ,  $^{13}\text{C-NMR}$ , EA, GPC and UV-VIS spectroscopy. Results revealed that all of the synthesized dendrimers are in good purity and yield.

By means of proton binding sites of dendrimers, they can be used in many applications like as MRI contrasting agents in target drug delivery [58], cancer therapy [59], gene delivery [60] and tumor screening [61]. As its formerly stated in the introduction, not only physical properties of dendrimers like intrinsic viscosity, metal absorption affinity, molecular conformation but also many molecular properties of PAMAMs and surface functionalized derivatives are depend on the molecular charge and useful for many applications. Thus, it is important to develop necessary approach to accurately

characterize protonation constant (pKa) values of the proton binding sites of both amine terminated and surface functionalized PAMAMs.

Interactions of  $H^+$  and macromolecular polydentate ligands PAMAMs were both characterized by potentiometric and spectroscopic studies with the use of most recent computer programs Hyperquad and HypSpec. Without using these models, potentiometric titration data can only be used for the calculation of macroscopic protonation constants. Up to now, characterization of the protonation mechanisms of PAMAMs have been tried to be explained by potentiometric fitting models like site binding model [65], and Frumkin adsorption isotherm multishell structural model [76] together to enlighten the protonation mechanism of PAMAMs in aqueous solutions. However, a little attention has been paid for the characterization of PAMAMs by other methods like spectroscopic titrations and with advanced computer programs [79].

In this thesis, interactions of  $H^+$  and macromolecular polydentate ligands PAMAMs are investigated using different factor analysis techniques; such as PCA and EFA, and the number of absorbing species were firstly estimated rather than trying to apply directly fitting or traditional least square methods. By the combination of other chemometric approaches like MCR-ALS, unit spectra of PAMAMs and derivatives were estimated from aqueous solutions. Resulting spectra's were used for the protonation constant refinements in HypSpec program by considering some constraints. As a result, a new chemometric approach for the development and characterization of the protonation mechanism of PAMAMs were developed with the aid of advanced computer programs, and protonation constants of EDA, DETA and Jeffamine<sup>®</sup> T403 cored PAMAMs with different functionalities with amine, tris and carboxyl were calculated.

The ability of simultaneous metal complexation of dendrimer was investigated with the removal of uncomplexed Cu (II), Co (II), Ni (II), Cd (II), and Zn (II) from metal dendrimer mixture solution with LPR technique. Retentate metal concentrations were determined by AAS. pH role and effect of Jeffamine<sup>®</sup> T-403 cored P3.NH<sub>2</sub> and P4.NH<sub>2</sub> on the simultaneous removal of metal ions from aqueous solutions were also investigated. Results revealed that low pH could be used for the regeneration of metal complexed PAMAMs as all the metal ions were released from membrane. As the pH increases, P3.NH<sub>2</sub> and P4.NH<sub>2</sub> start slightly to be selective at pH 5 and selective at neutral pH 7. P3.NH<sub>2</sub> and P4.NH<sub>2</sub> retains only 65 % and 75 % Cu(II) at pH 7, respectively. It could be

so interfered that both generation of PAMAMs are selective to Cu(II) in the presence of Co(II), Ni(II), Cd(II), and Zn(II) at neutral pH 7. At high pH 9, both generations could remove all of the metal ions present in the media. The affinity of both generations towards metal ions were also observed in the same decreasing order Zn(II) > Co(II) > Ni(II) > Cu(II) > Cd(II) at pH 9. Only the Cu(II) retention increases with increasing generation and pH. Zn(II) and Co(II) are retained most over % 90 retention for both generations at pH 9. In conclusion, novel metal chelating abilities of polydentate ligands P3.NH<sub>2</sub> and P4.NH<sub>2</sub> were characterized by LPR technique and explained by EOP profiles of dendrimers in different pH values. Over neutral pH, P3.NH<sub>2</sub> and P4.NH<sub>2</sub> are stable enough to simultaneously bind Co (II), Ni (II), Cd (II), and Zn (II). Regeneration of metal laden PAMAMs could be achieved by decreasing the pH of aqueous solution. Increasing the number of functional groups did not cause reasonable effect in metal binding. That is, no linearity has been observed with the increasing generation number.

All the surface modified PAMAMs were used for the synthesis of metal nanoparticles. Investigation of the maximum metal loading capacity of tris and carboxyl terminated PAMAMs were determined by the titrations of PAMAMs with Cu<sup>2+</sup> ions and optimum molar ratios were calculated. The most sparingly evidence of successfully synthesis of Cu-DENs comes from color change from blue to golden brown to the disappearance of d-d complexation band ~680 nm and formation of monotonically increasing exponential absorption band towards to low wavelengths. The size of Cu clusters can be understood from the absence of a Mie plasmon peak at around 570 nm in UV-VIS spectra. The absence of this band indicates that Cu clusters are smaller than 5nm [131]. All of these observations were encountered and so the synthesis of Cu-DENs were successfully achieved. Catalytic properties of these novel series of Cu-DENs might be interesting for catalytic evaluation in organic synthesis in future studies

CAR has a restricted bioavailability because of its lower solubility. In this study CAR binding and solubility enhancement abilities of P4.NH<sub>2</sub> PAMAM dendrimer were investigated. Results obtained from phase solubility diagram revealed that increasing P4.NH<sub>2</sub> concentration increases the solubility of CAR. This could be maintained by the increasing number of deprotonated inner tertiary amine numbers at pH 7. In this pH, almost all of the primary amines of P4.NH<sub>2</sub> are protonated. This allow P4.NH<sub>2</sub> to make inclusion complex with CAR. Consequently, the limited water solubility of CAR could

be overcome by the formation of inclusion complexes with P4.NH<sub>2</sub>, which could be proposed as a new kind of drug carrier.

Finally, chemometric analysis of the experimental data designed with 3<sup>2</sup> full factorial experimental design from full spectra can convey large scale of information for the construction of multivariate chemometric models. Hence, data analysis and interpretation could be performed with good reliability and security. Modelling from full spectra can make multivariate calibration models superior as they convey more information compared to simple linear models. MLR, PCR and PLS calibration models were constructed in order to predict P2.NH<sub>2</sub> and P3.NH<sub>2</sub> generations concentrations from the binary mixtures of Jeffamine<sup>®</sup> T-403 cored PAMAMs. Built models were compared in terms of their root-mean-square error values, especially in terms of RMSEPs. Results revealed that developed PCR and PLS model could be successfully used for the simultaneous determination of the binary mixtures of PAMAMs. Indeed, PLS predicts slightly better. To sum up, this study is the first report concerning the purity assessment of PAMAMs by using chemometric methods so that developed model could be easily used in routine laboratory UV-VIS spectroscopy analysis without using any sample pretreatment in short time and for the screening of the dendrimer synthesis.

## REFERENCES

---

- [1] Esfand, R. and Tomalia, D.A., (2001). "Poly(amidoamine) (PAMAM) dendrimers: from biomimicry to drug delivery and biomedical applications", *Drug Discov. Today*, 6: 427-436.
- [2] Patri, A.K. Majoros, I.J. and Baker Jr, J.R., (2002). "Dendritic polymer macromolecular carriers for drug delivery", *Curr. Opin. Chem. Biol.*, 6: 466-471.
- [3] Boas, U. and Heegaard, P.M., (2004). "Dendrimers in drug research", *Chem Soc Rev*, 33: 43-63.
- [4] Kukowska-Latallo, J.F. Bielinska, A.U. Johnson, J. Spindler, R. Tomalia, D.A. and Baker, J.R., (1996). "Efficient transfer of genetic material into mammalian cells using Starburst polyamidoamine dendrimers", *P. Natl. Acad. Sci.*, 93: 4897-4902.
- [5] Eichman, J.D. Bielinska, A.U. Kukowska-Latallo, J.F. and Baker Jr, J.R., (2000). "The use of PAMAM dendrimers in the efficient transfer of genetic material into cells", *Pharm. Sci Technol. To.*, 3: 232-245.
- [6] Luo, D. Haverstick, K. Belcheva, N. Han, E. and Saltzman, W.M., (2002). "Polyethylene glycol-Conjugated PAMAM Dendrimer for Biocompatible, High-Efficiency DNA Delivery", *Macromolecules*, 35: 3456-3462.
- [7] Van Manen, H.J. van Veggel, F.C.J.M. and Reinhoudt, D.N., (2001). *Dendrimers IV: Metal Coordination, Self Assembly, Catalysis*, F. Vögtle and Schalley, C.A., ed. *Dendrimers IV: Metal Coordination, Self Assembly, Catalysis*. Berlin: Springer, 163-169.
- [8] Kim, J.-W. Choi, E.-A. and Park, S.-M., (2003). "Electrochemically Controlled Preparation of Platinum-Poly(amidoamine) Dendrimer Hybrid Nanowires and Their Characterization", *J. Electrochem. Soc.*, 150: E202-E206.
- [9] Crooks, R.M. Zhao, M. Sun, L. Chechik, V. and Yeung, L.K., (2000). "Dendrimer-Encapsulated Metal Nanoparticles: Synthesis, Characterization, and Applications to Catalysis", *Accounts Chem. Res.*, 34: 181-190.
- [10] Cheng, L. Pacey, G.E. and Cox, J.A., (2001). "Preparation and electrocatalytic applications of a multilayer nanocomposite consisting of phosphomolybdate and poly(amidoamine)", *Electrochim. Acta*, 46: 4223-4228.

- [11] Tülü, M. and Ertürk, A.S., (2012). Dendrimers as Antibacterial Agents, V. Bobbarala, ed. A Search for Antibacterial Agents. In Tech, 89-106.
- [12] Winnicka, K. Sosnowska, K. Wieczorek, P. Sacha, P.T. and Trynieszewska, E., (2011). "Poly(amidoamine) dendrimers increase antifungal activity of clotrimazole", *Biol. Pharm. Bull.*, 34: 1129-1133.
- [13] Winnicka, K. Wroblewska, M. Wieczorek, P. Sacha, P.T. and Trynieszewska, E., (2012). "Hydrogel of ketoconazole and PAMAM dendrimers: formulation and antifungal activity", *Molecules*, 17: 4612-4624.
- [14] Lee, S.C., (2001). Dendrimers in Nanobiological Devices, J.M.J. Fréchet and Tomalia, D.A., ed. Dendrimers and other dendritic polymers. Wiley, 547-554.
- [15] Frechet, J. and Tomalia, D., (2001). Dendrimers and Other Dendritic Polymers: John Wiley & Sons Ltd.
- [16] Tomalia, D.A. Baker, H. Dewald, J. Hall, M. Kallos, G. Martin, S. Roeck, J. Ryder, J. and Smith, P., (1985). "A New Class of Polymers: Starburst-Dendritic Macromolecules", *Polymer Journal*, 17: 117-132.
- [17] Buhleier, E. Wehner, W. and Vögtle, F., (1978). "'Cascade'- and 'Nonskid-Chain-like' Syntheses of Molecular Cavity Topologies", *Synthesis*, 1978: 155-158.
- [18] Denkewalter, R.G. Kolc, J.F. and Lukasavage, W.J., (1983). Macromolecular Highly Branched Homogeneous Compound, U.S. Patent, ed<sup>eds.</sup>: 4,410,688.
- [19] de Brabander-van den Berg, E.M.M. and Meijer, E.W., (1993). "Poly(propylene imine) Dendrimers: Large-Scale Synthesis by Heterogeneously Catalyzed Hydrogenations", *Angew. Chem. Int. Edit.*, 32: 1308-1311.
- [20] Wörner, C. and Mülhaupt, R., (1993). "Polynitrile- and Polyamine-Functional Poly(trimethylene imine) Dendrimers", *Angew. Chem. Int. Edit.*, 32: 1306-1308.
- [21] Tomalia, D.A., (1993). "Starburst/cascade dendrimers: fundamental building blocks for a new nanoscopic chemistry set", *Aldrichim. Acta*, 26: 91-101.
- [22] Newkome, G.R. Yao, Z. Baker, G.R. and Gupta, V.K., (1985). "Micelles. Part 1. Cascade molecules: a new approach to micelles. A [27]-arborol", *J. Org. Chem.*, 50: 2003-2004.
- [23] Hawker, C.J. and Frechet, J.M.J., (1990). "Preparation of polymers with controlled molecular architecture. A new convergent approach to dendritic macromolecules", *J. Am. Chem. Soc.*, 112: 7638-7647.
- [24] Miller, T.M. and Neenan, T.X., (1990). "Convergent synthesis of monodisperse dendrimers based upon 1,3,5-trisubstituted benzenes", *Chem. Mater.*, 2: 346-349.
- [25] Xu, Z. and Moore, J.S., (1993). "Rapid Construction of Large-size Phenylacetylene Dendrimers up to 12.5 Nanometers in Molecular Diameter", *Angew. Chem. Int. Edit.*, 32: 1354-1357.
- [26] Xu, Z. and Moore, J.S., (1993). "Synthesis and Characterization of a High Molecular Weight Stiff Dendrimer", *Angew. Chem. Int. Edit.*, 32: 246-248.
- [27] Majoros, I.J. and Baker, J.R., (2008). Dendrimer-based nanomedicine, Singapore; Hackensack, NJ: Pan Stanford ; Distributed by World Scientific.

- [28] Campagna, S. Ceroni, P. and Puntoriero, F., (2011). *Designing Dendrimers*: Wiley.
- [29] Calderón, M. and Strumia, M., (2013). "Hyperbranched and Hiperfunctionalized Materials from DEndritici Chemistry (Materials Hiperramificados E Hiperfuncionalizados Derivados de La Quimica Dendritica)", *Rev. LatinAm. Metal. Mat*, 33: 2-14.
- [30] Beezer, A.E. King, A.S.H. Martin, I.K. Mitchel, J.C. Twyman, L.J. and Wain, C.F., (2003). "Dendrimers as potential drug carriers; encapsulation of acidic hydrophobes within water soluble PAMAM derivatives", *Tetrahedron*, 59: 3873-3880.
- [31] Franc, G. and Kakkar, A.K., (2010). "'Click' methodologies: efficient, simple and greener routes to design dendrimers", *Chem. Soc. Rev.*, 39: 1536-1544.
- [32] Kim, C. Kim, H. Oh, M.-J. and Hong, J.-H., (2009). "Preparation and Unequivocal Identification of Chromophores-Substituted Carbosilane Dendrimers up to 7th Generations", *Bull. Korean Chem. Soc*, 30: 873.
- [33] Kappe, C.O., (2004). "Controlled Microwave Heating in Modern Organic Synthesis", *Angewandte Chemie International Edition*, 43: 6250-6284.
- [34] Sinnwell, S. and Ritter, H., (2007). "Recent Advances in Microwave-Assisted Polymer Synthesis", *Australian Journal of Chemistry*, 60: 729-743.
- [35] Zhang, C. Su, P. Umar Farooq, M. Yang, Y. Gao, X. and Hongjun, E., (2010). "Synthesis of polyamidoamine dendrimer-grafted silica with microwave assisted protocol", *Reactive and Functional Polymers*, 70: 129-133.
- [36] Iannelli, M. Alupei, V. and Ritter, H., (2005). "Selective microwave-accelerated synthesis and polymerization of chiral methacrylamide directly from methacrylic acid and (R)-1-phenyl-ethylamine", *Tetrahedron*, 61: 1509-1515.
- [37] Kappe, C.O., (2004). "Synthetic methods. Controlled microwave heating in modern organic synthesis", *Angew. Chem., Int. Ed.*, 43: 6250-6284.
- [38] de la Hoz, A. Díaz-Ortiz, A. and Moreno, A., (2007). "Review on non-thermal effects of microwave irradiation in organic synthesis", *Journal of Microwave Power and Electromagnetic Energy*, 41: 44.
- [39] de, I.H.A. Díaz-Ortiz, A. and Moreno, A., (2005). "Microwaves in organic synthesis. Thermal and non-thermal microwave effects", *Chem. Soc. Rev.*, 34: 164-178.
- [40] Kappe, C.O. Pieber, B. and Dallinger, D., (2013). "Microwave Effects in Organic Synthesis-Myth or Reality?", *Angew. Chem., Int. Ed.*, 52: 1088-1094.
- [41] Spivakov, B.Y. Geckeler, K. and Bayer, E., (1985). "Liquid-phase polymer-based retention [mdash] the separation of metals by ultrafiltration on polychelatogens", *Nature*, 315: 313-315.
- [42] Mullen, D.G. Desai, A. van Dongen, M.A. Barash, M. Baker, J.R. and Banaszak Holl, M.M., (2012). "Best Practices for Purification and Characterization of PAMAM Dendrimer", *Macromolecules*, 45: 5316-5320.

- [43] Peterson, J. Allikmaa, V. Subbi, J. Pehk, T. and Lopp, M., (2003). "Structural deviations in poly(amidoamine) dendrimers: a MALDI-TOF MS analysis", *European Polymer Journal*, 39: 33-42.
- [44] Tomalia, D.A. Naylor, A.M. and Goddard, W.A., (1990). "Starburst Dendrimers: Molecular-Level Control of Size, Shape, Surface Chemistry, Topology, and Flexibility from Atoms to Macroscopic Matter", *Angewandte Chemie International Edition in English*, 29: 138-175.
- [45] Kallos, G.J. Tomalia, D.A. Hedstrand, D.M. Lewis, S. and Zhou, J., (1991). "Molecular weight determination of a polyamidoamine Starburst polymer by electrospray ionization mass spectrometry", *Rapid Communications in Mass Spectrometry*, 5: 383-386.
- [46] Tolić, L.P. Anderson, G.A. Smith, R.D. Brothers Ii, H.M. Spindler, R. and Tomalia, D.A., (1997). "Electrospray ionization Fourier transform ion cyclotron resonance mass spectrometric characterization of high molecular mass Starburst™ dendrimers", *International Journal of Mass Spectrometry and Ion Processes*, 165–166: 405-418.
- [47] Lalwani, S. Venditto, V.J. Chouai, A. Rivera, G.E. Shaunak, S. and Simanek, E.E., (2009). "Electrophoretic Behavior of Anionic Triazine and PAMAM Dendrimers: Methods for Improving Resolution and Assessing Purity Using Capillary Electrophoresis", *Macromolecules*, 42: 3152-3161.
- [48] Islam, M.T. Shi, X. Balogh, L. and Baker, J.R., (2005). "HPLC Separation of Different Generations of Poly(amidoamine) Dendrimers Modified with Various Terminal Groups", *Analytical Chemistry*, 77: 2063-2070.
- [49] Scott, R.W.J. Wilson, O.M. and Crooks, R.M., (2004). "Synthesis, Characterization, and Applications of Dendrimer-Encapsulated Nanoparticles", *The Journal of Physical Chemistry B*, 109: 692-704.
- [50] Eller, K. Henkes, E. Rossbacher, R. and Höke, H., (2000). *Amines, Aliphatic*, ed. Ullmann's Encyclopedia of Industrial Chemistry. Wiley-VCH Verlag GmbH & Co. KGaA.
- [51] Schluter, A.D. and Rabe, J.P., (2000). "Dendronized polymers: synthesis, characterization, assembly at interfaces, and manipulation", *Angew. Chem., Int. Ed.*, 39: 864-883.
- [52] Froimowicz, P. Gandini, A. and Strumia, M., (2005). "New polyfunctional dendritic linear hybrids from terminal amine polyether oligomers (Jeffamine): synthesis and characterization", *Tetrahedron Lett.*, 46: 2653-2657.
- [53] Tulu, M. Aghatabay, N.M. Senel, M. Dizman, C. Parali, T. and Dulger, B., (2009). "Synthesis, characterization and antimicrobial activity of water soluble dendritic macromolecules", *Eur. J. Med. Chem.*, 44: 1093-1099.
- [54] Öztürk, K. Ertürk, A.S. Sarısözen, C. Tulu, M. and Çalış, S., "Cytotoxicity and in vitro characterization studies of synthesized Jeffamine-cored PAMAM dendrimers", *Journal of Microencapsulation*, 0: 1-10.
- [55] López-Andarias, J. Guerra, J. Castañeda, G. Merino, S. Ceña, V. and Sánchez-Verdú, P., (2012). "Development of Microwave-Assisted Reactions for PAMAM

- Dendrimer Synthesis", *European Journal of Organic Chemistry*, 2012: 2331-2337.
- [56] Diallo, M.S. Christie, S. Swaminathan, P. Balogh, L. Shi, X. Um, W. Papelis, C. Goddard, W.A., III and Johnson, J.H., Jr., (2004). "Dendritic Chelating Agents. 1. Cu(II) Binding to Ethylene Diamine Core Poly(amidoamine) Dendrimers in Aqueous Solutions", *Langmuir*, 20: 2640-2651.
- [57] Cohen, S.M. Petoud, S. and Raymond, K.N., (2001). "Synthesis and Metal Binding Properties of Salicylate-, Catecholate-, and Hydroxypyridinonate-Functionalized Dendrimers", *Chemistry – A European Journal*, 7: 272-279.
- [58] Khopade, A.J. Caruso, F. Tripathi, P. Nagaich, S. and Jain, N.K., (2002). "Effect of dendrimer on entrapment and release of bioactive from liposomes", *International Journal of Pharmaceutics*, 232: 157-162.
- [59] Wolinsky, J.B. and Grinstaff, M.W., (2008). "Therapeutic and diagnostic applications of dendrimers for cancer treatment", *Advanced Drug Delivery Reviews*, 60: 1037-1055.
- [60] Kim, Y. and Zimmerman, S.C., (1998). "Applications of dendrimers in bio-organic chemistry", *Curr. Opin. Chem. Biol.*, 2: 733-742.
- [61] Swanson, S.D. Kukowska-Latallo, J.F. Patri, A.K. Chen, C. Ge, S. Cao, Z. Kotlyar, A. East, A.T. and Baker, J.R., (2008). "Targeted gadolinium-loaded dendrimer nanoparticles for tumor-specific magnetic resonance contrast enhancement", *International journal of nanomedicine*, 3: 201-210.
- [62] Maiti, P.K. Çağın, T. Lin, S.-T. and Goddard, W.A., (2005). "Effect of Solvent and pH on the Structure of PAMAM Dendrimers", *Macromolecules*, 38: 979-991.
- [63] Böhme, U. Klenge, A. Hänel, B. and Scheler, U., (2011). "Counterion Condensation and Effective Charge of PAMAM Dendrimers", *Polymers*, 3: 812-819.
- [64] van Duijvenbode, R.C. Borkovec, M. and Koper, G.J.M., (1998). "Acid-base properties of poly(propylene imine)dendrimers", *Polymer*, 39: 2657-2664.
- [65] Cakara, D. Kleimann, J. and Borkovec, M., (2003). "Microscopic Protonation Equilibria of Poly(amidoamine) Dendrimers from Macroscopic Titrations", *Macromolecules*, 36: 4201-4207.
- [66] Ottaviani, M.F. Montalti, F. Romanelli, M. Turro, N.J. and Tomalia, D.A., (1996). "Characterization of Starburst Dendrimers by EPR. 4. Mn(II) as a Probe of Interphase Properties", *The Journal of Physical Chemistry*, 100: 11033-11042.
- [67] Kabanov, V.A. Zezin, A.B. Rogacheva, V.B. Gulyaeva, Z.G. Zansochova, M.F. Joosten, J.G.H. and Brackman, J., (1998). "Polyelectrolyte Behavior of Astramol Poly(propyleneimine) Dendrimers", *Macromolecules*, 31: 5142-5144.
- [68] Koper, G.J.M. van Genderen, M.H.P. Elissen-Román, C. Baars, M.W.P.L. Meijer, E.W. and Borkovec, M., (1997). "Protonation Mechanism of Poly(propylene imine) Dendrimers and Some Associated Oligo Amines", *Journal of the American Chemical Society*, 119: 6512-6521.

- [69] Borkovec, M. and Koper, G.J.M., (2000). "A Cluster Expansion Method for the Complete Resolution of Microscopic Ionization Equilibria from NMR Titrations", *Analytical Chemistry*, 72: 3272-3279.
- [70] Lee, I. Athey, B.D. Wetzel, A.W. Meixner, W. and Baker, J.R., (2002). "Structural Molecular Dynamics Studies on Polyamidoamine Dendrimers for a Therapeutic Application: Effects of pH and Generation", *Macromolecules*, 35: 4510-4520.
- [71] Betley, T.A. Banaszak Holl, M.M. Orr, B.G. Swanson, D.R. Tomalia, D.A. and Baker, J.R., (2001). "Tapping Mode Atomic Force Microscopy Investigation of Poly(amidoamine) Dendrimers: Effects of Substrate and pH on Dendrimer Deformation", *Langmuir*, 17: 2768-2773.
- [72] Pande, S. and Crooks, R.M., (2011). "Analysis of Poly(amidoamine) Dendrimer Structure by UV-Vis Spectroscopy", *Langmuir*, 27: 9609-9613.
- [73] Tulu, M. and Senel, M., (2008). "Dendritic polychelators: synthesis, characterization, and metal ion binding properties", *J. Appl. Polym. Sci.*, 109: 2808-2814.
- [74] Diallo, M.S. Balogh, L. Shafagati, A. Johnson, J.H. Goddard, W.A. and Tomalia, D.A., (1999). "Poly (amidoamine) dendrimers: a new class of high capacity chelating agents for Cu (II) ions", *Environmental Science & Technology*, 33: 820-824.
- [75] van Duijvenbode, R.C. Rajanayagam, A. Koper, G.J.M. Baars, M.W.P.L. de Waal, B.F.M. Meijer, E.W. and Borkovec, M., (1999). "Synthesis and Protonation Behavior of Carboxylate-Functionalized Poly(propyleneimine) Dendrimers", *Macromolecules*, 33: 46-52.
- [76] Niu, Y. Sun, L. and Crooks, R.M., (2003). "Determination of the Intrinsic Proton Binding Constants for Poly(amidoamine) Dendrimers via Potentiometric pH Titration", *Macromolecules*, 36: 5725-5731.
- [77] Cakara, D. and Borkovec, M., (2007). "Microscopic protonation mechanism of branched polyamines: Poly (amidoamine) versus poly (propyleneimine) dendrimers", *Croatica chemica acta*, 80: 421-428.
- [78] Diallo, M.S. Christie, S. Swaminathan, P. Johnson, J.H., Jr. and Goddard, W.A., III, (2005). "Dendrimer enhanced ultrafiltration. 1. Recovery of Cu(II) from aqueous solutions using PAMAM dendrimers with ethylene diamine core and terminal NH<sub>2</sub> groups", *Environ. Sci. Technol.*, 39: 1366-1377.
- [79] Krot, K.A. de Namor, A.F.D. Aguilar-Cornejo, A. and Nolan, K.B., (2005). "Speciation, stability constants and structures of complexes of copper(II), nickel(II), silver(I) and mercury(II) with PAMAM dendrimer and related tetraamide ligands", *Inorganica Chimica Acta*, 358: 3497-3505.
- [80] McBryde, W.A.E., (1968). "Constraints on the determination of stability constants for metal complexes. II. The iron(III) phenolates", *Canadian Journal of Chemistry*, 46: 2385-2392.
- [81] McBryde, W.A.E., (1974). "Spectrophotometric determination of equilibrium constants in solution", *Talanta*, 21: 979-1004.

- [82] Crisponi, G., (1997). "Spectrophotometric methods in the study of solution equilibria", *Reactive and Functional Polymers*, 34: 121-126.
- [83] Gans, P. Sabatini, A. and Vacca, A., (1996). "Investigation of equilibria in solution. Determination of equilibrium constants with the HYPERQUAD suite of programs", *Talanta*, 43: 1739-1753.
- [84] Motekaitis, R.J. and Martell, A.E., (1982). "Program PKAS: a novel algorithm for the computation of successive protonation constants", *Can. J. Chem.*, 60: 168-173.
- [85] Sabatini, A. Vacca, A. and Gans, P., (1992). "Mathematical algorithms and computer programs for the determination of equilibrium constants from potentiometric and spectrophotometric measurements", *Coord. Chem. Rev.*, 120: 389-405.
- [86] Frassinetti, C. Ghelli, S. Gans, P. Sabatini, A. Moruzzi, M.S. and Vacca, A., (1995). "Nuclear magnetic resonance as a tool for determining protonation constants of natural polyprotic bases in solution", *Anal. Biochem.*, 231: 374-382.
- [87] Sabatini, A. Vacca, A. and Gans, P., (1974). "Miniquad. General computer program for the computation of formation constants from potentiometric data", *Talanta*, 21: 53-77.
- [88] Gampp, H. Maeder, M. Meyer, C.J. and Zuberbuehler, A.D., (1985). "Calculation of equilibrium constants from multiwavelength spectroscopic data - I. Mathematical considerations", *Talanta*, 32: 95-101.
- [89] Gans, P. Sabatini, A. and Vacca, A., (1985). "SUPERQUAD: an improved general program for computation of formation constants from potentiometric data", *J. Chem. Soc., Dalton Trans.*: 1195-1200.
- [90] Zuberbuehler, A.D. and Kaden, T.A., (1982). "TITFIT, a comprehensive program for numerical treatment of potentiometric data by using analytical derivatives and automatically optimized subroutines with the Newton-Gauss-Marquardt algorithm", *Talanta*, 29: 201-206.
- [91] "Jplus consulting ", Available at: <http://jplusconsulting.com/products/reactlab-equilibria/>. Accessed 13.12, 2013.
- [92] Tauler, R. and Casassas, E., (1989). "Principal component analysis applied to the study of successive complex formation data in Cu(II)–ethanolamine systems", *Journal of Chemometrics*, 3: 151-161.
- [93] Ayscough, P.B. Brooks, B.R. and Evans, H.E., (1964). "Electron spin resonance studies on the photolysis of azo compounds at -196°", *J. Phys. Chem.*, 68: 3889-3890.
- [94] Varga, L.P. and Veatch, F.C., (1967). "Nature of hafnium-chloranilic acid metallochrome by matrix rank, contour mapping, and iterative analysis of absorption spectra", *Anal. Chem.*, 39: 1101-1109.
- [95] Malinowski, E.R., (1977). "Theory of error in factor analysis", *Anal. Chem.*, 49: 606-612.
- [96] Malinowski, E.R., (1977). "Determination of the number of factors and the experimental error in a data matrix", *Anal. Chem.*, 49: 612-617.

- [97] Cartwright, H., (1987). "Determination of the dimensionality of spectroscopic data by submatrix analysis", *Journal of Chemometrics*, 1: 111-120.
- [98] Gampp, H. Maeder, M. Meyer, C.J. and Zuberbuehler, A.D., (1986). "Calculation of equilibrium constants from multiwavelength spectroscopic data - IV. Model-free least-squares refinement by use of evolving factor analysis", *Talanta*, 33: 943-951.
- [99] Tauler, P. and Casassas, E., (1989). "Application of principal component analysis to the study of multiple equilibria systems. Study of copper(II)/salicylate/mono-, di- and triethanolamine systems", *Anal. Chim. Acta*, 223: 257-268.
- [100] Tauler, R. Casassas, E. and Izquierdo-Ridorsa, A., (1991). "Self-modeling curve resolution in studies of spectrometric titrations of multiequilibria systems by factor analysis", *Anal. Chim. Acta*, 248: 447-458.
- [101] Casassas, E. Tauler, R. and Marques, I., (1994). "Interactions of H<sup>+</sup> and Cu(II) Ions with Poly(adenylic acid): Study by Factor Analysis", *Macromolecules*, 27: 1729-1737.
- [102] Tulu, M. and Geckeler, K.E., (1999). "Synthesis and properties of hydrophilic polymers. Part 7. Preparation, characterization and metal complexation of carboxy-functional polyesters based on poly(ethylene glycol)", *Polym. Int.*, 48: 909-914.
- [103] Rivas, B.L. Pereira, E.D. and Moreno-Villoslada, I., (2003). "Water-soluble polymer–metal ion interactions", *Progress in Polymer Science*, 28: 173-208.
- [104] Cojocar, C. and Zakrzewska-Trznadel, G., (2007). "Response surface modeling and optimization of copper removal from aqua solutions using polymer assisted ultrafiltration", *Journal of Membrane Science*, 298: 56-70.
- [105] Cañizares, P. Pérez, A. Camarillo, R. and Linares, J.J., (2004). "A semi-continuous laboratory-scale polymer enhanced ultrafiltration process for the recovery of cadmium and lead from aqueous effluents", *Journal of Membrane Science*, 240: 197-209.
- [106] Korus, I. Bodzek, M. and Loska, K., (1999). "Removal of zinc and nickel ions from aqueous solutions by means of the hybrid complexation–ultrafiltration process", *Separation and Purification Technology*, 17: 111-116.
- [107] Maketon, W. and Ogden, K.L., (2009). "Synergistic effects of citric acid and polyethyleneimine to remove copper from aqueous solutions", *Chemosphere*, 75: 206-211.
- [108] Muslehiddinoglu, J. Uludag, Y. Ozbelge, H.O. and Yilmaz, L., (1998). "Effect of operating parameters on selective separation of heavy metals from binary mixtures via polymer enhanced ultrafiltration", *J. Membr. Sci.*, 140: 251-266.
- [109] Molinari, R. Poerio, T. and Argurio, P., (2008). "Selective separation of copper(II) and nickel(II) from aqueous media using the complexation–ultrafiltration process", *Chemosphere*, 70: 341-348.

- [110] Juang, R.-S. and Chiou, C.-H., (2000). "Ultrafiltration rejection of dissolved ions using various weakly basic water-soluble polymers", *Journal of Membrane Science*, 177: 207-214.
- [111] Aroua, M.K. Zuki, F.M. and Sulaiman, N.M., (2007). "Removal of chromium ions from aqueous solutions by polymer-enhanced ultrafiltration", *Journal of Hazardous Materials*, 147: 752-758.
- [112] Zakrzewska-Trznadel, G. and Harasimowicz, M., (2002). "Removal of radionuclides by membrane permeation combined with complexation", *Desalination*, 144: 207-212.
- [113] Cojocar, C. Zakrzewska-Trznadel, G. and Jaworska, A., (2009). "Removal of cobalt ions from aqueous solutions by polymer assisted ultrafiltration using experimental design approach. part 1: Optimization of complexation conditions", *Journal of Hazardous Materials*, 169: 599-609.
- [114] Cojocar, C. Zakrzewska-Trznadel, G. and Miskiewicz, A., (2009). "Removal of cobalt ions from aqueous solutions by polymer assisted ultrafiltration using experimental design approach: Part 2: Optimization of hydrodynamic conditions for a crossflow ultrafiltration module with rotating part", *Journal of Hazardous Materials*, 169: 610-620.
- [115] Dambies, L. Jaworska, A. Zakrzewska-Trznadel, G. and Sartowska, B., (2010). "Comparison of acidic polymers for the removal of cobalt from water solutions by polymer assisted ultrafiltration", *Journal of Hazardous Materials*, 178: 988-993.
- [116] Stumm, W. and Morgan, J.J., (1996). *Aquatic chemistry: chemical equilibria and rates in natural waters*: Wiley.
- [117] Geckeler, K.E. and Volchek, K., (1996). "Removal of Hazardous Substances from Water Using Ultrafiltration in Conjunction with Soluble Polymers", *Environmental Science & Technology*, 30: 725-734.
- [118] Spivakov, B.Y. Geckeler, K. and Bayer, E., (1985). "Liquid-phase polymer-based retention - the separation of metals by ultrafiltration on polychelators", *Nature (London)*, 315: 313-315.
- [119] Juang, R.-S. and Chen, M.-N., (1997). "Removal of Copper(II) Chelates of EDTA and NTA from Dilute Aqueous Solutions by Membrane Filtration", *Ind. Eng. Chem. Res.*, 36: 179-186.
- [120] Sanli, O. and Asman, G., (2000). "Removal of Fe(III) ions from dilute aqueous solutions by alginic acid-enhanced ultrafiltration", *J. Appl. Polym. Sci.*, 77: 1096-1101.
- [121] Canizares, P. Perez, A. and Camarillo, R., (2002). "Recovery of heavy metals by means of ultrafiltration with water-soluble polymers: calculation of design parameters", *Desalination*, 144: 279-285.
- [122] Diallo, M.S. Christie, S. Swaminathan, P. Johnson, J.H. and Goddard, W.A., (2005). "Dendrimer Enhanced Ultrafiltration. 1. Recovery of Cu(II) from Aqueous Solutions Using PAMAM Dendrimers with Ethylene Diamine Core and Terminal NH<sub>2</sub> Groups", *Environmental Science & Technology*, 39: 1366-1377.

- [123] Diallo, M.S., (2009). Chapter 11 - Water Treatment by Dendrimer-Enhanced Filtration: Principles and Applications, N. Savage Diallo, M. Duncan, J. Street, A. and Sustich, R., ed. Nanotechnology Applications for Clean Water. Boston: William Andrew Publishing, 143-155.
- [124] Jawor, A. and Hoek, E.M.V., (2010). "Removing Cadmium Ions from Water via Nanoparticle-Enhanced Ultrafiltration", *Environmental Science & Technology*, 44: 2570-2576.
- [125] Rether, A. and Schuster, M., (2003). "Selective separation and recovery of heavy metal ions using water-soluble N-benzoylthiourea modified PAMAM polymers", *Reactive and Functional Polymers*, 57: 13-21.
- [126] Crooks, R.M. Zhao, M. Sun, L. Chechik, V. and Yeung, L.K., (2001). "Dendrimer-encapsulated metal nanoparticles: synthesis, characterization, and applications to catalysis", *Accounts of Chemical Research*, 34: 181-190.
- [127] Knapen, J.W.J. van, d.M.A.W. de, W.J.C. van, L.P.W.N.M. Wijkens, P. Grove, D.M. and van, K.G., (1994). "Homogeneous catalysts based on silane dendrimers functionalized with arylnickel(II) complexes", *Nature (London)*, 372: 659-663.
- [128] Tomalia, D.A. and Dvornic, P.R., (1994). "What promise for dendrimers?", *Nature (London)*, 372: 617-618.
- [129] Alivisatos, A.P., (1996). "Semiconductor Clusters, Nanocrystals, and Quantum Dots", *Science*, 271: 933-937.
- [130] Balogh, L. and Tomalia, D.A., (1998). "Poly(Amidoamine) Dendrimer-Templated Nanocomposites. 1. Synthesis of Zerovalent Copper Nanoclusters", *Journal of the American Chemical Society*, 120: 7355-7356.
- [131] Zhao, M. Sun, L. and Crooks, R.M., (1998). "Preparation of Cu Nanoclusters within Dendrimer Templates", *Journal of the American Chemical Society*, 120: 4877-4878.
- [132] Esumi, K. Suzuki, A. Yamahira, A. and Torigoe, K., (2000). "Role of Poly(amidoamine) Dendrimers for Preparing Nanoparticles of Gold, Platinum, and Silver", *Langmuir*, 16: 2604-2608.
- [133] Gröhn, F. Bauer, B.J. Akpalu, Y.A. Jackson, C.L. and Amis, E.J., (2000). "Dendrimer Templates for the Formation of Gold Nanoclusters", *Macromolecules*, 33: 6042-6050.
- [134] Zheng, J. and Dickson, R.M., (2002). "Individual Water-Soluble Dendrimer-Encapsulated Silver Nanodot Fluorescence", *Journal of the American Chemical Society*, 124: 13982-13983.
- [135] Zhao, M. and Crooks, R.M., (1999). "Intradendrimer Exchange of Metal Nanoparticles", *Chemistry of Materials*, 11: 3379-3385.
- [136] Curtis, A.C. Duff, D.G. Edwards, P.P. Jefferson, D.A. Johnson, B.F.G. Kirkland, A.I. and Wallace, A.S., (1988). "A Morphology-Selective Copper Organosol", *Angewandte Chemie International Edition in English*, 27: 1530-1533.

- [137] Lisiecki, I. and Pileni, M.P., (1993). "Synthesis of copper metallic clusters using reverse micelles as microreactors", *Journal of the American Chemical Society*, 115: 3887-3896.
- [138] Chen, P. Yang, Y. Bhattacharya, P. Wang, P. and Ke, P.C., (2011). "A Tris-Dendrimer for Hosting Diverse Chemical Species", *The Journal of Physical Chemistry C*, 115: 12789-12796.
- [139] Beezer, A. King, A. Martin, I. Mitchel, J. Twyman, L. and Wain, C., (2003). "Dendrimers as potential drug carriers; encapsulation of acidic hydrophobes within water soluble PAMAM derivatives", *Tetrahedron*, 59: 3873-3880.
- [140] Twyman, L.J. Beezer, A.E. Esfand, R. Hardy, M.J. and Mitchell, J.C., (1999). "The synthesis of water soluble dendrimers, and their application as possible drug delivery systems", *Tetrahedron Letters*, 40: 1743-1746.
- [141] Liu, M. Kono, K. and Fréchet, J.M., (2000). "Water-soluble dendritic unimolecular micelles:: Their potential as drug delivery agents", *Journal of Controlled Release*, 65: 121-131.
- [142] Esfand, R. and Tomalia, D.A., (2001). "Poly(amidoamine) (PAMAM) dendrimers: from biomimicry to drug delivery and biomedical applications", *Drug Discovery Today*, 6: 427-436.
- [143] Beezer, A.E. King, A.S.H. Martin, I.K. Mitchell, J.C. Twyman, L.J. and Wain, C.F., (2003). "Dendrimers as potential drug carriers; encapsulation of acidic hydrophobes within water soluble PAMAM derivatives", *Tetrahedron*, 59: 3873-3880.
- [144] Kolhe, P. Misra, E. Kannan, R.M. Kannan, S. and Lieh-Lai, M., (2003). "Drug complexation, in vitro release and cellular entry of dendrimers and hyperbranched polymers", *International Journal of Pharmaceutics*, 259: 143-160.
- [145] Milhem, O.M. Myles, C. McKeown, N.B. Attwood, D. and D'Emanuele, A., (2000). "Polyamidoamine Starburst® dendrimers as solubility enhancers", *International Journal of Pharmaceutics*, 197: 239-241.
- [146] Abderrezak, A. Bourassa, P. Mandeville, J.S. Sedaghat-Herati, R. and Tajmir-Riahi, H.A., (2012). "Dendrimers bind antioxidant polyphenols and cisplatin drug", *PloS one*, 7: e33102.
- [147] Devarakonda, B. Otto, D.P. Judefeind, A. Hill, R.A. and de Villiers, M.M., (2007). "Effect of pH on the solubility and release of furosemide from polyamidoamine (PAMAM) dendrimer complexes", *International Journal of Pharmaceutics*, 345: 142-153.
- [148] Yiyun, C. Tongwen, X. and Rongqiang, F., (2005). "Polyamidoamine dendrimers used as solubility enhancers of ketoprofen", *European Journal of Medicinal Chemistry*, 40: 1390-1393.
- [149] Yiyun, C. and Tongwen, X., (2005). "Solubility of nicotinic acid in polyamidoamine dendrimer solutions", *European Journal of Medicinal Chemistry*, 40: 1384-1389.

- [150] Filipowicz, A. and Wołowicz, S., (2011). "Solubility and in vitro transdermal diffusion of riboflavin assisted by PAMAM dendrimers", *International Journal of Pharmaceutics*, 408: 152-156.
- [151] Giordanengo, R. Mazarin, M. Wu, J. Peng, L. and Charles, L., (2007). "Propagation of structural deviations of poly(amidoamine) fan-shape dendrimers (generations 0–3) characterized by MALDI and electrospray mass spectrometry", *International Journal of Mass Spectrometry*, 266: 62-75.
- [152] Brothers Ii, H.M. Piehler, L.T. and Tomalia, D.A., (1998). "Slab-gel and capillary electrophoretic characterization of polyamidoamine dendrimers", *Journal of Chromatography A*, 814: 233-246.
- [153] Joliffe, I. and Morgan, B., (1992). "Principal component analysis and exploratory factor analysis", *Statistical methods in medical research*, 1: 69-95.
- [154] Martens, H., (1991). *Multivariate calibration*: John Wiley & Sons.
- [155] Martens, H. and Martens, M., (2000). "Modified Jack-knife estimation of parameter uncertainty in bilinear modelling by partial least squares regression (PLSR)", *Food quality and preference*, 11: 5-16.
- [156] Aşçı, B. Dönmez, Ö.A. Bozdoğan, A. and Sungur, S., (2011). "Simultaneous Determination of Paracetamol, Pseudoephedrine Hydrochloride, and Dextromethorphan Hydrobromide in Tablets Using Multivariate Calibration Methods Coupled With HPLC-DAD", *Journal of Liquid Chromatography & Related Technologies*, 34: 1686-1698.
- [157] Dönmez, Ö.A. Aşçı, B. Bozdoğan, A. and Sungur, S., (2011). "Simultaneous determination of potassium guaiacolsulfonate, guaifenesin, diphenhydramine HCl and carbetapentane citrate in syrups by using HPLC-DAD coupled with partial least squares multivariate calibration", *Talanta*, 83: 1601-1605.
- [158] Dinç, E. Yücesoy, C. and Onur, F., (2002). "Simultaneous spectrophotometric determination of mefenamic acid and paracetamol in a pharmaceutical preparation using ratio spectra derivative spectrophotometry and chemometric methods", *Journal of Pharmaceutical and Biomedical Analysis*, 28: 1091-1100.
- [159] Palabiyik, İ.M. Dinç, E. and Onur, F., (2004). "Simultaneous spectrophotometric determination of pseudoephedrine hydrochloride and ibuprofen in a pharmaceutical preparation using ratio spectra derivative spectrophotometry and multivariate calibration techniques", *Journal of Pharmaceutical and Biomedical Analysis*, 34: 473-483.
- [160] Autumn, K. Liang, Y.A. Hsleh, S.T. Zesch, W. Chan, W.P. Kenny, T.W. Fearilng, R. and Full, R.J., (2000). "Adhesive force of a single gecko foot-hair", *Nature (London)*, 405: 681-686.
- [161] Sunder, A. Heinemann, J. and Frey, H., (2000). "Controlling the growth of polymer trees: concepts and perspectives for hyperbranched polymers", *Chemistry*, 6: 2499-2506.
- [162] Burchard, W., (1972). "Angular distribution of rayleigh scattering from branched polycondensates. Amylopectin and glycogen types", *Macromolecules*, 5: 604-610.

- [163] Buhleier, E. Wehner, W. and Vögtle, F., (1978). "'Cascade"- and "Nonskid-Chain-like" Syntheses of Molecular Cavity Topologies", *Synthesis-stuttgart*, 1978: 155-158.
- [164] Tomalia, D.A. Baker, H. Dewald, J. Hall, M. Kallos, G. Martin, S. Roeck, J. Ryder, J. and Smith, P., (1985). "A New Class of Polymers - Starburst-Dendritic Macromolecules", *Polymer Journal*, 17: 117-132.
- [165] Fischer, M. and Vögtle, F., (1999). "Dendrimers: From Design to Application—A Progress Report", *Angewandte Chemie International Edition*, 38: 884-905.
- [166] Archut, A. and Vogtle, F., (1998). "Functional cascade molecules", *Chem Soc Rev*, 27: 233-240.
- [167] Tomalia, D.A., (2005). "Birth of a new macromolecular architecture: dendrimers as quantized building blocks for nanoscale synthetic polymer chemistry", *Progress in Polymer Science*, 30: 294-324.
- [168] Supattapone, S. Nguyen, H.-O.B. Cohen, F.E. Prusiner, S.B. and Scott, M.R., (1999). "Elimination of prions by branched polyamines and implications for therapeutics", *Proceedings of the National Academy of Sciences*, 96: 14529-14534.
- [169] Hawker, C.J. Wooley, K.L. and Frechet, J.M.J., (1993). "Unimolecular micelles and globular amphiphiles: dendritic macromolecules as novel recyclable solubilization agents", *J. Chem. Soc., Perkin Trans. 1*: 1287-1297.
- [170] Turnbull, W.B. and Stoddart, J.F., (2002). "Design and synthesis of glycodendrimers", *Rev. Mol. Biotechnol.*, 90: 231-255.
- [171] Roy, R. and Kim, J.M., (1999). "Amphiphilic p-tert-butylcalix[4]arene scaffolds containing exposed carbohydrate dendrons", *Angew. Chem., Int. Ed.*, 38: 369-372.
- [172] Majoral, J.-P. and Caminade, A.-M., (1999). "Dendrimers Containing Heteroatoms (Si, P, B, Ge, or Bi)", *Chem. Rev. (Washington, D. C.)*, 99: 845-880.
- [173] Newkome, G.R. Moorefield, C.N. and Vögtle, F., (2008). *Dendritic Molecules: Concepts, Syntheses, Perspectives*: Wiley.
- [174] Zeng, F. and Zimmerman, S.C., (1997). "Dendrimers in supramolecular chemistry: from molecular recognition to self-assembly", *Chem. Rev. (Washington, D. C.)*, 97: 1681-1712.
- [175] Moors, R. and Voegtle, F., (1993). "Preparation of dendrimeric polyamines", *Chem. Ber.*, 126: 2133-2135.
- [176] Boas, U. and Heegaard, P.M.H., (2004). "Dendrimers in drug research", *Chem Soc Rev*, 33: 43-63.
- [177] Hawker, C.J. and Frechet, J.M.J., (1990). "Preparation of polymers with controlled molecular architecture. A new convergent approach to dendritic macromolecules", *J. Am. Chem. Soc.*, 112: 7638-7647.
- [178] Miller, T.M. and Neenan, T.X., (1990). "Convergent synthesis of monodisperse dendrimers based upon 1,3,5-trisubstituted benzenes", *Chem. Mater.*, 2: 346-349.

- [179] Antoni, P. Hed, Y. Nordberg, A. Nyström, D. von Holst, H. Hult, A. and Malkoch, M., (2009). "Bifunctional Dendrimers: From Robust Synthesis and Accelerated One-Pot Postfunctionalization Strategy to Potential Applications", *Angewandte Chemie International Edition*, 48: 2126-2130.
- [180] McElhanon, J.R. and McGrath, D.V., (2000). "Toward Chiral Polyhydroxylated Dendrimers. Preparation and Chiroptical Properties", *The Journal of Organic Chemistry*, 65: 3525-3529.
- [181] Liang, C.O. and Fréchet, J.M.J., (2005). "Incorporation of Functional Guest Molecules into an Internally Functionalizable Dendrimer through Olefin Metathesis", *Macromolecules*, 38: 6276-6284.
- [182] Hecht, S. and Fréchet, J.M.J., (2001). "Dendritic Encapsulation of Function: Applying Nature's Site Isolation Principle from Biomimetics to Materials Science", *Angewandte Chemie International Edition*, 40: 74-91.
- [183] Nanjwade, B.K. Behra, H.M. Derkar, G.K. Manvi, F.V. and Nanjwade, V.K., (2009). "Dendrimers: Emerging polymers for drug-delivery systems", *European Journal of Pharmaceutical Sciences*, 38: 185-196.
- [184] Frechet, J., (1994). "Functional polymers and dendrimers: reactivity, molecular architecture, and interfacial energy", *Science*, 263: 1710-1715.
- [185] Mourey, T.H. Turner, S.R. Rubinstein, M. Frechet, J.M.J. Hawker, C.J. and Wooley, K.L., (1992). "Unique behavior of dendritic macromolecules: intrinsic viscosity of polyether dendrimers", *Macromolecules*, 25: 2401-2406.
- [186] Roberts, J.C. Bhargat, M.K. and Zera, R.T., (1996). "Preliminary biological evaluation of polyamidoamine (PAMAM) Starburst dendrimers", *J Biomed Mater Res*, 30: 53-65.
- [187] Malik, N. Wiwattanapatapee, R. Klopsch, R. Lorenz, K. Frey, H. Weener, J.W. Meijer, E.W. Paulus, W. and Duncan, R., (2000). "Dendrimers: relationship between structure and biocompatibility in vitro, and preliminary studies on the biodistribution of 125I-labelled polyamidoamine dendrimers in vivo", *J Control Release*, 65: 133-148.
- [188] Jevprasesphant, R. Penny, J. Jalal, R. Attwood, D. McKeown, N.B. and D'Emanuele, A., (2003). "The influence of surface modification on the cytotoxicity of PAMAM dendrimers", *Int. J. Pharm.*, 252: 263-266.
- [189] Dykes, G.M., (2001). "Dendrimers: a review of their appeal and applications", *Journal of Chemical Technology & Biotechnology*, 76: 903-918.
- [190] Balzani, V. Ceroni, P. Gestermann, S. Kauffmann, C. Gorka, M. and Vogtle, F., (2000). "Dendrimers as fluorescent sensors with signal amplification", *Chem. Commun. (Cambridge)*: 853-854.
- [191] Valerio, C. Fillaut, J.-L. Ruiz, J. Guittard, J. Blais, J.-C. and Astruc, D., (1997). "The dendritic effect in molecular recognition: ferrocene dendrimers and their use as supramolecular redox sensors for the recognition of small inorganic anions", *J. Am. Chem. Soc.*, 119: 2588-2589.

- [192] James, T.D. Shinmori, H. Takeuchi, M. and Shinkai, S., (1996). "A saccharide 'sponge'. Synthesis and properties of a dendritic boronic acid", *Chem. Commun.*: 705-706.
- [193] Fischer, M. and Vogtle, F., (1999). "Dendrimers: from design to application - a progress report", *Angew. Chem., Int. Ed.*, 38: 885-905.
- [194] Wiener, E.C. Brechbiel, M.W. Brothers, H. Magin, R.L. Gansow, O.A. Tomalia, D.A. and Lauterbur, P.C., (1994). "Dendrimer-based metal chelates: a new class of magnetic resonance imaging contrast agents", *Magn. Reson. Med.*, 31: 1-8.
- [195] Toth, E. Pubanz, D. Vauthey, S. Helm, L. and Merbach, A.E., (1996). "High-pressure NMR kinetics. 72. The role of water exchange in attaining maximum relaxivities for dendrimeric MRI contrast agents", *Chem. - Eur. J.*, 2: 1607-1615.
- [196] Van, H.R. Kamer, P.C.J. Van, L.P.W.N.M. and Reek, J.N.H., (2002). "Dendrimers as Support for Recoverable Catalysts and Reagents", *Chem. Rev.* (Washington, DC, U. S.), 102: 3717-3756.
- [197] Scott, R.W.J. Datye, A.K. and Crooks, R.M., (2003). "Bimetallic Palladium-Platinum Dendrimer-Encapsulated Catalysts", *J. Am. Chem. Soc.*, 125: 3708-3709.
- [198] Kollner, C. and Togni, A., (2001). "Synthesis, characterization, and application in asymmetric catalysis of dendrimers containing chiral ferrocenyl diphosphines", *Can. J. Chem.*, 79: 1762-1774.
- [199] Yang, Z.-w. Kang, Q.-x. Ma, H.-c. Li, C.-l. and Lei, Z.-q., (2004). "Oxidation of cyclohexene by dendritic PAMAMSA-Mn(II) complexes", *J. Mol. Catal. A: Chem.*, 213: 169-176.
- [200] Bedford, R.B. Singh, U.G. Walton, R.I. Williams, R.T. and Davis, S.A., (2005). "Nanoparticulate palladium supported by covalently modified silicas: synthesis, characterization, and application as catalysts for the Suzuki coupling of aryl halides", *Chem. Mater.*, 17: 701-707.
- [201] Ottaviani, M.F. Bossmann, S. Turro, N.J. and Tomalia, D.A., (1994). "Characterization of starburst dendrimers by the EPR technique. 1. Copper complexes in water solution", *Journal of the American Chemical Society*, 116: 661-671.
- [202] Kreibig, U. and Vollmer, M., (2010). *Optical Properties of Metal Clusters*: Springer.
- [203] Morgan, M.T. Nakanishi, Y. Kroll, D.J. Griset, A.P. Carnahan, M.A. Wathier, M. Oberlies, N.H. Manikumar, G. Wani, M.C. and Grinstaff, M.W., (2006). "Dendrimer-Encapsulated Camptothecins: Increased Solubility, Cellular Uptake, and Cellular Retention Affords Enhanced Anticancer Activity In vitro", *Cancer Research*, 66: 11913-11921.
- [204] Tekade, R.K. Dutta, T. Gajbhiye, V. and Jain, N.K., (2009). "Exploring dendrimer towards dual drug delivery: pH responsive simultaneous drug-release kinetics", *Journal of Microencapsulation*, 26: 287-296.

- [205] Dutta, T. and Jain, N.K., (2007). "Targeting potential and anti-HIV activity of lamivudine loaded mannosylated poly (propyleneimine) dendrimer", *Biochim Biophys Acta*, 1770: 681-686.
- [206] Dutta, T. Garg, M. and Jain, N.K., (2008). "Targeting of efavirenz loaded tuftsin conjugated poly(propyleneimine) dendrimers to HIV infected macrophages in vitro", *Eur J Pharm Sci*, 34: 181-189.
- [207] Dutta, T. Agashe, H.B. Garg, M. Balakrishnan, P. Kabra, M. and Jain, N.K., (2007). "Poly (propyleneimine) dendrimer based nanocontainers for targeting of efavirenz to human monocytes/macrophages in vitro", *J Drug Target*, 15: 89-98.
- [208] Morgan, M.T. Nakanishi, Y. Kroll, D.J. Griset, A.P. Carnahan, M.A. Wathier, M. Oberlies, N.H. Manikumar, G. Wani, M.C. and Grinstaff, M.W., (2006). "Dendrimer-encapsulated camptothecins: increased solubility, cellular uptake, and cellular retention affords enhanced anticancer activity in vitro", *Cancer Res*, 66: 11913-11921.
- [209] Cheng, Y. Wu, Q. Li, Y. and Xu, T., (2008). "External electrostatic interaction versus internal encapsulation between cationic dendrimers and negatively charged drugs: which contributes more to solubility enhancement of the drugs?", *J Phys Chem B*, 112: 8884-8890.
- [210] Liu, M. Kono, K. and Fréchet, J.M.J., (2000). "Water-soluble dendritic unimolecular micelles:: Their potential as drug delivery agents", *Journal of Controlled Release*, 65: 121-131.
- [211] Newkome, G.R. Yao, Z. Baker, G.R. and Gupta, V.K., (1985). "Micelles. Part 1. Cascade molecules: a new approach to micelles. A [27]-arborol", *The Journal of Organic Chemistry*, 50: 2003-2004.
- [212] Stevelmans, S. van Hest, J.C.M. Jansen, J.F.G.A. van Boxtel, D.A.F.J. de Brabander-van den Berg, E.M.M. and Meijer, E.W., (1996). "Synthesis, Characterization, and Guest-Host Properties of Inverted Unimolecular Dendritic Micelles", *Journal of the American Chemical Society*, 118: 7398-7399.
- [213] Devarakonda, B. Hill, R.A. and de Villiers, M.M., (2004). "The effect of PAMAM dendrimer generation size and surface functional group on the aqueous solubility of nifedipine", *International Journal of Pharmaceutics*, 284: 133-140.
- [214] Chauhan, A.S. Sridevi, S. Chalasani, K.B. Jain, A.K. Jain, S.K. Jain, N.K. and Diwan, P.V., (2003). "Dendrimer-mediated transdermal delivery: enhanced bioavailability of indomethacin", *Journal of Controlled Release*, 90: 335-343.
- [215] Lee, I. Athey, B.D. Wetzel, A.W. Meixner, W. and Baker, J.R., Jr., (2002). "Structural Molecular Dynamics Studies on Polyamidoamine Dendrimers for a Therapeutic Application: Effects of pH and Generation", *Macromolecules*, 35: 4510-4520.
- [216] Rietveld, I.B. Bouwman, W.G. Baars, M.W.P.L. and Heenan, R.K., (2001). "Location of the Outer Shell and Influence of pH on Carboxylic Acid-Functionalized Poly(propyleneimine) Dendrimers", *Macromolecules*, 34: 8380-8383.

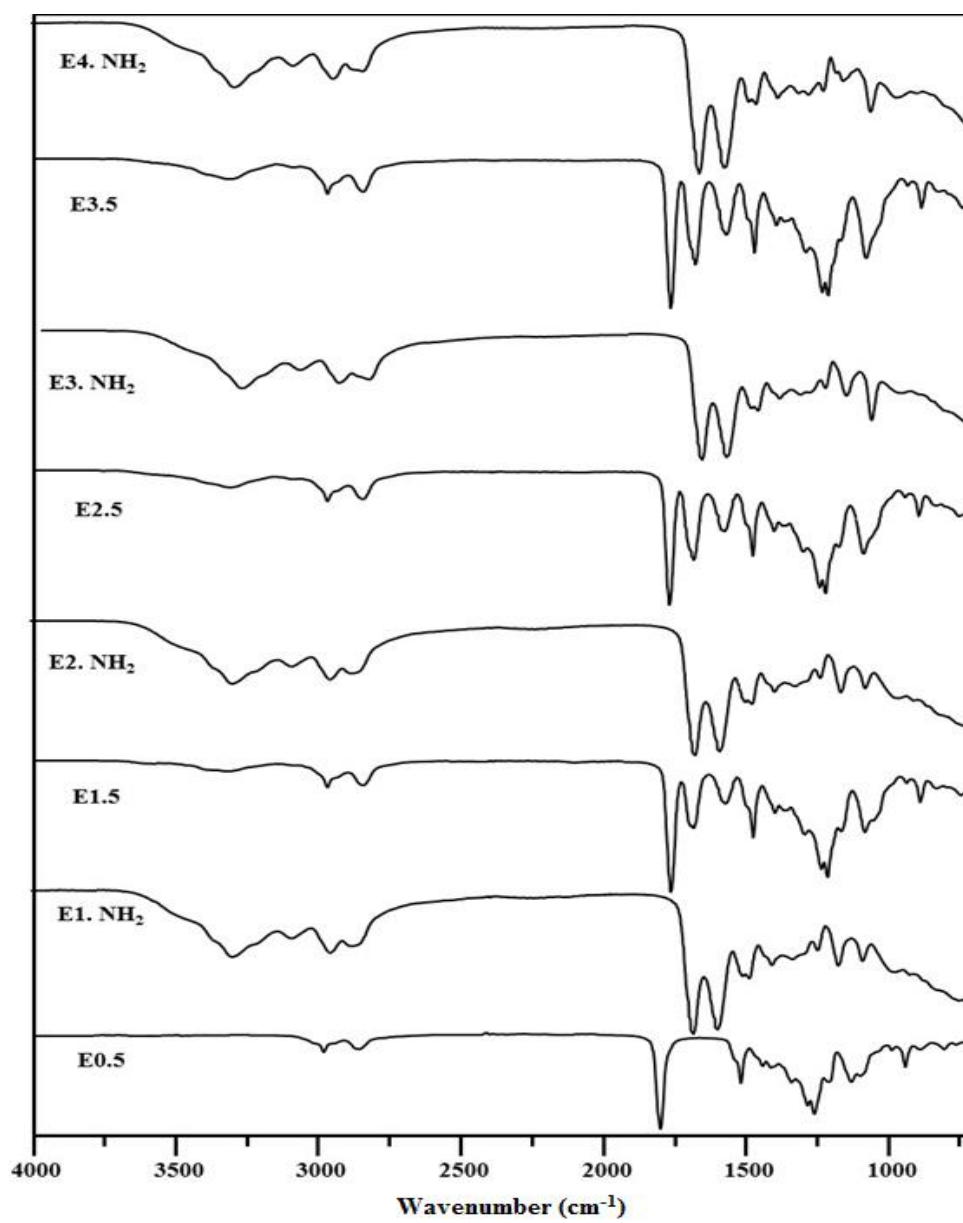
- [217] Asthana, A. Chauhan, A. Diwan, P. and Jain, N., (2005). "Poly(amidoamine) (PAMAM) dendritic nanostructures for controlled sitespecific delivery of acidic anti-inflammatory active ingredient", *AAPS PharmSciTech*, 6: E536-E542.
- [218] Palencia, M. Rivas, B.L. Pereira, E. Hernández, A. and Prádanos, P., (2009). "Study of polymer–metal ion–membrane interactions in liquid-phase polymer-based retention (LPR) by continuous diafiltration", *J. Membrane Sci.*, 336: 128-139.
- [219] Diallo, M.S. Arasho, W. Johnson Jr, J.H. and Goddard Iii, W.A., (2008). "Dendritic chelating agents. 2. U (VI) binding to poly (amidoamine) and poly (propyleneimine) dendrimers in aqueous solutions", *Environmental Science & Technology*, 42: 1572-1579.
- [220] Hayes, B.L., (2002). *Microwave synthesis: chemistry at the speed of light*: CEM Pub.
- [221] (1989). "Introduction to Microwave Sample Preparation: Theory and Practice", *Analytical Chemistry*, 61: 330A-330A.
- [222] Pearson, K., (1901). "LIII. On lines and planes of closest fit to systems of points in space", *Philosophical Magazine Series 6*, 2: 559-572.
- [223] Hotelling, H., (1933). "Analysis of a complex of statistical variables into principal components", *Journal of educational psychology*, 24: 417.
- [224] Abdi, H. and Williams, L.J., (2010). "Principal component analysis", *Wiley Interdisciplinary Reviews: Computational Statistics*, 2: 433-459.
- [225] Esbensen, K.H. and Geladi, P., (2009). 2.13 - Principal Component Analysis: Concept, Geometrical Interpretation, Mathematical Background, Algorithms, History, Practice, S.D. Brown Tauler, R. and Walczak, B., ed. *Comprehensive Chemometrics*. Oxford: Elsevier, 211-226.
- [226] Brereton, R., (2009). *Chemometrics for Pattern Recognition*: Wiley.
- [227] Brereton, R.G., (2003). *Chemometrics: data analysis for the laboratory and chemical plant*: John Wiley & Sons.
- [228] Martens, H. and Naes, T., (1989). *Multivariate Calibration*: Wiley.
- [229] Otto, M., (2007). *Chemometrics*: Wiley.
- [230] Malinowski, E.R., (1991). *Factor Analysis in Chemistry*: Wiley.
- [231] Maeder, M. and de Juan, A., (2009). 2.16 - Two-Way Data Analysis: Evolving Factor Analysis, S.D. Brown Tauler, R. and Walczak, B., ed. *Comprehensive Chemometrics*. Oxford: Elsevier, 261-274.
- [232] Gampp, H. Maeder, M. Meyer, C.J. and Zuberbuehler, A.D., (1985). "Evolving factor analysis of spectrophotometric titrations: forget about the law of mass action?", *Chimia*, 39: 315-317.
- [233] de Juan, A. Rutan, S.C. and Tauler, R., (2009). 2.19 - Two-Way Data Analysis: Multivariate Curve Resolution – Iterative Resolution Methods, S.D. Brown Tauler, R. and Walczak, B., ed. *Comprehensive Chemometrics*. Oxford: Elsevier, 325-344.

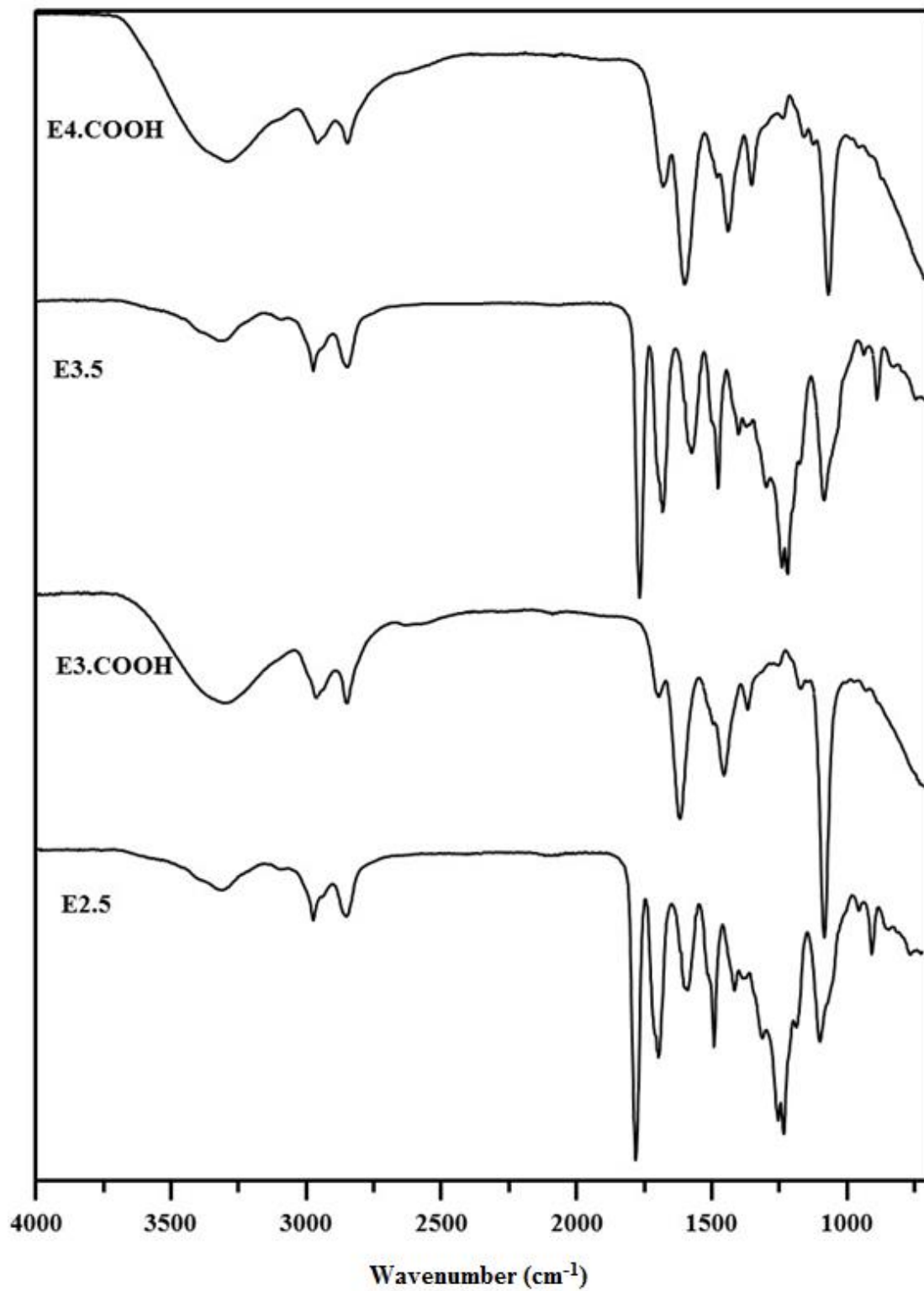
- [234] Vandeginste, B.G.M. Derks, W. and Kateman, G., (1985). "Multicomponent self-modeling curve resolution in high-performance liquid chromatography by iterative target transformation analysis", *Anal. Chim. Acta*, 173: 253-264.
- [235] Gemperline, P.J., (1984). "A priori estimates of the elution profiles of the pure components in overlapped liquid chromatography peaks using target factor analysis", *J. Chem. Inf. Comput. Sci.*, 24: 206-212.
- [236] Tauler, R. Smilde, A. and Kowalski, B., (1995). "Selectivity, local rank, three-way data analysis and ambiguity in multivariate curve resolution", *Journal of Chemometrics*, 9: 31-58.
- [237] Tauler, R., (1995). "Multivariate curve resolution applied to second order data", *Chemom. Intell. Lab. Syst.*, 30: 133-146.
- [238] Mason, C. Maeder, M. and Whitson, A., (2001). "Resolving factor analysis", *Anal Chem*, 73: 1587-1594.
- [239] Maeder, M. and Neuhold, Y.M., (2007). *Practical Data Analysis in Chemistry*: Elsevier Science.
- [240] Manne, R. and Grande, B.-V., (2000). "Resolution of two-way data from hyphenated chromatography by means of elementary matrix transformations", *Chemometrics and Intelligent Laboratory Systems*, 50: 35-46.
- [241] Mahalanobis, P.C., (1936). "On the generalized distance in statistics", *Proceedings of the National Institute of Sciences (Calcutta)*, 2: 49-55.
- [242] Ward, J.H., (1963). "Hierarchical Grouping to Optimize an Objective Function", *Journal of the American Statistical Association*, 58: 236-244.
- [243] Wise, M.B.G., N. B. Bro, R. Shaver, J. M. Winding, W. Koch, R. S., (2006). *Chemometrics Tutorial for PLS\_Toolbox and Solo*, USA: Eigenvector Research, Inc.
- [244] Erickson, C.L. Lysaght, M.J. and Callis, J.B., (1992). "Relationship between digital filtering and multivariate regression in quantitative analysis", *Analytical Chemistry*, 64: 1155A-1163A.
- [245] Næs, T. and Martens, H., (1988). "Principal component regression in NIR analysis: Viewpoints, background details and selection of components", *Journal of Chemometrics*, 2: 155-167.
- [246] Esbensen, K.H. Guyot, D. Westad, F. and Houmoller, L.P., (2002). *Multivariate Data Analysis: In Practice : an Introduction to Multivariate Data Analysis and Experimental Design*: Camo Process AS.
- [247] Wold, S. Ruhe, A. Wold, H. and Dunn, I. W., (1984). "The Collinearity Problem in Linear Regression. The Partial Least Squares (PLS) Approach to Generalized Inverses", *SIAM Journal on Scientific and Statistical Computing*, 5: 735-743.
- [248] Geladi, P. and Kowalski, B.R., (1986). "Partial least-squares regression: a tutorial", *Analytica Chimica Acta*, 185: 1-17.
- [249] Lorber, A. Wangen, L.E. and Kowalski, B.R., (1987). "A theoretical foundation for the PLS algorithm", *Journal of Chemometrics*, 1: 19-31.

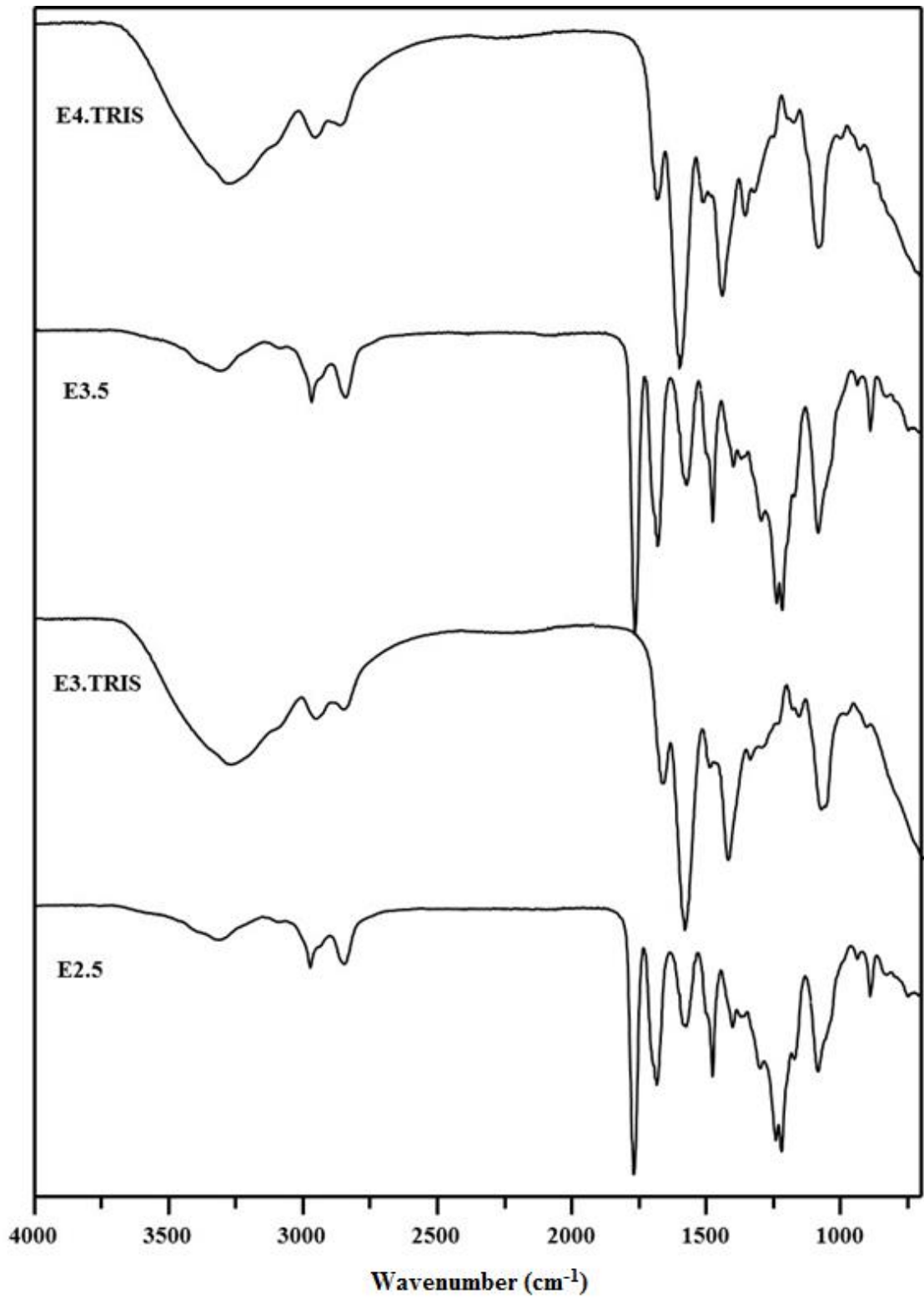
- [250] Höskuldsson, A., (1996). Prediction methods in science and technology. 1. Basic theory: Thor Publ.
- [251] Majoros, I.J. Keszler, B. Woehler, S. Bull, T. and Baker, J.R., (2003). "Acetylation of Poly(amidoamine) Dendrimers", *Macromolecules*, 36: 5526-5529.
- [252] Majoros, I.J. Thomas, T.P. Mehta, C.B. and Baker, J.R., (2005). "Poly(amidoamine) Dendrimer-Based Multifunctional Engineered Nanodevice for Cancer Therapy", *Journal of Medicinal Chemistry*, 48: 5892-5899.
- [253] Sabatini, A. Vacca, A. and Gans, P., (1992). "Mathematical algorithms and computer programs for the determination of equilibrium constants from potentiometric and spectrophotometric measurements", *Coordination Chemistry Reviews*, 120: 389-405.
- [254] Feng, Z.V. Lyon, J.L. Croley, J.S. Crooks, R.M. Vanden Bout, D.A. and Stevenson, K.J., (2009). "Synthesis and Catalytic Evaluation of Dendrimer-Encapsulated Cu Nanoparticles. An Undergraduate Experiment Exploring Catalytic Nanomaterials", *Journal of Chemical Education*, 86: 368.
- [255] Higuchi, T. and Connors, K.A., (1965). "Phase-solubility techniques", *Advan. Anal. Chem. Instr.*, 4: 117-212.
- [256] Şahin, S. Işık, E. and Demir, C., (2012). "Prediction of Total Phenolic Content in Extracts of Prunella Species from HPLC Profiles by Multivariate Calibration", *ISRN Chromatography*, 2012.
- [257] Esfand, R. and Tomalia, D.A., (2001). Laboratory Synthesis of Poly(amidoamine) (PAMAM) Dendrimers, J. Frechet and Tomalia, D., ed. *Dendrimers and Other Dendritic Polymers*. John Wiley & Sons Ltd, 587-604.
- [258] La Regina, G. Gatti, V. Piscitelli, F. and Silvestri, R., (2010). "Open Vessel and Cooling while Heating Microwave-Assisted Synthesis of Pyridinyl N-Aryl Hydrazones", *ACS Combinatorial Science*, 13: 2-6.
- [259] Kappe, C.O. Pieber, B. and Dallinger, D., (2013). "Microwave Effects in Organic Synthesis: Myth or Reality?", *Angewandte Chemie International Edition*, 52: 1088-1094.
- [260] Temel, G. Parali, T. Tulu, M. and Arsu, N., (2010). "Photopolymerization of acrylamide with benzophenone/methylated- $\beta$ -cyclodextrin inclusion complex in the presence of jeffamine based dendrimers as coiniciators in aqueous media", *J. Photoch. Photobio. A*, 213: 46-51.
- [261] Kojima, C. Kono, K. Maruyama, K. and Takagishi, T., (2000). "Synthesis of Polyamidoamine Dendrimers Having Poly(ethylene glycol) Grafts and Their Ability To Encapsulate Anticancer Drugs", *Bioconjugate Chemistry*, 11: 910-917.
- [262] Xu, M. Chen, Q.R. Kumar, D. Stass, S.A. and Mixson, A.J., (1998). "In Vivo Gene Therapy with a Cationic Polymer Markedly Enhances the Antitumor Activity of Antiangiogenic Genes", *Molecular Genetics and Metabolism*, 64: 193-197.

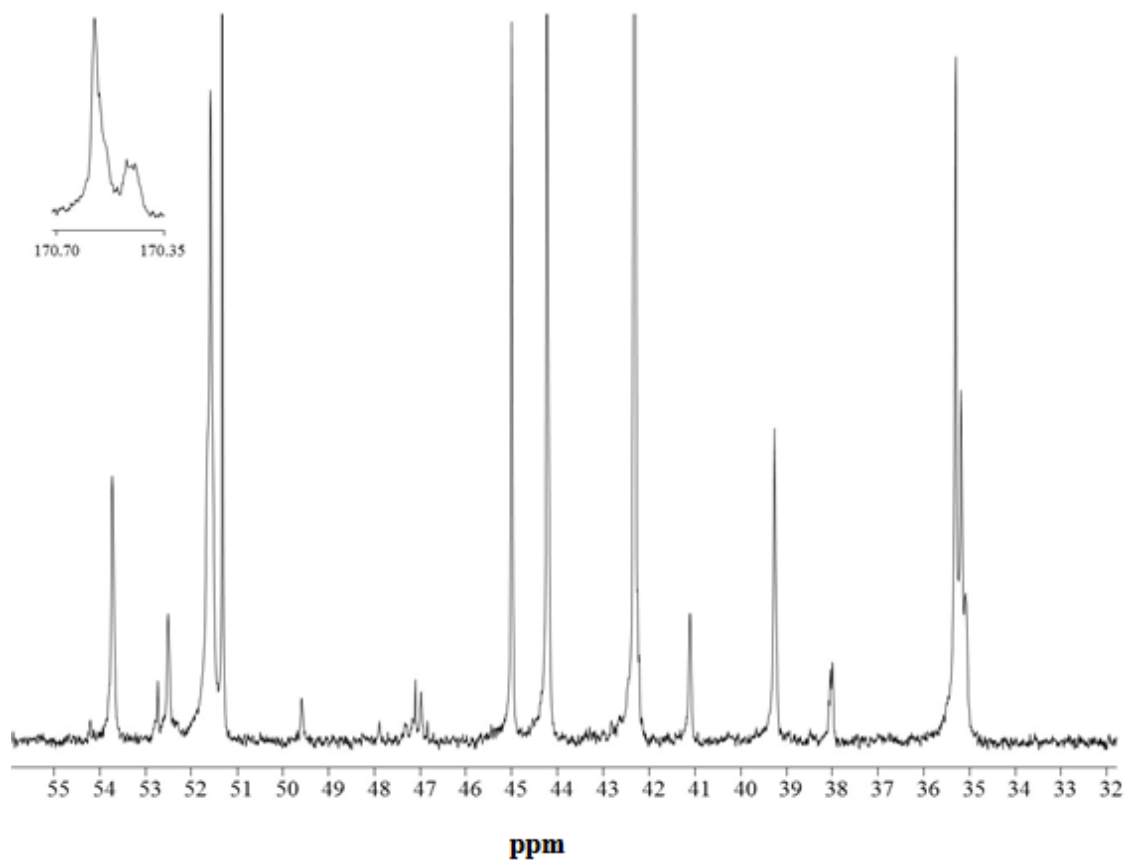
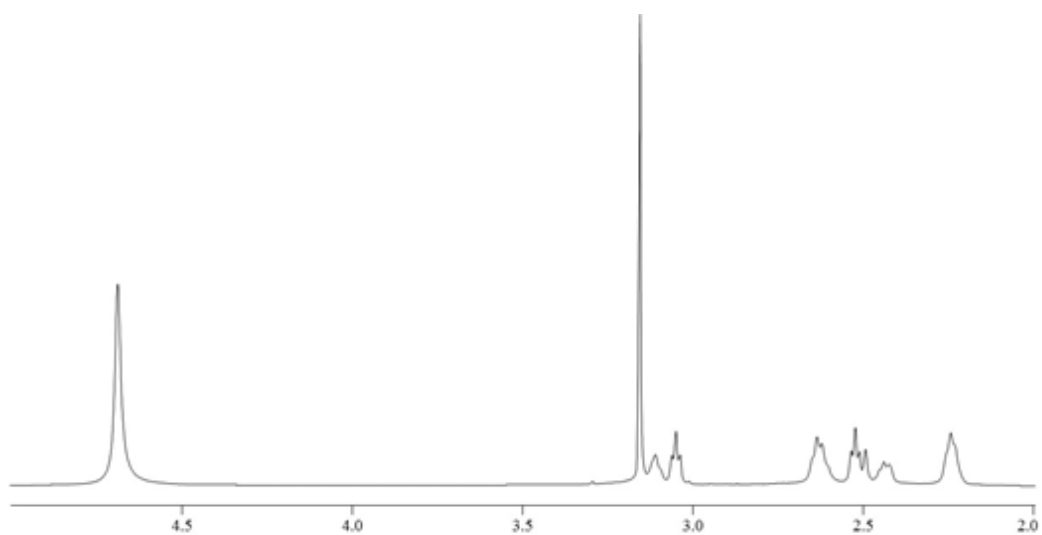
- [263] Malik, N. Wiwattanapatapee, R. Klopsch, R. Lorenz, K. Frey, H. Weener, J.W. Meijer, E.W. Paulus, W. and Duncan, R., (2000). "Dendrimers:: Relationship between structure and biocompatibility in vitro, and preliminary studies on the biodistribution of 125I-labelled polyamidoamine dendrimers in vivo", *Journal of Controlled Release*, 65: 133-148.
- [264] Newkome, G.R. Baker, G.R. Arai, S. Saunders, M.J. Russo, P.S. Theriot, K.J. Moorefield, C.N. Rogers, L.E. Miller, J.E. and et, a., (1990). "Cascade molecules. Part 6. Synthesis and characterization of two-directional cascade molecules and formation of aqueous gels", *J. Am. Chem. Soc.*, 112: 8458-8465.
- [265] Diallo, M.S. Balogh, L. Shafagati, A. Johnson, J.H., Jr. Goddard, W.A., III and Tomalia, D.A., (1999). "Poly(amidoamine) Dendrimers: A New Class of High Capacity Chelating Agents for Cu(II) Ions", *Environ. Sci. Technol.*, 33: 820-824.
- [266] Sun, L. and Crooks, R.M., (2002). "Interactions between Dendrimers and Charged Probe Molecules. 1. Theoretical Methods for Simulating Proton and Metal Ion Binding to Symmetric Polydentate Ligands", *The Journal of Physical Chemistry B*, 106: 5864-5872.
- [267] Kleinman, M.H. Flory, J.H. Tomalia, D.A. and Turro, N.J., (2000). "Effect of Protonation and PAMAM Dendrimer Size on the Complexation and Dynamic Mobility of 2-Naphthol", *The Journal of Physical Chemistry B*, 104: 11472-11479.
- [268] Crooks, R.M. Zhao, M. Sun, L. Chechik, V. and Yeung, L.K., (2000). "Dendrimer-Encapsulated Metal Nanoparticles: Synthesis, Characterization, and Applications to Catalysis", *Accounts of Chemical Research*, 34: 181-190.
- [269] Patri, A.K. Majoros, I.J. and Baker Jr, J.R., (2002). "Dendritic polymer macromolecular carriers for drug delivery", *Current Opinion in Chemical Biology*, 6: 466-471.
- [270] Liu, M. and Fréchet, J.M.J., (1999). "Designing dendrimers for drug delivery", *Pharmaceutical Science & Technology Today*, 2: 393-401.
- [271] D'Emanuele, A. and Attwood, D., (2005). "Dendrimer–drug interactions", *Advanced Drug Delivery Reviews*, 57: 2147-2162.
- [272] Cotton, F.A., (1999). *Advanced Inorganic Chemistry*: Wiley.
- [273] Kabanov, V. Zezin, A. Rogacheva, V. Gulyaeva, Z.G. Zansochova, M. Joosten, J. and Brackman, J., (1998). "Polyelectrolyte behavior of astramol poly (propyleneimine) dendrimers", *Macromolecules*, 31: 5142-5144.
- [274] Skoog, D.A., (2004). *Fundamentals of Analytical Chemistry*: Thomson-Brooks/Cole.
- [275] Yokoi, H. and Isobe, T., (1969). "ESR and Optical Absorption Studies of the Copper(II) Complexes of Ethylenediamine and Its Alkyl Derivatives", *Bulletin of the Chemical Society of Japan*, 42: 2187-2193.
- [276] Kennedy, B.P. and Lever, A.B.P., (1973). "Charge-transfer spectra of bis(diamine)copper(II) complexes and their correlation with other electronic, vibrational, and thermodynamic properties", *Journal of the American Chemical Society*, 95: 6907-6913.

- [277] Amundsen, A.R. Whelan, J. and Bosnich, B., (1977). "Biological analogs. Nature of the binding sites of copper-containing proteins", *Journal of the American Chemical Society*, 99: 6730-6739.
- [278] Hirlekar, R. and Kadam, V., (2009). "Preparation and characterization of inclusion complexes of carvedilol with methyl- $\beta$ -cyclodextrin", *Journal of Inclusion Phenomena and Macrocyclic Chemistry*, 63: 219-224.

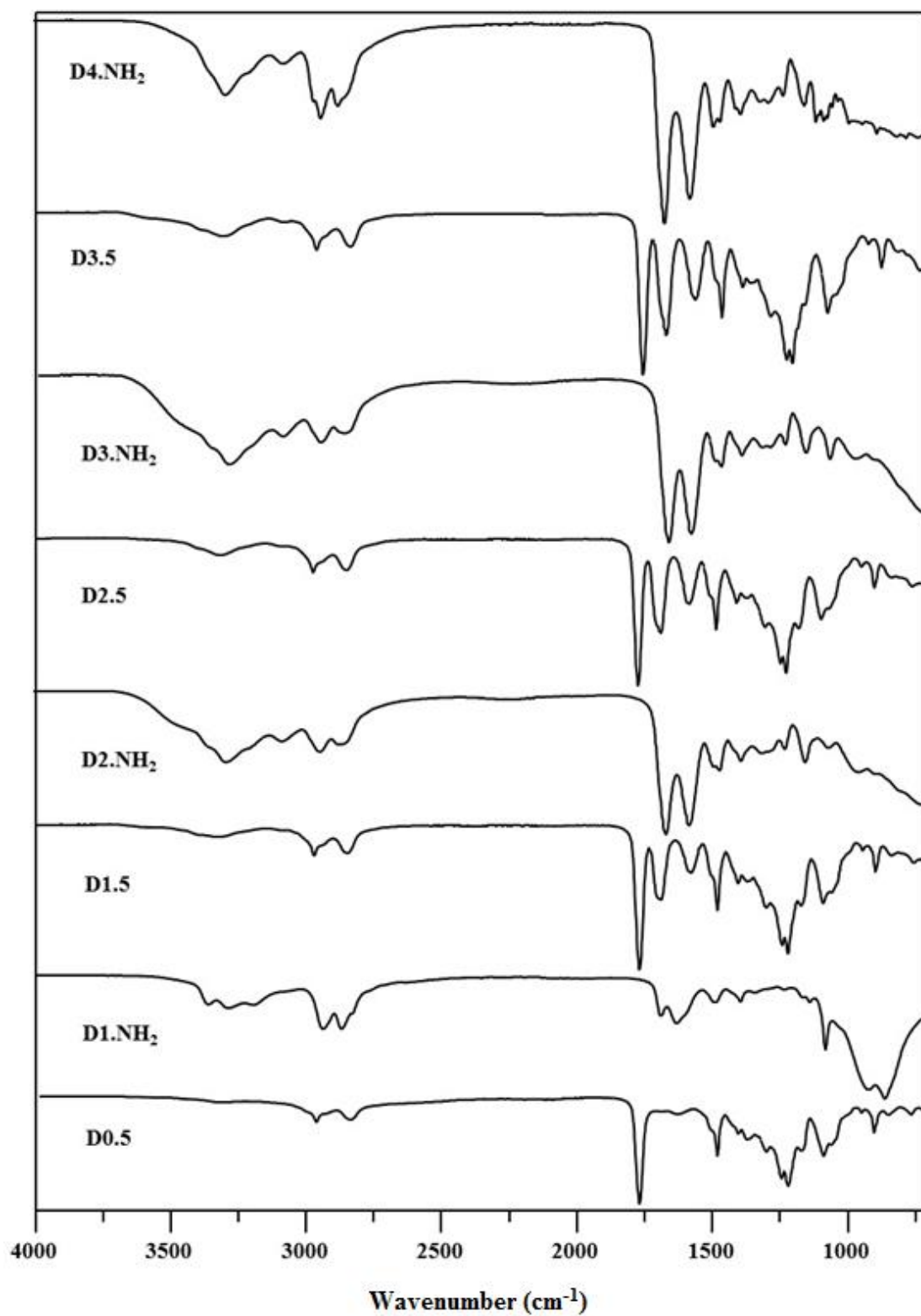
ATR-IR,  $^1\text{H}$  AND  $^{13}\text{C}$  NMR SPECTRA

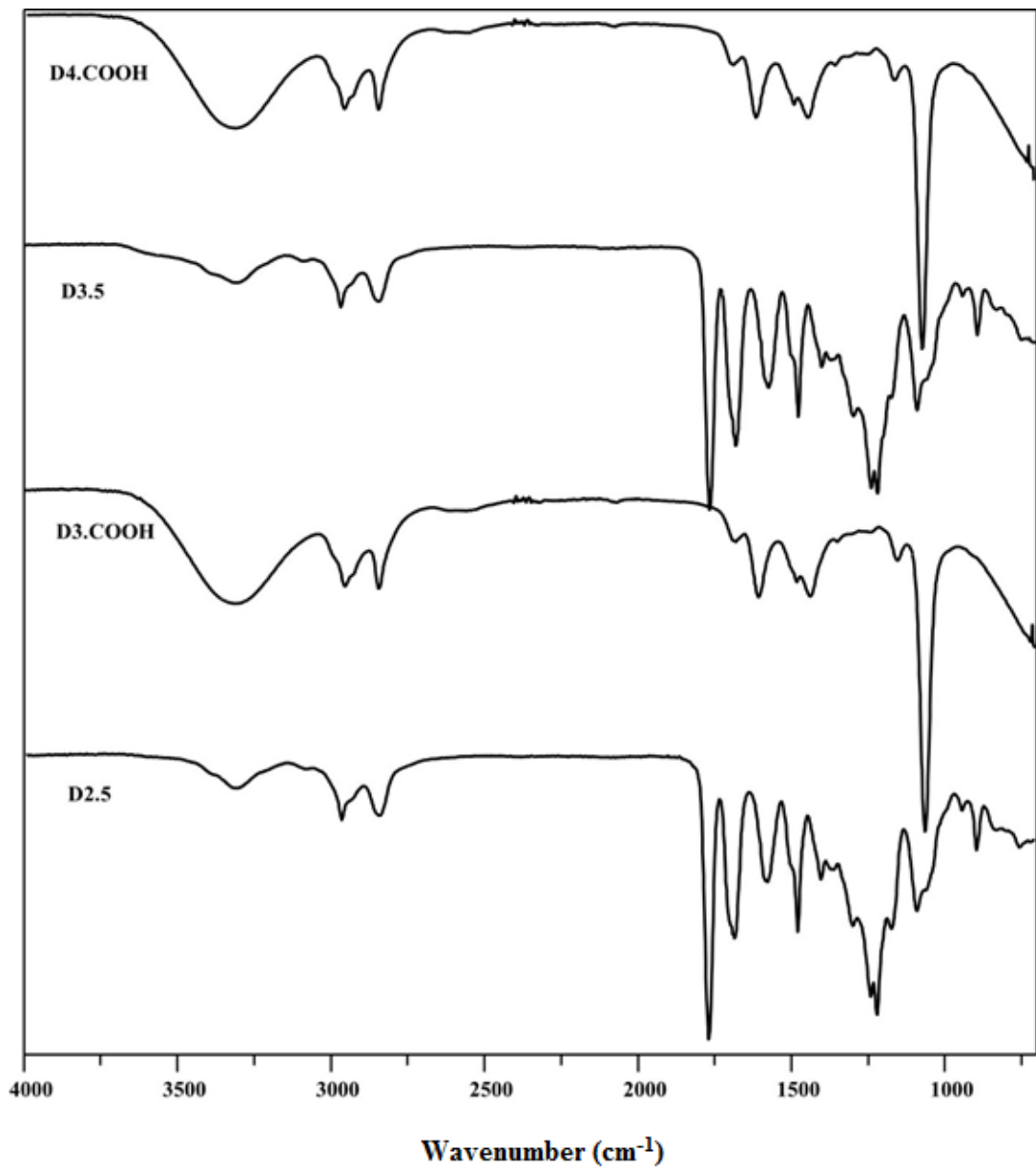


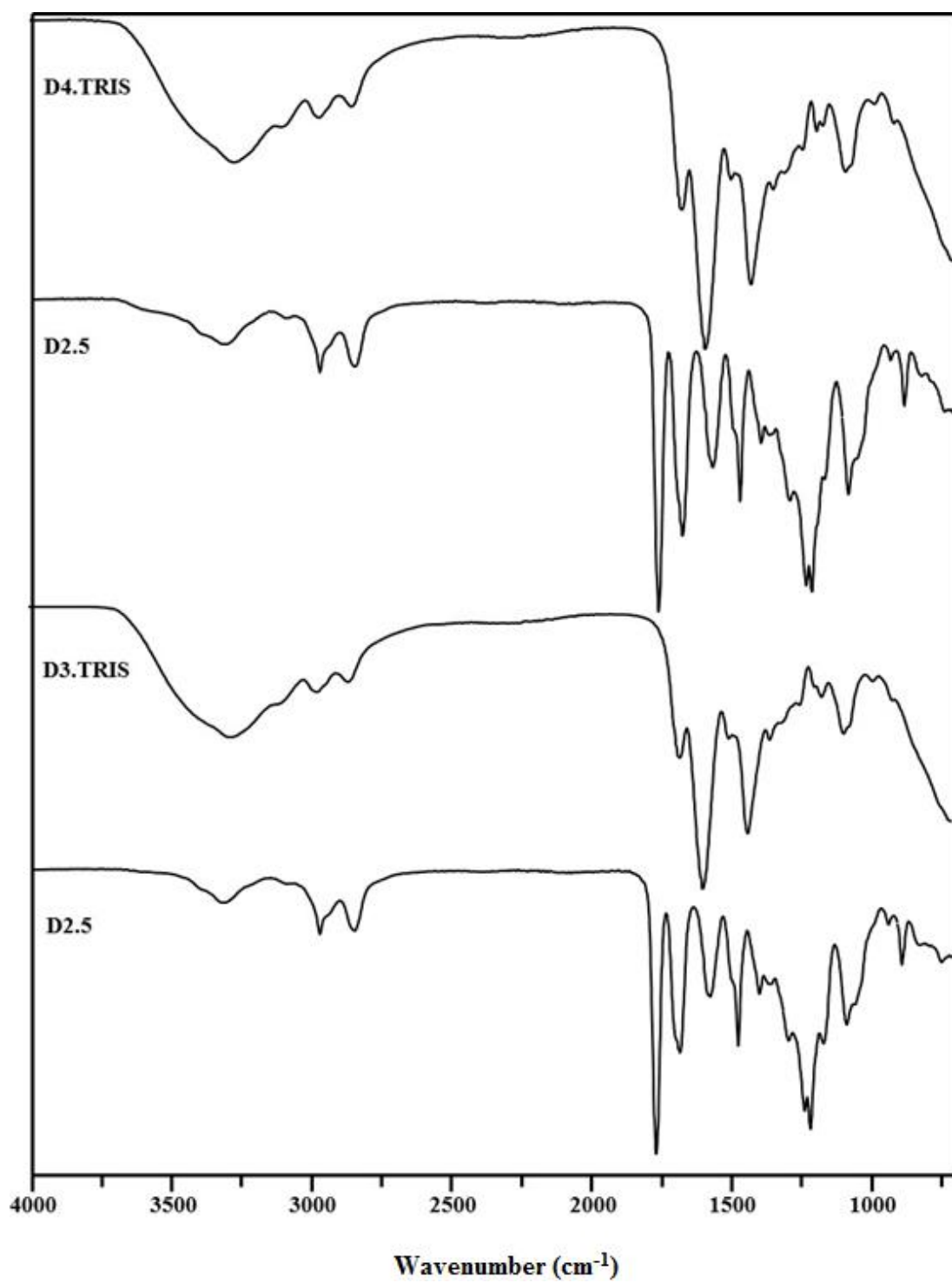


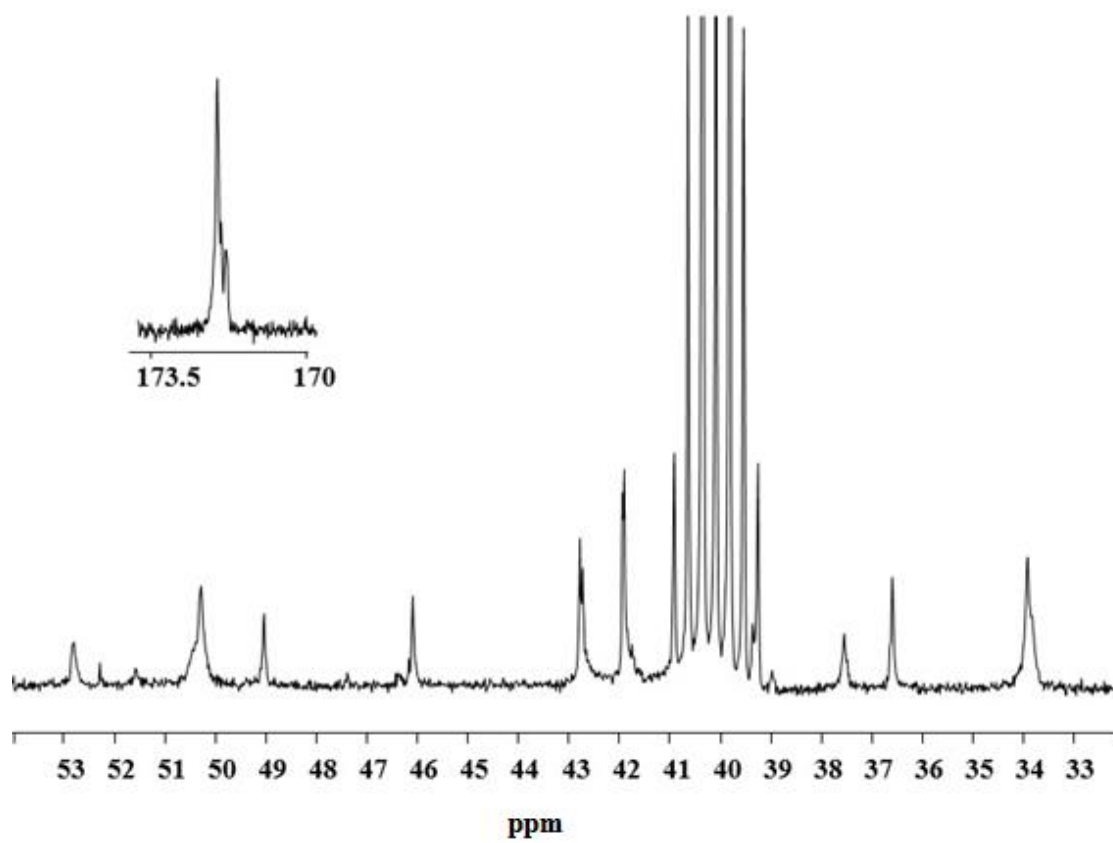
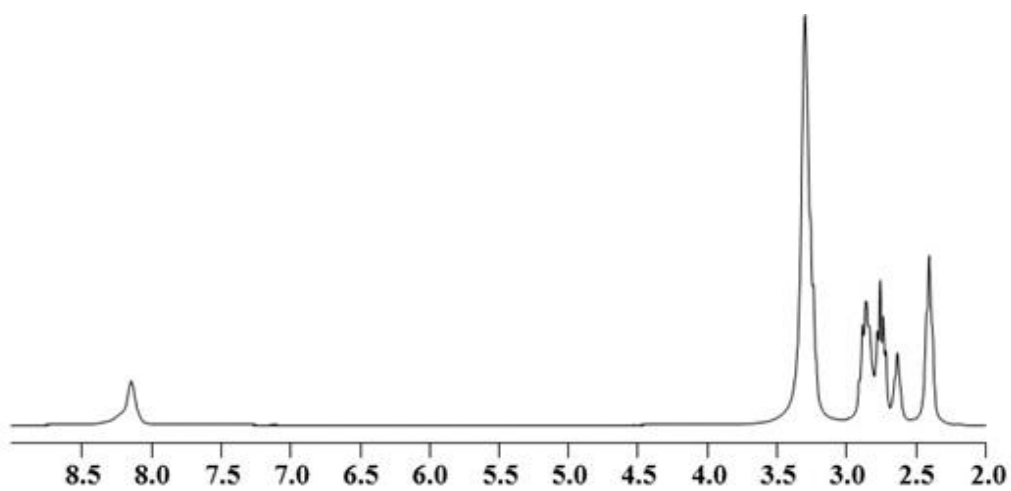


EDA 4.0-D<sub>2</sub>O Solvent

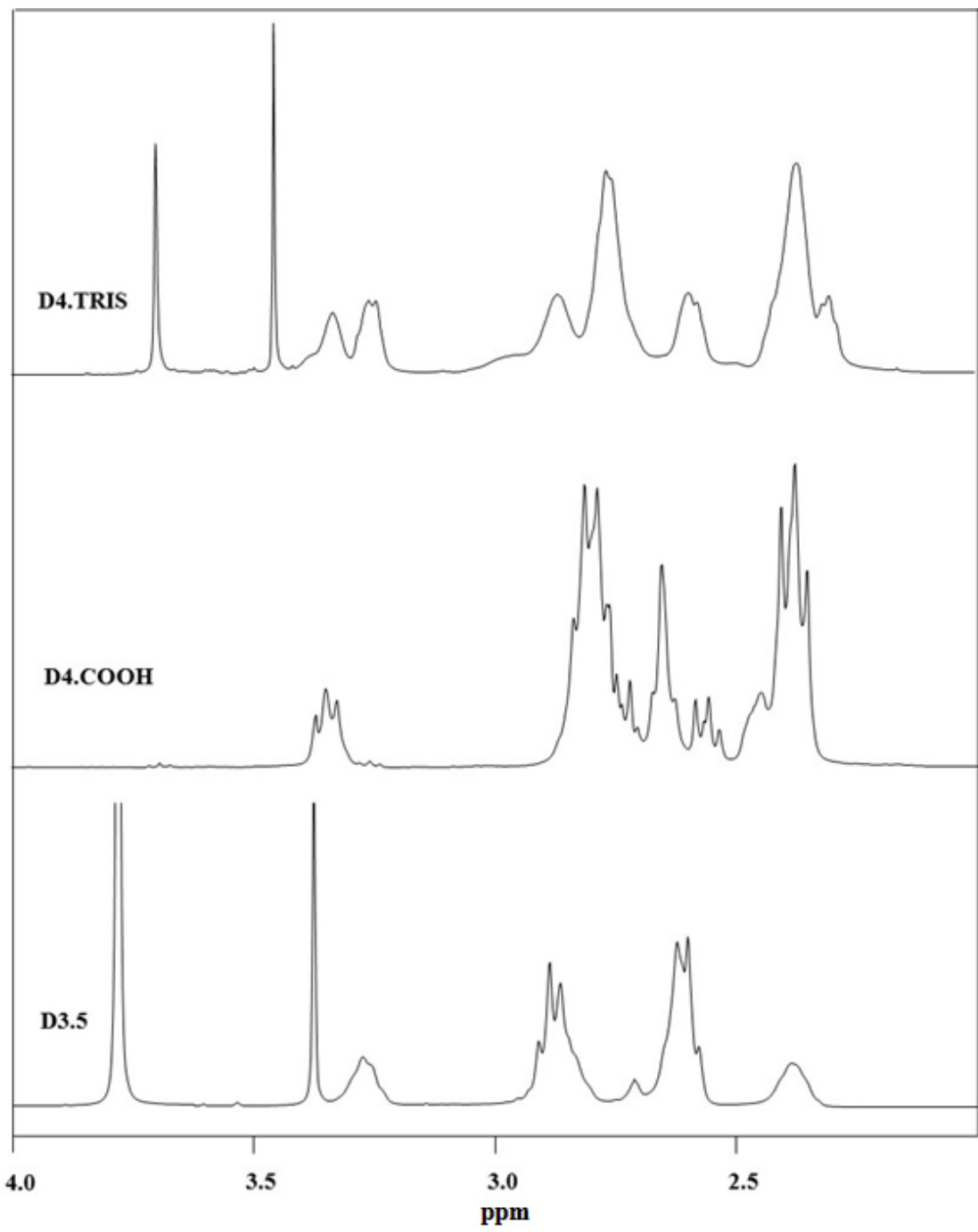




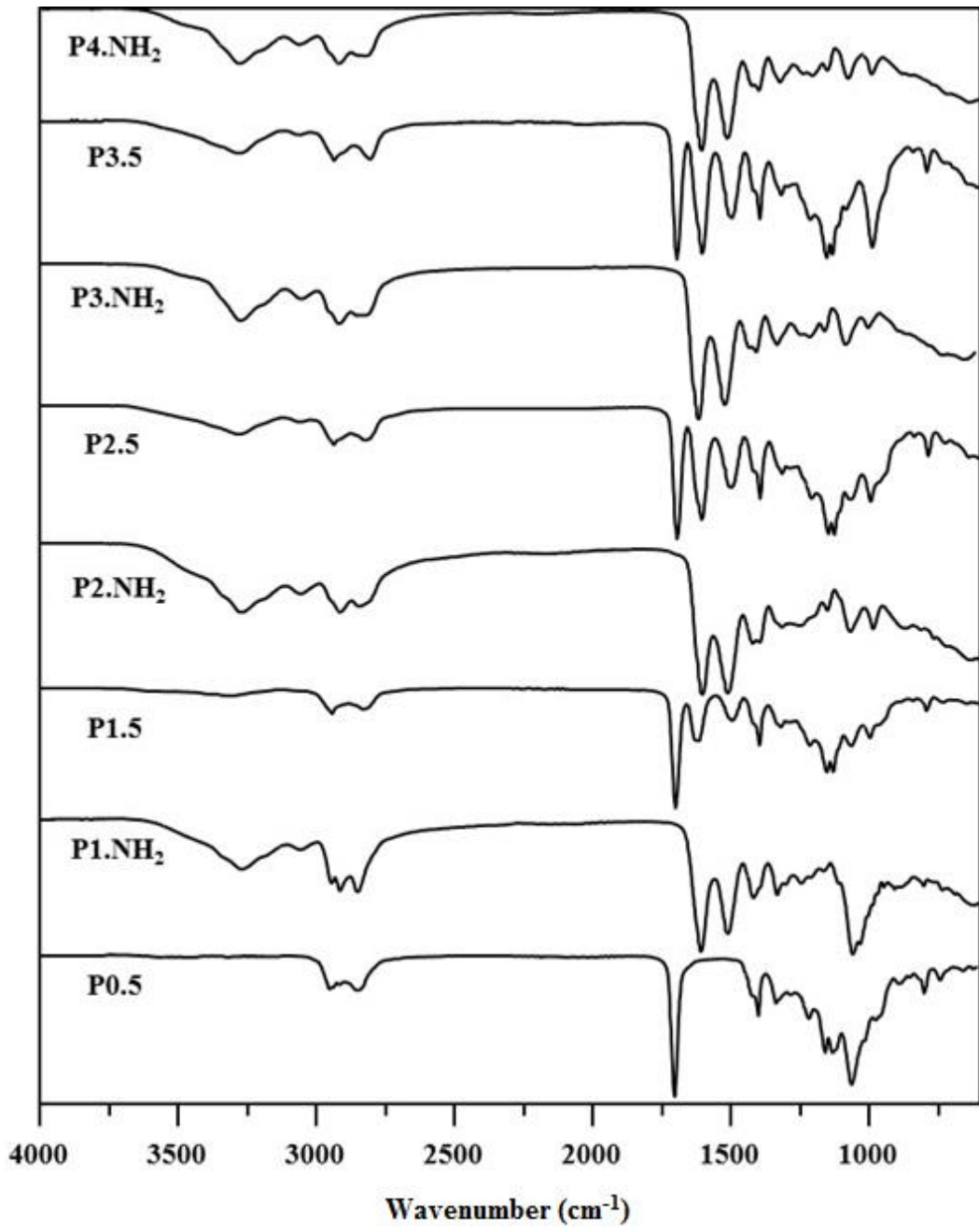


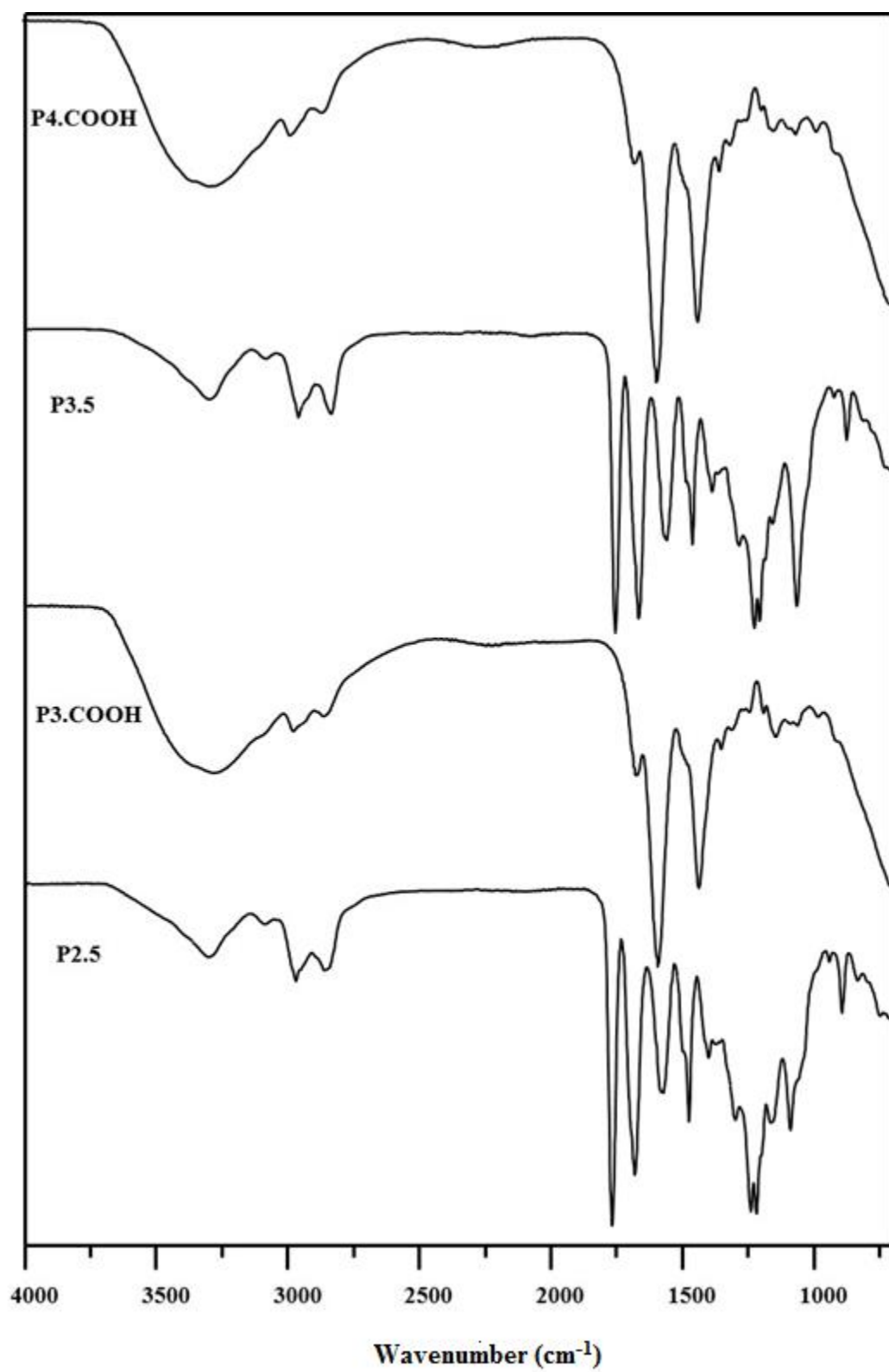


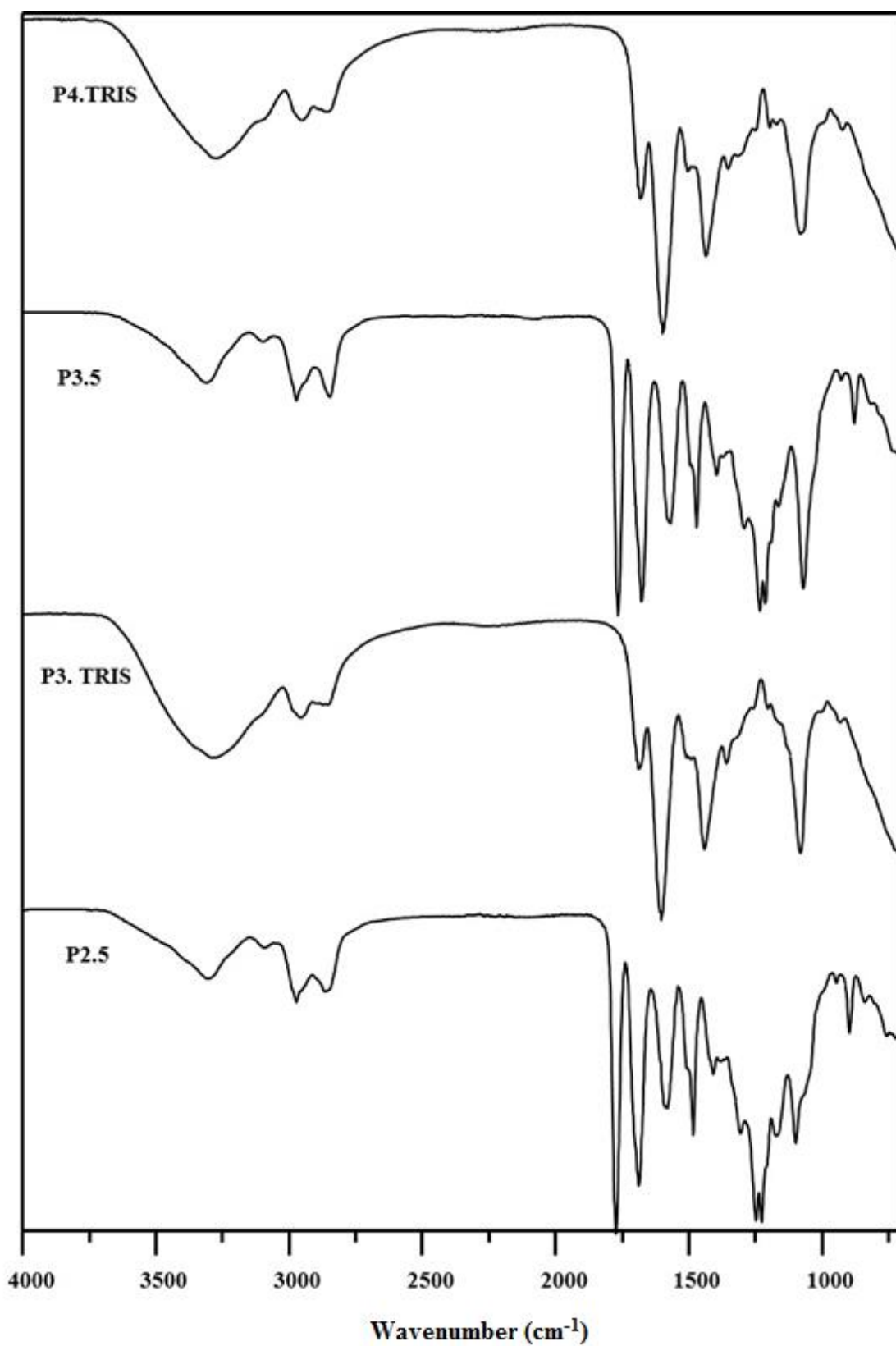
D4.NH<sub>2</sub>-DMSO Solvent

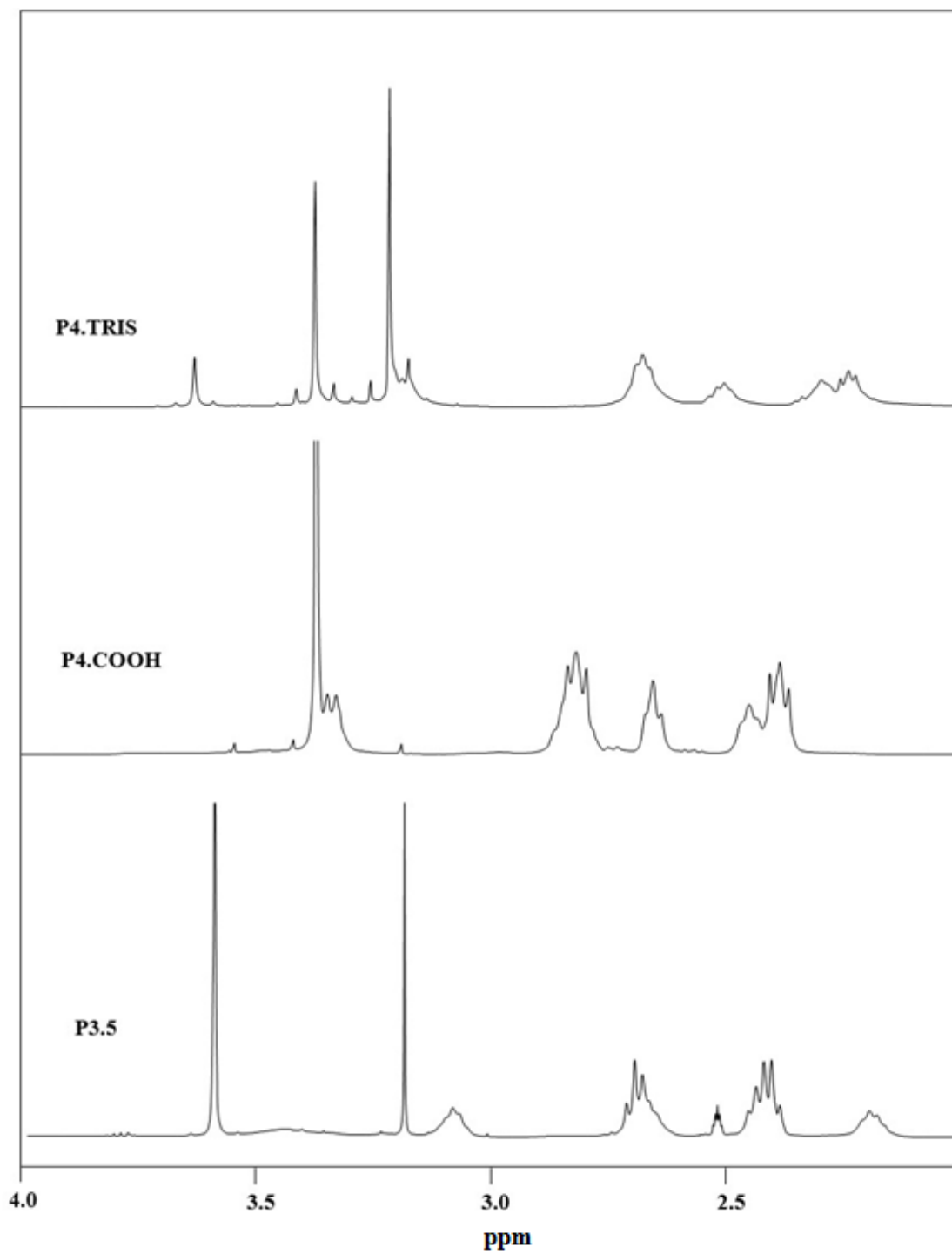


D3.5-DMSO, D4.COOH-D<sub>2</sub>O, D4.TRIS-CD<sub>3</sub>OD

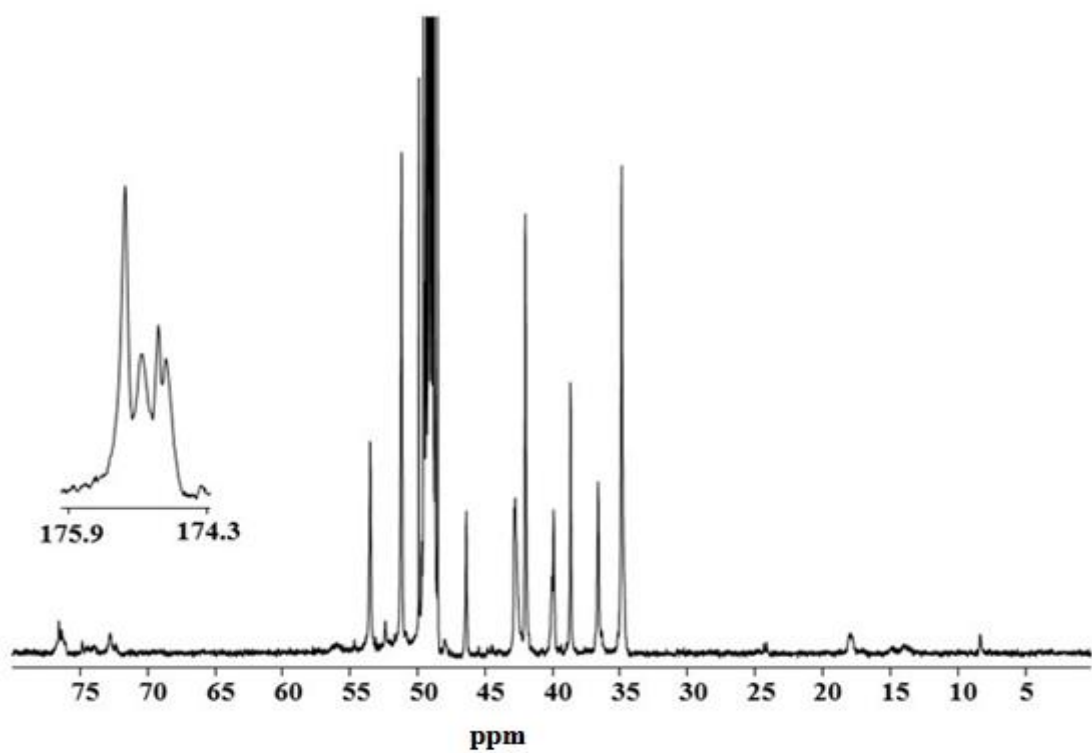
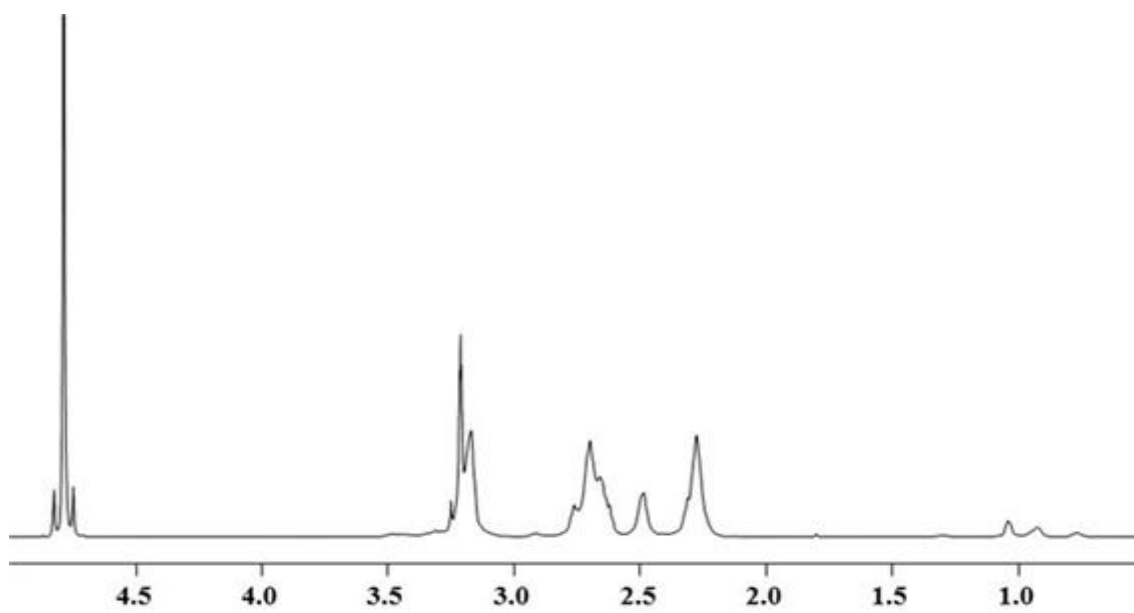








DMSO, D<sub>2</sub>O, CD<sub>3</sub>OD



P4.NH<sub>2</sub>-CD<sub>3</sub>OD Solvent

## CURRICULUM VITAE

---

### PERSONAL INFORMATION

**Name Surname** : Ali Serol ERTÜRK  
**Date of birth and place** : 14.02.1983 Malatya  
**Foreign Languages** : English  
**E-mail** : aserturk@yildiz.edu.tr, aserturk@gmail.com

### EDUCATION

| <b>Degree</b> | <b>Department</b>    | <b>University</b>           | <b>Date of Graduation</b> |
|---------------|----------------------|-----------------------------|---------------------------|
| Master        | Analytical Chemistry | Suleyman Demirel University | 2009                      |
| Undergraduate | Chemistry Education  | Boğaziçi University         | 2007                      |
| High School   |                      | Gönen Anatolian High School | 2000                      |

### WORK EXPERIENCE

| <b>Year</b> | <b>Corporation/Institute</b> | <b>Enrollment</b>  |
|-------------|------------------------------|--------------------|
| 2010        | Yıldız Technical University  | Research Assistant |
| 2008        | Adıyaman University          | Research Assistant |

## PUBLISHERMENTS

### Papers

1. **Ali S. Ertürk**, Metin Tülü, Abdürrezzak E. Bozdoğan, Tezcan Paralı, Microwave Assisted Synthesis of Jeffamine Cored PAMAM Dendrimers, European Polymer Journal, DOI: 10.1016/j.eurpolymj.2013.12.018, (2013) Accepted
2. Ozturk K., **Erturk A.**, Sarisözen C., Tulu M., Calis M., Cytotoxicity and In Vitro Characterization Studies of Synthesized Jeffamine-Cored PAMAMs, Journal of Microencapsulation , Vol. 30, Issue 5, pp. 1-10, (2013)

### Conference Papers

#### A. National Proceedings

1. **Ali Serol Ertürk**, Metin Tülü, Abdürrezzak Emin Bozdoğan, Spectroscopic Determination of the Proton Binding Constants of PAMAMs, XIII Ulusal Spektroskopi Kongresi, pp. 176, (2013)
2. **Ali Serol Ertürk**, Metin Tülü, Abdürrezzak Emin Bozdoğan, Simultaneous Determination of Different Generation PAMAM Dendrimer Mixtures with UV-VIS Spectroscopy, XIII Ulusal Spektroskopi Kongresi, pp. 177, (2013)
3. **Ertürk, A. S.**, Paralı, T., Bozdoğan, A., Tülü, M., PAMAM Tipi Dendrimerlerde Yüzey Modifikasyonu, 26. Ulusal Kimya Kongresi, pp. 17-18, (2012)
4. **Ertürk, A. S.**, Paralı, T., Tülü, M., Bozdoğan, A. E., PAMAM Dendrimerlerin İlaç Salınım Sistemleri Uygulamaları, 26. Ulusal Kimya Kongresi, pp. 64-65, (2012)
5. **Ertürk, A. S.**, Paralı, T., Bozdoğan, A., Tülü, M., PAMAM Dendrimerlere Metal Bağlanımın Spektroskopik Tespiti, 26. Ulusal Kimya Kongresi , pp. 62-63, (2012)

## **B. International Proceedings**

1. Metin Tülü, **A. Serol Ertürk**, A. Emin Bozdoğan. Synthesis of Dendritic Macroramolecules And Their Metal Complexation Studies, 44th World Chemistry Congress, 517, (2013)
2. **A. Serol Ertürk**, A. Emin Bozdoğan, Metin Tülü, Determination Of The Proton Binding Constants Of Dendrimers With Hyperquad, 44th World Chemistry Congress, 1051, (2013).
3. **A. Serol Ertürk**, Metin Tülü, A. Emin Bozdoğan. Removal Of Metal Ions From Aqueous Solutions By Polymer Assisted Ultrafiltration, 44th World Chemistry Congress, 1052, (2013)
4. **Ali Serol Ertürk**, Metin Tülü, Abdürrezzak Emin Bozdoğan. Determination of Different Generations from Binary Mixture of Jeffamine Cored PAMAMs by UV-VIS Spectroscopy, 2<sup>nd</sup> International Conference on New Trends in Chemometrics and Applications, 62, (2013).
5. **Ertürk, A. S.**, Gürbüz, M. U., Paralı, T., Bozdoğan, A. E., Tülü, M. , Selective Metal Complexation Of Novel Dendritic Macromolecules, 44th World Chemistry Congress, pp. 1268, (2013)
6. **Ertürk, A. S.**, Tülü, M., Bozdoğan, A. E. , Removal Of Metal Ions From Aqueous Solutions By Polymer Assisted Ultrafiltration, 44th World Chemistry Congress, pp. 1052, (2013)
7. **Ertürk, A. S.**, Bozdoğan, A. E., Tülü, M., Determination of The Proton Binding Constants of Dendrimers With Hyperquad, 44th World Chemistry Congress, pp. 1051, (2013)
8. Tülü, M., **Ertürk, A. S.**, Bozdogan, A. E., Synthesis of Dendritic Macromolecules and Their Metal Complexation Studies, 44 World Chemistry Congress, pp. 517, (2013)

9. Ozturk, K., Sarisozen, C., **Erturk, A. S.**, Tulu, M., Calis, S., Effect of Generation Number and Concentration on In Vitro Characterization and Cytotoxicity of Dendrimers, 2012 AAPS Annual Meeting and Exposition, (2012)
10. Dizman, C.,Paralı, T., **Ertürk, A. S.**, Tülü, M., Dendrimers as Potential Drug Carriers; Microwave-Assisted Synthesis of PAMAM Type Dendrimers, International Syposium on Drug Research & Development, pp. 35-36, (2011)

### **Books**

1. Tülü M., **Ertürk A. S.**, A Search for Antibacterial Agents, pp. 89-106, (2012)

### **Projects**

1. Dendritik Ligantların Sentezi ve Analitik Uygulamaları, DOP, Araştırmacı, 2012-07-01 - 2014-07-01
2. Çok Dişli Selat Ajanı Sentezi ve Çok Değişkenli Kalibrasyon Yöntemleri İle Metal İyonlarının Kantitatif Tayininde Kullanılması, Araştırmacı, KAP, 2011-09-01 - 2013-03-01
3. PAMAM Tipi Dendrimerlerinin Sentezi ve Biyolojik Özelliklerinin Araştırılması, Araştırmacı, KAP, 2011-09-01 - 2013-03-01
5. Suda Çözünür Makromoleküllerin Sentezi Ve Ağır Metallerle Kompleksleşme Kapasitelerinin İncelenmesi, Araştırmacı, KAP, 2011-09-01 - 2013-03-01

### **AWARDS**

1. Best poster award, 2<sup>nd</sup> International Conference on New Trends in Chemometrics and Applications, 58, (2013).